Discovery of a new type of ribosome-associated complex in *Caenorhabditis elegans*

Dissertation zur Erlangung des

akademischen Grades eines

Doktors der Naturwissenschaften

(Dr.rer.nat.)

vorgelegt von

Sachs, Nadine

an der

Mathematisch-Naturwissenschaftliche Sektion

Fachbereich Biologie

Konstanz, 2019

Tag der mündlichen Prüfung: 19.07.2019

1. Referentin: Prof. Dr. Elke Deuerling

2. Referent: Prof. Dr. Jörg Hartig

„Lache, wenn es nicht zum Weinen reicht“
HERBERT GRÖNEMEYER

TABLE OF CONTENTS

1. Abstract

Cellular fitness depends on proper *de novo* protein folding, translocation and degradation. All these pathways ensure protein homeostasis (proteostasis) within the cell. Maintenance of proteostasis is sustained by many factors that assist proteins to adopt their correct three-dimensional structure and to reach their specific subcellular destination. A class of proteins called molecular chaperones escorts proteins throughout their lifetime and facilitates protein folding and degradation to ensure a balanced cellular protein homeostasis. *De novo* protein biogenesis at the ribosome is a particularly error-prone process and is therefore guided by specialized ribosome-tethered chaperone systems. These chaperones facilitate co-translational protein folding by preventing unfavorable intramolecular interactions of the nascent polypeptide chain by a mechanism that is driven by coordinated substrate binding and release.

Part A: The ribosome-associated complex (RAC)

In eukaryotes co-translational protein folding is assisted by a conserved chaperone triad consisting of the heterodimeric ribosome-associated complex (RAC) and an Hsp70. RAC serves as a co-chaperone of the Hsp70 and is composed of a J-domain protein (Zuo1) and an atypical Hsp70 (Ssz1). The function of Ssz-like Hsp70s in RAC is poorly understood, as it lacks both ATPase and substrate binding activity. This unique chaperone complex organization is assumed to be evolutionary conserved in eukaryotes. However, while Zuotin-related proteins are present in all organisms, Ssz1 homologs appear to be absent in many metazoan species including nematodes and many arthropods. Seemingly, in these organisms a structurally and functionally different RAC system has evolved.

This thesis describes one of these non-canonical RAC systems found in the nematode *Caenorhabditis elegans*. In *C. elegans* a canonical, catalytically-active Hsp70 (HSP-1) forms a stable heterodimeric complex with the Zuo1 homolog DNJ-11 (ceRAC). Interestingly, complex formation induces a remodeling of the conventional Hsp70 function resulting in repressed ATPase and substrate binding activity. Nevertheless, the complexed Hsp70 transiently binds nascent chains at the ribosome via the canonical peptide binding cleft. Thus, not only Ssz-like proteins but also classical Hsp70 chaperones can serve as a RAC subunit. These findings reveal for the first time an Hsp70 inhibitory interaction by a J-domain protein and highlight the function of a low-affinity substrate-binding Hsp70 in RAC for co-translational protein folding.

Part B: The nascent polypeptide-associated complex (NAC)

At the ribosome the heterodimer NAC is the first factor that binds nascent chains and ensures proper ER protein targeting. However, the exact mode of action at the ribosome as well as its proposed chaperone activity remained enigmatic. The second part of this study demonstrates that *in vitro* NAC supports refolding of denatured luciferase by the Hsp70 system, providing direct evidence that NAC exerts chaperone function also independent from its ribosome association. A potential off-ribosome chaperone function of NAC was further supported by the finding that *in vivo* a substantial fraction of NAC is not ribosome bound. Moreover, the study revealed that the positively charged ribosome binding domain, the N-terminus of βNAC (N-βNAC), is essential for direct chaperone function toward polyglutamine (PolyQ) proteins. Apart from its function as chaperone entity, the N-terminal tail of the βNAC subunit inserts into the ribosomal tunnel extending up to the peptidyl transferase center. Thus, N-βNAC senses protein properties early during protein biogenesis and guides the newly synthesized polypeptide through the ribosomal tunnel. It was hypothesized that this tunnel probing of NAC senses empty and early translating ribosomes to block unproductive association of other co-translational protein biogenesis factors like RAC. Indeed, it could be shown *in vitro* that wildtype NAC, but not a ribosome-binding mutant variant, detaches RAC from ribosomes. NAC is as abundant as ribosomes, thus this finding supports the hypothesis that NAC orchestrates ribosome association of other low abundant protein biogenesis factors to ensure correct *de novo* folding and transport.

2. Zusammenfassung

Die Protein-Homöostase trägt grundlegend zur Fitness einer jeden Zelle bei. An der Aufrechterhaltung dieses Gleichgewichts sind in Eukaryoten zahlreiche Faktoren beteiligt, die *de novo* Proteinfaltung, zellulären Proteintransport sowie -abbau unterstützen. Diese Mechanismen sind essentiell für die Funktionalität von Proteinen und dadurch im gleichen Maße für die Lebensfähigkeit der Zelle. Eine Proteinklasse namens „Molekulare Chaperone" unterstützt hierbei die Faltung und den Abbau der Substrate und begleitet dadurch Polypeptide auf deren gesamten Lebensweg. Ein erster Kontakt von Chaperonen und Substraten findet bereits während der Proteinbiogenese an Ribosomen statt, da dieser Prozess sehr fehleranfällig ist. Hier agieren spezifizierte Chaperon-Systeme, die die Faltung neu synthetisierter Polypeptide unterstützen. Die Substratbindung/ -freisetzung durch Chaperone verhindert nachteilige intramolekulare Kontakte der Peptidkette.

Teil A: Der Ribosome-associated complex (RAC)

Die co-translationale Proteinfaltung in Eukaryoten wird von einer Chaperon-Triade begleitet. Diese besteht aus einem Hsp70, welches in seiner Chaperon-Aktivität von dem heterodimeren Ribosome-associated complex (RAC) unterstützt wird. Dieser Komplex besteht seinerseits aus einem J-Protein (Zuo1) und einem atypischen Hsp70 (Ssz1). Die Funktion der Ssz-Untereinheit ist bisher unklar, da weder eine ATP Hydrolyse noch eine Bindung von Substraten durch diese Proteine beobachtet wurde. Zunächst scheint der einzigartige Aufbau des RAC-Komplexes in Eukaryoten evolutionär konserviert zu sein, jedoch existieren in allen eukaryotischen Organismen nur Zuotin-Homologe. Ssz-Homologe sind in allen Fadenwürmern (Nematoden) und in einer großen Anzahl an Gliederfüßern (Arthropoden) nicht vorhanden, was darauf hinweist, dass diese Arten ein funktionell verändertes RAC-System evolviert haben.

Diese Arbeit analysiert das RAC-System im Fadenwurm *Caenorhabditis elegans*. In *C. elegans* bilden ein gewöhnliches, katalytisch-aktives Hsp70 (HSP-1) und das Zuo1-Homolog DNJ-11 einen stabilen, heterodimeren Komplex (ceRAC). Die Komplexbildung führt zu einer Umgestaltung von HSP-1, sichtbar in einer reprimierten ATPase- und Substratbindeaktivität. Interessanterweise bindet die HSP-1-Untereinheit des Komplexes noch immer transient an Polypeptidketten, die den ribosomalen Tunnel verlassen. Diese Interaktion findet über die normale Hsp70-Substratbindetasche statt. Diese Beobachtungen zeigen, dass RAC sowohl Ssz-ähnliche Hsp70 als auch gewöhnliche Hsp70 enthalten kann. Hierdurch wird deutlich, dass in allen RAC-Systemen ein Hsp70 mit niedriger Substrat-Affinität benötigt wird, um eine co-translationale Proteinfaltung an Ribosomen zu ermöglichen.

Teil B: Der Nascent polypeptide-associated complex (NAC)

NAC ist ein Heterodimer und der erste eukaryotische Faktor, der Kontakt zu Polypeptiden aufnimmt, wenn diese das Ribosom verlassen. Zudem konnte gezeigt werden, dass der erfolgreiche co-translationale Transport von Proteinen zum ER nur durch die Aktivität von NAC gewährleistet werden kann. Der exakte Wirkmechanismus sowie die vermutete Chaperon-Funktion von NAC sind bisher nicht vollständig geklärt. Der zweite Abschnitt dieser Arbeit zeigt, dass NAC im Stande ist, das Hsp70-System *in vitro* bei der Rückfaltung von denaturierter Luciferase zu unterstützen. Dies zeigt, dass NAC auch unabhängig vom Ribosom eine Funktion erfüllt. Dies wurde durch die Beobachtung bestätigt, dass ein Großteil von NAC *in vivo* nicht an Ribosomen gebunden vorliegt. Des Weiteren konnte gezeigt werden, dass NAC eine direkte Chaperon-Aktivität auf krankheitsassoziierte Proteine, wie Polyglutamin-Proteine (PolyQ) ausübt. Hierfür ist der geladene N-Terminus von βNAC (N-βNAC) essentiell. Unabhängig von der Chaperon Funktion kann N-βNAC in den ribosomalen Tunnel inserieren und die neu synthetisierte Polypepitdkette bereits am Peptidyltransferase-Zentrum des Ribosoms kontaktieren. NAC kann hierdurch bereits sehr früh die Eigenschaften der neu translatierten Proteine erkennen und sie durch den Tunnel begleiten. Es wurde vermutet, dass diese Tunnel-Insertion von NAC in leere und früh translatierende Ribosomen unproduktive Bindung von anderen co-translationalen Faktoren blockiert. Tatsächlich konnte *in vitro* gezeigt werden, dass RAC von Wildtyp-NAC am Ribosom verdrängt werden kann. Eine NAC-Ribosom-Bindemutante war zu dieser Verdrängung nicht im Stande. NAC ist in gleicher Anzahl vorhanden wie Ribosomen, daher kann postuliert werden, dass NAC am Ribosom andere, weniger abundante Proteinbiogenese-Faktoren zeitlich arrangiert, um eine erfolgreiche Proteinfaltung sowie einen korrekten Proteintransport zu gewährleisten.

3. Introduction

3.1 Protein folding and aggregation

All cellular processes depend on a functional proteome that acts in a broad range of cellular pathways. To fulfill their specific tasks these polypeptides need to adopt their correct three-dimensional structure. In the 1970s Anfinsen postulated that the amino acid sequence of polypeptides encodes all information needed for three-dimensional protein folding as small denatured proteins fold spontaneously into their native structure (Anfinsen, 1973). Nevertheless, during folding proteins need to manage their path through a distinct energy landscape which may force them into non-native but kinetically favored structures.

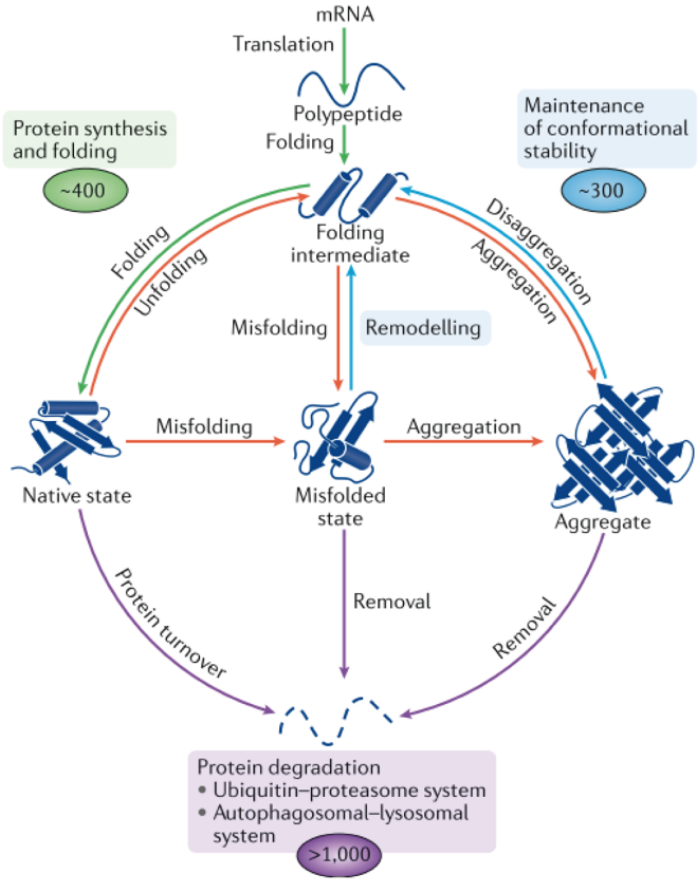

Figure 1: Protein folding pathways and quality control mechanisms in eukaryotes. In humans *de novo* protein folding is supported by ~400 proteins (green line). The native three-dimensional protein structure is maintained by approximately 300 factors (blue lines) which prevent unfavorable conformations and protein aggregation of the client proteins in off-pathways (red line). If protein refolding fails, misfolded proteins and protein deposits are eliminated via the protein degradation pathway by ubiquitination and proteasomal activity or by phagocytosis (purple line). Figure reprinted by permission from Macmillan Publishers Ltd: Nature Reviews Molecular Cell Biology, 2019 Feb 7. doi: 10.1038/s41580-019-0101-y., Hipp *et al.*, copyright 2019.

Partially folded or non-native proteins often expose hydrophobic amino acid residues that promote aberrant inter- or intramolecular interactions which lead to protein aggregation or misfolding (Hipp *et al*, 2019). To prevent unfavorable interactions mammalian cells possess approximately 2,000 proteins that act in protein quality control pathways including protein synthesis and folding, structural maintenance and protein degradation (Fig. 1) (Klaips *et al*, 2018).
Under stress conditions, however, protein quality control mechanisms can fail evident by many diseases that are characterized by misfolded or aggregated polypeptides causing cellular or tissue-specific toxicity. These pathological conditions include for example Alzheimer's (amyloid beta (Aβ)), Parkinson's (alpha-synuclein) or Huntigton's (PolyQ) disease. Protein folding is a demanding task for every cell and the maintenance of proteome integrity is even more challenging under aging conditions when the capacity of protein homeostasis (proteostasis) pathways declines dramatically (Labbadia & Morimoto, 2015).

The introduction will mainly focus on early protein folding and quality control mechanisms in eukaryotes which are mediated by specialized molecular chaperones that directly bind to translating ribosomes.

3.2 Protein biosynthesis by ribosomes

In all organisms the processing of genetic information is a fundamental step that guarantees a functional cellular environment. The dogma of molecular biology states that the conversion of this information traverses two basic steps that are called transcription and translation. Protein coding genes are first transcribed into RNA followed by translation of this messenger RNA (mRNA) by ribosomes into polypeptides.

3.2.1 Organization of ribosomes

Translation of mRNA into proteins is mediated by large ribonucleoprotein complexes, called ribosomes that harbor apart from mRNA also tRNA (transfer RNA) and ancillary factors to fulfill efficient protein synthesis. While all ribosomes consist of a large and small subunit, which are characterized by a specific composition of ribosomal RNA (rRNA) and proteins, the molecular size and building blocks differ between prokaryotes and eukaryotes. Prokaryotic 70S ribosomes are ∽ 2.4 MDa large complexes that consist of a small 30S and large 50S subunit (S= Svedberg unit) with 3 rRNA molecules (5S, 23S and 16S) and ∽ 54 ribosomal proteins. In contrast, eukaryotic 80S ribosomes are ∽ 4 MDa in size and comprise a 40S and 60S subunit with 4 rRNAs (18S, 5S, 5.8S and 28S) and ∽ 83 proteins (Ban *et al*, 2014; Bashan & Yonath, 2008). However, bacterial and

eukaryotic ribosomes share a common structural core of 34 proteins showing that translation by ribosomes is evolutionary conserved (Spahn *et al*, 2001).

Ribosome biogenesis is the most energy consuming process in the cell and regulated by nearly 200 different factors in eukaryotes (Karbstein, 2011). Under optimal growth conditions *Escherichia coli* contains around 55,000 ribosomes per cell, whereas in eukaryotes this number increases tremendously e.g. *Saccharomyces cerevisiae* contains 200,000 ribosomes and mammalian cells up to 5 million ribosomes (von der Haar, 2008; Bakshi *et al*, 2012; Hipp *et al*, 2019). The elongation speed varies from 20 aa/s in eukaryotes to 4-6 aa/s in prokaryotes, respectively (Kaiser & Liu, 2018; Young & Bremer, 2015).

Many sequential structure determinations of ribosomes during translation shed light on the mode of action and gave an impression on the complexity of this fundamental process. In 1980 the first ribosomal structure was published showing the crystal structure of the large ribosomal subunit of *Bacillus stearothermophilus* (Yonath *et al*, 1980). In the following years many publications followed revealing higher resolution structures of the bacterial (Schuwirth *et al*, 2005; Yusupov *et al*, 2008; Khusainov *et al*, 2016; Ban *et al*, 2000) and eukaryotic ribosome (Ben-Shem *et al*, 2010; Anger *et al*, 2013; Khatter *et al*, 2015; Spahn *et al*, 2001).

3.2.2 Structural features of eukaryotic ribosomes

The eukaryotic 40S subunit comprises the decoding center where mRNA and amino acid loaded tRNA meet. At the large 60S subunit catalytic amino acid polymerization takes place and the polypeptide chain leaves the ribosome through the resident exit tunnel (Fig. 2 A). Both subunits share the peptidyl transferase center (PTC) which encompasses the three binding sites, A (aminoacyl), P (peptidyl) and E (exit). The first loaded tRNA inserts at the mRNA codon presented in the A site and slides forward to the P site, thus a second tRNA can bind at the A site and a peptide bond of both presented amino acids is formed. This chain elongation processes further by continuous insertion of new amino acid loaded tRNAs , whereas empty tRNAs leave the ribosome through the E site (Bashan & Yonath, 2008). The exit tunnel is ∽ 100 Å long and forms a constriction site formed by the extended loops of the ribosomal proteins uL4 and uL22, 30 Å away from the PTC (Fig. 2 B). Here, the tunnel narrows down to ∽10 Å in diameter, while the tunnel expands to ∽20 Å at the mouth of the tunnel exit (Berisio *et al*, 2003; Ben-Shem *et al*, 2011; Beckmann *et al*, 2001; Ban *et al*, 2000). The narrow space inside the tunnel allows merely the folding of α-helical structures, however near the exit site even small tertiary structures may form (Nilsson *et al*, 2015; Kosolapov & Deutsch, 2009; Nissen *et al*, 2000). Completion of protein folding takes place outside the ribosomal tunnel.

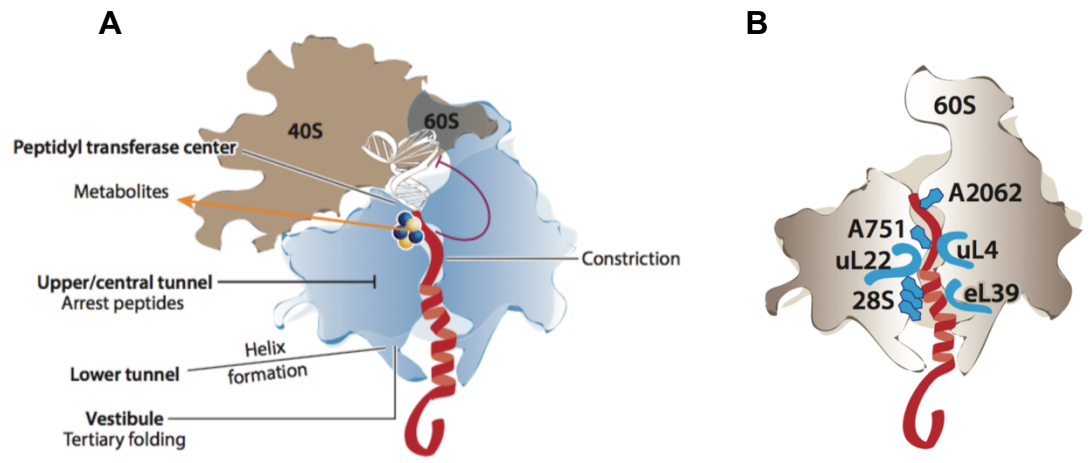

Figure 2: The eukaryotic ribosomes as center for protein biosynthesis (A) The 40S and 60S subunits of the ribosome host the peptidyl transferase center (PTC), where peptide-bonds between amino acids are formed and where nascent polypeptide chains enter the ribosomal tunnel. The polypeptide (red) traverses through the constriction site of the tunnel and in the lower tunnel section is able to form first secondary structures, like α-helices. Metabolites that inhibit translation often interact directly with the PTC. **(B)** The constriction site in the ribosomal tunnel is formed by the extended loops of the ribosomal proteins uL4 and uL22, preventing any initial folding of the nascent polypeptide. Figure republished by permission from Annual Review of Biochemistry, from Kramer et al., 2018 Dec 3. doi: 10.1146/annurev-biochem-013118-111717., copyright 2018, permission conveyed through Copyright Clearance Center, Inc..

At the tunnel exit an assembly of different ribosomal proteins provides a hub for different ribosome-associated factors that assist protein folding, maturation, trafficking or modification of the nascent polypeptide chains. These anchor proteins include uL22, uL23, uL29 and eL31 as well as eL39 and eL19 (Fig. 3). Ribosomal proteins uL23 and uL29 are bound by methionine aminopeptidases (MAPs) which cleave off the N-terminal methionine during translation. The same ribosomal proteins are recognized by SRP54, a subunit of the signal recognition particle, which mediates the co-translational targeting of substrates destined for the endoplasmic reticulum (ER) (Nyathi & Pool, 2015; Fujii *et al*, 2018; Pool *et al*, 2002; Voorhees & Hegde, 2015). N-acetyltransferases (NATs), the nascent polypeptide-associated complex (NAC) and the ribosome-associated complex (RAC) associate with uL22 and eL31 near the tunnel exit (Lee *et al*, 2016; Zhang *et al*, 2014; Peisker *et al*, 2008; Knorr *et al*, 2019; Pech *et al*, 2010; Wegrzyn *et al*, 2006; Zhang *et al*, 2012). Functions of NAC and RAC are presented in more detail in **chapter 3.4**.

It becomes obvious that the tunnel exit site at the ribosome is a platform for many factors that act on the nascent chain immediately as it reaches out of the save tunnel environment into the crowded cytosol. Overlapping contact sites of these factors reveal that simultaneous binding is either difficult or impossible.

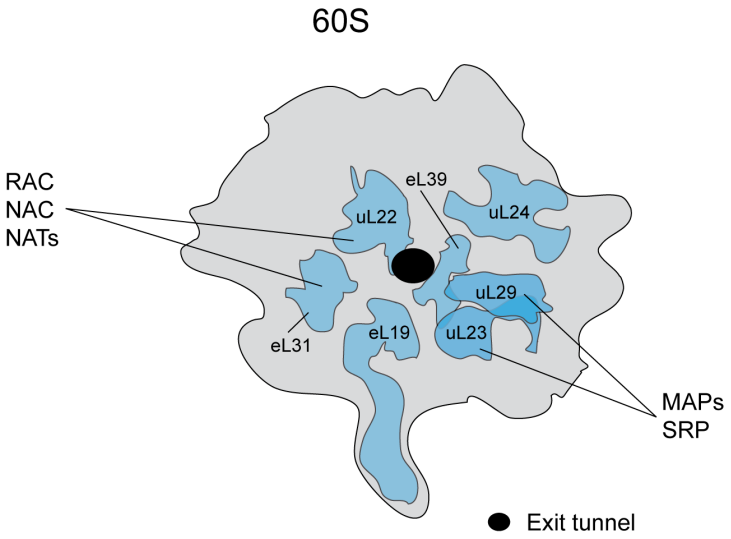

Figure 3: The eukaryotic 60S ribosomal subunit as platform for modification, trafficking and maturation factors of newly synthesized proteins (PDB 3O58). Ribosomal proteins (blue) directly positioned at the tunnel exit function as a hub for different factors involved in co-translational protein folding, sorting and modification. N-acetyltransferases (NATs), the ribosome-associated complex (RAC) and the nascent polypeptide-associated complex (NAC) share contact sites at uL22 and eL31. The signal recognition particle (SRP) involved in protein transport of the nascent polypeptide chain to the ER and the methionine aminopeptidases (MAPs) associate with uL29 and uL23.

3.3 Molecular chaperones

Molecular chaperones are defined as proteins that help other proteins to adopt their native fold without being part of their final structure (Hartl, 1996). Chaperones preserve cellular protein homeostasis and regulate diverse pathways including *de novo* protein folding, prevention of aggregation, protein unfolding and disaggregation, protein targeting, as well as protein degradation (Kim *et al*, 2013). The next subchapter will focus on the diversity of the eukaryotic chaperone network.

3.3.1 Classes of molecular chaperones

Molecular chaperones are highly miscellaneous concerning their subcellular localization, mode of action, energy dependence and substrate specificity, therefore these heat shock proteins (HSPs) are divided into different subclasses (Hipp *et al*, 2019). Numbering of the various chaperone families refers generally to the molecular size of these proteins, however, there are exceptions.

Small heat shock proteins (sHSPs)

The members of this chaperone class are heterogenous in size (12-45 kDa) and act ATP-independently. Their main function is the prevention of protein aggregation ("holding chaperone" function) by association with non-native protein structures without direct refolding activity. sHSPs form higher oligomers via their conserved alpha-crystallin domain (Haslbeck & Vierling, 2015). Moreover, sHSPs sequester misfolded proteins into large inclusions thereby detoxifying these protein species. This sequestration was shown to be cytoprotective during aging in long-lived nematode *daf-2* mutants (Walther *et al*, 2015).

Hsp70s

These 70 kDa heat shock proteins represent the major subclass of chaperones, which reside in the cytosol, ER or mitochondria. They act in *de novo* protein folding, aggregation prevention and disaggregation by an ATP dependent cycle which is driven by their co-chaperones (JDPs and nucleotide exchange factors) (Mayer & Bukau, 2005). Hsp70 transiently shield hydrophobic segments (aggregation-prone sequences) in polypeptides, which contain 5-7 amino acid stretches enriched in hydrophobic entities and flanked by positively charged residues (Flynn *et al*, 1991; Rüdiger *et al*, 1997). The detailed mechanism of Hsp70's mode of action including function of the co-chaperones is described in **chapter 3.3.2**.

J-domain proteins (JDPs; Hsp40s)

JDPs are a very diverse subset of molecular chaperones which act as Hsp70 co-chaperones. They are characterized by a conserved J-domain which is essential for the ATPase stimulation of Hsp70s. In addition, JDPs recruit Hsp70s to their substrates and cellular compartments (Liberek *et al*, 1991; Greene *et al*, 1998). In **chapter 3.3.3** subclasses of JDPs are described including further information about the role as co-chaperones.

TRiC

TRiC is a chaperonin of ~1-MDa in size, which resides in the cytosol and is responsible for the folding of a small subset of proteins (10% of the proteome), e.g. actin and tubulin. The complex is composed of two octameric rings in which the 60 kDa subunits are aligned back-to-back. This structure enables effective folding of protein substrates in an isolated, protective chamber (Saibil, 2013; Lopez *et al*, 2015). Hsp70s can hand-over unfolded substrates to TRiC by direct contact to the chaperonin (Cuéllar *et al*, 2008).

HSP60

HSP60s, also called chaperonins, are formed by two heptameric rings composed of ~60 kDa subunits, which are stacked back-to-back. These heat shock proteins are ATP-dependent and work together with their HSP10 co-chaperones in folding and transport of mitochondrial proteins (Hipp *et al*, 2019). Hsp60s were shown to be involved in cell cycle regulation and apoptosis (Ghosh *et al*, 2008).

HSP90

HSP90 chaperones are involved in diverse cellular signaling pathways. Their substrates include steroid hormone receptors, kinases or oncogenic proteins. HSP90s function as homodimers that interact with their client proteins mainly at late folding stages. This chaperone class supports protein folding by an ATP-dependent chaperone cycle characterized by large conformational changes traversing an open V-shape stage and a closed packed structure engulfing the substrate (Saibil, 2013; Mayer, 2010).

HSP100

HSP100 respresent AAA+ATPases of ~100 kDa size, which are present in yeast and chloroplasts of plants performing unfolding and disaggregation of client proteins that cooperate with the Hsp70 chaperone family (Balchin *et al*, 2016; Hipp *et al*, 2019).

HSP110

HSP110 (~100 kDa) chaperones serve as metazoan nucleotide exchange factor for Hsp70s during protein disaggregation (Rampelt *et al*, 2012).

3.3.2 Hsp70 structure and chaperone cycle

The Hsp70 chaperone family prevents protein aggregation, promotes folding of clients into their native state and facilitates refolding of aggregated proteins (Mayer & Bukau, 2005).

Hsp70 chaperones interact with their substrates in a defined and well controlled cycle that is characterized by ATP hydrolysis and large intramolecular conformational changes. Studies on the Hsp70 mode of action, both biochemically and structurally, were mainly conducted with *E. coli* DnaK. All Hsp70s share a N-terminal nucleotide-binding domain (NBD; 45 kDa) and a C-terminal substrate-binding domain (SBD; 25 kDa), which is subdivided into an α- and β-subunit according to their three-dimensional structure (Fig. 4). The NBD consists of 4 subdomains (IA, IIA, IB and

IIB) that are highly flexible enabling nucleotide exchange by widening of the nucleotide binding cleft (Zhang & Zuiderweg, 2004). Both domains are connected via a flexible interdomain linker containing a characteristic hydrophobic patch (DVLLLD), which is highly conserved in Hsp70s. This linker is mainly involved in the allosteric regulation between the SBD and NBD of Hsp70s (Kityk *et al*, 2015; Vogel *et al*, 2006).

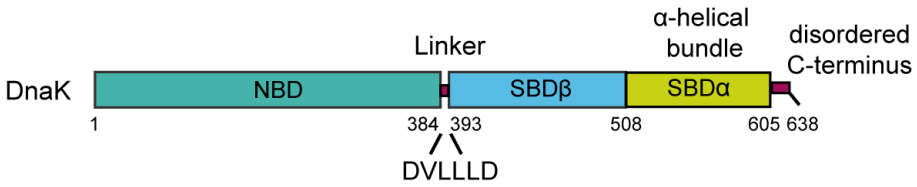

Figure 4: Domain structure of *E. coli* DnaK. Hsp70s harbor a N-terminal nucleotide-binding domain (NBD) and a substrate-binding domain (SBD) connected via a short linker that is characterized by a highly conserved hydrophobic sequence (DVLLLD). The SBD is further subdivided into a SBDβ and SBDα unit, which in the ADP-bound state enclose the client protein whereby the SBDα serves as a "lid".

In the ATP-bound state the SBDα and SBDβ are separated and docked on the NBD allowing only low affinity substrate binding of the SBD. In this state the interdomain linker of DnaK binds in a hydrophobic crevice of the NBD and interacts with the NBD subdomains IA and IIA, whereas the SBDα and SBDβ are detached from each other and bound by the NBD on two sites (Kityk *et al*, 2012; Swain *et al*, 2007) (Fig. 5 left panel). This globular state impedes with ATP hydrolysis as the basal ATP hydrolysis rate was shown to be very low (3×10^{-4} to 1.6×10^{2} s^{-1}) (Zhuravleva *et al*, 2012; Mayer & Bukau, 2005). The ATP cycle of Hsp70s is regulated by co-chaperones consisting of J-domain proteins (JDPs) and nucleotide exchange factors (more details see **chapter 3.3.3** and **3.3.4**). JDPs deliver protein substrates to their Hsp70 chaperone partners by transient contact to the NBD, thereby triggering structural rearrangements in the Hsp70 that result in a decrease in the activation energy of ATP hydrolysis and release of the interdomain linker from the NBD. The SBD rotates, dissociates from the NBD and transforms into an extended structure wherein the substrate gets enclosed by the two SBD subunits while SBDα functions as a "lid" (Mayer & Kityk, 2015). Peptide binding to the SBD leads to large changes of the ATP-bound Hsp70 in the interdomain linker and NBD. Therefore, substrate binding and lid closure are enabled even before ATP hydrolysis (Rist *et al*, 2006; Vogel *et al*, 2006). In this structural conformation and after ATP hydrolysis the affinity to substrates is high and client release occurs only after nucleotide exchange (Fig. 5, right panel). NEFs facilitate opening of the nucleotide binding cleft, which enables ADP and P_i exchange by ATP accompanied by substrate release, as the SBD adopts the compact structure on the NBD resetting the ATP-bound low affinity Hsp70 state (Polier *et al*, 2008; Bracher & Verghese, 2015). In the Hsp70 cycle the interdomain linker plays a major role in the allosteric communication

of the NBD and SBD and couples substrate binding to ATP hydrolysis as it was demonstrated that mutations in the hydrophobic linker abolishes ATPase stimulation by J-domain proteins (Laufen *et al*, 1999). How exactly Hsp70s act on their substrates is still under debate, however it is postulated that these chaperones exert a force on their clients, which is called "entropic pulling" resulting in a partially unfolding of the substrate (Goloubinoff & Rios, 2007).

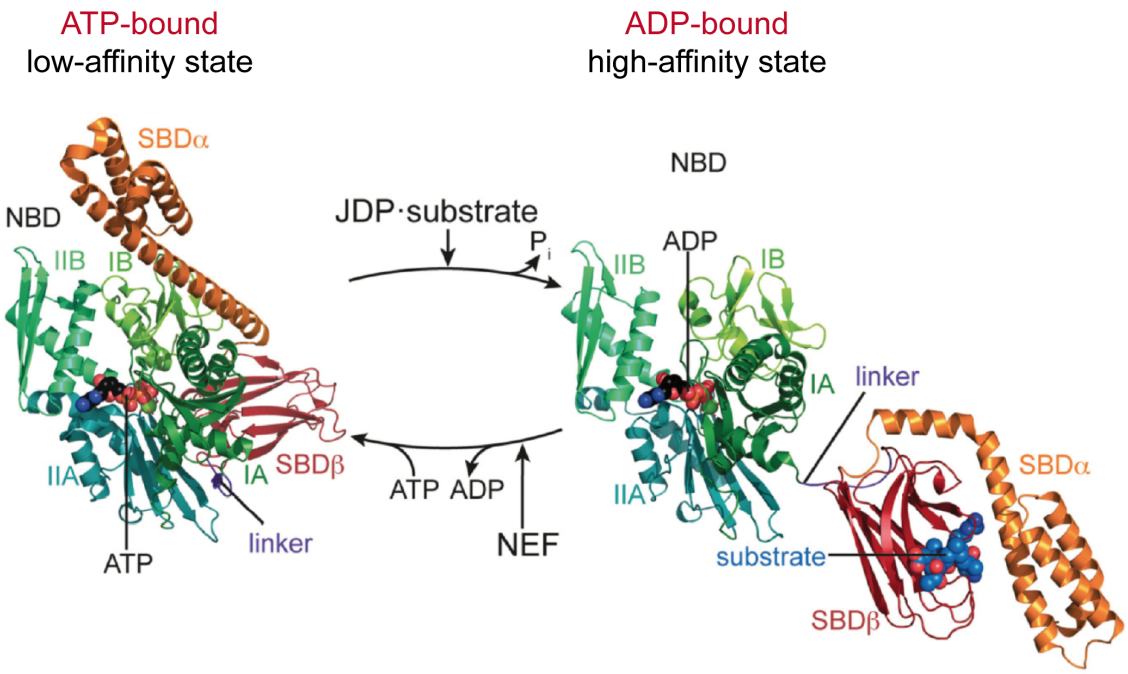

Figure 5: Allosteric regulation of *E. coli* DnaK during Hsp70 cycle. In the ATP-bound state the Hsp70 substrate binding domains (SBDα and SBDβ) are attached to the nucleotide binding domain (NBD; green). The interdomain linker (purple) contacts the NBD subdomains IA and IIA. In this so-called open state substrates show only a low-affinity to the SBD. Upon substrate delivery via J-domain proteins (JDP), structural rearrangements lead to linker detachment and extension and consequently to ATPase stimulation. In the ADP state the substrate can be enclosed by the SBD subdomains wherein the SBDα serves as a "lid". This closed ADP state is characterized by a high affinity substrate binding. Client protein release is enabled by the action of nucleotide exchange factors (NEFs), which widen the nucleotide binding cleft allowing ADP and P_i release. Figure adapted from (Mayer & Kityk, 2015) under a CC BY 4.0 license.

3.3.3 J-domain proteins (JDPs; Hsp40s)

Already in the 1990s it was postulated that JDPs are functionally interconnected with Hsp70s (Szabo *et al*, 1994; Laufen *et al*, 1999). In the literature, JDPs are synonymously called Hsp40s and are originally described as relatives of the *E. coli* DnaJ, which share a conserved helical 70 aa residue with a flexible loop (J-domain) (Kampinga *et al*, 2018). This loop is characterized by a His-Pro-Asp motif (HPD) that is known to be essential for ATPase stimulation of Hsp70s (Cheetham & Caplan, 1998). However, JDPs are constitutively expressed and are not heat inducible (Hageman & Kampinga, 2009). Except for the J-domain as a common feature, the family of JDPs are

miscellaneous and thus they are divided into three major groups corresponding to their domain structures (Fig. 6). Class A displays a C-terminal J-domain, a Glycine/Phenylalanine-rich stretch (G/F), two homologous C-terminal beta barrel domains (CTD) and a dimerization domain at the far C-terminal end. The CTDI includes a zinc-binding motif (Zn), which is absent in Class B JDPs (Fig. 6). Class C is structurally highly diverse and the J-domain is shifted from the very N-terminus (Craig & Marszalek, 2017). However, this classification is under debate and a subdivision on the basis of substrate specificity has been proposed (Kampinga *et al*, 2018). The G/F region was shown to be involved in both, the regulation of J-domain dynamics and thus modulating ATPase stimulation of Hsp70s, and additionally in substrate binding (Huang *et al*, 1999; Perales-Calvo *et al*, 2010). However, how JDPs of class A and B bind their substrates is still under debate but it seems that there are several low-affinity binding sites which allow simultaneous interaction with the client protein (Mayer & Gierasch, 2018).

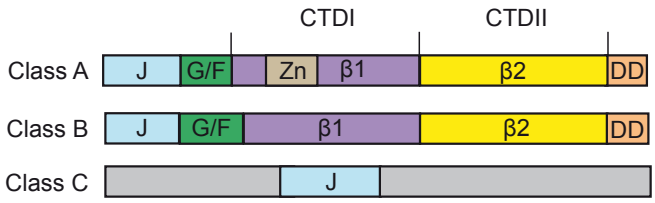

Figure 6: Domain structure of JDPs. J-domain proteins are subdivided into classes corresponding to their structural composition. All classes harbor a J-domain (JD). G/F: glycine/phenylalanine-rich region. CTD: C-terminal domain I and II. Zn: Zinc-binding motif. DD: dimerization domain. Figure adapted from Journal of Biological Chemistry. Mayer and Gierasch. Recent advances in the structural and mechanistic aspects of Hsp70 molecular chaperones. J. Biol. Chem. 2019; 294:2085-2097. © 2019 Mayer and Gierasch

As outlined in **chapter 3.3.2** JDPs not only act in Hsp70 ATPase stimulation but also in substrate delivery to the Hsp70 chaperone family. Some JDPs are specific for one substrate whereas other JDPs have a large pool of diverse clients (Craig & Marszalek, 2017). Interestingly, *in vivo* Hsp70s are 10 times more abundant than their JDP co-chaperones, thus JDPs function efficiently at substoichiometric concentrations (Kampinga *et al*, 2018). Under physiological conditions JDPs dimerize via their DD domain and in *E. coli* it was shown that dimerization of class A DnaJ is essential for efficient substrate binding (Shi *et al*, 2005). JDPs do not always interact and deliver client proteins to Hsp70s. Hsp70s are also specifically guided to cellular compartments by a single J-domain tethered to this cellular site (Craig & Marszalek, 2017). Structural analysis could reveal the detailed mechanism of JDPs in the Hsp70 cycle. The J-domain helix II docks via the HPD motif to the Hsp70 linker in the ATP state (Fig. 5). Through this interaction the catalytic residues of the NBD are structurally altered allowing ATP hydrolysis. In addition, delivery of the client protein to

the SBDβ triggers detachment of the SBD from the NBD resulting in the high affinity extended state of Hsp70 (Fig. 5, right panel) (Kityk *et al*, 2018, 2015; Malinverni *et al*, 2017).
Interestingly, studies showed that during protein refolding JDPs of subclasses A and B can act synergistically with Hsp70s in protein disaggregation of a wide range of different aggregate sizes (Nillegoda *et al.*, 2015, 2018).

3.3.4 Nucleotide exchange factors (NEFs)

Nucleotide exchange factors are subdivided into three types (GrpE, BAG and HspBP1), which share no sequence similarities (Bukau *et al*, 2006). Among these classes the mode of action underlying nucleotide release in Hsp70s is diverse. However, all NEFs cause a structural rearrangement in the NBD that leads to an opening of the nucleotide binding cleft (Harrison *et al*, 1997; Sondermann *et al*, 2001; Shomura *et al*, 2005). *In vitro* studies revealed that the concentration of NEFs applied in protein folding reactions together with Hsp70s is delicate as concentrations above a critical threshold can have an opposing effect leading to inhibition of the Hsp70 chaperone cycle (Gassler 2001, Nollen, 2000) Generally, NEFs promote protein folding reactions at concentrations 10-20 times less than their JDP counterpart (Diamant & Goloubinoff, 1998).

3.4 Protein quality control at the ribosome

To enable appropriate protein folding of nascent chains in the crowded cellular environment, the ribosome hosts a broad quality control machinery directly at the ribosome tunnel exit as shown in Figure 3. This chapter will mainly focus on molecular chaperones which associate with ribosomes, and assist *de novo* co-translational protein folding.

In *E. coli* nascent polypeptides are processed by the ATP-independent chaperone Trigger Factor (TF) which transiently binds to ribosomes in a 1:1 stoichiometry near the ribosomal proteins L23 and L29 (Kramer *et al*, 2002). Interestingly, biochemical and crystallographic studies showed that TF and SRP can simultaneously bind to ribosomes although they occupy the same ribosomal sites (Raine *et al*, 2004; Schlünzen *et al*, 2005). Deletion of TF is not lethal as the loss can be compensated by other off-ribosome chaperone systems like DnaK or GroEL, which were shown to share a partially overlapping substrate pool with TF (Deuerling *et al*, 1999; Teter *et al*, 1999). Upon ribosome exit hydrophobic patches of newly synthesized proteins are shielded by TF and are thereby prevented from unfavorable intramolecular contacts as the chaperone adopts a dragon shape structure when bound to 50S ribosomes keeping nascent chains in a folding-competent state

(Tomic *et al*, 2006; Ferbitz *et al*, 2004). *In vitro* studies by Saio *et al.* showed that TF binds substrates via four independent hydrophobic pockets that, in sum, accommodate up to 50 hydrophobic residues of nascent chains. However, TF binds its substrates with low affinity and the interaction is very dynamic showing high on- and off-rates (Patzelt *et al*, 2002; Saio *et al*, 2014).

In eukaryotes co-translational protein folding is accomplished by a more complex chaperone network involving two structurally and functionally distinct ribosome-tethered systems, RAC (**r**ibosome-**a**ssociated **c**omplex) and NAC (**n**ascent polypeptide-**a**ssociated **c**omplex) that are evolutionary highly conserved. These complexes bind to ribosomes near the nascent peptide tunnel exit and are thus enabled to control early steps of protein folding and targeting in a co-translational manner (Koplin *et al*, 2010; Rospert *et al*, 2002; Deuerling *et al*, 2019).

3.4.1 The nascent polypeptide-associated complex (NAC)

NAC binds in a 1:1 stoichiometry to ribosomes and is the first factor that contacts nascent polypeptide chains as soon as they emerge from the ribosomal tunnel. NAC is highly abundant and expressed in equimolar levels compared to ribosomes (Wiedmann *et al*, 1994; del Alamo *et al*, 2011). Eukaryotic NAC is a heterodimer consisting of an α- and β-subunit whereas archaea express an αNAC homodimer. In yeast, NAC is encoded by three different genes, namely Egd1 (β), Egd2 (α) and Btt1 (β') in contrast to higher eukaryotes which possess only two genes encoding αNAC and βNAC. In all species dimer formation is mediated by the conserved NAC domain that is present in both subunits and forms a compact β-barrel like structure (Fig. 7 A and B) (Liu *et al*, 2010; Wang *et al*, 2010). Apart from the NAC domain, the α-subunit harbors a **ub**iquitin **a**ssociated (UBA) domain at the C-terminus, which was shown to negatively regulate the chaperone activity of NAC as deletion of the UBA domain enhanced the protein aggregation suppression activity of NAC in yeast (Ott *et al*, 2015). However, apart from this observation the function of the NAC UBA domain remains enigmatic. Ribosome binding of NAC is mediated by a conserved positively-charged ribosome binding motif ^{23}RRK-(X_n)-KK^{31} in the N-terminus of β-NAC, which positions the heterodimer close to the ribosomal tunnel exit as indicated by crosslinks to uL23, eL31 and uL22 (Wegrzyn *et al*, 2006; Pech *et al*, 2010; Zhang *et al*, 2012). In addition, also crosslinks of α-NAC to uL29 were observed expanding the contact surface of the heterodimer at the tunnel exit (Nyathi & Pool, 2015). Yeast cells lacking NAC show no obvious phenotype, however, in higher eukaryotes NAC is essential as deletion results in embryonic lethality in *D. melanogaster*, *C. elegans* and mice (Bloss *et al*, 2003; Deng & Behringer, 1995; Markesich *et al*, 2000). Moreover, NAC depletion in *C. elegans* leads to a shortened median lifespan showing that NAC also exerts a critical

housekeeping function in animals after development (Gamerdinger *et al*, 2015). Furthermore, it has been shown in *C. elegans* that NAC dissociates from ribosomes and is sequestered by protein aggregates under stress conditions like heat and aging, suggesting that NAC also possesses a ribosome-independent function (Kirstein-Miles *et al*, 2013).

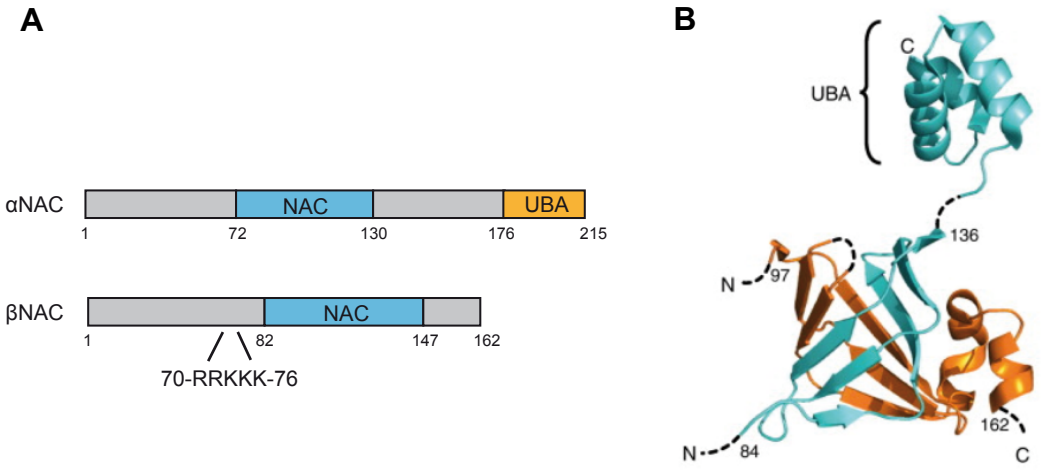

Figure 7: Domain representation and structure of the NAC subunits. (A) Schematic showing of the NAC domains. αNAC and βNAC share a common NAC domain which is essential for heterodimer formation between the subunits. Ribosome binding is mediated by a charged region in the N-terminus of βNAC (^{70}RRKKK^{76}). αNAC is extended by a C-terminal ubiquitin-associated domain (UBA) of so far unknown function. **(B)** Structural model of the NAC heterodimer using structures of the archaeal UBA domain (PDB 1TR8) and the human NAC domain heterodimer (PDB 3LKX). αNAC is highlighted in cyan and βNAC is presented in orange. Dashed lines indicate unresolved parts of the structure. Reprinted from Trends in Biochemical Sciences, Vol. 37, No.7, Steffen Preissler and Elke Deuerling, Ribosome-associated chaperones as key players in proteostasis, p. 274-283, Copyright (2012), with permission from Elsevier.

Already in 1996, it was postulated that NAC regulates the fidelity of SRP-dependent protein targeting to the ER (Powers & Walter, 1996). Indeed, *in vitro* studies showed that proteins, which have not yet exposed the signal peptide for SRP binding to ribosomes, depend on the presence of NAC (Zhang *et al*, 2012). Consistent with these observations depletion of NAC in *C. elegans* results in a strong ER and moderate mitochondrial stress response. It has been shown that NAC suppresses autonomous ER translocon binding of ribosomes that translate polypeptides not destined for the ER. Thus, NAC acts as negative regulator for ER targeting and thereby ensures a specific binding of translating ribosomes to the Sec61 complex. In consequence, upon depletion of NAC translating ribosomes are mistargeted to the ER leading to incorrect import of mitochondrial proteins into the ER (Gamerdinger *et al*, 2015; del Alamo *et al*, 2011).

Although the presence of NAC near the ribosome tunnel exit indicates an additional role in co-translational protein folding, detailed knowledge about substrate contact sites are missing and the potential function as a chaperone has yet to be proven.

3.4.2 The ribosome-associated complex (RAC)

Yeast (*S. cerevisiae*)

Co-translational protein folding in yeast is assisted by the ribosome-associated complex (RAC) (Preissler & Deuerling, 2012), which promotes ATP hydrolysis and substrate binding of an additional Hsp70 called Ssb. RAC consists of Zuotin (Zuo1), a J-domain protein, and Ssz1, a non-canonical Hsp70 (Huang *et al*, 2005; Yam *et al*, 2005) (Fig. 9, left panel).

RAC is tethered to the ribosome by the Zuo1 subunit, while Ssz1 shows no direct ribosome interaction (Gautschi *et al*, 2001). Zuo1 contacts both ribosomal subunits at rRNA helix 24, eL22 and eL31 (60S) and rRNA helix 59 of the 40S. On the side of Zuo1, contact sites comprise two lysines (Zuo1: R247 and R251) that enable 60S contact (Kaschner *et al*, 2015), and in addition two other regions that facilitate ribosome association with the 40S (340-356 aa) and 60S (285-302 aa) (Zhang *et al.*, 2014; Lee *et al.*, 2016). Zuo1 stretches from the polypeptide tunnel exit of the 60S ribosomal subunit up to a helical RNA element of the 40S that elongates into the decoding center of the ribosome. The structural data imply that RAC might affect conformational dynamics of the ribosome and thereby stalls or slows down translation. This raises the hypothesis that polypeptides with folding problems may recruit RAC to regulate their elongation speed and to allow the RAC-Ssb chaperone system to assist their folding (Lee *et al*, 2016; Zhang *et al*, 2014; Peisker *et al*, 2008).

It was shown that the J-domain of Zuo1 is required for RAC function *in vivo* and *in vitro* (Gautschi *et al*, 2002) and Ssb function relies on ATPase stimulation by this Zuo1 domain to exert co-translational protein folding (Huang *et al*, 2005). Cells expressing a J-domain mutated Zuotin version ($Zuo1^{H128Q}$) resemble the phenotype of a complete Zuo1 knockout illustrating the important function of this protein domain *in vivo* (Hundley *et al*, 2002; Gautschi *et al*, 2002). Indeed, Zuo1 is the only JDP that is able to stimulate Ssb's ATPase as it was shown that deletion of either Ssb or Zuo1 display the same phenotype, which is manifested in severe growth defects at high temperature or in the presence of translation inhibitor paromomycin (Yan *et al*, 1998).

The exact function of Ssz1 in RAC is not yet elucidated. Huang and coworkers showed that stimulation of Ssb's ATPase by Zuo1 is only possible when Zuo1 is in complex with Ssz1 (Huang *et al*, 2005). Interestingly, Ssz1 binds ATP but was rather weak due to a wider nucleotide binding cleft. However, binding or hydrolysis of ATP by Ssz1 is not crucial for its function (Conz *et al*, 2007) and also not required to stimulate Ssb (Huang *et al*, 2005). Crystal structures of the ATP-bound Ssz1 ATPase domain confirmed that this Hsp70 is catalytically inert as five residues in the active site of the nucleotide-binding domain (NBD), critical to hydrolyze ATP, are replaced (Leidig *et al*, 2013). Moreover, Ssz1 is characterized by a shortened substrate-binding domain (SBD) which argues for an inefficient substrate binding property due to the lack of the lid domain (SBDα) (Gautschi *et al*,

2001; Hundley *et al*, 2002; Huang *et al*, 2005). Indeed, substrate binding of Ssz1 could not be observed so far and the substrate-binding domain of Ssz1 was shown to be dispensable for the *in vivo* function of RAC (Hundley *et al*, 2002). Biochemical studies showed that RAC formation occurs via the N-Terminus of Zuo1, as the interaction with Ssz1 is abolished when an N-terminally truncated version of Zuo1 is expressed (Fiaux *et al*, 2010). The observed interaction between Ssz1 and Zuo1 in RAC represents a stable complex rather than a canonical Hsp70/JDP/substrate interaction as complex formation is stable in the presence of ATP (Gautschi *et al*, 2001) and upon J-domain mutation ($Zuo1^{H128Q}$) (Gautschi *et al*, 2002) . X-ray crystallographic studies give insight into this unique complex formation of Ssz1 and Zuo1 as outlined below (Weyer *et al.*, 2017; for more information see **chapter 3.4.3**). The function of RAC is not restricted to translating ribosome, as Zuo1 and Jjj1, another J-domain protein, were shown to assist ribosome assembly in the nucleus. Both proteins associate with 60S precursors in the nucleus and share the same ribosome binding motif, the Zuotin homology region (ZHR) (Albanèse *et al*, 2010; Kaschner *et al*, 2015). Moreover, overexpression of Jjj1 can partially compensate for the loss of Zuo1 by recruiting the Hsp70 Ssa to the ribosome (Meyer *et al*, 2007).

Ssb is a yeast specific Hsp70 that binds in a 1:1 stoichiometry to ribosomes where it contacts nascent chains, though the presence of this Hsp70 is restricted to fungi. Ssb exists in two isoforms, called Ssb1 and Ssb2 (from here on together termed Ssb), which are functionally redundant as deletion of one Ssb isoform shows no apparent phenotype (Craig & Jacobsen, 1985). Ssb contacts the ribosome with two distinct intramolecular patches characterized by positive charge, one in the C-terminal lid domain and one site within the SBD (KRR-motif) (Hanebuth *et al*, 2016). Contact sites at the ribosome comprise the rRNA expansions ES24, ES39, ES41 as well as the ribosomal proteins uL29, eL39 and eL19 (Gumiero *et al*, 2016). Although Ssb is as abundant as ribosomes, at steady state only 50% of Ssb molecules are ribosome-bound whereas the other half resides freely in the cytosol (Raue *et al*, 2007; Peisker *et al*, 2010). Ssb binds a high variety of nascent chains, including cytosolic and nuclear proteins, and especially assists folding of polypeptides with complex domain structures and an increased aggregation propensity (Willmund *et al*, 2013; Pechmann *et al*, 2013). Yeast cells deleted for Ssb (*ssbΔ*) are hypersensitive to certain translation inhibitors and display a cold sensitive phenotype (Nelson *et al*, 1992). Yam and coworkers observed that in the absence of Ssb the cytosolic Hsc70 Ssa can interact with nascent chains, however, Ssb is unable to compensate for the loss of Ssa (Yam *et al*, 2005; Boorstein *et al*, 1994). Interestingly, high Ssb protein levels can substitute for Ssz1 loss (Gautschi *et al*, 2002) and restore translation fidelity (Conz *et al*, 2007).

In addition to co-translational protein folding, Ssb was shown to act in ribosome biogenesis and cellular signaling indicating a crucial off-ribosome function of this Hsp70 in yeast (Von Plehwe *et al*, 2009; Koplin *et al*, 2010; Albanèse *et al*, 2010). Protein aggregation in *ssbΔ* is enhanced upon

additional loss of NAC, indicating a partially overlapping function of these ribosome-tethered systems in *de novo* protein folding (Koplin *et al*, 2010). Nucleotide exchange in Ssb is managed by the NEFs Sse1, Fes1 and Sln1 (Shaner *et al*, 2006; Sondermann *et al*, 2002; Dragovic *et al*, 2006).

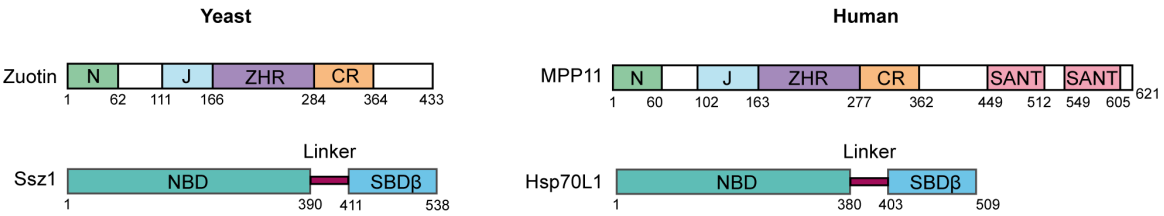

Figure 8: Components of the ribosome-associated complex (RAC) in *S. cerevisiae* and human cells. The JDPs Zuotin and MPP11 are characterized by a Zuotin homology region (ZHR) and a conserved J-domain (J) essential for Hsp70 ATPase stimulation. Ribosome binding is accomplished by the charged region (CR). The C-terminus of MPP11 in humans is extended by two SANT domains. The function of these domains in context of the ribosome is so far unknown. Ssz1 and Hsp70L1 are non-canonical Hsp70s marked by a shortened substrate binding domain (SBD) lacking the α-helical lid and a compromised ATPase. Four residue replacements in the nucleotide binding domain (NBD) of Ssz1 and Hsp70L1 deactivate the catalytic domain and inhibit ATP hydrolysis. In both Ssz-like Hsp70s the interdomain linker is significantly enlarged compared to canonical Hsp70s (compare DnaK Fig. 4).

Mammals

In mammalian cells the ribosome-associated complex (mRAC) is composed of MPP11, a Zuo1 homolog, and Hsp70L1, an Ssz-like protein (Fig. 8) (Jaiswal *et al*, 2011; Otto *et al*, 2005; Hundley *et al*, 2005). Since a ribosome binding, Ssb-like protein is missing, cytosolic Hsp70s are recruited to the ribosome via mRAC (Jaiswal *et al*, 2011) (Fig. 9, right panel).

As seen in **figure 8**, the domain structure is highly conserved between yeast and human. However, MPP11 includes two SANT domains at the C-terminus that are normally known to function in histone tail binding and chromatin remodeling (Boyer *et al*, 2004). MPP11 binds to yeast ribosomes in a *zuo1Δ* strain and is able to complement the growth phenotype of both *zuo1Δ* and *zuo1ΔssbΔ* yeast cells, concluding that MPP11 functions independent of Ssb. Indeed, *in vitro* MPP11 stimulates exclusively the ATPase of the cytosolic yeast Hsc70 Ssa but not of Ssb (Hundley *et al*, 2005). The Ssz-like protein Hsp70L1 was able to functionally interact with Zuo1, however, this was not the case between MPP11 and Ssz1 (Otto *et al.*, 2005). MPP11 knockdown cells are characterized by reduced Hsp70L1 and ribosomal protein levels and show hypersensitivity to translation inhibitors (Jaiswal *et al*, 2011). Interestingly, mRAC can stimulate the ATPase of Hsp70 and Hsc70 but only functionally interacts with Hsp70 at the ribosome. For MPP11 function ATP-binding to Hsp70L1 is mandatory, and similar to yeast Zuo1 the ATPase seems to be inactivated and peptide binding

could not be observed so far (Jaiswal *et al*, 2011). Many cancer types reveal high levels of MPP11 and early metastatic events in breast cancer were linked to MPP11 activity (Resto *et al*, 2000; Greiner *et al*, 2003; Kaymak *et al*, 2018). Moreover, nucleotide excision repair at DNA lesions involves MPP11 mediated chromatin decondensation and E3 ligase remodeling, revealing an important off-ribosome function (Gracheva *et al.*, 2016; Chitale and Richly, 2017).

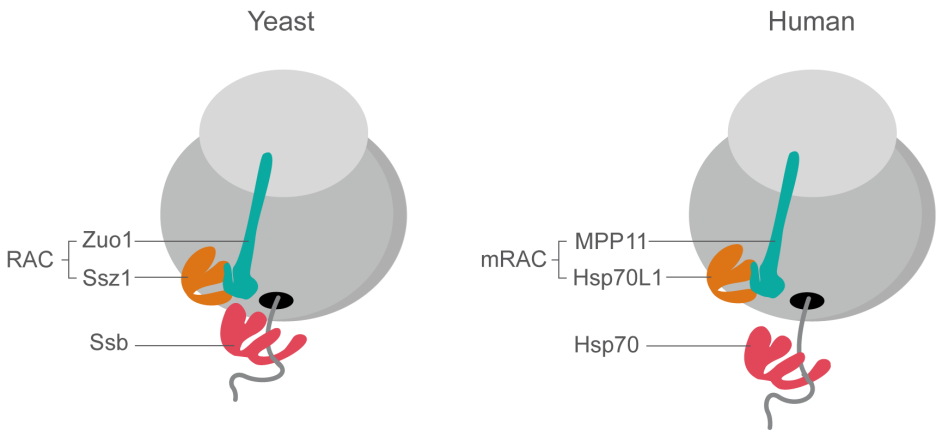

Figure 9: Ribosome-associated chaperone triad at the yeast and mammalian ribosome. The ribosome-associated complex (RAC) is comprised of a JDP subunit (Zuo1; MPP11) and a non-canonical Hsp70 (Ssz1; Hsp70L1). In both species ribosome anchoring is facilitated by the J-domain chaperones Zuo1 and MPP11, respectively. RAC serves as a co-chaperone of an additional Hsp70, Ssb in *S. cerevisiae* and Hsp70 in mammals, whereas Ssb is directly ribosome-bound and mammalian Hsp70 is recruited to the ribosome. Through its J-domain RAC induces ATP hydrolysis in partner Hsp70s thereby recruiting the chaperone contact to the nascent polypeptide chain and co-translational protein folding. The role of the catalytically inactive Ssz1 and Hsp70L1 proteins has not yet been clarified.

In conclusion, yeast and mammals facilitate co-translational protein folding both via a ribosome-tethered chaperone triad composed of an Hsp70/JDP dimer and an additional Hsp70. This Hsp70 is either ribosome-associated (yeast) or recruited by RAC (mammals). Both species share an Ssz-like protein whose function is still under debate as it lacks ATPase and substrate binding capacity.

3.4.3 Unique structure of the yeast ribosome-associated complex

To understand the function of RAC it is critical to understand how this heterodimeric complex is formed. *In vitro* data revealed that the N-terminus (1-62 aa) of the Zuotin subunit is crucial for complex formation and that deletion of the complete C-terminus of Ssz1 (interdomain linker and SBD) abolishes interaction as well (Conz *et al*, 2007; Fiaux *et al*, 2010). So far, there is no complete structure of this high molecular weight complex available but crystallization of the *Chaetomium thermophilum* Zuo1-Ssz1 complex revealed a unique assembly of the heterodimer comprising the

N-terminus of Zuo1 (Zuo1N; 19-60 aa) and the entire Ssz1 subunit (Fig. 10A) (Weyer *et al*, 2017). The structure was solved in the ATP-bound state of Ssz1. In the ATP state the interdomain linker of canonical Hsp70s, that consist of a well-structured β-sheet, is docked via a conserved hydrophobic motif on the NBD subdomain IA and IIA (Fig. 5; left panel) (Kityk *et al*, 2012)..

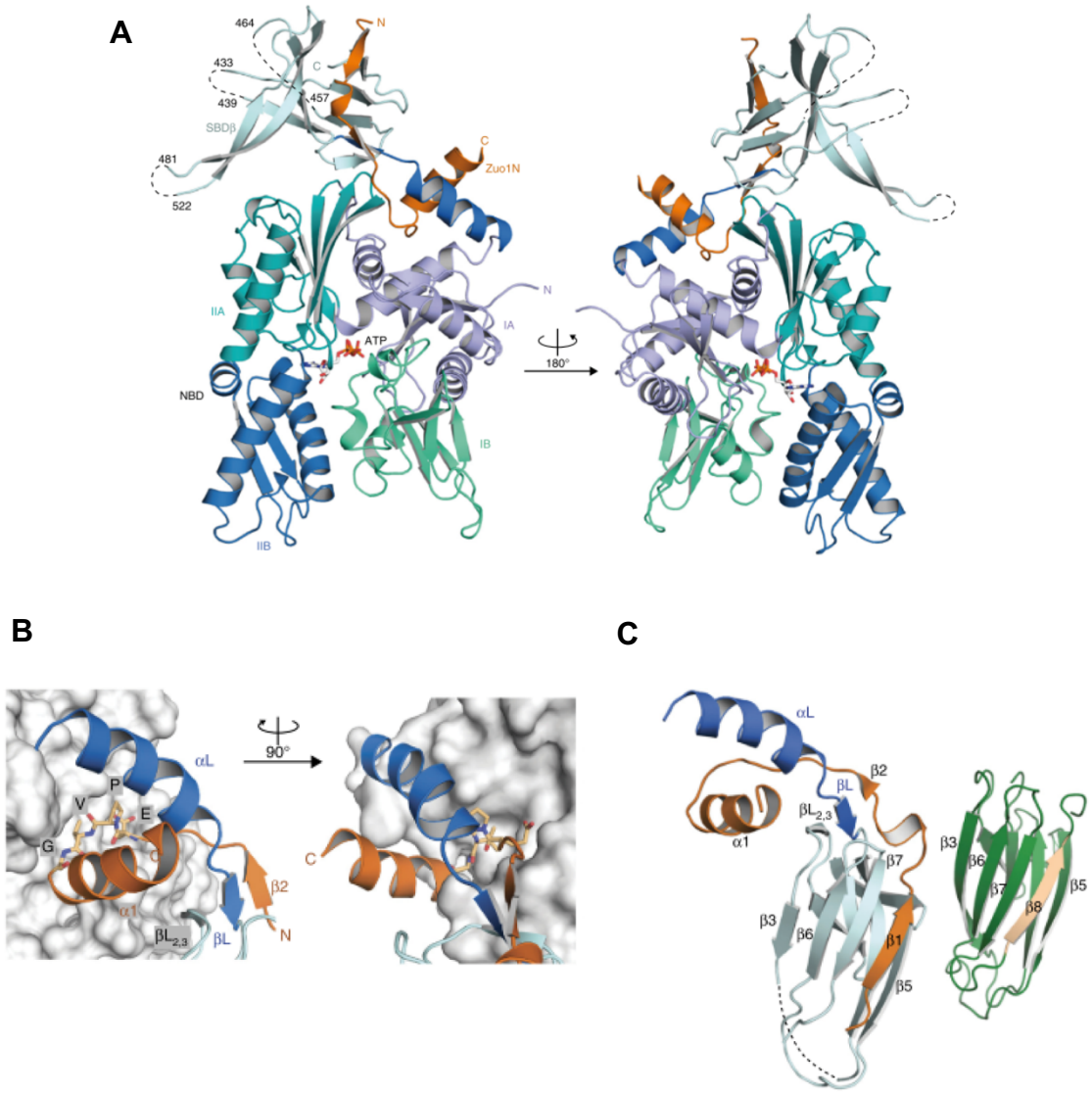

Figure 10: Crystal structure of Zuo1N-Ssz1 complex of *C. thermophilum*. (A) Structure of the Zuo1N-Ssz1 complex in the ATP-bound state. The four subdomains of the NBD (IA, IIA, IB, IIB) are highlighted in purple, cyan, green and blue. In this state the Ssz1 SBDβ (light blue) and the interdomain linker (dark blue) are detached from the NBD. The Zuo1 N-terminus (Zuo1N; orange) contacts all three domains of Ssz, the SBD, the interdomain linker and the NBD. **(B)** Zoom-in of the contact between the Ssz1 interdomain linker (dark blue) and the Zuo1 N-terminus (orange), the Ssz1 NBD is indicated in grey. Direct interaction of the linker and Zuo1N is comprised by the Zuo1 motif EPVG, between the α-helix and the β-sheet (presented in sticks). **(C)** Complementation of Ssz SBDβ (light blue) by the β1 sheet of Zuo1N (orange) (left panel). Dark blue: interdomain linker of Ssz1. Model of the SBDβ of DnaK in the ADP-bound state (green). The β8 sheet, which is complemented in the RAC structure, is shown in pale orange (right panel). Figures reprinted by permission from Macmillan Publishers Ltd: Nature Structural and Molecular Biology, Feb;24(2):144-151., Weyer *et al.*, copyright 2017.

However, in yeast RAC the linker of the Ssz1 lacks the hydrophobic motif but is extended by an α-helical motif. Instead of binding to the NBD, the interdomain linker of Ssz1 is detached from the Ssz1 NBD and is bound by an α-helix of Zuo1N (Fig 10 A; dark blue). A conserved motif (EPVG) in Zuo1N interacts with the interdomain linker binding groove of Ssz1 (Fig. 10 B), positioning Zuo1 at the interface of the NBD and SBDα, contacting the NBD subdomain IIA (Weyer *et al*, 2017). Thus, the linker of Ssz1 is detached from the NBD and the linker binding cleft is permanently occupied by Zuo1N. In addition, the structure revealed a complementation of the missing β8 strand of Ssz1's SBDβ by the β1-sheet of Zuo1N (Fig. 10 C).
In conclusion, the partial RAC structure confirms a unique interaction between a JDP and a non-canonical Hsp70. However, the precise role of Ssz1 in this heterodimer is poorly understood.

3.5 The model organism *C. elegans*

In 1963 Sydney Brenner introduced the nematode *Caenorhabditis elegans* (*Caeno*, recent; *rhabditis*, rod; *elegans*, nice) as model organism for studies in developmental biology and neurology. *C. elegans* is a roundworm of 1 mm in length which lives in soil environments in most regions of the world. As a non-infectious and non-pathogenic nematode, the worms are easy to breed and handle. *C. elegans* is a post mitotic organism and most individuals of the population are hermaphrodites (959 cells) whereas 0.05% are male worms (1031 cells) (Brenner, 1974). Upon self-fertilization wildtype nematodes lay around 300 eggs, however, when inseminated by a male worm the number of progenies increases tremendously to 1,000 eggs per individual (Sin *et al*, 2014). They feed on bacteria and during development they travers four molting larval stages, L1-4 (Fig. 11). Under unfavorable environmental conditions like heat stress, starving or population crowding stress, *C. elegans* can develop into dauer stages after L1 to survive harsh conditions (Cassada & Russell, 1975). The nematodes undergo one life cycle in approximately three days (Fig. 11) and live on average for 20 days at 20°C (Brenner, 1974).
A major advantage is that synchronized populations can easily be generated by hypochlorite bleaching as only eggs survive the procedure. To maintain a synchronized culture, *C. elegans* worms are treated with Floxuridine (FUdR), an inhibitor of DNA replication, at the L4 stage which suppresses development of further progeny (Mitchell *et al*, 1979). Different proteomic studies showed that between 40-80% of the 21,000 protein coding genes of *C. elegans* share human orthologs, making this nematode a suitable model for basic or disease oriented research (The C. elegans Consortium, 1998; Lai *et al*, 2000; Shaye & Greenwald, 2011).

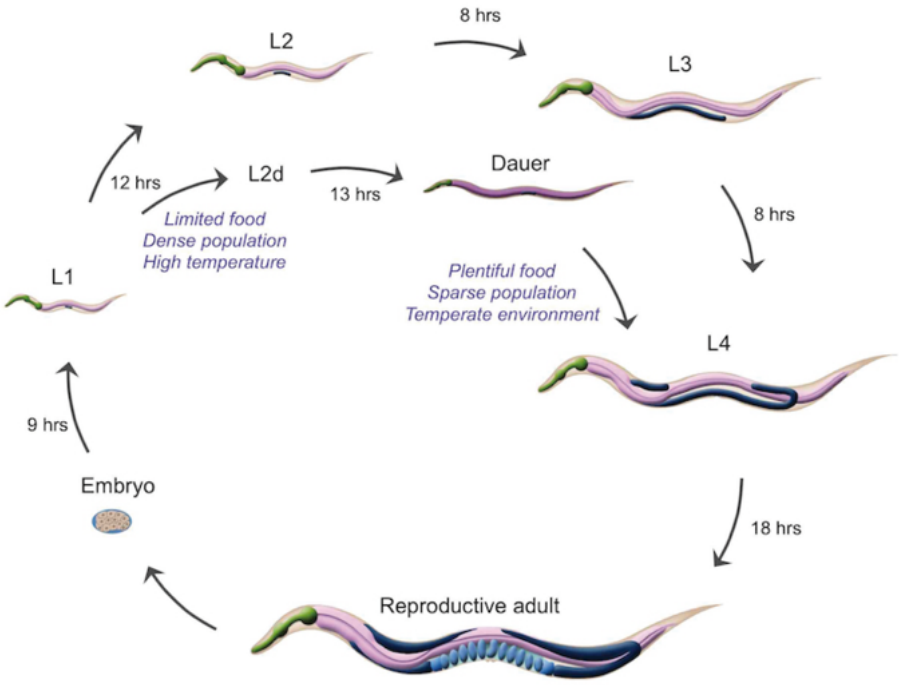

Figure 11: Life cycle of the nematode *C. elegans*. After egg-lay the nematodes travers 4 different molting larval stages and reach adulthood after approximately three days. When exposed to environmental stressors L1 larvae can develop into dauer larvae and resume normal development under more favorable conditions. © http://www.wormatlas.org.

3.5.1 The Hsp70 system in *C. elegans*

In *C. elegans* heat shock proteins are involved in protein quality control in a variety of cellular compartments. The nematodes are sensitive towards temperatures above 28°C manifested by failures in reproduction and growth stagnation. Continuous heat stress finally leads to the death of *C. elegans*. Expression of heat shock proteins was observed at elevated temperatures between 29°C and 35°C (Heschl & Baillie, 1990). *C. elegans* worms possess 8 Hsp70s, 31 J-domain proteins and 6 nucleotide exchange factors (NEFs). The Table A1 (appendix) gives an overview of the *C. elegans* "chaperome" based on: wormbase.org; Brehme *et al.*, 2014 and the *C. elegans* RNAi feeding clones & v1.1 feeding library (Dharmacon™).

4. Objectives

Appropriate *de novo* protein folding at the ribosome is a fundamental process that defines cellular fitness. Protein biogenesis is highly error-prone, given the high translation rate and folding challenges of the newly synthesized polypeptides. Thus, translation depends on the correct function of molecular chaperones and other ribosome-bound factors.

Part A: Characterization of a non-canonical RAC system in the nematode *C. elegans*

The ribosome-associated complex (RAC) is a system supporting protein homeostasis and has been extensively studied both in *S. cerevisiae* and mammalian cells. This complex acts as co-chaperone of an Hsp70 that associates with nascent polypeptide chains. RAC is a stable heterodimer of a J-domain protein (JDP) (yeast: Zuo1, human: MPP11) and an atypical Hsp70 (yeast: Ssz1, human: Hsp70L1) that is characterized by an inactive ATPase and a shortened substrate binding domain. The JDP subunit stimulates the ATP hydrolysis of the extra Hsp70 to support client protein folding. Up to now, the function of Ssz-like subunits in the ribosome-bound chaperone triad is poorly understood and still under debate. Many studies indicate a stabilizing role of Ssz1 towards the JDP subunit, however, ATP hydrolysis and substrate binding of Ssz1 seem to be negligible for proper RAC function. Sequence alignments revealed that nematodes lack an Ssz-like protein but possess a Zuo1 homolog, called DNJ-11, suggesting that functionally different RAC systems have evolved in eukaryotes. The aim of this thesis was to examine the composition and the mode of action of the RAC system in the nematode *C. elegans*. The following questions were addressed:

- Are nematodes the sole animal phylum which lacks an Ssz-like RAC subunit?
- Does DNJ-11 represent a functional homolog of Zuo1/MPP11?
- Does DNJ-11 depend on a complex partner? Is there a RAC-like system in *C. elegans*?
- Which Hsp70 isoform of *C. elegans* facilitates co-translational protein folding at the ribosome?

Part B: Dissecting the chaperone function of the nascent polypeptide-associated complex (NAC)

NAC is a ribosome-associated factor that interacts with nascent polypeptide chains and coordinates proper protein targeting to the ER. A direct chaperone function has been proposed but not demonstrated yet. Questions that were addressed in this side project were:

- Does NAC exhibit chaperone function *in vitro*?
- Does NAC show an off-ribosome function?
- Are RAC and NAC able to bind simultaneously to ribosomes?

5. Results – Part A

The main findings presented in this chapter resulted in a manuscript that was submitted recently (Sachs *et al.*, 2019, see appendix). This study was a joint collaborative work with contributions of other researchers, which are listed below:

***In vitro* translation and crosslinking (Fig. 34)**
Annalena Wallisch, Department of Biology, Molecular Microbiology, University of Konstanz
Single turn-over ATPase measurements (Fig. 29 and 36 B)
Dr. Roman Kityk, Centre for Molecular Biology of Heidelberg University (ZMBH), DKFZ-ZMBH Alliance, Heidelberg
Structural modeling and molecular dynamics simulations (Fig. 33)
Dr. Christoph Globisch, Department of Chemistry, Computational and Theoretical Chemistry, University of Konstanz
Phylogenetic analyses of Ssz- and Zuo-like proteins (Fig. 12 and 13)
Prof. Matthias P. Mayer, Centre for Molecular Biology of Heidelberg University (ZMBH), DKFZ-ZMBH Alliance, Heidelberg
Microinjection of *C. elegans*
Dr. Martin Gamerdinger, Department of Biology, Molecular Microbiology, University of Konstanz

5.1 A variety of organisms lack Ssz-like proteins

It was assumed that RAC is highly conserved in eukaryotes as Zuo1 homologs are widely spread throughout the eukaryotic kingdom. However, during the course of this work phylogenetic analyses conducted by **Prof. Matthias P. Mayer** (ZMBH Heidelberg) showed that Ssz-like proteins are absent in many organisms. To search for Ssz-like proteins, protein sequences of yeast Ssz1 and human Hsp70L1 were blasted against the UniRef90 Database using the server of the European Bioinformatics Institute (Chojnacki *et al*, 2017). The search yielded 1000 sequence clusters comprising 5200 sequences for Ssz1 and 3267 sequences for Hsp70L1, which were aligned. These sequence clusters also included sequences coding for canonical Hsp70s. Therefore, the sequences were further selected for specific Ssz1/Hsp70L1 features that included mutations of conserved residues for ATP hydrolysis and Hsp70 allosteric function (Leidig *et al*, 2013; Huang *et al*, 2005). Proteins that shared at least 30% sequence identity with Ssz1 or Hsp70L1 and which showed a total sequence length between 500 and 600 amino acids were scored as Ssz/Hsp70L1-like. The identified matches were diverse in sequence length and identity but shared common Ssz/Hsp70L1-like features that distinguished them from canonical Hsp70s (cHsp70s). Unexpectedly, Ssz1-like protein sequences were found exclusively in BLAST searches of fungal organisms (Fig. 12 A). In contrast, the Hsp70L1 search includes matches from diverse organisms (Fig. 12 B).

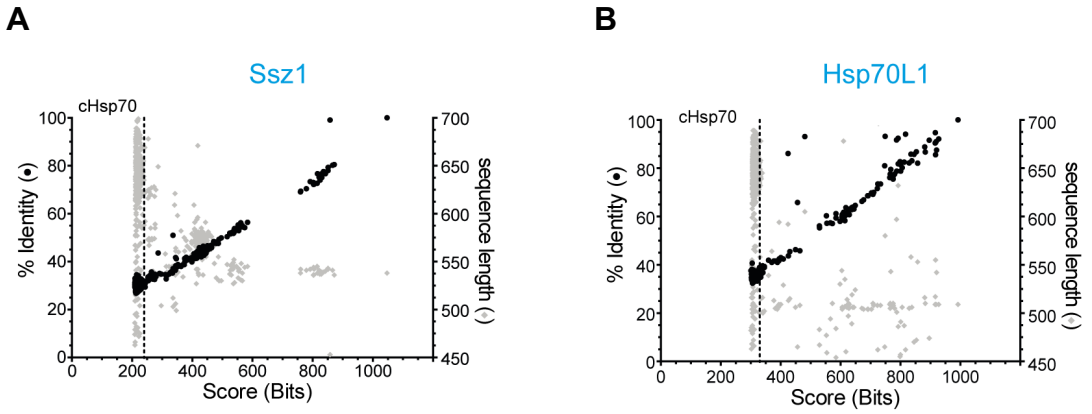

Figure 12: Conservation of Ssz1 and Hsp70L1 in eukaryotes. BLAST search results on UniRef90 Database using yeast Ssz1 **(A)** and human Hsp70L1 **(B)** as query. The relative degree of identity (left y-axis, black dots) and the sequence length (right y-axis, grey dots) are plotted against the alignment score from the BLAST search result. Dashed lines indicate to which score the sequence belongs to. Sequences on the left side of the line exhibit features of canonical Hsp70s (cHsp70). Ssz-like **(A)** and Hsp70L1-like **(B)** protein sequences are illustrated on the right side of the line. Proteins with Ssz-like features were exclusively found in fungi. Hsp70L1-like sequences were found in diverse organisms, except plant and nematodes. Identities were assessed with Clustal Ω multiple sequence comparison. Analysis and presentation were prepared by Prof. Matthias P. Mayer.

To further validate the presence of Hsp70L1 orthologs in different organisms, the BLAST search focused on all four taxonomic groups of Vertebrata, Arthropoda, Nematoda and Viridiplantae (green plants). All Arthropoda clades (Crustacea, Myriapoda, Chelicerata and Insecta) comprised Hsp70L1-like proteins and the obtained sequences were derived from 35 different organisms. However, the BLAST search indicated that plants and nematodes lack Hsp70L1-like proteins. To further specify the BLAST analysis, all Hsp70 protein sequences from *Caenorhabditis elegans* (wormbase.org), *Drosophila melanogaster* (flybase.org) and *Arabidopsis thaliana* (arabidopsis.org) were extracted from the respective databases and scored for Ssz/Hsp70L1-like protein characteristics. No sequence matches were retrieved for *C. elegans* and for *D. melanogaster*. An Hsp70L1 homolog was identified in *A. thaliana* and used as query for the BLAST search in Viridiplantae detecting 150 Hsp70L1-like sequences. To visualize the conservation of Hsp70L1-like proteins present throughout eukaryotes, the obtained proteins (amino acid sequence length and identity) were plotted against the BLAST alignment score. As query the human (Vertebrates), the *Daphnia magna* (Arthropoda, Nematoda) and the *A. thaliana* (Viridiplantae) Hsp70L1-like proteins were used. Figure 13 illustrates the widespread presence of Hsp70L1 homologs in vertebrates (Fig. 13 A) and green plants (Fig. 13 D). However, nematodes lack Hsp70L1-like proteins and only a subset of arthropods were shown to express a noncanonical Hsp70 (Fig. 13 B and C).

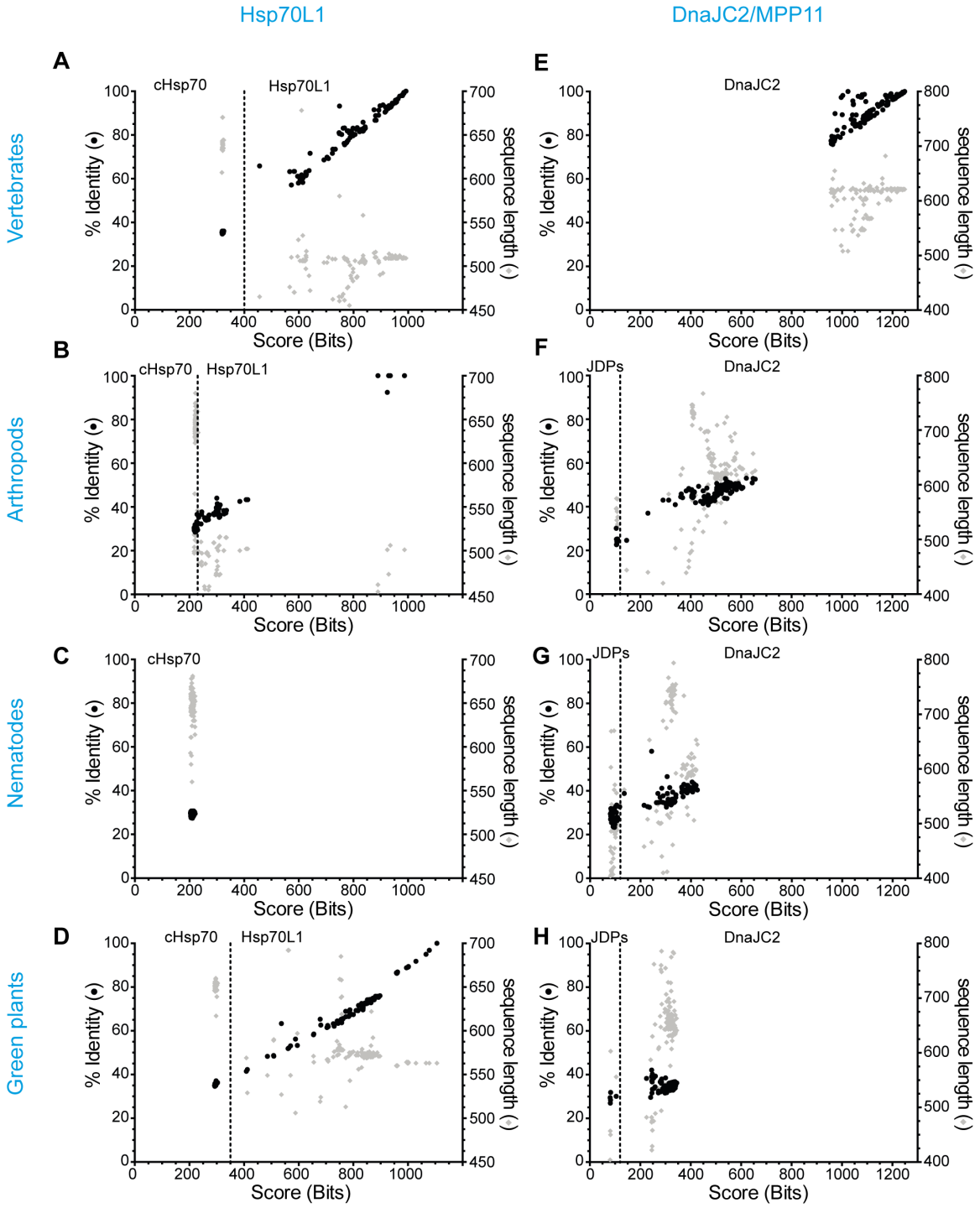

Figure 13: Conservation of Hsp70L1 and DnaJC2 in evolution. Results of BLAST searches on UniProtKB taxonomic subsets of vertebrates **(A, E)**, arthropods **(B, F)**, nematodes **(C, G)**, and green plants **(D, H)** using human Hsp70L1 **(A)**, *D. magna* Hsp70L1 **(B, C)**, *A. thaliana* Hsp70L1 **(D)**, and human DnaJC2 **(E-H)** as query. The relative degree of identity (left y-axis, black dots) and the sequence length (right y-axis, grey dots) are plotted versus the alignment score from the BLAST search result. Dashed lines indicate to which score the sequence exhibited features to: on the right side of the line either to Hsp70L1 **(A-D)** or DnaJC2 **(E-H),** on the left side of the line to classical Hsp70s **(cHsp70, A-D)** and other J-domain proteins **(JDPs, E-H)**, respectively. Sequence similarities were determined by Clustal Ω multiple sequence comparison. Analysis was performed by Prof. Matthias P. Mayer.

Yet, BLAST searches against the human RAC JDP partner (MPP11/DnaJC2) identified matches in all tested taxonomic subsets confirming the high protein sequence conservation of the ribosome-bound JDP (Fig. 13 E-H). These data suggest that during evolution RAC underwent alterations in nematodes and many arthropods.

5.2 Features of the Zuo1 homolog DNJ-11

5.2.1 Zuotin homologs in eukaryotes

The ribosome-associated complex (RAC) of *C. elegans* has not been characterized yet. Phylogenetic analyses showed that nematodes lack an Ssz-like protein making the investigation of RAC in these species even more intriguing. Previous studies pointed out that the *C. elegans* J-domain protein DNJ-11 shares a high sequence similarity to yeast Zuo1 and human MPP11 (Table A2) (Hatzold & Conradt, 2008; Kirstein-Miles *et al*, 2013; Chen *et al*, 2014). Overall, DNJ-11 shares 23.5% identity with Zuo1 and 34.5% identity with MPP11 and is classified as class C JDP. This diverse class of JDPs is mainly characterized by the presence of the J domain downstream of the N-terminus (Mayer & Gierasch, 2018). In addition to the J-domain and a charged region (CR), DNJ-11 and MPP11 contain two SANT domains at the C-terminus that generally function in chromatin remodeling by binding to histones (Fig. 14) (Boyer *et al*, 2002). However, whether RAC exerts a nuclear function via the SANT domains or whether they act on the ribosome is unknown.

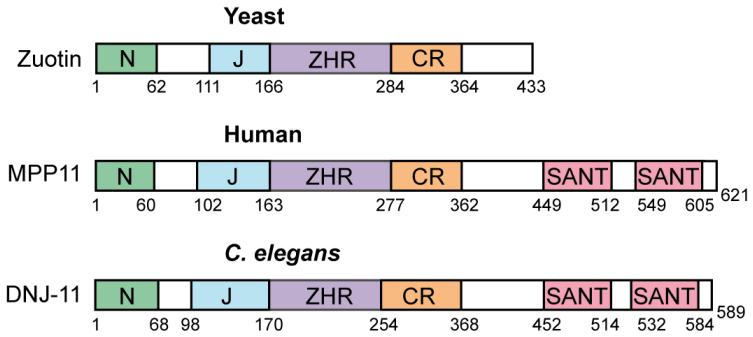

Figure 14: Schematic representation of different eukaryotic ribosome-associated JDPs. The Zuotin homology region (ZHR) is a common feature of all ribosome-associated JDPs. The N-terminal domain (N) is conserved and was shown to be essential in yeast for heterodimerization with Ssz1. ATPase stimulation of Hsp70s is enabled by the J-domain (J), which comprises a conserved HPD (histidine-proline-aspartic acid) motif. The charged region (CR) is essential for ribosome binding. In addition, MPP11 and DNJ-11 contain two negatively charged SANT domains at the C-terminus.

To further characterize DNJ-11, sequence alignments of Zuo1 homologs in yeast, human and different nematode species were performed.

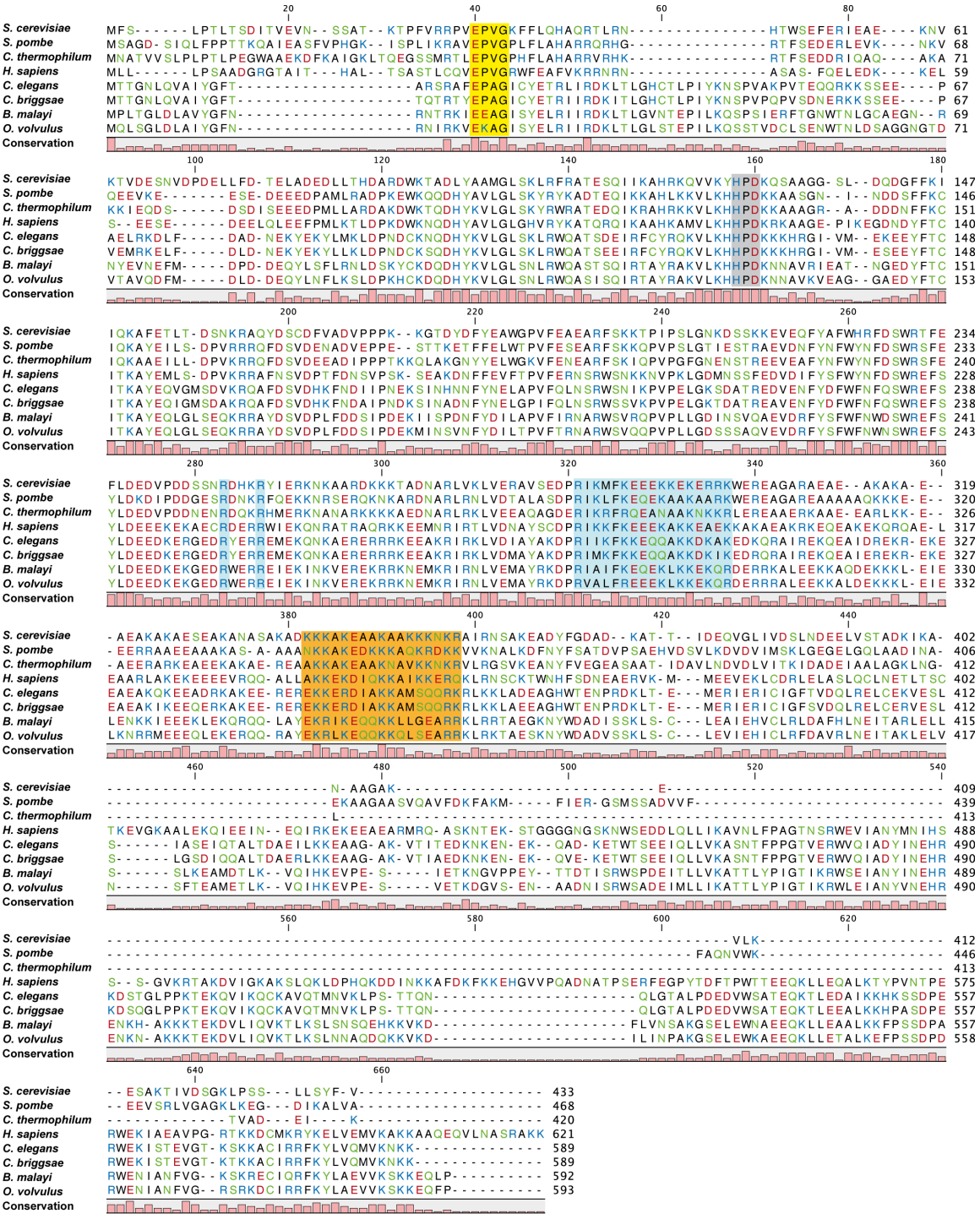

Figure 15: Sequence alignment of Zuo1 homologs found in yeast, humans and nematodes. The conserved HPD motif critical to act as a J-domain co-factor is highlighted in grey. Amino acid residues and regions involved in 60S binding are highlighted in light blue and the 40S contact site is shown in orange. The EPVG motif, known to be involved in yeast RAC formation is highlighted in yellow. Amino acids are colored on the basis of their properties: positively charged (blue), negatively charged (red), hydrophobic (black) and neutral (green).

The alignments were analyzed with respect to the presence of ribosome binding regions. Amino acid residues that are required for ribosome binding are conserved (Fig. 15). These binding regions include two lysines (Zuo1: R247 and R251), which mediate interaction with the 60S ribosomal subunit (Kaschner *et al*, 2015). In addition, two regions that facilitate ribosome association with the 40S (Fig. 15, orange) and 60S (Fig. 15, light blue) are also conserved (Zhang *et al.*, 2014; Lee *et al.*, 2016). Interestingly, the EPVG motif that is essential for RAC formation in yeast, is also highly conserved in nematodes (Fig. 15, yellow). This motif was shown to interact with the interdomain linker binding groove of Ssz1 (Weyer *et al*, 2017). All JDPs contain a highly conserved HPD motif which is critical for ATPase stimulation of Hsp70s (Greene *et al*, 1998) (Fig. 15, grey).
Altogether, the presented sequence alignments indicate strong homology between DNJ-11 and Zuo1/MPP11 providing the basis of a more profound analysis of RAC in *C. elegans*.

5.2.2 DNJ-11 binds to ribosomes *in vivo* and *in vitro*

As DNJ-11 shares many functionally important sequence features with Zuo1 and MPP11, the potential role of this J-domain protein as co-translational chaperone was examined in *C. elegans*. First, the ribosome binding manner was investigated *in vivo* as well as *in vitro*. Polysome profile analysis in young adult N2 nematodes (day 2 adults) showed that DNJ-11 comigrates with 80S ribosomes and polysomes (Fig. 16 A). However, approximately 50% of DNJ-11 was found to be ribosome-unbound (soluble).
To further investigate the ribosome binding manner of DNJ-11, ribosome-sedimentation assays using increasing salt concentrations were performed. Already at 150 mM KOAc, DNJ-11 completely dissociates from ribosomes (Fig. 16 B). This indicates that the interaction between DNJ-11 and the ribosome is weak and far more transient when compared to other ribosome-associated factors like NAC (Fig. 16 B). In comparison, Zuo1 and MPP11 showed an attenuated salt sensitivity (150-250 mM) (Yan *et al*, 1998; Otto *et al*, 2005). To confirm ribosome binding *in vitro*, recombinant DNJ-11 was incubated with 80S *C. elegans* ribosomes in the presence of 120 mM KOAc (physiological conditions). After sucrose cushion ultracentrifugation the supernatant and pellet fractions were analyzed by immunoblotting (Fig. 16 C). The addition of ribosomes shifted DNJ-11 into the ribosomal pellet fraction. An increase in DNJ-11 concentration (4 µM) resulted in a pronounced saturation of this association (Fig. 16 C).
To confirm the specificity of the observed ribosome binding and exclude an incidental co-migration of DNJ-11 with large ribosomal particles in the sucrose gradient, polysomes were digested by RNAse A resulting in elevated monosome levels (Fig. 17 A). If DNJ-11 binds specifically to ribosomes, it will shift along with ribosomes to the 80S fraction after RNAse A treatment.

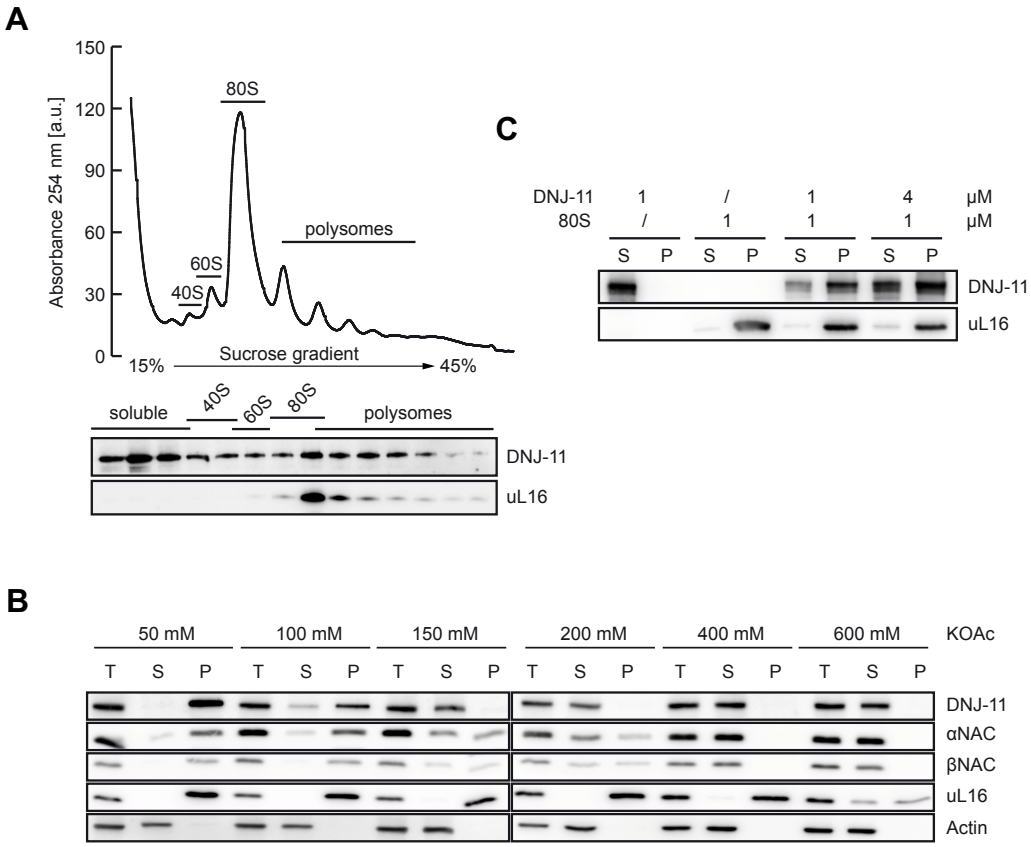

Figure 16: Ribosome binding of DNJ-11 *in vivo* and *in vitro*. (A) Polysome profile of N2 wildtype worms (day 2 adults) under low salt conditions (50 mM KOAc). Total lysate was loaded on a sucrose gradient (15%-45%) and ribosomal species were separated by ultracentrifugation. Fractions were analyzed by immunoblotting using a DNJ-11 specific antibody. uL16 served as marker for the large ribosomal subunit. **(B)** Synchronized wildtype worms were harvested at day 2 of adulthood. Total lysates were adjusted to equal A_{260} units in different salt concentrations. After ultracentrifugation samples (supernatant (S), pellet (P)) were analyzed by immunoblotting using DNJ-11 and NAC specific antibodies. uL16 served as a ribosomal and actin as cytosolic marker. T, total lysates **(C)** *In vitro* ribosome association of DNJ-11. Recombinant DNJ-11 was incubated with 80S *C. elegans* ribosomes in presence of 120 mM KOAc. DNJ-11 ribosome binding was verified by immunoblotting by separation of the soluble (S) and pellet (P) fraction by ultracentrifugation. uL16 served as ribosomal marker.

In previous studies yeast and human polysomes were digested with 250 µg/mL RNAse A (Kaschner *et al*, 2015; Otto *et al*, 2005). Strikingly, treatment of *C. elegans* polysomes with this nuclease concentration resulted in a total digestion of the ribosomal RNA. Thus, nematode ribosomes were far more sensitive to RNase A treatment and incubation with 1 to 5 µg/mL RNAse A for 5 min on ice was more than sufficient to observe polysome disruption in this species (Fig. 17 A). Surprisingly, DNJ-11 did not accumulate in the 80S fraction after nuclease treatment, though DNJ-11 protein levels increased in the soluble fraction (1 µg/mL) (Fig. 17 B). Upon treatment with 5 µg/mL RNase A, ribosome binding of DNJ-11 was completely abolished when compared to untreated or 1 µg/mL RNase A conditions.

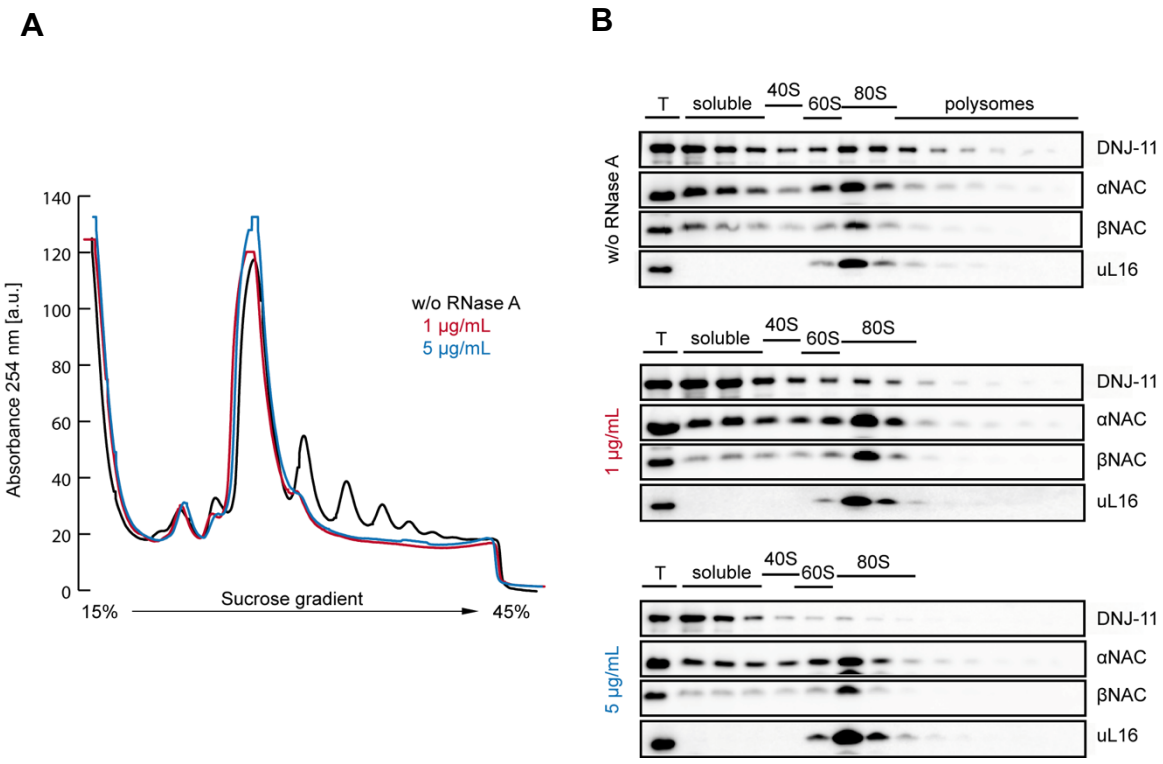

Figure 17: Ribosome binding of DNJ-11 is diminished upon RNAse A treatment. Total lysate (T) of young wildtype N2 *C. elegans* worms (day 2 adults) was incubated with (1 µg/mL or 5 µg/mL) or without RNase A for 5 min on ice. **(A)** Ribosomal species were separated by sucrose gradient centrifugation (15-45%). **(B)** Samples were analyzed by immunoblotting using specific antibodies against DNJ-11 and NAC. uL16 served as marker of the large ribosomal subunit.

Here, RNAse A application might lead to digestion of a ribosome exposed rRNA helix that is essential for DNJ-11 ribosome binding. Interestingly, ribosome binding of NAC was not altered upon nuclease treatment (Fig. 17 B).

In sum, all analyses strongly support that DNJ-11 associates with ribosomes *in vivo* and *in vitro* and this interaction was shown to be salt-sensitive.

5.2.3 DNJ-11 is predominantly expressed in gonads and embryos

The observed ribosome binding of DNJ-11 both *in vivo* and *in vitro* suggests a role in co-translational protein folding, as described for Zuo1 or MPP11 (Yan *et al*, 1998; Otto *et al*, 2005). Protein GFP fusion and immunofluorescence analyses of Zuo1 homologs in eukaryotes indicated a predominant cytosolic localization (Otto *et al*, 2005; Yan *et al*, 1998). However, a low nuclear abundance of Zuo1 homologs cannot be excluded as it was shown that Zuo1 associates with nuclear 60S intermediates during ribosome biogenesis (Albanèse *et al*, 2010) and the SANT domains of MPP11 (Fig. 14) are known to be involved in chromatin remodeling and histone tail binding (Boyer *et al*, 2002).

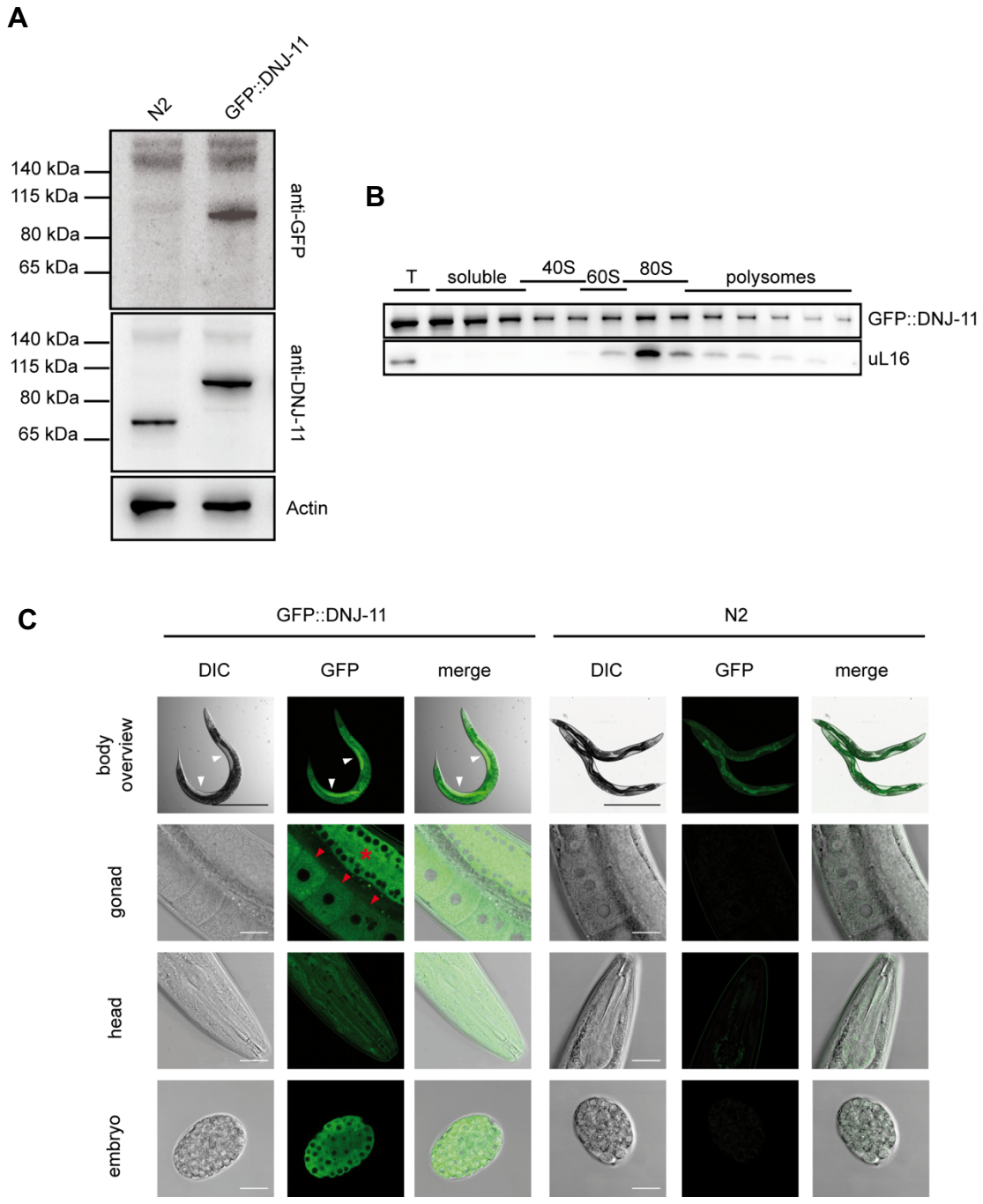

Figure 18: Characterization of the *C. elegans* GFP::DNJ-11 knock-in strain. (A) Expression of DNJ-11 and GFP::DNJ-11 in N2 and knock-in worms. DNJ-11 was detected by GFP or DNJ-11 specific antibodies. Actin served as loading control. **(B)** Ribosome association of GFP-tagged DNJ-11 in GFP::DNJ-11 transgenic worms using polysome profiling. uL16 served as ribosomal marker. T, total **(C)** Young adults and embryos of *C. elegans* were anesthetized with 25 mM levamisole and fluorescence was assessed with a Leica TCS SP8 confocal microscope. White arrowheads, gonads; red arrowheads, oocytes; red asterisk, gonad syncytium. Wildtype N2 worms (right panel) were used as background control in the fluorescence channel. Body overview: scale bar = 500 µm; others, scale bar = 20 µm. DIC, differential interference contrast.

DNJ-11 expression patterns were analyzed both in different tissues and on a subcellular level. Thus, the N-terminus of DNJ-11 was chromosomally GFP-tagged. To exclude any influence of GFP on DNJ-11 in the knock-in strain, GFP::DNJ-11 protein level and its ribosome binding capability were verified by polysome profiling and immunoblotting (Fig. 18 A and B). Microscopic fluorescence analyses showed that GFP::DNJ-11 is distributed throughout the worm. The highest protein abundance was detected in the distal gonads and in embryos (Fig. 18 C, left panel, white/red arrow heads) and zoomed-in images revealed a predominant cytosolic localization (Fig. 18 C, gonad and embryo). As N2 worms only showed a faint autofluorescence signal in the gut resulting from glycosylated anthranilic acid (Coburn & Gems, 2013). Thus, it can be concluded that the observed cytosolic signal of GFP::DNJ-11 is specific (Fig. 18 C, right panel).

To investigate the potential nuclear localization of DNJ-11, nuclei of *C. elegans* (day 1 adults) were isolated and analyzed via immunoblotting. The detection of DNJ-11 in the cytosolic extract confirms the observed expression in the cytosol (Fig. 18 C and Fig. 19). Moreover, DNJ-11 was detected in the nuclei fraction, which showed high amounts of Histone H3 (Fig. 19). However, the nuclear fraction showed slight GAPDH and tubulin signals, and the cytosolic fraction contained marginal Histone H3 contaminations. Thus, a clear nuclear presence of DNJ-11 could not be shown.

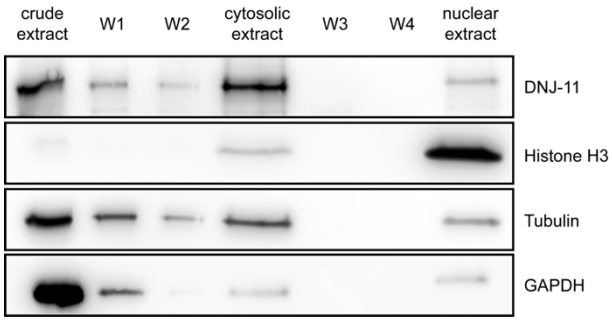

Figure 19: DNJ-11 is predominantly located in the cytosol. Nuclei and cytosolic fractions of young adult wildtype nematodes were prepared using sequential extraction and washing (W) steps. DNJ-11 was detected by immunoblotting using a specific antibody. Histone H3 served as nuclear marker, tubulin and GAPDH were used as cytosolic markers.

In sum, DNJ-11 shows a strong cytosolic accumulation. However, a partial nuclear localization cannot be excluded as DNJ-11 may also act on a transcriptional level via its SANT domains.

5.2.4 DNJ-11 complements the growth defect of *zuo1Δ* yeast cells

Ribosome-bound Ssb is specific for fungi and absent in higher eukaryotes (Pfund *et al*, 2001). While Zuo1 and Ssz1 are conserved in humans (MPP11 and Hsp70L1) (Jaiswal *et al*, 2011), so far only the Zuotin homolog DNJ-11 is identified in the metazoan *C. elegans*. Protein sequence BLASTs showed that Ssz-like proteins are absent in nematodes (Fig. 13). It seems that the setup of this system diverged over time, and it is unclear if this is accompanied by functional differences in diverse eukaryotes. To investigate, if the function of ribosome-associated chaperones is evolutionary conserved, complementation studies in *S. cerevisiae* were performed.

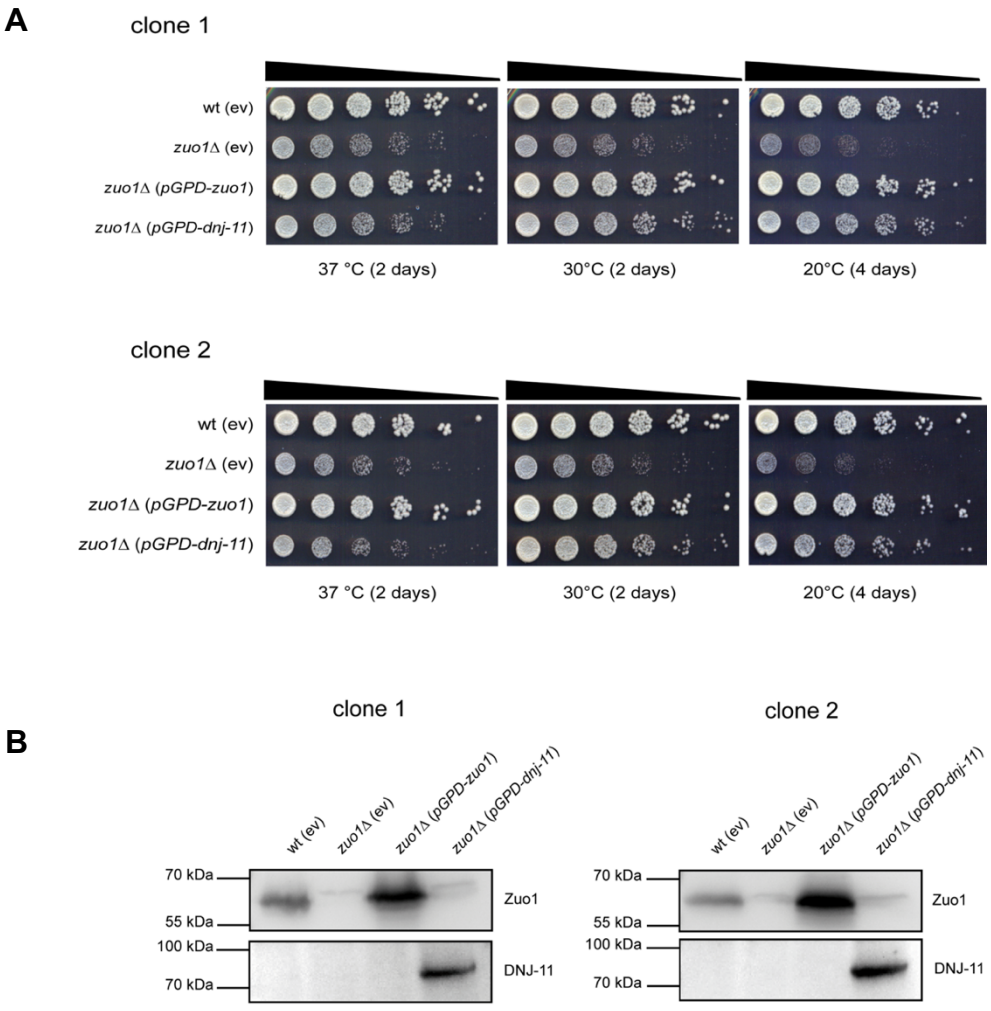

Figure 20: Expression of DNJ-11 in *Δzuo1 S. cerevisiae* cells rescues growth defect.(A) Growth analyses of wildtype yeast cells (wt) and *zuo1Δ* yeast cells transformed with either the empty GPD vector (ev) or plasmids coding for *zuo1* or *dnj-11*. Serial dilutions of two clones were spotted on synthetic complete media without histidine (SD-His) and were incubated at indicated temperatures for 2 or 4 days, respectively. **(B)** Expression levels of Zuotin and DNJ-11 in yeast cells, which were used in the growth analyses in (A). Proteins were detected via specific antibodies.

The constitutive GPD promoter and CYC1 terminator were used to express DNJ-11 in yeast. The stable protein expression of DNJ-11 was confirmed by immunoblotting (Fig. 20 B) and the growth of multiple yeast clones was tested. The expression of DNJ-11 in *Δzuo1* yeast cells could rescue the growth defect at a growth temperature of 20°C (Fig. 20 A). However, the complementation effect was less significant at 37°C, most likely due to DNJ-11 folding stress.

It seems that DNJ-11 is functional in yeast, but still it remains unclear how this JDP interacts with the yeast Hsp70 family.

5.2.5 Protein depletion and specific mutations of DNJ-11 alter brood size and development of *C. elegans*

Zuo1 in yeast and MPP11 in human cells are non-essential proteins. However, deletion of Zuo1 leads to growth defects (Yan *et al*, 1998; Zhang *et al*, 1992) and HeLa cells depleted of MPP11 are characterized by a decreased doubling time (Jaiswal *et al*, 2011). To characterize the conserved function of Zuotin homologs in eukaryotes, phenotypic effects caused by endogenous protein depletion using RNAi and genomic deletion of *dnj-11* (*dnj-11(bc212)*) were examined. DNJ-11 expression levels in these worms were analyzed by immunoblot analysis (Fig. 21 A). Worms depleted of DNJ-11 showed an increased embryonic mortality, a reduced brood size and a delay in larval maturation of approximately 24 h (Hatzold & Conradt, 2008). In addition to the effect on larval development, the depletion and deletion of DNJ-11 decreased the median life span of the nematodes (Fig. 21 B). Thus, DNJ-11 exhibits a general role, both during development and adulthood.

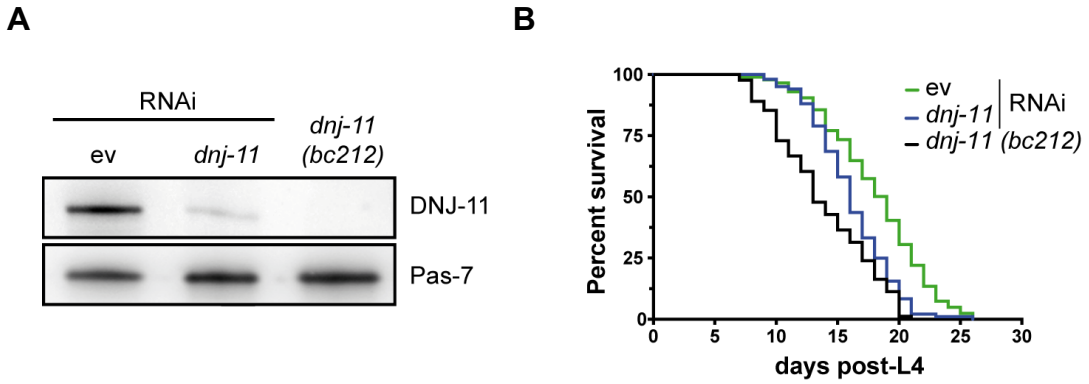

Figure 21: Effect of DNJ-11 depletion and deletion on *C. elegans* median life span. (A) Protein expression levels at day 3 of adulthood in total lysates of wildtype N2 worms fed with bacteria transformed either the empty vector (ev) or *dnj-11* RNAi plasmid, were compared to *dnj-11* knockout worms (*dnj-11(bc212)*). Samples were separated by SDS-PAGE and analyzed by immunoblotting. Pas-7 served as loading control. **(B)** Kaplan-Meier survival curves. Median life span of *C. elegans* wildtype strain N2 grown on the indicated RNAi bacteria as in (A) by feeding and *dnj-11*(*bc212*). N2 median life span = 19 days, *dnj-11* RNAi = 16 days, *dnj-11(bc212)* = 13 days.

Next, the *in vivo* importance of the HPD motif and the SANT domains of DNJ-11 was assessed with respect to worm development and brood size. To address the functional relevance of these protein domains, worms expressing either a mutation in the HPD motif or lacking both SANT domains were generated. Both mutants (hereafter DNJ-11^{H129Q} and DNJ-11$^{\Delta SANT}$) were expressed from a single integrated transgene in the DNJ-11 knockout background (*dnj-11(bc212)*). As control, the gene coding for wildtype DNJ-11 was integrated into *dnj-11(bc212)*. Expression of the transgenes was driven under the native DNJ-11 promoter and expression levels were analyzed by immunoblot (Fig. 22 A).

Comparison of the brood size showed that deletion of DNJ-11 significantly reduced the progeny number when compared to N2 or DNJ-11^{WT} complemented knockout worms (Fig. 22 B, **P<0.01) (Hatzold & Conradt, 2008). Previous studies performed in *E. coli* showed that the HPD motif is indispensable in the Hsp70/JDP cycle, both as interaction platform with Hsp70s, and as essential motif for ATPase stimulation (Tsai & Douglas, 1996; Wall *et al*, 1994). The transgenic DNJ-11^{H129Q} worms were used to investigate the essential role of DNJ-11 as functional JDP partner of a ribosome-tethered Hsp70. Interestingly, mutations in the HPD motif caused a decrease in progeny numbers (Fig. 22 B, *P<0.05). Although DNJ-11^{H129Q} is approximately 50% less expressed compared to wildtype DNJ-11 (Fig. 22 A), DNJ-11^{H129Q} worms showed an increased number in progeny compared to *dnj-11*(*bc212*). In addition, both DNJ-11 knockout and HPD mutation had a strong effect on worm development as both *dnj-11(bc212)* and DNJ-11^{H129Q} expressing worms did not reach the adult state after 72 h post egg-lay (Fig. 22 C). This observation is in line with described slow growth rates of yeast cells expressing Zuo1^{H128Q} (Hundley *et al*, 2002). These data show that the J-domain is essential for full DNJ-11 function *in vivo*. However, apart from the JDP function other protein domains or features seem to be important.

As seen for HPD mutation, the deletion of both SANT domains reduced the brood size significantly (Fig. 22 B). Surprisingly, DNJ-11$^{\Delta SANT}$ expressing worms reached the adult state 72 h post egg lay unlike worms of the *dnj-11*(*bc212*) or DNJ-11^{H129Q} strain. However, none of the mutations resulted in a sterile phenotype as all strains were able to produce progenies (Fig. 22 B). The observed phenotypic alterations of DNJ-11^{H129Q} can be assigned to the canonical function of the HPD motif, however, the role of the SANT domains remains ambiguous. Previously, this motif was characterized as transcriptional activator module (Boyer *et al*, 2002), thus the observed phenotype of DNJ-11$^{\Delta SANT}$ might originate from alterations in transcriptional activity. Yet, ribosome binding efficiency of the mutant was tested. Indeed, *in vivo* DNJ-11$^{\Delta SANT}$ showed no binding to 80S ribosomes compared to wildtype or DNJ-11^{H129Q} (Fig. 22 D). This might indicate that the SANT domains are used as auxiliary anchor points at ribosomes apart from the charged region. These data are in line with the observation that human MPP11 lacking one SANT domain is less efficient

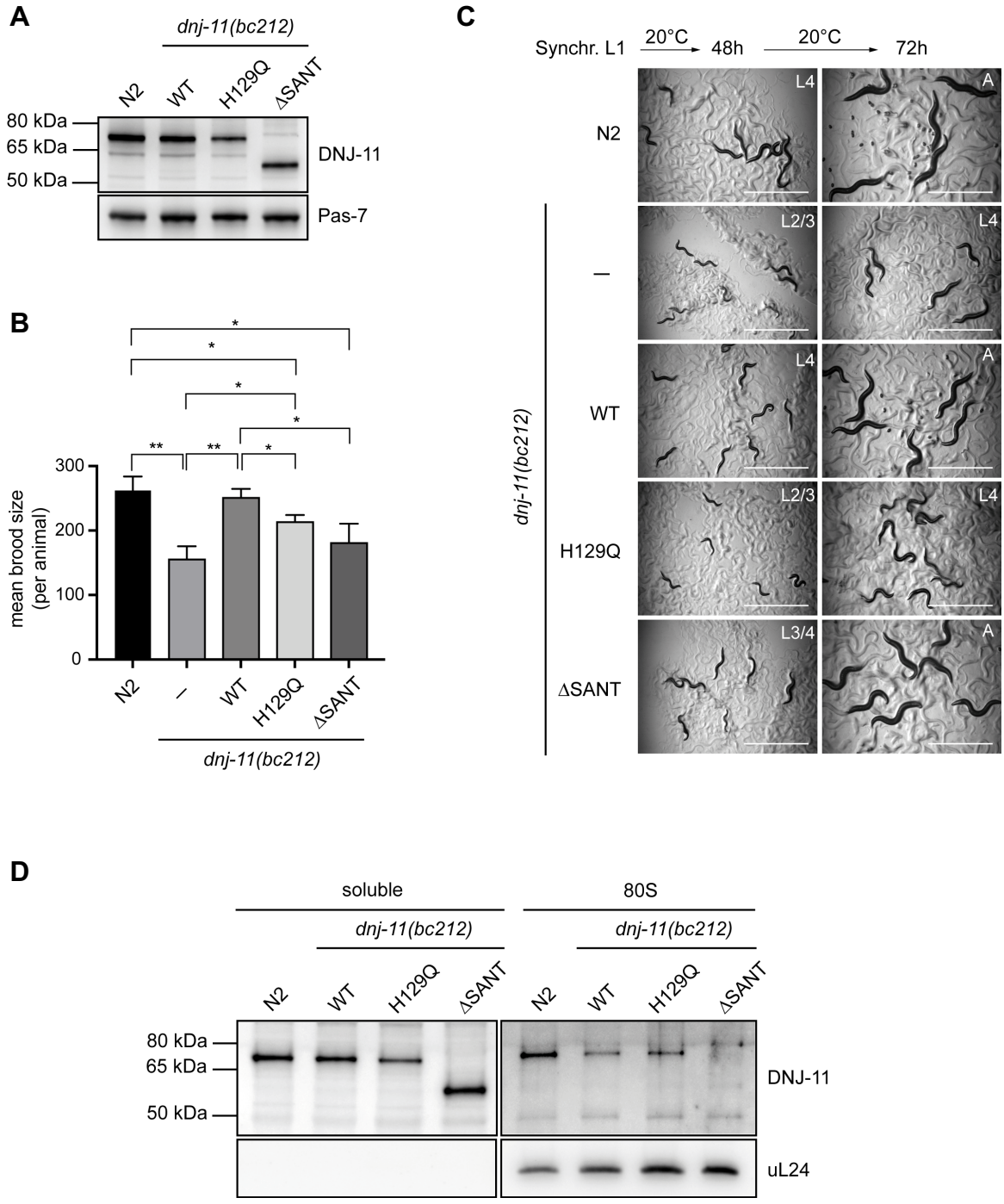

Figure 22: Impact of DNJ-11 knockout, HPD motif mutation and SANT domain deletion on *C. elegans* development. (A) Western Blot analysis of protein expression levels of DNJ-11 WT and DNJ-11 mutants in *C. elegans* (day 1 adulthood). H129Q, residue substitution in HPD motif; ΔSANT, complete deletion of both C-terminal SANT domains. DNJ-11 was detected via a specific antibody. Pas-7 served as loading control. N2, *C. elegans* wildtype; *dnj-11(bc212)*, DNJ-11 knockout**. (B)** Mean brood size of indicated *C. elegans* strains. An unpaired Student's t-test was used to assess significance (*P<0.05; **P<0.01). Data are presented as mean ± SD (n=3 with 20 worms per analysis and strain). **(C)** Bright field microscopic images showing the developmental stages of the different *C. elegans* strains after 48 and 72 h. Scale bar = 1 mm. Synchr., synchronized; L, larval stage 1-4; A, adult **(D)** *C. elegans* total lysates were fractionated by a sucrose gradient (15-45%) and soluble as well as 80S fractions were collected. Aliquots of fractions were analyzed by immunoblot using DNJ-11 and uL24 specific antibodies. uL24 served as marker for the large ribosomal subunit.

to complement the growth phenotype of *Δzuo1Δssz1* in concert with Hsp70L1 (Otto *et al*, 2005). However, Otto and coworkers did not analyze ribosome binding of the mutant. The importance of the SANT domains in ribosome binding is underlined by the fact that *in vivo* ribosome association was diminished by a single FLAG-tag at the C-terminus downstream of these domains (data not shown).

In sum, both the J-domain function and the SANT domains are important for the cellular function of DNJ-11 *in vivo*.

5.2.6 DNJ-11 has no impact on global translation rates

In yeast, deletion of Zuo1 causes a clear defect in ribosome biogenesis. This defect is visible as shoulders on the 80S and polysome peaks (halfmers) in polysome profiles (Albanèse *et al*, 2010). Considering DNJ-11 as Zuo1 homolog, it was investigated whether the depletion or deletion of DNJ-11 has an effect on ribosome assembly or ribosome biogenesis.

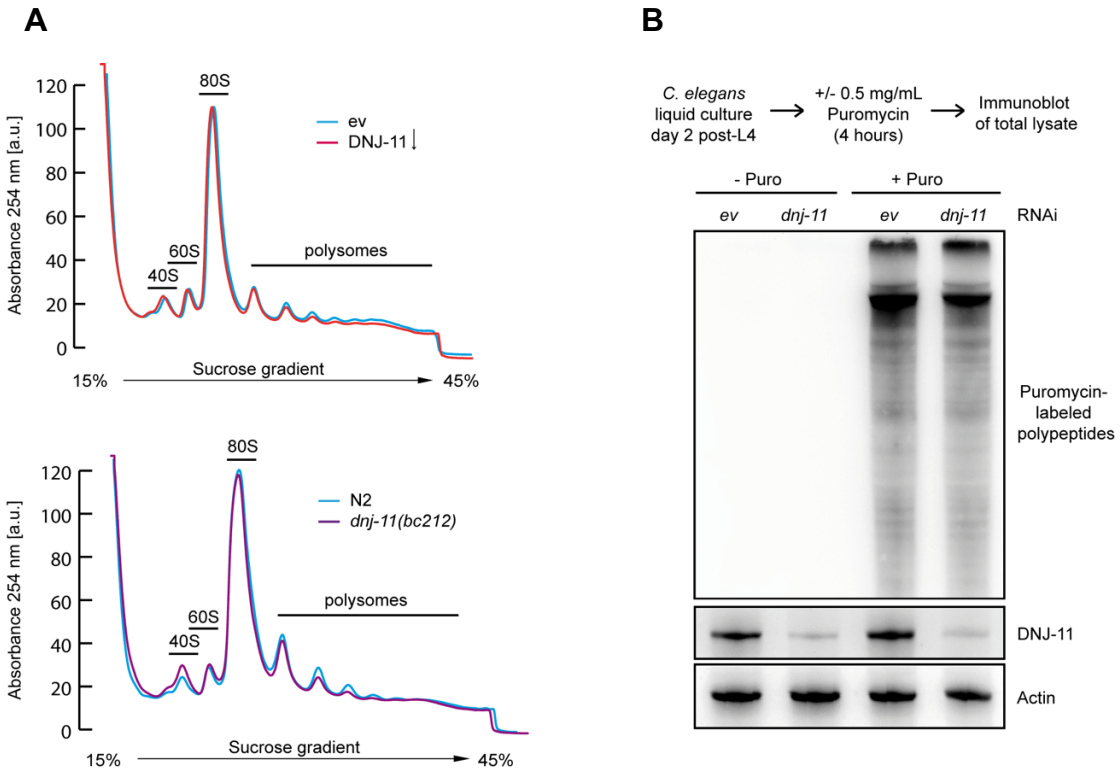

Figure 23: Impact of DNJ-11 depletion or knockout on ribosome biogenesis and overall translation rate. **(A)** Polysome analysis of wildtype worms versus *dnj-11*-depleted worms (*dnj-11* RNAi) or *dnj-11(bc212)* nematodes (day 3 adults). RNAi treatment was performed after hatching. ev, empty vector. DNJ-11 ↓, DNJ-11 depletion **(B)** SUrface SEnsing of Translation method applied in liquid culture of *C. elegans*. At day 2 of adulthood worms were either treated with (0.5 mg/mL) for four hours. Total lysates were analyzed by immunoblotting and puromycin-labeled polypeptides were probed with a specific puromycin antibody. Knockdown efficiency of DNJ-11 was detected via DNJ-11 specific antibodies. Actin served as loading control. Puro, Puromycin.

In *C. elegans* no significant differences in polysome profiles of DNJ-11-depleted or *dnj-11(bc212)* worms were observed (Fig. 23 A). As the height and shape of polysome peaks showed no differences it can be assumed that worms lacking DNJ-11 are not hampered in cellular translation activity.
In addition, a more sensitive technique called SUrface SEnsing of Translation (SUnSET) was applied to quantify global protein synthesis (Schmidt *et al*, 2009; Arnold *et al*, 2014). This approach is based on *in vivo* puromycin-labeling of newly translated polypeptides. By incubating of *C. elegans* with puromycin in liquid culture the Tyr-tRNA mimetic is ingested by the worms and attached at the C-terminus of the nascent chains during ongoing translation. This modification inhibits the translocation of the tRNA to the P site of the ribosome leading to premature chain termination and release of the polypeptide chain (Yarmolinsky & Haba, 1959). After four hours of puromycin treatment the worms were harvested, and total lysates were prepared. To detect changes in the translation rate of wildtype compared to DNJ-11-depleted worms, puromycin-labeled proteins were probed with a specific puromycin antibody. Likewise, this technique did not reveal any *in vivo* impact of DNJ-11 on the overall number of translated polypeptides (Fig. 23 B).

5.3 The *C. elegans* ribosome-associated complex (ceRAC)

J-domain proteins are co-chaperones of the Hsp70 chaperone family. JDPs are essential for Hsp70 ATPase stimulation and guidance of protein substrates to the Hsp70 machinery (Szabo *et al*, 1994; McCarty *et al*, 1995; Hartl *et al*, 2011). At the ribosome RAC acts as co-translational chaperone recruiting an extra Hsp70 to bind nascent polypeptide chains. Thus, these heat shock proteins work together as a functional triad to maintain proper quality control at the ribosome. However, the Ssz-like protein subunit of RAC is characterized by an inactive ATPase and a shortened substrate binding domain (Preissler & Deuerling, 2012). In the previous chapters it was shown that DNJ-11 is a functional homolog of yeast Zuotin and human MPP11. Interestingly, the genome of *C. elegans* does not encode an Ssz-like protein, therefore it remains an open question if a RAC-like complex exists in nematodes.

5.3.1 HSP-1 forms a stable heterodimeric complex with DNJ-11

It is so far unknown, if DNJ-11 is functional and able stimulate a cytosolic Hsp70 on its own, or if a complex partner is needed, similar to the yeast and human RAC systems (Otto *et al*, 2005; Gautschi *et al*, 2002). To address this question, co-immunoprecipitation experiments were performed in wildtype nematodes. DNJ-11 was co-precipitated with a 70 kDa protein in a 1:1 stoichiometry (Fig. 24 A). Mass-spectrometric analyses identified the second protein as HSP-1. The interaction

between DNJ-11 and HSP-1 was stable in presence of ATP arguing against an Hsp70/substrate interaction as substrates are released from Hsp70s in the ATP-bound conformation (Fig. 24 B). Moreover, the heterodimeric DNJ-11-HSP-1 complex (herein ceRAC) was very stable withstanding even high salt concentrations (500 mM NaCl) (Fig. 24 C).

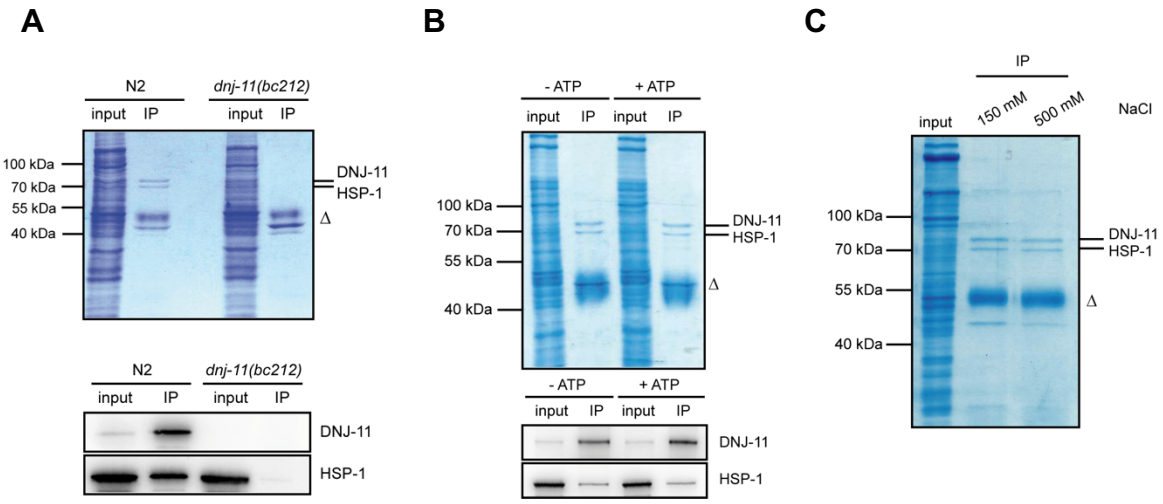

Figure 24: DNJ-11 forms a stable heterodimeric complex with HSP-1. Coomassie-stained gels of DNJ-11 co-immunoprecipitation under different conditions **(A)** DNJ-11 pulldown in N2 and *dnj-11(bc212) C. elegans* (day 2 of adulthood) using a DNJ-11 specific antibody. DNJ-11 and HSP-1 were identified by mass spectrometry and were detected in immunoblot analyses using specific DNJ-11 and HSP-1 antibodies. Δ, IgG heavy chain. **(B, C)** Pulldown of DNJ-11 in N2 *C. elegans* (day 2 of adulthood) using a DNJ-11 specific antibody. Co-immunoprecipitation was performed in presence or absence of 5 mM ATP **(B)** or in the presence of low and high salt concentrations **(C)**. Δ, IgG heavy chain

HSP-1 represents the single Hsp70 in *C. elegans* that is constitutively expressed (Hsc70) compared to the three inducible cytosolic Hsp70 proteins (Hsp-70, F44E5.4, F44E5.5), which are predominantly expressed under stress conditions (Table A1) (Guhathakurta et al, 2002; Snutch et al, 1988). In contrast to yeast Ssz1 or human Hsp70L1, HSP-1 is assumed to be a fully active cytosolic Hsc70 with a functional ATPase (Fig. 26 yellow residues) and a regular substrate binding domain including the C-terminal lid domain (SBDα) (Fig. 25). The hydrophobic interdomain linker between the NBD and SBD in canonical Hsp70s, like HSP-1, is longer compared to the linker of Ssz-like proteins (Fig. 25 and 26 grey residues). *C. elegans* HSP-1 was shown to exhibit chaperone-like function *in vivo* and *in vitro* and was described as one of the key players in metazoan protein disaggregation (Sankhala *et al*, 2012; Rampelt *et al*, 2012; Nillegoda *et al*, 2015). In *C. elegans* HSP-1 is essential, as HSP-1-depleted animals show larval arrest (Kamath *et al*, 2003; Gaiser *et al*, 2011). Moreover, appropriate muscle function is regulated by the Hsp70 cycle of HSP-1 (Papsdorf *et al*, 2014). Nevertheless, HSP-1 could not be linked to a ribosome-associated activity yet.

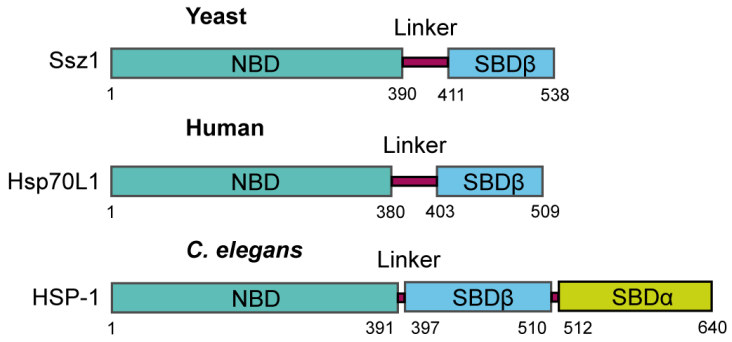

Figure 25: Hsp70 subunit of RAC from different eukaryotic species. Schematic representation of conserved domains in Hsp70s of RAC: nucleotide binding domain (NBD), substrate-binding domain (SBDβ) and the "lid" domain (SBDα). Ssz1 and Hsp70L1 are characterized by a long interdomain linker between the NBD and SBD and the absence of the helical SBDα.

The previous data indicate that *C. elegans* evolved a non-canonical RAC system. Thus, it needs to be clarified if ceRAC can act on its own or if an additional Hsp70 is needed, as seen in yeast (Ssb) or humans (Hsp70). To investigate whether complex formation with HSP-1 is critical for DNJ-11 function *in vivo*, HSP-1 was depleted by RNAi. Knockdown of HSP-1 decreased DNJ-11 protein levels despite 2-fold increased *dnj-11* mRNA levels (Fig. 27 A) suggesting that DNJ-11 is unstable *in vivo* without its complex partner. These data illustrate that the stability of DNJ-11 strictly depends on complex formation with HSP-1 *in vivo*, similar to the JDP subunit of RAC in yeast and human cells (Jaiswal *et al*, 2011; Huang *et al*, 2005). In contrast, HSP-1 is expressed in excess compared to DNJ-11 (Fig. 24 A; compare input and IP ratios) and stable in absence of DNJ-11(Fig. 27 B). As the single Hsc70 in *C. elegans*, HSP-1 does not exclusively depend on DNJ-11. In contrast, depletion of the DNJ-11 homolog MPP11 in mammalian cells resulted in reduced Hsp70L1 and uL22 ribosome levels (Jaiswal *et al*, 2011). However, in *C. elegans* no impact on ribosomal protein levels in *dnj-11(bc212)* nematodes was observed (Fig. 27 C).

All observations indicate that *C. elegans* evolved a non-canonical RAC system consisting of a constitutively expressed Hsp70 (HSP-1) and a ribosome-bound JDP (DNJ-11). ceRAC could be recombinantly expressed in *E. coli* and purified as stable heterodimeric complex using a three-step purification protocol (see methods and Fig. 28 A).

As shown before, DNJ-11 binds 80S ribosomes *in vitro* (Fig. 16 C), thus ribosome association of ceRAC was tested to analyze a DNJ-11 dependent HSP-1 tethering to the ribosome. Under physiological conditions (120 mM KOAc) recombinant ceRAC efficiently bound to *C. elegans* 80S ribosomes and high salt concentrations (300 mM KOAc) led to dissociation from ribosomes (Fig. 28 C). Apparently, also HSP-1 alone showed ribosome binding ability that could be explained by interaction with residual nascent polypeptides, though ribosomes were treated with puromycin

during purification. Interestingly, it was not possible to reconstitute ceRAC *in vitro* by mixing separately purified DNJ-11 and HSP-1 neither with nor without ATP (Fig. 28 B). This observation indicates that the complex most likely needs to be assembled co-translationally.

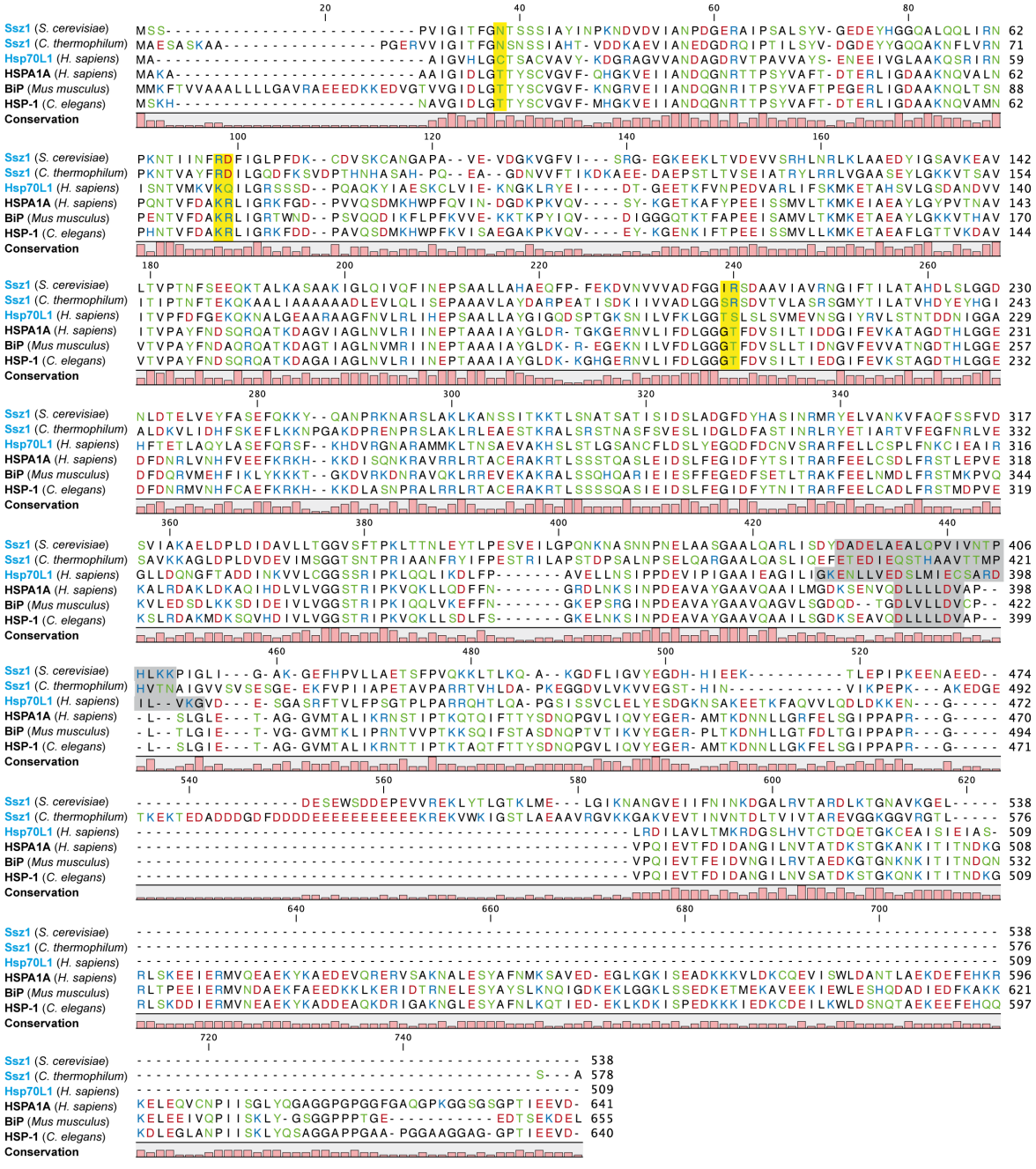

Figure 26: Sequence alignment of Ssz-like proteins and canonical Hsp70s in different eukaryotic species. Ssz-like proteins (blue), canonical Hsp70 (black). Catalytic residues of the NBD are highlighted in yellow, the hydrophobic linker between the NBD and SBD is marked in grey. Amino acids are colored on the basis of their properties: positively charged (blue), negatively charged (red), hydrophobic (black) and neutral (green).

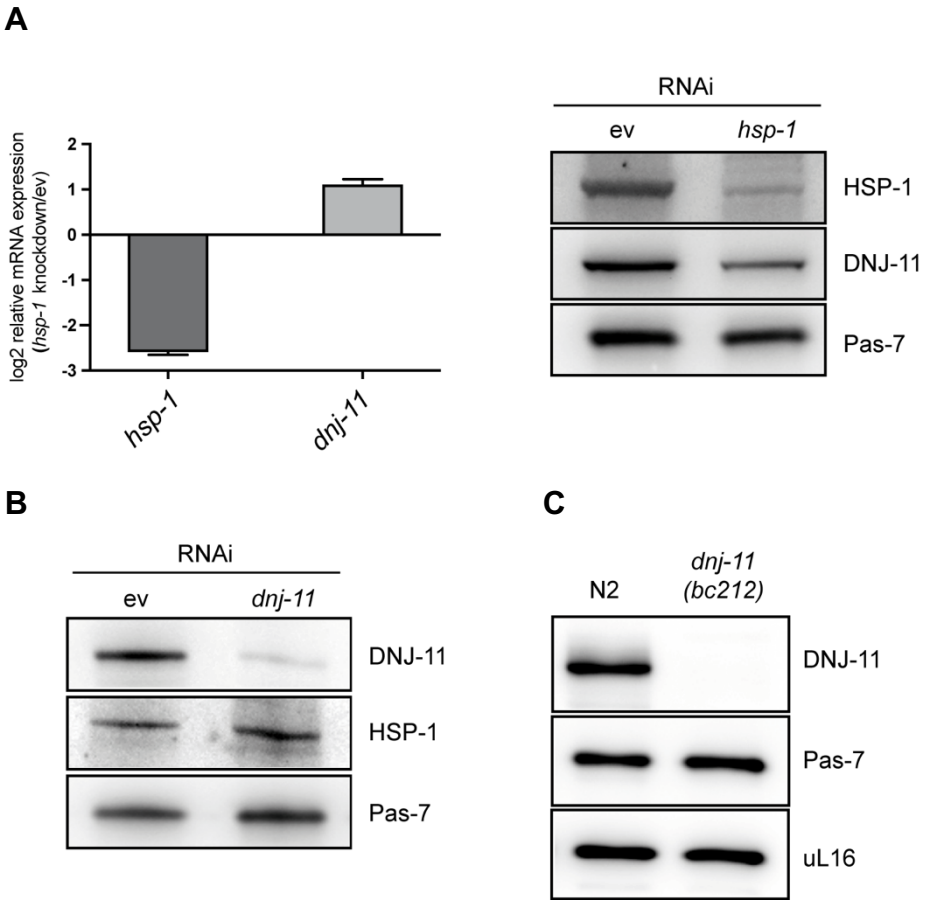

Figure 27: DNJ-11 stability depends on HSP-1 *in vivo*. (A) mRNA (left) and protein (right) levels of HSP-1 and DNJ-11 in HSP-1- depleted nematodes (day 3 of adulthood) analyzed via qPCR and immunoblotting, respectively. In the qPCR experiment relative mRNA expression levels were calculated in comparison to empty vector (ev) control animals. *Ama-1* was used as reference gene. Relative expression was calculated via the $2^{-(\Delta\Delta Ct)}$ method. Data are presented as mean ± SD (n=2). RNAi treatment was started at L4 larval stage. Protein levels of HSP-1 and DNJ-11 were analyzed by immunoblotting. Pas-7 served as loading control. **(B)** Immunoblot analysis of protein levels of DNJ-11 and HSP-1 in DNJ-11-depleted *C. elegans* worms (day 3 of adulthood). RNAi was started at L1 larval stage. Membrane was probed with DNJ-11 and HSP-1 specific antibodies. Pas-7 served as protein loading control. **(C)** Ribosomal protein level in wildtype (N2) versus *dnj-11(bc212)* worms. Indicated proteins were detected with specific antibodies. Pas7 served as loading control. uL16 served as maker for ribosomal protein levels.

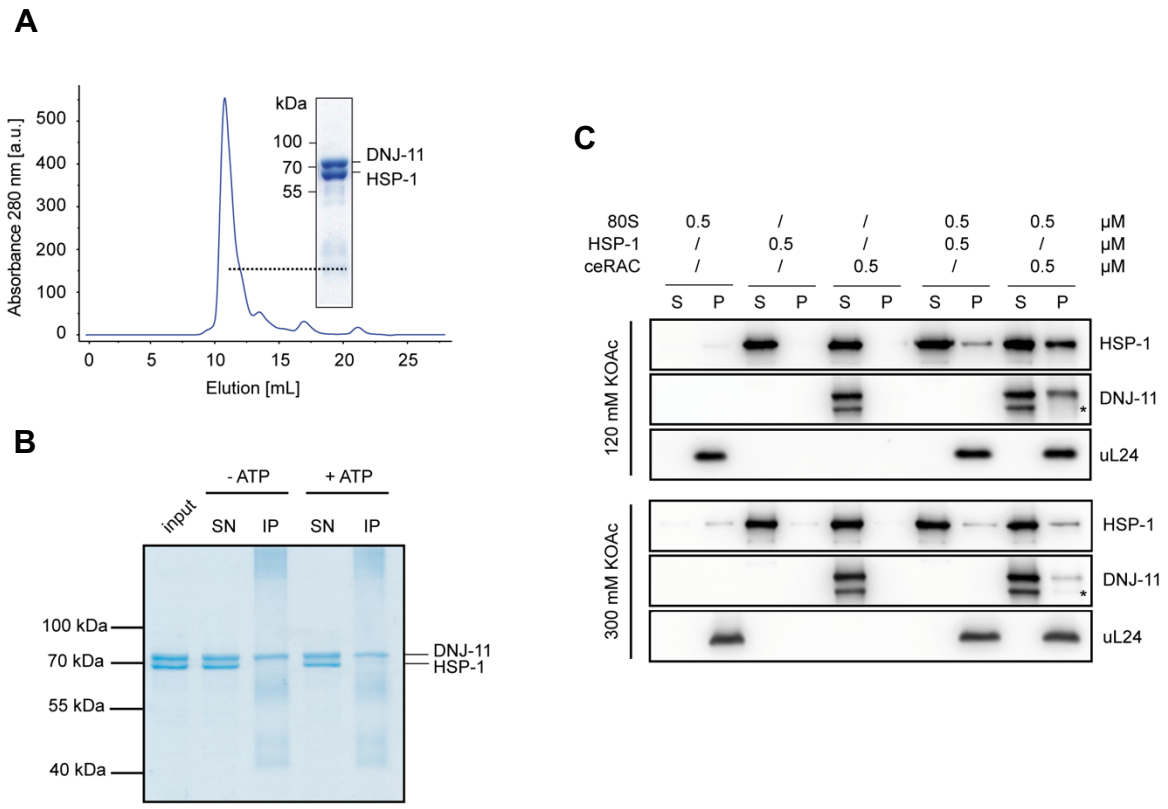

Figure 28: *In vitro* ribosome association and complex formation of ceRAC. (A) DNJ-11 and HSP-1 were recombinantly co-expressed in *E. coli* and the complex was purified via ion-exchange and size-exclusion chromatography (SEC). Record of SEC run is shown, and sample of the highest peak was applied to SDS-PAGE and Coomassie-staining. a.u., arbitrary units **(B)** Coomassie-stained gel of *in vitro* ceRAC formation using co-immunoprecipitation. Single recombinant HSP-1 and DNJ-11 (input) were incubated at 20°C for 15 min. in presence or absence of 5 mM ATP and subsequently incubated with DNJ-11 antibody. DNJ-11 was finally pulled down via Protein A magnetic beads. SN, supernatant; IP, immunoprecipitation. **(C)** 80S *C. elegans* ribosomes (+ Puromycin) were incubated with recombinant HSP-1 or ceRAC in presence of 120 mM or 300 mM KOAc. Soluble (S) and pellet (P) fractions were separated by ultracentrifugation. DNJ-11 and HSP-1 ribosome binding was verified via immunoblotting. uL24 served as ribosomal marker. *, degradation product of DNJ-11.

All findings imply that HSP-1 forms a stable ribosome-bound complex with DNJ-11 and is crucial to stabilize the JDP *in vivo*. These data show a stable complex formation between an active Hsc70 and a JDP, which has never been described before.

5.3.2 ceRAC formation decreases the ATP hydrolysis rate of HSP-1

Peptide binding and ATPase activity are dispensable for the function of Ssz-like proteins (Preissler & Deuerling, 2012; Leidig *et al*, 2013). By now, the exact function of these Hsp70s is not resolved but it is assumed that Ssz-like proteins are needed to stabilize their JDP partner and act as a scaffold between the JDP and the extra Hsp70 (Fiaux *et al*, 2010).

Previous results of this thesis showed that in *C. elegans* DNJ-11 forms a stable heterodimer with HSP-1, the canonical Hsc70 of nematodes. It remains to be clarified if HSP-1 in ceRAC is capable to perform chaperone-like function autonomously or if an additional Hsc70/Hsp70 is needed. Therefore, *in vitro* ATPase activity of HSP-1 alone and in complex with DNJ-11 was determined by ATP single turnover measurements in cooperation with **Dr. Roman Kityk** (ZMBH Heidelberg). Basal hydrolysis rates of HSP-1 (rate: 3.06 x 10^{-4} s^{-1}) and ceRAC (rate: 9.54 x 10^{-4} s^{-1}) are similar. Strikingly, the turnover rates illustrated that the ATPase of HSP-1 in the heterodimer can only be mildly stimulated when an additional JDP (DNJ-11) was added (rate: 2.76 x 10^{-3} s^{-1}) (Fig. 29). The significant decline in the hydrolysis rate is most obvious when compared to HSP-1 stimulated by DNJ-11 (rate: 6.99 x 10^{-3} s^{-1}) or DNJ-13 (rate: 1.27 x 10^{-2} s^{-1}). As a positive DNJ-13 was used as it is known to be a functional cytosolic J-domain partner of HSP-1 (Papsdorf *et al*, 2014; Sun *et al*, 2012).

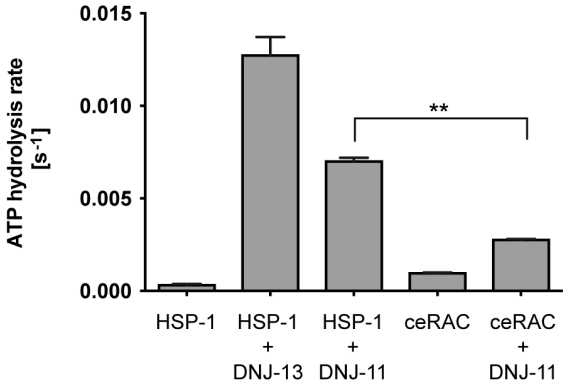

values / chaperones	ATP hydrolysis rate [s^{-1}]	SD [s^{-1}]
HSP-1 basal	3.06 x 10^{-4}	1.25 x 10^{-4}
ceRAC basal	9.54 x 10^{-4}	8.73 x 10^{-5}
HSP-1 + DNJ-11	6.99 x 10^{-3}	3.64 x 10^{-4}
HSP-1 + DNJ-13	1.27 x 10^{-2}	1.17 x 10^{-3}
ceRAC + DNJ-11	2.76 x 10^{-3}	9.72 x 10^{-5}

Figure 29: ATP hydrolysis rates of free HSP-1 versus DNJ-11 complexed HSP-1 (ceRAC). The ATP hydrolysis rates of different chaperone combinations were determined under single-turnover conditions. [α-^{32}P]ATP–HSP-1 or [α-^{32}P]ATP–ceRAC complexes were incubated with buffer, DNJ-13, DNJ-11 or ceRAC. At different time points the ATP and ADP levels were analyzed by thin-layer chromatography. Hydrolysis rates per second are shown. Data are presented as mean ± SD (n=3). An unpaired Student's t-test was used to assess significance (**P<0.01). ceRAC, HSP-1-DNJ-11 complex. Study was performed by Dr. Roman Kityk.

These observations show that the ATPase activity of HSP-1 is strongly decreased in ceRAC suggesting that HSP-1 in ceRAC is functionally remodeled.

5.3.3 HSP-1 in ceRAC shows diminished peptide binding and protein refolding activity

Since HSP-1 in ceRAC shows repressed ATPase activity, it was interesting to investigate whether HSP-1 in the complex can still bind peptides and substrates. In this context, nascent chain contact of yeast Ssz1 and human Hsp70L1 at the ribosome has not yet been observed excluding so far any Hsp70 activity in context of translation (Hundley *et al*, 2002). To investigate peptide binding of HSP-1 in ceRAC, both HSP-1 and ceRAC were incubated with a small dansyl-labeled Hsp70 binding peptide (D-NR peptide; 7 kDa) in presence or absence of DNJ-13 and 5 mM ATP. Proteins were subsequently loaded on a Superdex200 column to separate potential protein-peptide complexes from the free, unbound peptide.

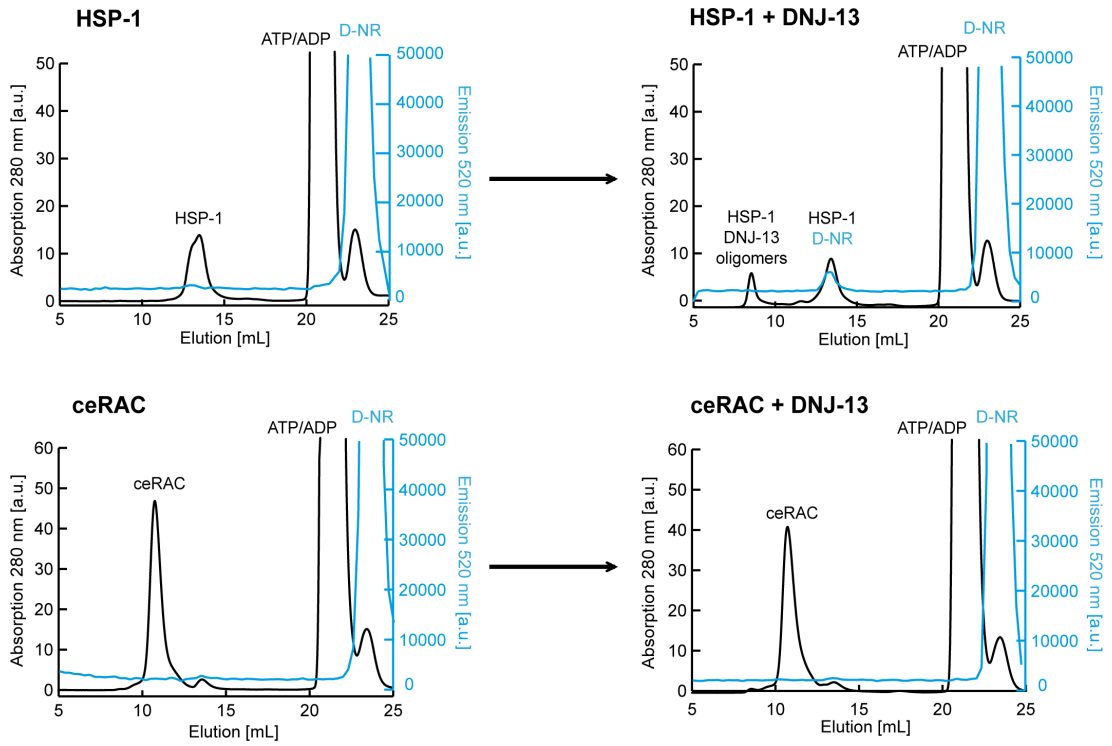

Figure 30: *In vitro* peptide binding of free HSP-1 versus HSP-1 in ceRAC. Peptide binding analyses of HSP-1 or ceRAC in presence and absence of DNJ-13. Proteins were incubated with 80 µM D-NR peptide and 5 mM ATP for 30 min at 20°C and loaded on a Superdex200 gelfiltration column. Diagrams show the elution profile of the proteins (absorbance, black line) and the fluorescence emission of the D-NR peptide (520 nm, blue line). a.u., arbitrary units.

The results showed that HSP-1 efficiently binds the D-NR peptide in presence of DNJ-13 (Fig. 30, upper panel) but HSP-1 in ceRAC does not (Fig. 30, lower panel). However, a potential transient and weak peptide interaction of ceRAC cannot be excluded considering that only stable HSP-1-peptide complexes can be detected with the SEC approach.

Next, the substrate refolding ability of HSP-1 and HSP-1 in ceRAC was investigated. Therefore, an *in vitro* protein refolding assay was established based on the well-known Hsp70 substrate luciferase (Sun *et al*, 2012; Schröder *et al*, 1993). Chemically denatured luciferase was incubated with different chaperone combinations in presence of the substrate luciferin and an ATP regenerating system. To measure substrate refolding, luminescence was recorded over time in a microplate reader. Like Sun and coworkers showed, HSP-1 in combination with DNJ-13 was able to refold and reactivate luciferase (Fig. 31, red square) (Sun *et al*, 2012). However, the refolding acivity of HSP-1 in complex with DNJ-11 was strongly decreased (Fig. 31 ceRAC + DNJ-13; yellow triangle). The activity of HSP-1 in ceRAC, however, was not entirely lost indicating residual chaperone activity of the complexed Hsp70.

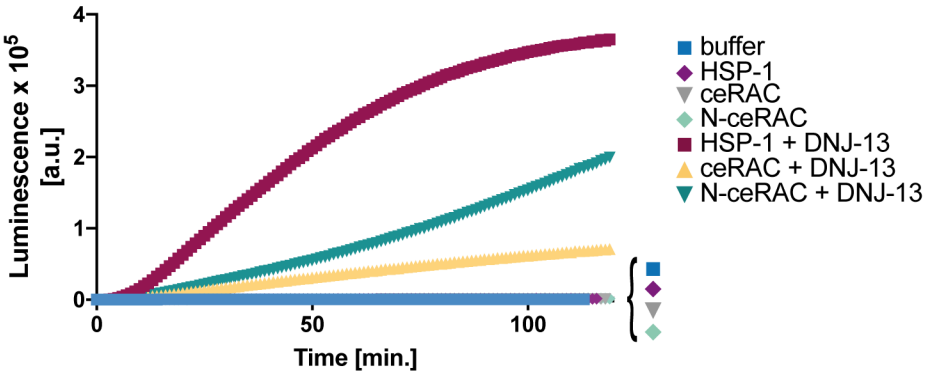

Figure 31: Refolding activity of HSP-1 in ceRAC. Chemically denatured luciferase was incubated for 120 min at 20°C in the presence of indicated chaperone combinations in buffer containing luciferin, ATP and an ATP regenerating system. Luminescence was measured every minute. a.u., arbitrary units; N-ceRAC, DNJ-11N-HSP-1.

5.3.4 The DNJ-11 N-terminus is essential for ceRAC formation

Previous studies showed that in yeast the N-terminus of Zuo1 is essential for RAC formation (Weyer *et al*, 2017; Lee *et al*, 2016; Fiaux *et al*, 2010). To investigate whether ceRAC is assembled in a similar manner, the N-terminus of DNJ-11 (2-35 aa) was deleted in the *E. coli* ceRAC expression vector. *In vitro* pulldown assays of His^6-SUMO-DNJ-11ΔN using Ni-NTA agarose clearly showed that HSP-1 does not interact with DNJ-11ΔN (data not shown) suggesting that also in nematodes the ceRAC the N-terminus of the JDP is necessary for complex formation. Next, it was tested whether the N-terminus of DNJ-11 is sufficient for complex formation with HSP-1. Indeed, a stable complex between the N-terminus of DNJ-11 (2-42 aa) and HSP-1 was generated in *E. coli* and could be purified (N-ceRAC) (Fig. 32). Purification of the DNJ-11N-HSP-1 complex was performed in presence of ATP excluding potential substrate interaction between the small N-terminal peptide

and HSP-1. Interestingly, HSP-1 in N-ceRAC showed a strongly reduced luciferase refolding activity (Fig. 31; N-ceRAC + DNJ-13; green triangle).

All results demonstrate that *C. elegans* reprograms a regular Hsc70 in ceRAC showing Ssz-like features. This functional remodeling occurs upon complex formation with the ribosome-bound JDP DNJ-11. Here the DNJ-11 N-terminus alone is sufficient to decrease HSP-1 activity (Fig. 31).

5.3.5 Molecular dynamics simulation of DNJ-11N-HSP-1 interaction

To gain insight into the remodeling effect of DNJ-11 on HSP-1 in ceRAC, structural homology modeling on the basis of the crystallized yeast Zuo1N-Ssz1 complex (Weyer *et al*, 2017) was performed in cooperation with **Dr. Christoph Globisch** (Department of Chemistry, Computational and Theoretical Chemistry, University of Konstanz).

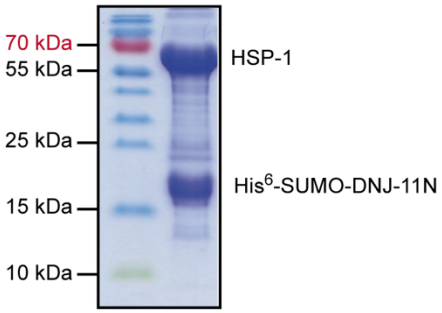

Figure 32: Pulldown of HSP-1 by His^6-SUMO-DNJ-11N. Coomassie stained gel of HSP-1 pulldown by His^6-SUMO-DNJ-11N (2-42 aa) using Ni-NTA agarose in presence of 5 mM ATP.

In the Zuo1N-Ssz1 crystal structure the interdomain linker of Ssz1 is detached from the NBD and the linker binding groove is occupied by Zuo1N contacting the Ssz1 NBD subdomain I and II via a conserved EPVG motif (Fig. 10 B; Weyer *et al.*, 2017). In the Zuo1 homolog of *C. elegans* this motif (^{Zuotin}EPVG/EPAG^{DNJ-11}) as well as a helical motif directly downstream of this motif are conserved (Fig. 15 yellow residues and Fig. 33 A). In Zuo1 this helical motif was shown to interact with a helical element in the interdomain linker of Ssz1 (Weyer *et al*, 2017). Thus, DNJ-11N might interact similarly with the linker binding groove of HSP-1 NBD and also potentially with the HSP-1 linker. However, in canonical Hsp70s the interdomain linker is much shorter than in Ssz-like proteins (Fig. 26; grey residues) and lacks the α-helix that is bound by Zuo1. In order to model the structure of ceRAC, the available Zuo1N-Ssz structure (PBD 5mb9) was used as a template. The truncated SBD of Ssz1, which shows major differences to the HSP-1 SBD, was omitted. Molecular dynamics simulations were performed with the homology model to determine the stability of the DNJ-11N-HSP-1 interaction and special emphasis was put on the helical propensity of the DNJ-11N peptide

and its potential interactions with the interdomain linker of HSP-1. During the simulations, occasional partial unfolding and fast refolding of the N-terminal DNJ-11 peptide confirmed its assumed helical structure (Fig. 33 E). Moreover, the molecular dynamics simulations revealed that the EPAG motif of DNJ-11 (21-24 aa) stably interacts with the hydrophobic groove of HSP-1. An overview of interacting residues and hydrogen bonding residues are presented in the sequence alignment and tables (Fig. 33 A, C and D). The conserved DNJ-11 EPAG motif as well as the conserved residues C26, Y27 and E28 were shown to interact with HSP-1. On the HSP-1 side, the stretch GIFEV (216-220 aa) in the hydrophobic groove and the residues R172, N175, T178 and Q377 interacted with DNJ-11N. Throughout all simulations the HSP-1 interdomain linker was characterized by a high motility and no stable interaction with DNJ-11N was observed (compare Fig. 33 B, left and right panel).

In sum, the structural model predicts interaction between the conserved EPAG motif of DNJ-11N and the hydrophobic linker binding groove of the HSP-1-NBD. Thus, the interdomain linker of HSP-1 in the ATP-bound state seems to no longer bind to the NBD and is replaced by the DNJ-11 N-terminal peptide binding to the NBD linker groove. In this structure the HSP-1 linker shows high flexibility and no stable contact to DNJ-11N in contrast to yeast RAC (Fig. 33B). Allosteric communication in the Hsp70 cycle is regulated by the interdomain linker of Hsp70s which attaches and detaches from the NDB to regulate substrate binding as well as substrate release and ATP hydrolysis (Mayer & Kityk, 2015). Occupation of the linker binding groove by DNJ-11N thus likely leads to an impaired allosteric communication between the NBD and SBD in HSP-1 explaining the observed repressed ATPase and peptide binding activity of HSP-1 in ceRAC.

Figure 33 (page 52): Molecular dynamics (MD) simulations of the DNJ-11N-HSP-1 interaction. **(A)** Alignment of Ssz1/HSP-1 and Zuo1/DNJ-11. The blue highlighted regions correspond to stable/conserved interactions between HSP-1 and DNJ-11 during MD simulations. **(B)** Comparison of the DNJ-11N-HSP-1 structural model (left) with the crystal structure of Zuo1N-Ssz1 (right) showing the NBD of HSP-1/Ssz1(blue), the interdomain linker of HSP-1/Ssz1 (grey) and the interacting loop-helix motif of DNJ-11/Zuotin (orange). Left: Model of DNJ-11N-HSP-1. Side chains of residues forming stable interactions between DNJ-11N and HSP-1 during MD simulations are indicated and colored according to the residue type (gray hydrophobic, green hydrophilic, red negatively charged and blue positively charged). A ghost like representation (light grey) of various HSP-1 interdomain linker conformations that occurred during the simulations demonstrate its high mobility and only transient interactions with DNJ-11N (orange). **(C, D)** Stable intermolecular contacts **(C)** and hydrogen-bonding residues **(D)** observed during the MD simulations of the DNJ-11N-HSP-1 model. **(E)** Snapshots illustrating the high helical propensity of the DNJ-11N peptide (orange) and the high mobility of the NBD-SBD linker (grey). Blue, HSP-1-NBD. MD simulation and data presentation by Dr. Christoph Globisch

A

B

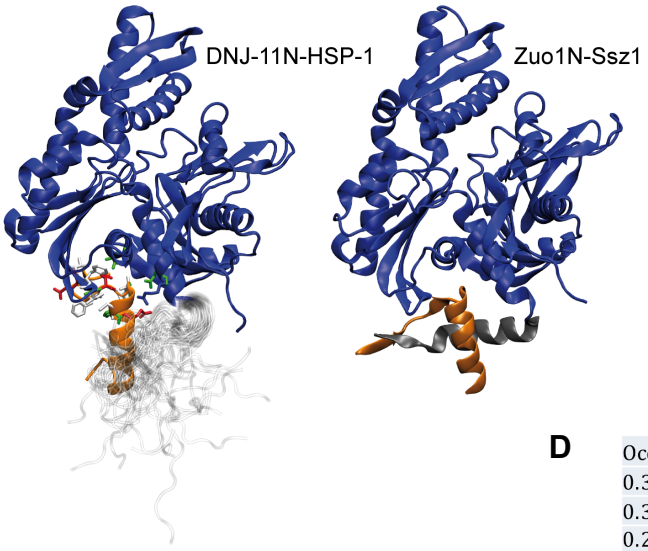

C

Occupancy	contact pair			
	HSP-1		DNJ-11	
0.669	GLN	377	GLY	24
0.905	GLN	377	ALA	23
0.666	VAL	220	GLU	21
0.812	GLU	219	GLU	21
0.858	GLU	219	PHE	20
0.983	PHE	218	GLU	21
0.948	PHE	218	PHE	20
0.551	ILE	217	TYR	27
0.738	GLY	216	CYS	26
0.772	THR	178	GLU	21
0.681	ASN	175	GLU	21

D

Occupancy	Donor		Acceptor	
0.351	THR	178	GLU	21
0.323	ASN	175	GLU	21
0.227	ASN	175	GLU	21
0.228	ARG	172	PRO	22
0.252	ARG	172	GLU	28
0.267	CYS	26	GLY	216
0.644	GLY	24	GLN	377
0.957	GLU	21	PHE	218

E

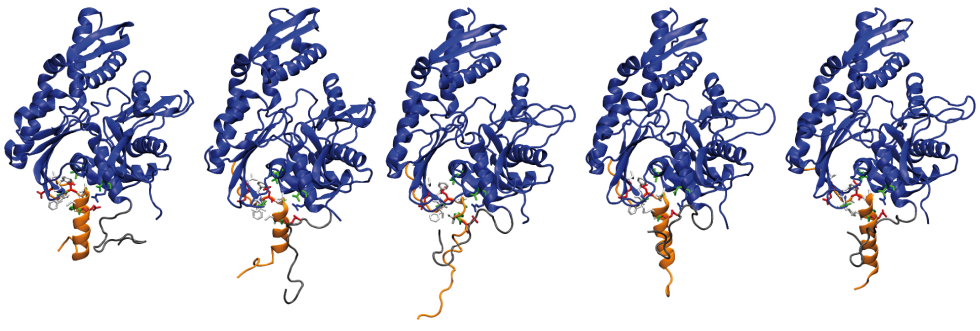

5.3.6 ceRAC interacts with nascent chains at the ribosome

The biochemical and structural data suggest that HSP-1 in ceRAC might be captured in the ATP-bound state in an open conformation that allows, if at all, only low affinity binding to protein substrates (Mayer & Kityk, 2015). The *in vitro* peptide binding analysis (Fig. 30) was not suitable to detect very transient interactions which may occur during translation at ribosomes. To investigate if ceRAC directly interacts with nascent chains, *in vitro* translation and crosslinking experiments were performed by **Annalena Wallisch** (AG Deuerling, University of Konstanz). In reticulocyte lysates a 85 aa long segment of the cytosolic human glucose-6-phosphate isomerase (GPI) was *in vitro* translated and radioactively labeled with [S^{35}]-methionine. The translated mRNA lacked a stop-codon leading to ribosome stalling and generation of stable ribosome nascent-chain complexes (RNCs) carrying nascent chains of a defined length. During translation newly synthesized proteins traverse the ribosomal tunnel of 100 Å length (Wilson & Beckmann, 2011), thus, assuming a fully extended amino acid is 3 – 3.4 Å long, the ribosomal tunnel would be occupied by 30-40 aa (Jha & Komar, 2011; Lu & Deutsch, 2005; Yonath *et al*, 1987; Ban *et al*, 2000). Consequently, ~45-55 aa of the model substrate GPI are exposed outside the tunnel. After *in vitro* translation, these ribosome nascent-chain complexes were pelleted via high salt sucrose cushion centrifugation washing off all ribosome-associated factors. The RNCs were incubated with HSP-1, ceRAC or yeast RAC and crosslinked using the amine-reactive chemical crosslinker DSS. As negative control an HSP-1 variant, HSP-1^{V439F}, was used. The amino acid conversion in the hydrophobic peptide binding pocket abolishes substrate binding (Rüdiger *et al*, 2000; Mayer *et al*, 2000). However, complex formation of ceRAC was not altered due to this mutation, thus this heterodimer could be successfully purified. NAC, which is known to efficiently bind to short nascent chains (see Results -Part B), was used as positive control for nascent chain crosslinking. Finally, crosslinked products between the radiolabeled tRNA-nascent chains and proteins were visualized by immunoblotting and autoradiography.

As expected, addition of NAC resulted in a strong nascent-chain-tRNA crosslink, whereas the buffer control only showed unspecific background signals (Fig. 34, blue arrow). HSP-1 alone did not crosslink to the nascent chain, presumably because a ribosome tethered JDP was missing. However, ceRAC showed a dominant crosslink of approximately 100 kDa in size that matches the size of an HSP-1 (70 kDa) - NC-tRNA (34 kDa) complex (Fig. 34, red arrow). This crosslink was weaker with ceRAC containing the substrate binding deficient HSP-1^{V439F} mutant of ceRAC. Additional crosslink bands might present either HSP-1-NC-tRNA complexes containing several intra-HSP-1 crosslinks or crosslinks to DNJ-11. Addition of HSP-1 to ceRAC did not lead to

increased intensity of the crosslink bands (Fig. 34, red arrow). This observation argues against a simultaneous binding of ceRAC and HSP-1 to the 85 aa long nascent chain.

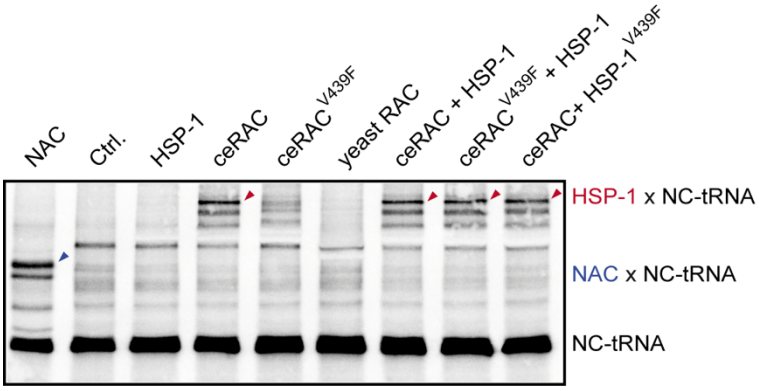

Figure 34: ceRAC binds nascent chains at the ribosome. (A) *In vitro* translation of the cytosolic 85 aa long model substrate GPI in rabbit reticulocyte extract. Stable ribosome nascent-chain complexes (RNCs) were generated by translation of a transcript lacking a stop codon. After translation RNCs were incubated with indicated chaperone combinations. An only buffer control was included (Ctrl.). Proteins were labeled with [S^{35}]-methionine and crosslinked using the amine residue crosslinker DSS. Samples were separated by SDS-gel electrophoresis and crosslinked products were visualized by autoradiography. The substrate binding deficient HSP-1 mutant HSP-1^{V439F} was used as negative control. NC, nascent chain. Experiment was performed by Annalena Wallisch.

Surprisingly, addition of ceRAC^{V439F} in combination with uncomplexed HSP-1 showed a crosslink which resembles the observed pattern of wildtype ceRAC. Thus, ceRAC can recruit an additional HSP-1 to nascent chains independently from its own substrate interaction. However, for yeast RAC no crosslinked products could be observed.

5.3.7 ceRAC functionally cooperates with HSP-1

All *in vitro* experiments showed that HSP-1 in ceRAC is functionally remodeled showing repressed ATPase and substrate binding activity. Consequently, ceRAC is not able to comply full chaperone function at the ribosome. However, crosslinking experiments indicated that ceRAC binds nascent polypeptide chains already early during translation and serves therefore more likely as a guiding chaperone and cofactor that recruits additional Hsp70s to nascent substrates. The J-domain of DNJ-11 most likely stimulates the ATPase of a free HSP-1. To further validate the function of ceRAC as co-chaperone, D-NR peptide binding analyses by SEC were performed. Indeed, the presence of HSP-1 induced D-NR peptide of HSP-1 (Fig. 36 A). This finding is consistent with single turnover ATP measurements showing that ceRAC stimulates ATP hydrolysis in HSP-1

(Fig. 36 B). Additionally, *in vitro* ribosome sedimentation experiments showed that HSP-1 is recruited by ceRAC to 80S RNCs (Fig. 36 C, compare +80S pellet fractions). The findings that ceRAC acts as a cofactor of an additional HSP-1 *in vitro* is consistent with the observed developmental defect in worms expressing the J-domain dead mutant DNJ-11^{H129Q} (Fig. 22 B and C). Nevertheless, to exclude any impact of this mutation on ceRAC complex formation, co-immunoprecipitation experiments were performed. As expected, complex formation is not perturbed by the amino acid replacement (Fig. 35), thus the observed phenotype resulted from inefficient HSP-1 stimulation via DNJ-11 at the ribosome. However, *in vitro* the ceRAC-HSP-1 system was ineffective in refolding of denatured luciferase (Fig. 36 D).

In sum, these data suggest that also in nematodes a chaperone triad acts in co-translational protein folding, similar to yeast and human cells.

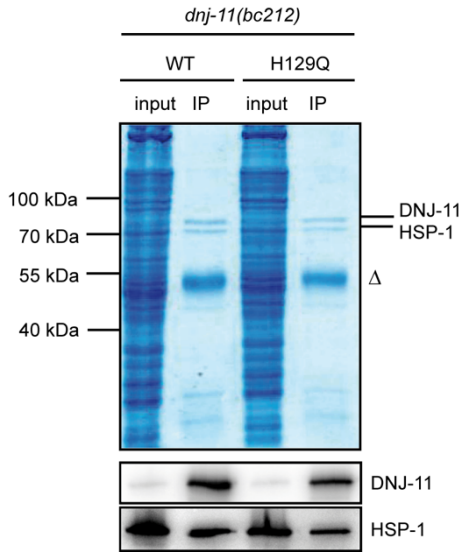

Figure 35: Complex formation of ceRAC is not impeded by HPD motif mutation in DNJ-11. Pulldown of ceRAC in total lysates of DNJ-11 wildtype (DNJ-11^{WT}) or DNJ-11 QPD mutant (DNJ-11^{H129Q}) expressing worms (*dnj-11(bc212)* background) by DNJ-11 antibodies. Samples of the input and IP were analyzed by SDS-PAGE and Coomassie staining or immunoblotting. DNJ-11 and HSP-1 were detected by specific antibodies. Δ, IgG heavy chain.

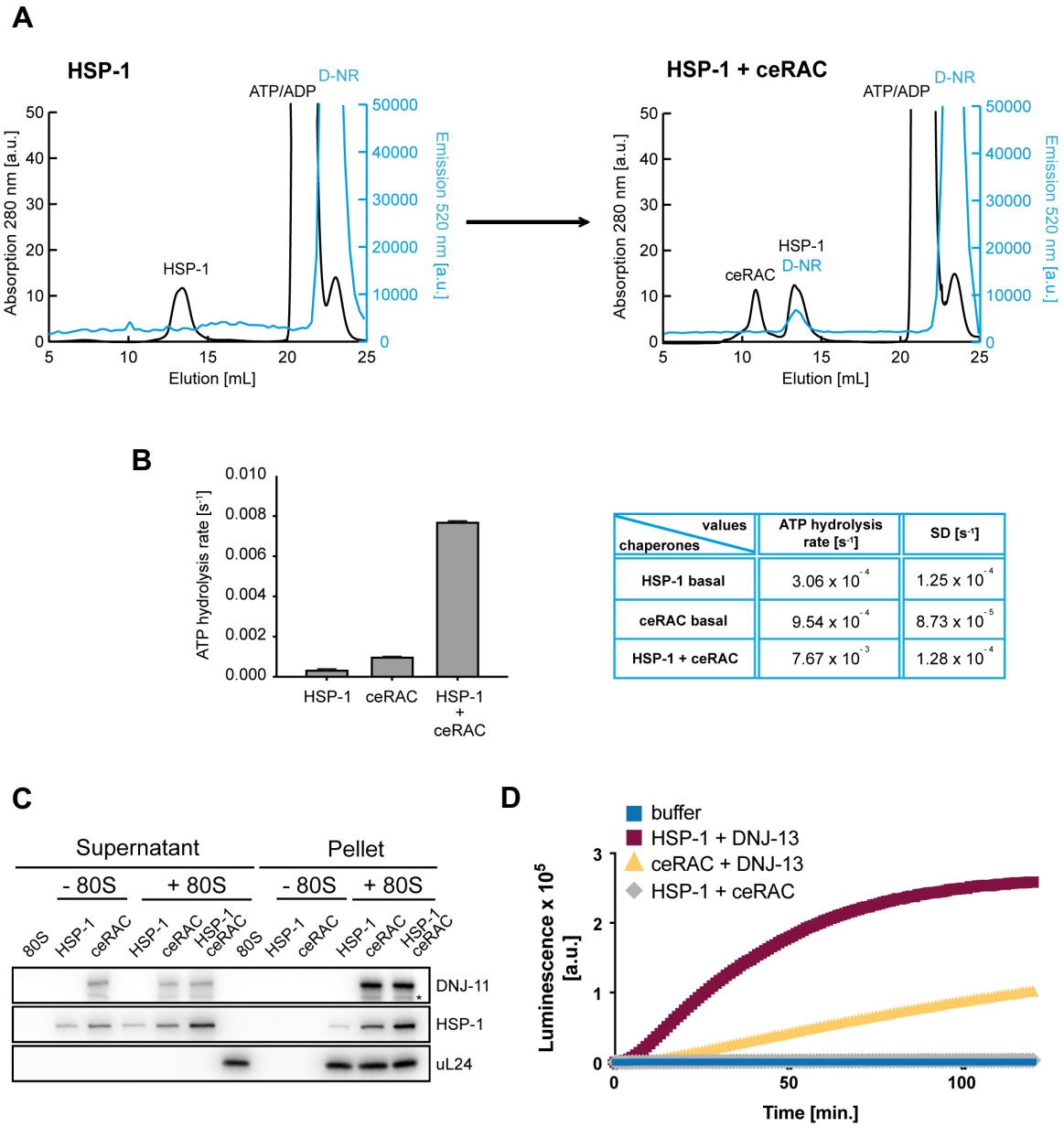

Figure 36: Functional cooperation of ceRAC and HSP-1. (A) Peptide binding analyses of HSP-1 in presence and abscence of ceRAC. Proteins were incubated with 80 µM D-NR peptide and 5 mM ATP for 30 min at 20°C and subsequently loaded on a Superdex200 gel filtration column. Elution profile (absorbance at 280 nm, black) and fluorescence of D-NR peptide (emission 520 nm, blue) are shown. **(B)** ATP hydrolysis rates of indicated chaperone combinations were determined under single-turnover conditions. [α-^{32}P]ATP–HSP-1 or [α-^{32}P]ATP–ceRAC complexes were incubated with buffer or ceRAC. At different time points ATP and ADP levels were analyzed by thin-layer chromatography. Hydrolysis rates per second are shown. Data are presented as mean ± SD (n=3). ceRAC, HSP-1-DNJ-11 complex. Experiment was performed by Dr. Roman Kityk. **(C)** *In vivo* ribosome sedimentation analysis. Purified HSP-1 and ceRAC were incubated with 80S *C. elegans* ribosomes as indicated (30 min, 18°C). In simultaneously binding approaches, ribosomes were preincubated with ceRAC, HSP-1 was subsequently added and incubated for additional 5 minutes. After ultracentrifugation, proteins in the supernatant and pellet fractions were analyzed by immunoblotting. **(D)** Chemically denatured luciferase was incubated for 120 min at 20°C in the presence of different chaperone combinations in buffer containing luciferin, ATP and an ATP regenerating system. Luciferase refolding was measured by recording the luminescence every minute using a microplate reader.

5.3.8 ceRAC function during heat and aging stress

The proteostasis network efficiency decreases tremendously during aging, thus imposing a considerable burden on every organism (Walther *et al*, 2015). Aging is accompanied by a decline in the overall translation rate evident by a decrease in polysome amount in *C. elegans* (Kirstein-Miles *et al*, 2013). To assess potential effects of aging on ceRAC, soluble protein levels of DNJ-11 and HSP-1 at day 2 and day 12 of adulthood were compared.

Translation shut down during aging was clearly reflected by reduction in uL16 protein levels (Fig. 37 A). Similarly, also the protein levels of DNJ-11 but not HSP-1 were strongly decreased. To investigate if the decline in DNJ-11 protein levels correlates with a decrease in *dnj-11* transcription, mRNA levels of young and old nematodes were compared. As control the mRNA expression of two inducible Hsp70s (*C12C8.1* and *F44E5.4*) was analyzed. As expected, their mRNA levels were strongly elevated at day 12 of adulthood (Brehme *et al*, 2014). Interestingly, transcript levels of *dnj-11* and also of *hsp-1* were unaltered in aged worms (Fig. 37 B). Hence, the observed decrease in DNJ-11 protein levels cannot be explained by lower *dnj-11* gene expression.

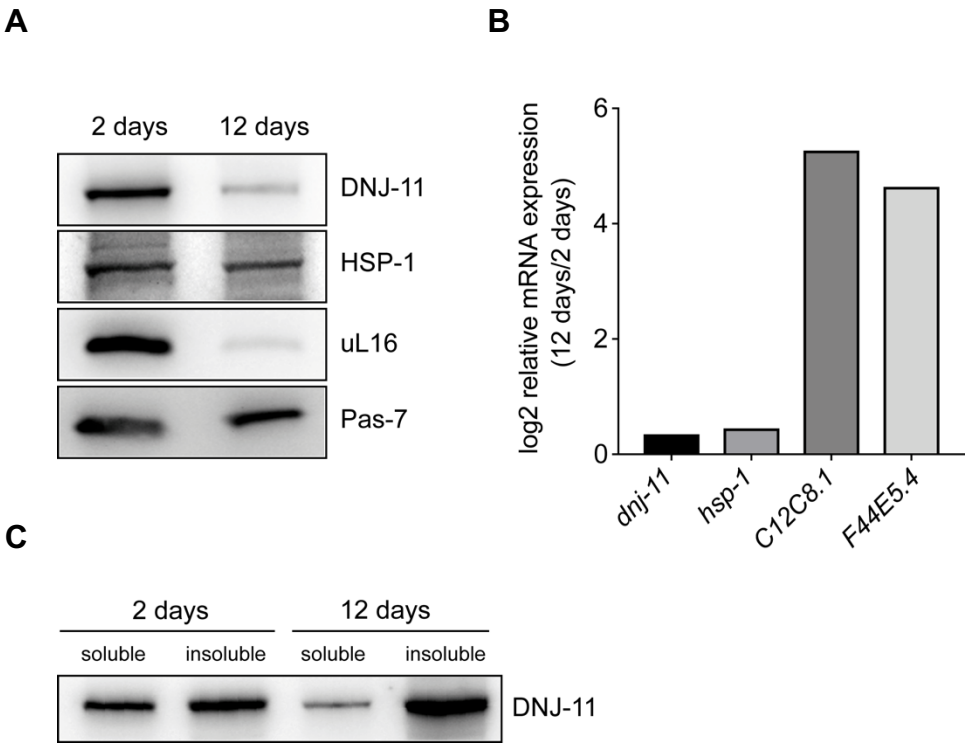

Figure 37: Function of ceRAC during aging. (A) Immunoblot analyses of soluble protein pool of wildtype nematodes at day 2 and day 12 of adulthood. Proteins were detected by specific antibodies. Pas-7 served as loading control. **(B)** Relative mRNA expression of different chaperones in 12 days versus 2 days old adult worms was determined by qPCR. *Ama-1* served as reference gene. Change in expression was calculated using the $2^{-(\Delta\Delta Ct)}$ method. **(C)** Soluble and insoluble (2% SDS) DNJ-11 protein levels in worms at indicated age were analyzed by immunoblotting using a specific DNJ-11 antibody.

Indeed, immunoblot analyses showed that during aging DNJ-11 significantly shifts to the insoluble protein fraction (Fig. 37 C). This shift might indicate aggregation of DNJ-11 or it can be speculated that the ceRAC chaperone complex might associate with protein aggregates, which strongly accumulate in aging worms (Walther *et al*, 2015; David *et al*, 2010). However, as class C J-domain protein, DNJ-11 was so far not considered as part of the disaggregation machinery in *C. elegans* (Nillegoda *et al*, 2015, 2017; Kirstein *et al*, 2017). A potential ribosome-independent function of ceRAC remains to be investigated.

During their life cycle organisms have to cope with different kind of stressors, which include apart from aging also abiotic stresses like heat shock. The gene expression of many chaperones from different families is induced upon heat shock (Lindquist, 1980). To elucidate the impact of heat stress on ceRAC expression, nematodes were heat shocked at 35°C for one hour and recovered for 24 hours at 20°C. As expected, the mRNA levels of cytosolic heat inducible Hsp70s (*C12C8.1* and *F44E5.4*) were strongly elevated (Fig. 38). In contrast, expression of HSP-1 was only slightly increased (2-fold). These observations are consistent with earlier published work showing an increase in HSP-1 mRNA levels of 2-6 fold after heat shock (Heschl & Baillie, 1990; Snutch *et al*, 1988). The transcript levels of DNJ-11 did not change after heat shock, suggesting that ceRAC is not a stress-regulated chaperone complex.

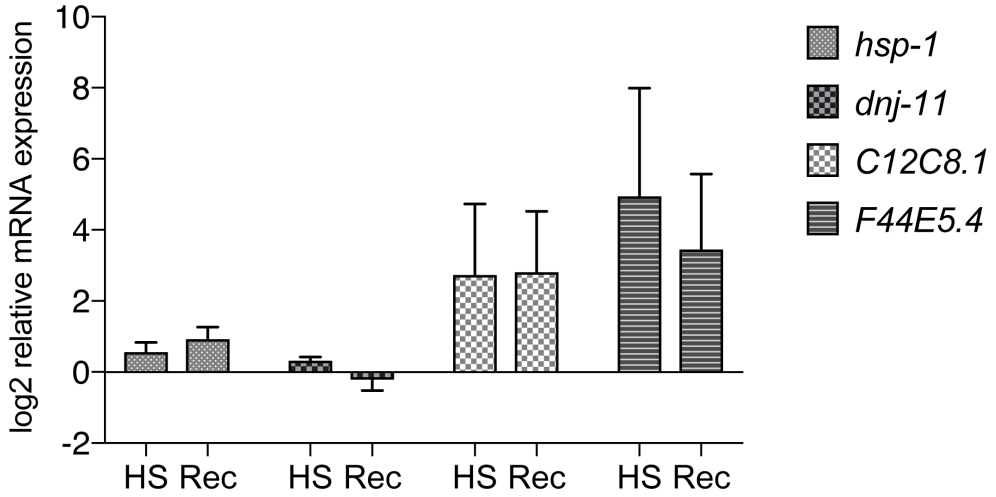

Figure 38: Transcript levels of chaperones after heat shock and recovery phase. *C. elegans* (day 2 of adulthood) were heat shocked at 35°C for one hour and recovered at 20°C for 24 hours. Transcript levels of indicated chaperones were determined via qPCR. *Ama-1* served as reference gene. Relative expression was calculated via the $2^{-(\Delta\Delta Ct)}$ method. Data are presented as mean ± SD (n=3). HS, heat shock. Rec, Recovery.

5.4 The mammalian ribosome-associated complex (mRAC)

5.4.1 Depletion of HSPA14 reduces MPP11 protein levels

RAC was assumed to be conserved in higher eukaryotes. However, nematodes display an animal phylum that lacks the Ssz1 component of RAC and instead uses a canonical Hsc70 with reconfigured catalytic activity to serve as a low affinity binding chaperone at the ribosome. These findings raise the question, why many eukaryotes still use an atypical Hsp70 without any detectable activity. It remains unknown, how flexible this RAC system might be in organisms which possess an Ssz1 homolog. Do Zuotin homologs in these species partner with a classical Hsc70/Hsp70 when Ssz-like proteins are absent? Are non-canonical Hsp70s required or can those be replaced by canonical Hsc70/Hsp70s? To answer this question, further experiments focused on mRAC in human HEK293 cells. Cancer cells are generally characterized by a high translation rate and studies showed that many cancer types show a tremendous overexpression of the human Zuotin homolog MPP11 (Greiner *et al*, 2003; Resto *et al*, 2000; Imamura *et al*, 2018). First, ribosome binding of MPP11 was investigated using sucrose density gradient fractionation analyses. Polysome profiles showed a typical ribosomal pattern and illustrate highly active translation evident by high levels of late polysome species (Fig. 39). MPP11 associated with 80S ribosomes and polysomes consistent with the observation by Otto and coworkers (Otto *et al.*, 2005). Though, a large fraction of MPP11 was ribosome unbound and found in the soluble part of the density gradient.

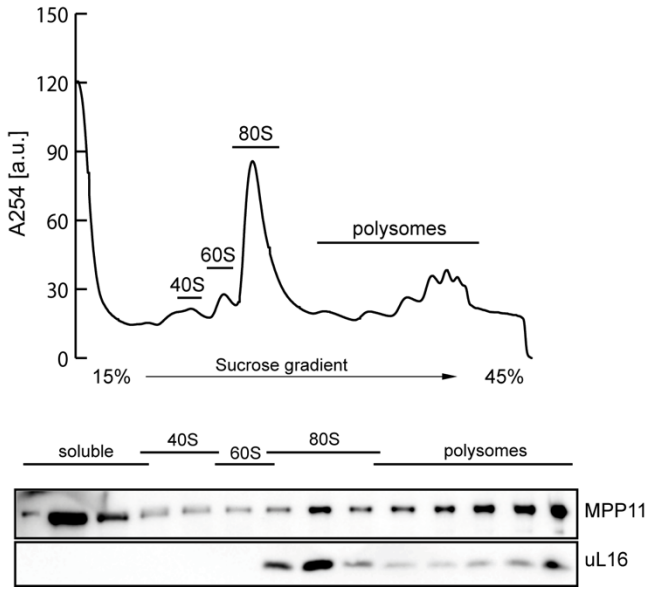

Figure 39: Ribosome association of MPP11 in HEK293 cells. Ribosomal species were separated by sucrose density gradient (15%-45%) fractionation. Fractions throughout the gradient were analyzed by immunoblotting. MPP11 was detected by a specific antibody and uL16 served as ribosomal marker.

Next, the Ssz1 homolog HSPA14 (Hsp70L1) was depleted in these HEK293 cells to investigate a possible partner switch in mRAC. The knockdown was performed by transfection of four different siRNAs and three different concentrations thereof. Cells were incubated with transfection media for either 24, 48 or 72 h. In 12-well plates the siRNA #1 and #4 showed the best results 48 and 72 h post transfection (Fig. 40 A). Depletion of HSPA14 led to diminished MPP11 protein levels suggesting that stability of MPP11 depends on its specific Hsp70 partner.

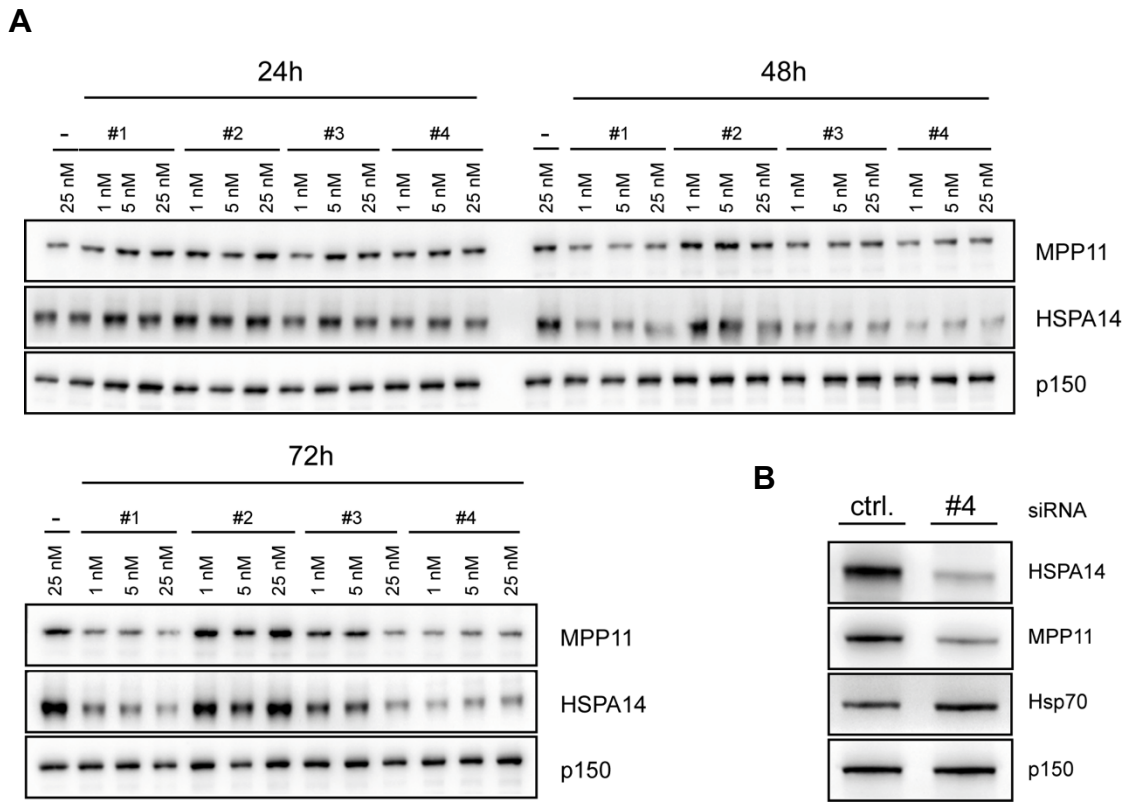

Figure 40: HSPA14 knockdown reduces MPP11 protein levels in HEK293 cells. (A) Knockdown of HSPA14 in HEK293 cells using four different siRNAs (#1-#4) in three varying concentrations (1, 5 and 25 nM). As control, cells were transfected with an unspecific siRNA at 25 nM concentration (-). Transfection was performed in 12 well plates. Cells were analyzed 24, 48 or 72 h post transfection. After cell lysis samples were adjusted to equal cell numbers and aliquots were analyzed by immunoblotting. Proteins were detected by specific antibodies. p150 served as loading control. **(B)** Knockdown of HSPA14 with siRNA #4 in 10 cm dishes. After blotting the membrane was probed with specific antibodies.

To confirm this result, knockdown with siRNA #4 was conducted in a larger scale using 10 cm dishes for transfection. Immunoblot analysis underlines the effect of HSPA14 depletion on MPP11 (Fig. 40 B). This finding agrees with the observation that MPP11 knockdown in HeLa cells reduces HSPA14 protein levels (Jaiswal *et al*, 2011). Interestingly, Hsp70 protein levels are slightly elevated arguing for a stress compensatory effect dealing with the loss of HSP14. To detect a possible partner

switch in mRAC, these cells were used to perform co-immunoprecipitation followed by mass spectrometric analyses. Unfortunately, the simultaneously depletion of MPP11 impeded with pull-down efficacy and so far, it was not possible to detect MPP11 association with canonical Hsc70/Hsp70.

These findings argue against a potential Hsp70 partner switch in mRAC, suggesting that the recruitment of classical Hsp70 as subunit of RAC only occurs in species that have not evolved an Ssz-like Hsp70, like nematodes.

6. Discussion and Outlook – Part A

Cellular homeostasis depends on correct *de novo* protein folding, transport and degradation. An imbalance in these pathways leads to formation of protein deposits which can cause cellular or tissue-specific toxicity as seen in many human diseases. Cells are able to cope with proteotoxic stress with the help of molecular chaperones which control major steps of protein maturation and degradation during protein lifetime. Already during protein biogenesis at ribosomes nascent polypeptide chains are guided by co-translational chaperones and targeting factors that guarantee successful processing, transport and folding.

In eukaryotes a ribosome-tethered chaperone triad assists newly synthesized polypeptides to fold in their three-dimensional structure. RAC consists of an ATPase deficient, truncated Hsp70 (yeast: Ssz1, human: Hsp70L1/HSPA14) and a J-domain protein (yeast: Zuo1, human: MPP11/DNAJC2), which facilitates ATP hydrolysis of an additional catalytically active Hsp70. Zuo1/MPP11 anchors the complex to the ribosome and positions the J-domain close to the ribosomal tunnel, where it stimulates the ATPase of an Hsp70, which then binds nascent chains. However, the exact role of Ssz1 and Hsp70L1 in RAC is poorly understood. The present study revealed that Ssz-like proteins are absent in nematodes and many arthropods, though Zuo1 homologs seem to be conserved in all eukaryotic species (Fig. 12 and 13). This observation indicates that functionally and structurally different RAC systems have evolved in eukaryotes.
During this study a new ribosome-associated complex (ceRAC) in *C. elegans* was identified and biochemically as well as structurally characterized revealing that also classical active Hsp70s can be functionally remodeled to serve as a RAC subunit.

The main findings of this study are summarized in the following:

I. In *C. elegans* the J-domain protein DNJ-11 directly binds in a salt-sensitive manner to ribosomes *in vitro* and *in vivo* and partially complements the growth defect of *Δzuo1* yeast cells, showing that DNJ-11 is a *bona fide* functional homolog of Zuotin.

II. DNJ-11 is most abundant in metabolically active tissues, like gonads and embryonic cells.

III. The constitutively expressed, catalytically active HSP-1 (Hsc70) forms a stable ribosome-bound heterodimeric complex with DNJ-11 (ceRAC), which is neither disrupted by ATP nor high salt concentrations.

IV. HSP-1 is functionally reconfigured in the complex with DNJ-11 showing repressed ATPase, peptide-binding and chaperone activity.

V. Complex formation of ceRAC is mediated by an interaction of the N-terminus of DNJ-11 with the HSP-1 interdomain linker binding groove preventing allosteric communication between the NBD and SBD of HSP-1, which explains the diminished ATP hydrolysis rate and refolding ability of HSP-1 in ceRAC.

VI. On the ribosome ceRAC acts as a holding chaperone that transiently binds and hands over newly synthesized nascent chains to an additional HSP-1.

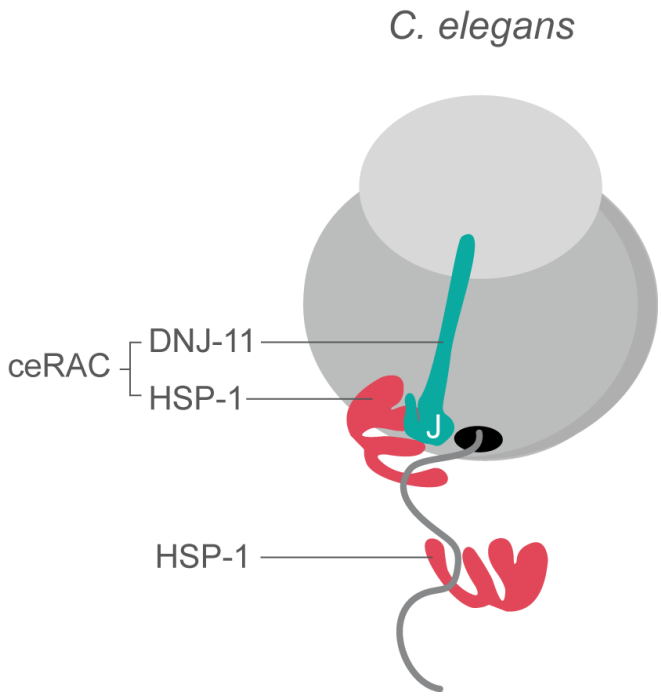

Figure 41: The ribosome-associated complex in *C. elegans* (ceRAC). Like in other eukaryotes, *de novo* protein folding in nematodes is assisted by a RAC-Hsp70 system. ceRAC consists of the J-domain protein DNJ-11 and the canonical, active HSP-1 (Hsc70). Ribosome binding is mediated by the DNJ-11 subunit positioning its J-domain (J), as well as its complex partner HSP-1, near the ribosomal tunnel exit. HSP-1 in ceRAC transiently contacts and likely hands over nascent polypeptide chains to another HSP-1 that is recruited by the J-domain of DNJ-11. It was shown that HSP-1 in ceRAC is functionally remodeled as ATPase, peptide binding and protein refolding activities are repressed.

The conserved function of RAC in eukaryotes

Using an active Hsc70 rather than an Ssz-like protein to build a RAC-like complex is a fascinating concept. However, the function of RAC systems seem to be conserved in eukaryotic species. Growth defects of *zuo1Δssz1Δ* cells were partially complemented by expression of human MPP11 and additional co-expression with Hsp70L1 even enhanced the growth of the complemented cells (Otto *et al*, 2005; Jaiswal *et al*, 2011). It seems that DNJ-11 is functional in yeast, but still it remains unclear how this JDP interacts with the yeast Hsp70 family. In human cells complementation assays revealed that MPP11 was unable to functionally interact with Ssz1 and it was therefore speculated that it might act together with a non-ribosome-bound cytosolic Hsp70, like Ssa (Otto *et al*, 2005). In line with this observation, MPP11 rescued both the growth of *Δzuo1* and *Δzuo1Δssb* showing that MPP11 does not require Ssb to function in yeast (Hundley *et al*, 2005). Moreover, MPP11 stimulated the ATPase of Ssa but not of Ssb (Hundley *et al*, 2005). Interestingly, Hsp70L1 forms a functional complex with Zuo1 (Otto *et al*, 2005). These studies show that RAC subunits are partially interchangeable in different species.

In this study, *C. elegans* DNJ-11 was found to partially complement the growth defect of *Δzuo1* cells (Fig. 20 A). Here, following questions need to be answered in future: Can DNJ-11 partner with Ssz1 or does DNJ-11 in yeast build a complex with a canonical Hsp70? Moreover, it needs to be investigated whether DNJ-11 acts as a J-domain cofactor of the yeast specific ribosome-bound Ssb or of a cytosolic Hsp70 such as Ssa. One can speculate that DNJ-11 is also not able to functionally interact with Ssb and might act in concert with a cytosolic Hsp70 as seen for the human homolog MPP11 (Hundley *et al*, 2005; Jaiswal *et al*, 2011).

A functional chaperone triad at the *C. elegans* ribosome

ceRAC was shown to be a very stable complex *in vivo*, which was shown by co-immunoprecipitation in presence of high salt concentrations (Fig. 24). However, knockdown experiments clearly confirmed that stability and function of DNJ-11 in *C. elegans* depends on its complex formation with HSP-1, reminiscent to the yeast and human orthologs that require their specific Hsp70 partner to become functionally active (Fig. 27 A) (Jaiswal *et al*, 2011; Huang *et al*, 2005). Moreover, instability of DNJ-11 in absence of HSP-1 contradicts with a possible Hsp70 partner switch in ceRAC. *Hsp-1* knockdown induced the expression of Hsp70 proteins (C12C8.1 and F44E5.4), but neither of these chaperones partnered with DNJ-11.

As shown for yeast and mammalian RAC, the J-domain is essential for proper function of ceRAC *in vivo* (Gautschi *et al*, 2002; Jaiswal *et al*, 2011). However, a loss-of-function mutation of the J-domain does not resemble the phenotype of a complete deletion of DNJ-11, thus other protein

domains are equally important (Fig. 22 B and C). Interestingly, DNJ-11$^{\Delta SANT}$ expressing nematodes showed a similar phenotype as DNJ-11^{H129Q} worms. Therefore, deletion or mutation of both domains might generate a complete knockout phenotype.

Canonical Hsp70s were shown to be stimulated by a variety of co-chaperones, thus they are not limited to one specific JDP partner (Craig & Marszalek, 2017). It can be envisioned that upon J-domain mutation in DNJ-11 other cytosolic JDPs (e.g. DNJ-13) are recruited to the ribosome to stimulate HSP-1's ATPase and support co-translational protein folding. Obviously, this system works less efficient *in vivo*, as seen for the expression of DNJ-11^{H129Q} (Fig. 22 B and C). In yeast, mutation of the HPD motif in the J-domain of Zuo1 leads to inefficient recruitment of Ssb to ribosomes and these cells resemble the phenotype of a *zuo1* knockout. Thus, Ssb is not able to functionally interact with another JDP except Zuo1 (Gautschi *et al*, 2002).

Proper function of HSP-1 at the ribosome depends on nucleotide exchange factors (NEFs). Nucleotide exchange of Ssb is achieved by three different NEFs, namely Sse1, Sln1 and Fes1 (Shaner *et al*, 2006; Sondermann *et al*, 2002; Dragovic *et al*, 2006). In humans, it was shown that Bag-1 functionally interacts with the mRAC/Hsp70 system (Jaiswal *et al*, 2011). In *C. elegans* three cytosolic NEFs are potential partners of the ceRAC/HSP-1 system (Bag-1, UNC-23 and Hsp110, see Table A3). Sun and coworkers showed that HSP-1 functions with Bag-1 in luciferase refolding (Sun *et al*, 2012), cooperates with Hsp110 in protein disaggregation (Rampelt *et al*, 2012), and nematode muscle functionality was shown to be dependent on cooperative function between HSP-1 and UNC-23 (Papsdorf *et al*, 2014). Thus, HSP-1 cooperates with all three cytosolic NEFs. Therefore, future investigations will focus on nucleotide exchange in the ceRAC/HSP-1 system at ribosomes and the specific NEF(s) involved.

Recently, it was postulated that Ssz1 homologs serve as guiding chaperones at the tunnel exit, passing on the nascent chain to an additional Hsp70 (Leidig *et al*, 2013; Weyer *et al*, 2017). This model suggests that a direct substrate interaction of RAC occurs at translating ribosomes. However, Ssz-like proteins miss the α-helical lid of the SBD and a direct interaction between nascent chains and Ssz-like proteins was not demonstrated yet. Nevertheless, lidless mutants of Hsc70 were shown to still exhibit substrate binding and release activity upon ATP binding (Mayer *et al*, 2000; Misselwitz *et al*, 1998). Moreover, previous studies showed that only the nucleotide binding domain and the interdomain linker are critical for RAC function arguing against a critical role of Ssz1 in co-translational protein folding (Hundley *et al*, 2002; Huang *et al*, 2005).

Thus, it can be speculated that in *C. elegans* the presence of an active Hsc70 instead of an Ssz-like protein enables peptide binding by RAC. Size exclusion chromatography approaches showed no peptide binding of HSP-1 in ceRAC (Fig. 30), thus a potential ceRAC-nascent chain interaction

might be rather transient and thus not detectable using purified components and peptide substrates *in vitro*. Strikingly, ceRAC crosslinked to radiolabeled nascent chains in *in vitro* translation approaches and this interaction obviously comprises the canonical peptide binding groove of HSP-1 (ceRAC^{V439F}). It is conceivable that organisms using a canonical Hsc70 in RAC rely on a low affinity chaperone system that hands over the nascent polypeptide to an additional Hsc70/Hsp70. Thus, at the ribosome ceRAC might hand over newly synthesized proteins to an extra HSP-1. Indeed, ceRAC and HSP-1 associate simultaneously with 80S ribosomes and HSP-1 binds the small D-NR peptide in presence of ceRAC (Fig. 36 A). These observations match with the measured ATPase stimulation of HSP-1 by ceRAC (Fig. 36 B). However, addition of both ceRAC and HSP-1 in the crosslink approach did not intensify the radioactive crosslink band to the model substrate (Fig. 34). This observation can be explained by the length of the cytosolic model substrate (GPI). Nascent chains of 85 aa in length expose only approximately 45-55 aa outside the ribosome, thereby simultaneous contact of ceRAC and HSP-1 might not be possible yet, due to steric hindrance. Nevertheless,

HSP-1 could engage the nascent chain when client contact of ceRAC (ceRAC^{V439F}) was inhibited (Fig. 34). Thus, substrate binding by ceRAC at the ribosome seems not to be a prerequisite for subsequent client binding by HSP-1. To analyze a simultaneous action of ceRAC and HSP-1 in *de novo* protein folding at the ribosome, RNCs with longer nascent chains need to be generated and also substrate specificity should be tested by translation of ER or mitochondrial substrates (e.g. mitochondrial Hsp60 or ER chaperone GRP78/BiP). This approach should also include NAC to test for sequential binding to longer model substrates by NAC and RAC, although both complexes do not bind simultaneously to ribosomes due to overlapping ribosome contact sites (Results part B). In contrast, yeast RAC showed no crosslink to the nascent chains (Fig. 34). It can be envisioned that the interaction is even more transient compared to ceRAC, or yeast does not depend on a low affinity Hsp70 at the ribosome (Hundley *et al*, 2002).

All obtained results in *C. elegans* point to a functional chaperone triad at the ribosome as seen in yeast and mammals (Preissler & Deuerling, 2012). Yet, ceRAC together with HSP-1 showed no luciferase refolding ability *in vitro* (Fig. 36 D). It can be speculated that *in vitro*, in contrast to the JDP DNJ-13, DNJ-11 in ceRAC does not guide protein substrates to the additional HSP-1. *In vivo* this chaperone triad is tethered to the ribosome and directly approaches the nascent polypeptide chain. Thus, there is no need for substrate guidance to HSP-1 via DNJ-11.

Structural modeling of the non-canonical DNJ-11-HSP-1 complex

Due to ceRAC-substrate crosslinks at the ribosome it can be speculated that HSP-1 is locked in the ATP low affinity state that shows high substrate-binding on and off-rates due to an open α-helical

SBD lid. Interestingly, structure modeling revealed a distinct interaction surface comprising the EPAG motif of the DNJ-11 N-terminus and the interdomain linker groove of HSP-1 (Fig. 33). Thus, RAC formation in yeast and nematodes is accomplished in a very similar way (Weyer *et al*, 2017). Nevertheless, it still needs to be investigated whether the interdomain linker of HSP-1 is as flexible as shown in the structural modeling (Fig. 33). In contrast to the yeast structure, the NBD of HSP-1 was omitted in molecular dynamic simulations and may influence linker flexibility.

Moreover, the ceRAC model predicts that HSP-1 adopts a state wherein the N-terminus of DNJ-11 occupies the interdomain linker contact site in the NBD preventing allosteric communication between the NBD and SBD of HSP-1. Inhibition of the interdomain communication of HSP-1 impedes with high affinity substrate binding and ATP hydrolysis (Kityk *et al*, 2015; Vogel *et al*, 2006). Hence, this specific structure can explain the low ATPase rate (Fig. 29) and the diminished luciferase refolding ability (Fig. 31) of HSP-1 in ceRAC. Strikingly, addition of the N-terminal DNJ-11 peptide *in trans* was ineffective in reprogramming HSP-1, because the peptide was bound as substrate, preventing a RAC-like complex formation with HSP-1 *in vitro* (data not shown).

In addition, *in vitro* reconstitution of ceRAC using separately purified DNJ-11 and HSP-1 is not possible (Fig. 28 B) and thus complex formation is most likely achieved co-translationally *in vivo*.

Moreover, the structure of yeast RAC revealed that the SBDβ lacks the β8 strand but is structurally complemented by a β-sheet of the Zuo1 N-terminus. Thus, Ssz1 comprises a potential substrate binding cleft. This SBDβ structure resembles the ADP-bound state of canonical Hsp70s, like DnaK (Weyer *et al*, 2017). Interestingly, in the ATP bound state of canonical Hsp70s, the β8 strand of the SBDβ is detached. It can be speculated that HSP-1 in ceRAC adopts this ATP-bound conformation of the SBDβ and the β-sheet of the DNJ-11 N-terminus structurally complements the detached β8 strand as seen in the yeast RAC structure (Weyer *et al*, 2017).

Interestingly, the canonical substrate binding groove in Ssz1 is characterized by an amino acid replacement (Fig. 26, HSP-1 V439, Ssz1 F446). This mutation might reduce substrate binding affinity *per se* due to a blockage of the hydrophobic substrate binding pocket as shown before for the DnaK^{V436F} mutant (Rüdiger *et al*, 2000).

The cellular function of *C.elegans* RAC

DNJ-11 in *C. elegans* is low abundant indicating substrate specificity of the ceRAC-HSP-1 system at ribosomes (Gamerdinger, 2016). In yeast it was shown that 2% of normal Zuo1 and Ssz1 levels are sufficient for normal growth (Hundley *et al*, 2002). Nevertheless, in life span analyses depletion of DNJ-11 to residual 11% resulted in a mild decrease in median lifespan showing that this ribosome-bound JDP is required during adulthood (Fig. 21 B). To investigate the specific function of ceRAC at ribosomes, pulldown of DNJ-11-associated ribosomes and microarray analyses of the

bound mRNAs can identify substrates that rely on specific co-translational guidance by the chaperone triad of ceRAC and HSP-1.

In addition, ceRAC is expressed in tissues with high metabolic rates, like the reproductive system and embryonic cells (Fig. 18 C). As previously shown by other researchers, DNJ-11 is important during embryogenesis and DNJ-11 knockout worms show a reduced brood size, developmental defects and slow growth (Hatzold & Conradt, 2008) (Fig. 22 B and C). Hatzold and Conradt revealed that DNJ-11 is required for the death of the neuro-secretory motoneuron sister cells during early embryonic development via transcription or translation of the transcription factor *ces-1* (Hatzold & Conradt, 2008).

The SANT domains

SANT domains are ~ 50 aa long protein motifs that are involved in chromatin remodeling and histone tail binding The term SANT originates from factors which harbor these domains ('switching-defective protein 3 (**S**wi3), adaptor 2 (**A**da2), nuclear receptor co-repressor (**N**-CoR), transcription factor (**T**F)IIIB')) (Boyer *et al*, 2004, 2002). Both *C. elegans* DNJ-11 and human MPP11 possess two SANT domains at the C-terminus (Fig. 14). In humans, MPP11 (DnaJC2/ZRF1) was recently identified as epigenetic regulator of gene transcription in stem cells and cancer (Aloia *et al*, 2015; Richly *et al*, 2010). Apart from its role at the ribosome, DNJ-11 might also function in transcription regulation. In the present study neither GFP-tagging of DNJ-11 nor analysis of the nuclear extract could show a distinct nuclear presence of DNJ-11 (Fig. 18 C and 19). However, an off-ribosome function of DNJ-11 was not analyzed in this study. Thus, a possible impact on transcription was not tested.

Yet, for the first time this study showed that the SANT domains facilitate ribosome binding (Fig. 22 D). Yeast Zuotin lacks the SANT domains, thus the internal charged region is mainly required for ribosome association (Yan *et al*, 1998; Lee *et al*, 2016). It can be speculated that in *C. elegans* the SANT domains present an additional ribosome binding motif apart from the charged region enabling contact of the DNJ-11 C-terminus to RNA element(s) of the 40S subunit or even contact to the mRNA. Indeed, the second SANT domain at the far C-terminus shows an overall positive net charge and ribosome association of DNJ-11 was indeed very sensitive towards RNase A digest (Fig. 17).

Coomassie staining of recombinant wildtype ceRAC often showed a faint lower weight degradation product that was also detected by the anti-DNJ-11 antibody in immunoblot analyses. Interestingly, this protein product was not able to bind to 80S ribosomes *in vitro* (Fig. 28 C, asterisk). *In vitro* a small fraction of ceRAC might be degraded at the C-terminal end of DNJ-11 (SANT domains),

thereby preventing ribosome binding. However, this hypothesis has to be confirmed by mass spectrometric analyses. Interestingly, recombinant DNJ-11$^{\Delta SANT}$ and ceRAC$^{\Delta SANT}$ were far more stable than their wildtype versions and even less susceptible to temperature as well as freeze and thaw cycles indicating that these domains are unstable protein entities.

Functions of ceRAC in translation

In yeast, Zuo1 spans both ribosome subunits and contacts the 40S at rRNA helix 59, which stretches directly into the ribosome decoding center (Lee *et al*, 2016). Like in yeast, one can speculate that RNA contact enables ceRAC to sense specific mRNA properties and transfer this signal to the decoding center slowing down translation speed during biogenesis of challenging transcripts (Zhang *et al*, 2014). It was shown before that elongation speed varies along one mRNA and thereby facilitates folding of specific protein domains at the ribosome tunnel exit (O'Brien *et al*, 2012; Rodnina, 2016). The detection of ceRAC/HSP-1 clients can reveal protein domains or structural features that are specifically dependent on this chaperone system during co-translational protein folding.

Zuo1 homologs are highly abundant in cells and tissues with high translation rates (cancer cells, yeast, the reproductive system). MPP11 is highly abundant in cancer cells (Imamura *et al*, 2018) and the *in vivo* ratio of Zuo1 to ribosomes is 1:1 (Yan *et al*, 1998; Gautschi *et al*, 2001). However, recent studies showed that *in vivo* only every third ribosome is occupied by Zuo1 (Wang *et al*, 2012; Raue *et al*, 2007). Off-ribosome function of Zuo1 includes ribosome-biogenesis, manifested in shoulders on the 80S and polysome peaks (halfmers) in polysome profiles of *zuo1Δ* cells (Albanèse *et al*, 2010). Additionally, HeLa cells depleted of MPP11 showed decreased ribosome abundance (Jaiswal *et al*, 2011). However, DNJ-11 is a low abundant protein (Gamerdinger, 2016) and depletion of DNJ-11 had no significant effect on ribosome biogenesis, ribosomal protein levels or the overall translation rate in *C. elegans* (Fig. 23 and 27 C). Though, Zuotin homologs show differences in the effect on ribosomal protein levels and translation. These opposing roles might be explained by both the varying abundance of the Zuo1 homologs and the overall metabolic rate in different eukaryotic species or cell types.

HSP-1 is the only Hsc70 in *C. elegans*, and thus likely exhibits a broad function in cellular protein homeostasis. To dissect the specific role of ceRAC HSP-1 in translation, mutations must be specifically inserted into the complex-bound HSP-1. Therefore, transgenic strains expressing a DNJ-11/HSP-1 fusion protein can be generated. Insertion of a flexible linker between both proteins will facilitate complex formation. However, choosing the correct DNJ-11 terminus for linker

connection is quite a challenge as the N-terminus is essential for complex formation with HSP-1 and the C-terminus is involved in ribosome binding. These transgenic strains facilitate the insertion of mutations into the ATPase as well as into the substrate binding pocket of HSP-1 to elucidate the specific role of the complexed HSP-1 at the ribosome.

Crystal structure of ceRAC

This study shows for the first time a stable complex formation between an active Hs70 and a JDP. The discovery of this new ribosome-associated complex in *C. elegans* will leave many open questions. A lot of them were discussed in this chapter, however, to further investigate this special complex, structure elucidation will be necessary. Structure modeling gave first insights on how this heterodimer may form *in vivo* and could explain the reprogramming of HSP-1 in ceRAC. However, to gain crystal structures of DNJ-11 in complex with HSP-1 the flexibility of HSP-1 and instability of DNJ-11 should be diminished. Thus, for crystallization approaches ceRAC$^{\Delta SANT}$ or the DNJ-11N-HSP-1 complex should be used. Structure elucidation can also be facilitated by intramolecular disulfide bond generation (E48C, C243V, C268A, C307N, Q533C, C575V) to stabilize HSP-1 in the ATP-bound conformation (Kityk *et al*, 2012).

In sum, this study shows that ceRAC exhibits a dual role at *C. elegans* ribosomes. During *de novo* protein biogenesis ceRAC exerts both J-domain function towards an Hsp70 and in addition acts as a low affinity chaperone.

7. Results – Part B

This part of the thesis focuses on two studies examining the ribosome-associated factor NAC. Parts of these studies were conducted as side projects and contributions to this collaborative work are presented below:

I. "Dual role of ribosome binding domain of NAC as a potent suppressor of protein aggregation and aging-related proteinopathies"

Shen *et al.*, 2019 (Mol Cell 74, 1–13)

Koning Shen[1], Martin Gamerdinger[2], Rebecca Chan[1], Karina Gense[2], Esther M. Martin[3], Nadine Sachs[2], Patrick D. Knight[3], Renate Schlömer[2], Antonio N. Calabrese[3], Katie L. Stewart[3], Lukas Leiendecker[2], Ankit S. Baghel[1], Sheena E. Radford[3], Judith Frydman[1], Elke Deuerling[2]

[1] Department of Biology, Stanford University, Stanford, CA 94305-5430, USA
[2] Department of Biology, Molecular Microbiology, University of Konstanz, 78457 Konstanz, Germany
[3] Astbury Centre for Structural Molecular Biology, School of Molecular and Cellular Biology, Faculty of Biological Sciences,University of Leeds, Leeds LS2 9JT, UK

Contributions: *C. elegans* polysome analysis
In vitro luciferase refolding assays

II. "*Ab initio* guidance of nascent polypeptides inside the ribosomal tunnel by NAC"

Gamerdinger *et al.*, 2019 (manuscript in revision)

Martin Gamerdinger[1], Kan Kobayashi[2], Annalena Wallisch[1], Stefan G. Kreft[1], Carolin Sailer[3], Renate Schlömer[1], Nadine Sachs[1], Ahmad Jomaa[2], Florian Stengel[3], Nenad Ban[2], Elke Deuerling[1]

[1] Department of Biology, Molecular Microbiology, University of Konstanz, 78457 Konstanz, Germany
[2] Department of Biology, Institute of Molecular Biology and Biophysics, ETH Zurich, Zurich, Switzerland
[3] Department of Biology, University of Konstanz, 78457 Konstanz, Germany

Contribution: *Ex vivo* ribosome binding competition analysis

In eukaryotes the nascent polypeptide-associated complex (NAC) was postulated to be the first factor that interacts with newly synthesized proteins directly at the ribosome (Wiedmann *et al.*, 1994; del Alamo *et al.*, 2011). NAC is a heterodimer consisting of an α- and β-subunit (Liu *et al*, 2010) that is expressed at equimolar levels relative to ribosomes and is therefore assumed to control early protein folding and co-translational protein sorting in the cell (Raue *et al*, 2007; Wiedmann & Prehn, 1999; Kirstein-Miles *et al*, 2013; Gamerdinger *et al*, 2015). The interaction mode with the ribosome or protein substrates remains poorly understood. A critical ribosome binding motif is

located in the N-terminus of βNAC (β-RRxxKKK) (Wegrzyn *et al*, 2006). However, also αNAC crosslinks to ribosomal proteins suggesting a more complex ribosome interaction mode (Nyathi & Pool, 2015). The substrate binding motifs in NAC are still unknown and the assumed *in vivo* chaperone function could not be confirmed so far. Moreover, it was shown that upon proteotoxic stress conditions NAC is sequestered to cytosolic aggregates, which indicates an additional off-ribosome function (Kirstein-Miles *et al*, 2013). The following two studies give new insights into on- and off-ribosome functions of NAC.

7.1 Dual role of ribosome binding domain of NAC as a potent suppressor of protein aggregation and aging-related proteinopathies

This study investigated the proposed chaperone function of NAC. *In vivo* as well as *in vitro* experiments were performed with special emphasis on the impact of this ribosome-associated factor on protein aggregation. In *C. elegans* it could be shown that *in vivo* wildtype NAC prevents aggregation of pathogenic proteins containing an extended polyglutamine (PolyQ) stretch, which cause several human neurodegenerative diseases like Huntington's disease and spinocerebellar ataxias. Interestingly, also a ribosome binding deficient NAC variant (^{29}RRK/AAA^{31}-NAC) effectively suppressed PolyQ protein aggregation. This finding suggests that NAC also exhibits off-ribosome chaperone function. Therefore, it was analyzed if *in vivo* a fraction of NAC is ribosome unbound. Polysome profile analysis of young wildtype nematodes supported this assumption as NAC associated not only with 80S ribosomes and polysomes but was also highly abundant in the soluble, non-ribosome-bound fraction (Fig. 42). The aggregation suppression activity of NAC on PolyQ proteins could be confirmed in *in vitro* analyses and the critical PolyQ binding domain was mapped to the highly charged N-terminal domain of βNAC. To exclude a NAC-specific effect on PolyQ polypeptides, it was of interest to investigate the activity of NAC on chemically denatured luciferase. As expected, denatured luciferase was effectively refolded upon incubation with the *C. elegans* Hsp70/JDP chaperone system (HSP-1 and DNJ-13) (Fig. 43 A). Human NAC neither showed refolding activity when added to denatured luciferase alone nor increased the refolding efficiency when added together with the Hsp70/JDP system (Fig. 43 A). However, incubation with NAC prior to the addition of the Hsp70/JDP chaperone system significantly enhanced refolding efficiency (Fig. 43 B, compare green and red curve). This effect seems to be specific, as a preincubation with GFP, a protein with an equal molar mass, did not enhance refolding activity of the Hsp70/JDP system (Fig. 43 B).

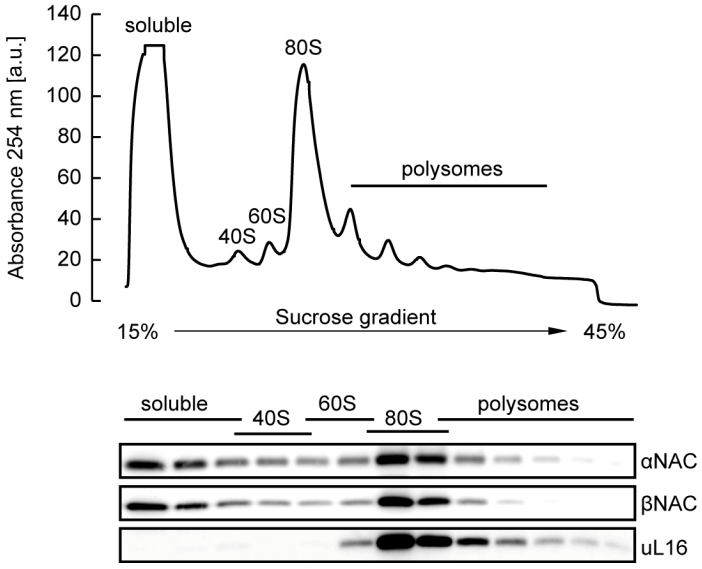

Figure 42: Distribution of NAC in polysome profiles. Ribosomal species of young adult *C. elegans* worms (day 2 of adulthood) were separated by sucrose density gradient (15%-45%) centrifugation. A polysome profile (upper panel) was recorded measuring the absorbance at 254 nm. Fractions throughout the gradient were analyzed by immunoblotting using a NAC specific antibody (lower panel). uL16 served as ribosomal marker.

These data suggest that NAC exerts a "holding" chaperone function maintaining luciferase in a refolding competent state, thus supporting subsequent reactivation via other chaperones systems. Strikingly, deletion of the βNAC N-terminus (ΔNβ-NAC) significantly reduced the "holding" chaperone activity of NAC, however ΔNβ-NAC showed residual chaperone function indicating other not yet identified chaperone domains of NAC (Fig. 43 C). Addition of *C. elegans* NAC showed a similar effect, though it was marginally less efficient in luciferase refolding than human NAC (Fig. 43 D), indicating a conserved NAC "holding" chaperone function.

In sum, this study provides direct evidence that NAC exhibits distinct chaperone activity towards a broad range of structurally and physiochemically diverse substrates, as well as denatured luciferase. Moreover, NAC was shown to act both co- and post-translationally. The N-terminus of βNAC is crucial for chaperone activity extending its function beyond that of a mere ribosome binding entity. The study furthermore indicates that in addition to the N-terminus of βNAC other not yet identified substrate interaction domains are present in NAC.

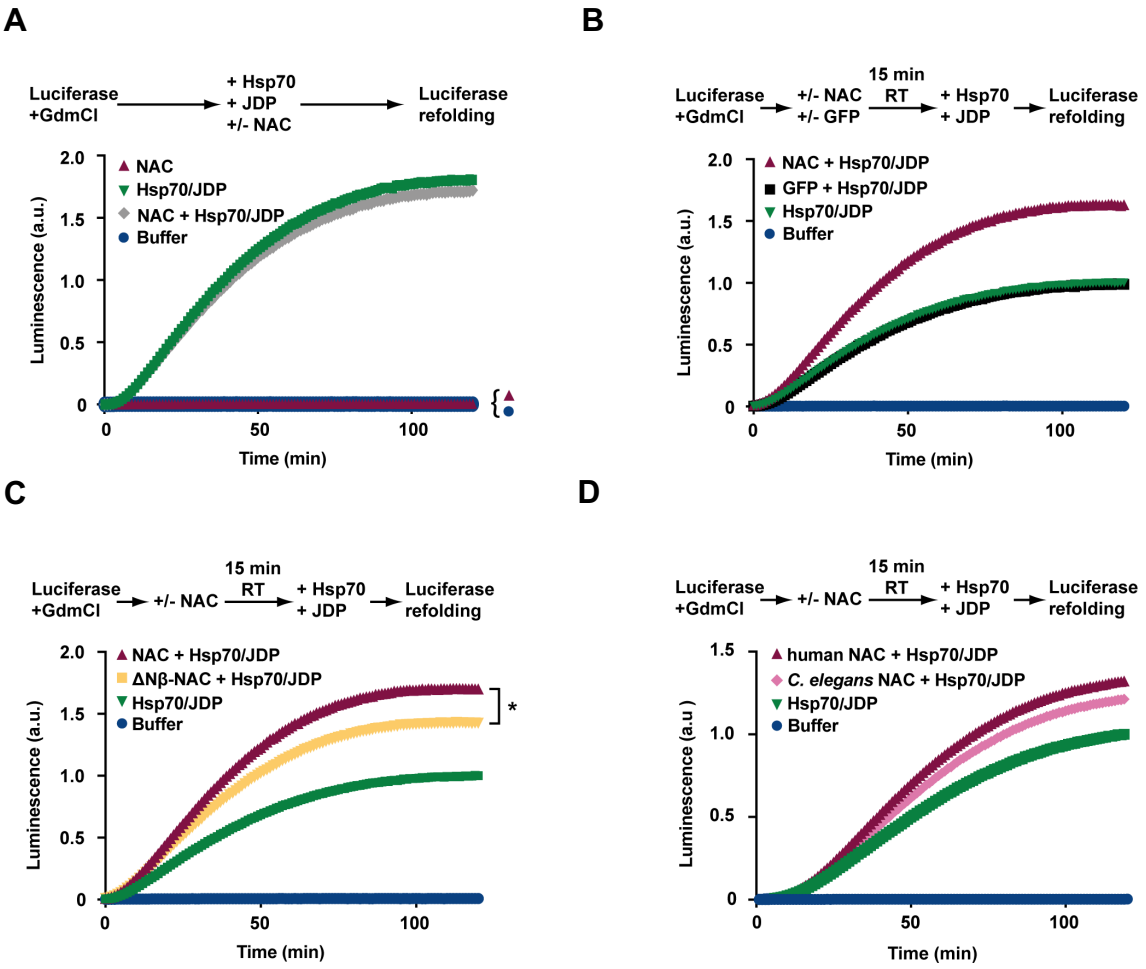

Figure 43: Chaperone function of NAC on luciferase refolding. (A) Refolding of chemically denatured luciferase was measured in the presence of NAC (red), an Hsp70/JDP system (green) and both combined (grey) using luciferin as substrate. Luminescence was recorded in a microplate reader every minute over two hours. **(B)** Denatured luciferase was incubated with (red) or without (green) human NAC for 15 min and refolding was initiated by addition of a Hsp70/JDP system. GFP (black) served as negative control. **(C)** Same assay as in (B) but with a human NAC variant lacking the βNAC N-terminus (ΔNβ-NAC). Significance was assessed by a one-way ANOVA and Tukey post hoc test, *p<0.05. **(D)** Same assay as in (B) but with *C. elegans* NAC (rose). a.u. = arbitrary units; GdmCl, Guanidinium chloride; RT, room temperature.

7.2 *Ab initio* chaperone guidance of nascent polypeptides inside the ribosomal tunnel by NAC

This work focused on the co-translational interaction mechanism of NAC at the ribosome investigating ribosome binding and substrate interaction using genetic, biochemical and structural (Cryo-EM) analyses.

The most striking finding was that NAC insert its βNAC N-terminus into the ribosomal tunnel, extending up to the peptidyl transferase center (PTC) where it binds newly synthesized polypeptide chains and escorts them to the cytosol. In this tunnel inserted conformation NAC prevents the association of other transiently ribosome-anchored factors like RAC, SRP or Sec61. These data suggest that NAC senses empty and early phase translating ribosomes and blocks the binding of other protein biogenesis factors. This hypothesis is supported by the finding that tunnel sensing by NAC is crucial for *in vivo* ER protein transport. To investigate if NAC also regulates simultaneous binding of RAC, biochemical *ex vivo* ribosome binding competition studies were performed. Addition of recombinant wildtype NAC to wildtype *C. elegans* lysate displaced DNJ-11 from ribosomes, whereas a ribosome binding mutant of NAC (^{29}RRK/AAA^{31} in β-NAC) had no effect on DNJ-11 binding (Fig. 44). These results suggest that RAC and NAC competitively bind to ribosomes and is consistent with the hypothesis that NAC orchestrates ribosome binding of other factors that reside at the ribosome exit site.

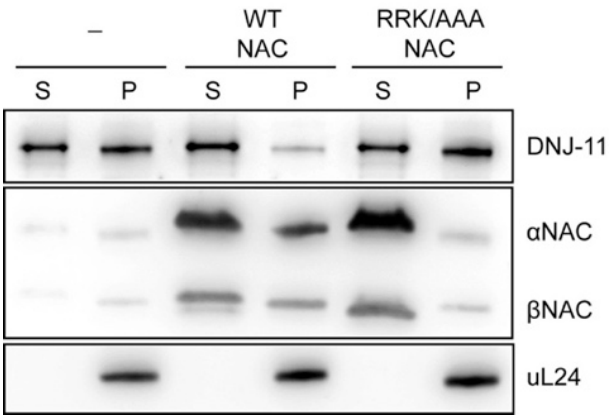

Figure 44: ***Ex vivo*** **ribosome binding competition of RAC and NAC.** WT NAC or a ribosome binding deficient NAC mutant (βNAC subunit (^{29}RRK/AAA^{31})) was added to *C. elegans* N2 lysate. Ribosomes were subsequently pelleted via sucrose cushion centrifugation. Supernatant (S) and pellet (P) fractions were subjected to immunoblotting. The membrane was probed with antibodies against DNJ-11 and NAC. uL24 served as ribosomal marker.

8. Materials

8.1 Laboratory equipment

Instrument	Device Model
Binoculars	LEICA MZ10F Olympus SZ51
Centrifuges	MiniSpin Plus, Eppendorf Centrifuge 5702, Eppendorf Centrifuge 5427R, Eppendorf Centrifuge 5430R, Eppendorf
Chemiluminescence imager	Fusion SL, PEQLAB
Cryo mill	MM400, Retsch
FPLC	Äkta™ purifier, GE Healthcare Äkta™ pure, GE Healthcare
French Press	SLM Aminco®, SLM Instruments, INC.
Gradient analyzer and fraction collector	Foxy, Teledyne ISCO
Gradient mixer	Gradient Master 107, BioComp Instruments Inc.
Image analyzer	Typhoon™ FLA 9500, GE Healthcare
Incubators	Infors Mulritron II, Infors AG APT.line™ KB(E5.1), Binder MaxQ8000, Thermofisher Scientific HettCube 600, Hettich Incubator
Micromanipulator	Bachofer
Microscopes	Confocal Laser-Scanning Microscope Leica TCS SP8 Leica DM5500
Multimode reader	TriStar² LB 942, Berthold Technologies
Photometer (UV/Vis)	Ultraspec 3100 pro, GE Healthcare
Power-supply	EV265 Consort
SDS-PAGE chamber	BioRad, München
Sonifier	Branson 450, Ermerson US
Test tube rotator	34528, Snjiders
Thermal cycler	Biometra Trio, Analytik Jena AG Biometra Tadvanced, Analytik Jena AG ABI 7500 Fast Real-Time PCR System, Applied Biosystems
Thermal shaker	Termomixer comfort, Eppendorf
Ultracentrifuges	Optima L-90K, Beckman Coulter Discovery M150 SE, Sorvall
UV Imager	red™ Personal Imaging System, ProteinSimple
Vortexer	Vortex Genie 2, Scientific Industries
Flow cytometry system	COPAS FlowPilot System, Union Biometrica
LUNA™ automated cell counter	Logos Biosystems, Inc.

8.2 Chemicals

Common chemicals were ordered from Sigma-Aldrich, Merck or Carl Roth, respectively. All additional chemicals are listed below:

Chemical	Manufacturer
[S^{35}]Met-label	Hartmann Analytic GmbH, Braunschweig
Aprotinin	Genaxxon, BioScience, Ulm
Bacto™ tryptone	BD, Sparks, USA
Bacto™ agar	BD, Sparks, USA
Bacto™ peptone	BD, Sparks, USA
Bacto™ yeast extract	BD, Sparks, USA
Bacto™ yeast nitrogen base (w/o amino acids)	BD, Sparks, USA
Bradford reagent (5x)	Bio-Rad Laboratories GmbH, München
Bromphenol blue	Serva, Heidelberg
Complete EDTA-free protease inhibitor cocktail (Tm complete)	Roche Diagnostics GmbH, Mannheim
COPAS Cleaning Solution	Union Biometrica, Holliston
D-Luciferin potassium salt	Synchem
Deoxyribonucleotidetriphosphate (dNTPs)	New England Biolabs, USA
DSS	Thermofisher Scientific GmbH
Floxuridine	LKT Laboratories, Inc.
Gen agarose LE	Genaxxon, BioScience, Ulm
Gibco® DMEM (1x) GlutaMAX	Thermofisher Scientific GmbH
Gibco® FCS	Thermofisher Scientific GmbH
Glycerol	VWR, Geldenaaksebaan, Belgium
GoTaq® qPCR Master-Mix	Promega, Madison, USA
Herring sperm DNA	Promega, Madison, USA
L-Uracil	AppliChem GmbH, Darmstadt
Leupeptin	Genaxxon, BioScience, Ulm
Levamisole	LKT laboratories, Inc.
Lipofectamin RNAi Max	Thermo Fisher Scientific GmbH
Magnesium-chloride	Acros Organic, New Jersey, USA
Manganese(II) chloride tetrahydrate	Riedel de Haën, Seelze
Midori Green	NIPPON Genetics EUROPE GmbH
Mineral Oil	Trinity Biotech, USA
N,N,N‘,N‘-Tetramethylethylendiamine (TEMED)	Serva, Heidelberg
Nonidet P-40	Fluka Biochemica, Neu-Ulm
Normocin™	InvivoGen, San Diego, USA
Nuclease-free water	Promega, USA
ON-TARGETplus Human HSPA14 (51182) siRNA	Dharmacon™
OptiMEM®	Thermofisher Scientific GmbH
Pepstatin A	Genaxxon, BioScience, Ulm
Phosphoenol-pyruvate	Roche Diagnostics GmbH, Mannheim
Protein A magnetic beads	New England Biolabs GmbH, USA
Protino® Ni-NTA/IDA Agarose	Machery-Nagel GmbH & Co. KG
Puromycin	InvivoGen, San Diego, USA
Rabbit Reticulocyte Lysate	Promega, USA
Sodium-chloride	VWR, Geldenaaksebaan, Belgium

8.3 General buffers

Buffer	Manufacturer/Composition
T4 DNA-ligase buffer (10x)	Fermentas, St. Leon-Rot, Deutschland
Taq DNA-polymerase buffer (10x)	New England Biolabs GmbH, USA
DNA loading dye (6x)	Fermentas, St. Leon-Rot, Deutschland
CutSmart Buffer (10x)	New England Biolabs GmbH, USA
Antarctic Phosphatase buffer (10x)	New England Biolabs GmbH, USA
Western Blot transfer (1x)	25 mM Tris base 192 mM glycine 0.02% (w/v) SDS 20% (v/v) methanol
SDS Stacking gel buffer	0.5 M Tris-HCl pH 6.8 0.4% SDS
SDS Separation gel buffer	1.5 M Tris-HCl pH 8.8 0.4% (w/v) SDS
Bis-Tris Gel buffer (3.5x)	1.25 M Bis-Tris-HCl pH 6.5-6.8
M9	85.6 mM NaCl 42 mM Na_2HPO_4 x 2 H_2O 36.7 mM KH_2PO_4 add after autoclaving: 1 mM $MgSO_4$
TBS-T (10x)	200 mM Tris-HCl pH 8.0 1.37 M NaCl 1% (v/v) Tween-20
TAE buffer (50x)	2 M Tris base 5.71% (v/v) acetic acid 50 mM EDTA pH 8.0
Phusion reaction buffer (10x)	100 mM Tris-HCl pH 8.8 500 mM KCl 20 mM MgCl 1% (v/v) Triton X-100
Ponceau S	0.2% (w/v) Ponceau S 5% (v/v) acetic acid
Protein sample buffer (5x)	255 mM Tris-HCl pH 6.8 5% SDS 715 mM β-ME 42.5% glycerol 0.35% (w/v) bromphenol blue
SDS protein lysis buffer (2x)	125 mM Tris-HCl pH 6.8 2 mM EGTA pH 8.0 4% (v/v) SDS 20% (w/v) sucrose (1x concentrated working buffer supplemented with 2x Tm complete)
MOPS running buffer (5x)	250 mM MOPS 250 mM Tris base 5 mM EDTA 0.5% SDS

Buffer	Manufacturer/Composition
Trace metal solution	5 mM EDTA 2 mM $FeSO_4$ 1 mM $MnCl_2$ 1 mM $ZnSO_4$ 0.1 mM $CuSO_4$
Coomassie blue staining solution	0.6% (w/v) Coomassie R250 50% (v/v) ethanol 10 % (v/v) acetic acid
Coomassie destaining solution	50% (v/v) ethanol 10% (v/v) acetic acid
BCA working solution	bicinchoninic acid solution with 0.08% (w/v) $CuSO_4$
RNAi buffer (1x)	60 mM KCl 6 mM HEPES-KOH pH 7.5 0.2 mM $MgCl_2$
PBS (1x)	137 mM NaCl 2.7 mM KCl 8 mM Na_2HPO_4 2 mM KH_2PO_4 pH 7.4 (HCl)

ECL solution (Enhanced Chemiluminescence solution)

Solution A	0.1 M Tris-HCl pH 8.6 25 mg luminol ad 100 mL ddH_2O
Solution B	11 mg p-cumaric acid ad 10 mL DMSO
Solution C	30% (v/v) H_2O_2

Solution ready for use: 1 mL solution A + 100 µL solution B + 1 µL solution C

8.4 Antibiotics

Antibiotic	Manufacturer	Working Solution
Ampicillin	AppliChem, USA	100 µg/mL (stock: 100 mg/mL in ddH_2O)
Tetracyclin	Sigma-Aldrich Chemie GmbH	10 µg/mL (stock: 10 mg/mL in ddH_2O)
Kanamycin	Carl Roth GmbH & Co. KG	50 µg/mL (stock: 50 mg/mL in ddH_2O)
Chloramphenicol	SERVA Electrophoresis GmbH	25 µg/mL (stock: 25 mg/mL in ethanol)
Spectinomycin	Sigma-Aldrich Chemie GmbH	50 µg/mL (stock: 50 mg/mL in ddH_2O)

8.5 Protease inhibitors

Protease Inhibitor	Working Solution
Aprotinin	10 µg/mL (stock: 10 mg/mL in ddH_2O)
Leupeptin	5 µg/mL (stock: 5 mg/mL in ddH_2O)
Pepstatin A	8 µg/mL (stock: 1 mg/mL in MeOH)

8.6 Molecular weight standards

Marker	Manufacturer
GeneRuler 1 kb DNA ladder	Fermentas, St. Leon-Rot, Deutschland
GeneRuler 100 bp DNA ladder	Fermentas, St. Leon-Rot, Deutschland
Prestained protein ladder	Fermentas, St. Leon-Rot, Deutschland

8.7 Yeast culture media

Amino acid dropout mix without L-Histidine, L-Uracil and L-Leucine was prepared and finally used for the preparation of minimal medium. To prepare – His minimal medium suitable amounts of the missing amino acids were added: **L-Uracil** (22.40 mg/L), **L-Leucine** (219.00 mg/L)

Dropout mix

Amino acid	Amount
L-Adenine	0.5 g
L-Alanine	2.0 g
L-Arginine	2.0 g
L-Asparagine	2.0 g
L-Aspartic acid	2.0 g
L-Cysteine	2.0 g
L-Glutamic acid	2.0 g
L-Glutamine	2.0 g
Glycine	2.0 g
L-Isoleucine	2.0 g
L-Lysine	2.0 g
L-Methionine	2.0 g
L-Phenylalanine	2.0 g
L-Proline	2.0 g
L-Serine	2.0 g
L-Threonine	2.0 g
L-Tryptophan	2.0 g
L-Tyrosine	2.0 g
L-Valine	2.0 g
Myo-Inositole	2.0 g
P-Aminobenzoic acid	0.2 g

Medium	Composition
YPD	1% (w/v) Bacto™ yeast extract 2% (w/v) Bacto™ peptone 2% (w/v) D-glucose (2% (w/v) Bacto™ agar)
Minimal medium	6.7 g/L Bacto™ yeast nitrogen base (w/o amino acids) 2.0 g/L amino acid dropout mix 2% (w/v) D-glucose (2% (w/v) Bacto™ agar)

8.8 Bacterial culture medium

Medium	Composition
LB-medium	1% (w/v) Bacto™ tryptone 0.5% (w/v) Bacto™ yeast extract 0.5% (w/v) sodium-chloride (1.5% (w/v) Bacto™ agar)

8.9 *Caenorhabditis elegans* culture media

Medium	Composition
NG plates (Nematode Growth)	2% (w/v) Bacto™ agar 0.25% (w/v) Bacto™ peptone 0.3% (w/v) NaCl 1 mM $CaCl_2$ 13 µM cholesterol 25 mM KPO_4 pH 6.0 1 mM $MgSO_4$
HG plates (High Growth)	2% (w/v) Bacto™ agar 2% (w/v) Bacto™ peptone 0.3% (w/v) NaCl 1 mM $CaCl_2$ 13 µM cholesterol 25 mM KPO_4 pH 6.0 1 mM $MgSO_4$
RNAi plates	2% (w/v) Bacto™ agar 0.25% (w/v) Bacto™ peptone 0.3% (w/v) NaCl 1 mM $CaCl_2$ 13 µM cholesterol 25 mM KPO_4 pH 6.0 1 mM $MgSO_4$ 100 mg/ml ampicillin 1 mM IPTG
S-medium *C. elegans* liquid culture	100 mM NaCl 5.7 mM K_2HPO_4 44 mM KH_2PO_4 13 µM cholesterol add after autoclaving: 10 mM 1 M K-Citrate (pH 6.0) 1% (v/v) Trace metal solution 3 mM $CaCl_2$ 3 mM $MgSO_4$
S-buffer *C.elegans* cryogenic storage	100 mM NaCl 6.45 mM K_2HPO_4 44 mM KH_2PO_4 (+ 30% (v/v) glycerol)

8.10 Mammalian cell culture medium

Designation	Basal medium	Additives
HEK293 culture medium	Gibco® DMEM (1x) GlutaMAX	10% FCS 100 µg/mL Normocin

8.11 *Caenorhabditis elegans* strains

Strain	Genotype	Source
N2	Wildtype (wild isolate)	CDC Minnesota
dnj-11(bc212)	[*tph-1p::gfp; bc212*] Codon 7 of *dnj-11* is transformed into a stop codon by C-to-T transition at position 21 of the nucleotide sequence	Hatzold and Conradt, 2008
GFP::DNJ-11 (DEU136)	*gamIs36* [*gfp::dnj-11*]	This study
DNJ-11^{WT} (DEU137)	*dnj-11(bc212); gamIs37* [*dnj-11p::WT-dnj-11; icd-2p::mCherry*]	This study
DNJ-11$^{\Delta SANT}$ (DEU138)	*dnj-11(bc212); gamIs38* [*dnj-11p:: Δ452-589-dnj-11; icd-2p::mCherry*]	This study
DNJ-11^{H129Q} (DEU139)	*dnj-11(bc212); gamIs38 [dnj-11p:: H129Q-dnj-11; icd-2p::mCherry]*	This study

8.12 *Saccharomyces cerevisiae* strains

Strain	Description	Genotype	Source
Y67	BY4741 (wt)	*MATa; his3Δ1; leu2Δ0; met15Δ0; ura3Δ0*	EUROSCARF
Y217	*zuo1Δ*	*MATa; his3Δ1; leu2Δ0; met15Δ0; ura3Δ0; YGR285C::kanMX*	EUROSCARF

8.13 *Escherichia coli* strains

Strain	Genotype	Source
DH5αZ1	F$^-$ φ80*lac*ZΔM15 Δ(*lac*ZYA$^-$*arg*F) U169 *rec*A1 *end*A1 *hsd*R17 (rk$^-$, mk$^+$) *pho*A *sup*E44 λ^- *thi*$^-$1 *gyr*A96 *rel*A1	Invitrogen
BL21(DE3) /pRARE	F$^-$ *omp*T *hsd*S$_B$(r_B^- m_B^-) *gal dcm* (DE3) /pRARE (Cam^R)	Novagen
OP50	Uracil auxotroph	CDC Minnesota
HT115 (DE)	F-, *mcr*A, *mcr*B, IN(*rrnD-rrnE*)1, *rnc14::Tn10*(DE3 lysogen: lavUV5 promoter -T7 polymerase)	Open Biosystems

8.14 Mammalian cells

Cells	Description	Source
HEK293	human embryonic kidney cells	AG T. U. Mayer, University of Konstanz

8.15 Plasmids

Expression in yeast

Nr.	Plasmid	Inserted gene(s)	Basic vector	Promoter	Marker	Reference
#856	p413GPD	/	/	*GPD*	Amp^R/ HIS3	Mumberg *et al.*, 1995
#1627	p413GPD-zuo1	*zuo1*	#856	*GPD*	Amp^R/ HIS3	This study
#1628	p413GPD-dnj-11	*dnj-11*	#856	*GPD*	Amp^R/ HIS3	This study

Recombinant Protein Expression

Nr.	Plasmid	Inserted gene(s)	Basic vector	Promoter	Marker	Reference
#540	pHis^6::SUMO	/	/	*T7*	Amp^R	AG Deuerling
#1422	pDS56-His^{6}Luciferase	*Firefly Luciferase*	pDS56	*T5*	Amp^R	AG Deuerling
#747	pZA4	*lacIq*	/	/	$Spec^R$	AG Deuerling
#46	pHis^6::SUMO::dnj-11	*dnj-11*	#540	*T7*	Amp^R	This study
#125	pHis^6::SUMO::hsp-1	*hsp-1*	#540	*T7*	Amp^R	This study
#83	pHis^6::SUMO:: dnj11::RBS::hsp-1	*dnj-11* and *hsp-1*	#46	*T7*	Amp^R	This study
#179	pHis^6::SUMO::dnj-13	*dnj-13*	#540	*T7*	Amp^R	This study
#251	pHis^6::SUMO:: dnj11N::RBS::hsp-1	*dnj11N* (2-42aa) and *hsp-1*	#83	*T7*	Amp^R	This study
#168	pHis^6::SUMO:: dnj11ΔN::RBS::hsp-1	*Δ2-35 dnj-11* and *hsp-1*	#83	*T7*	Amp^R	This study
#198	pHis^6::SUMO:: dnj11::RBS::hsp1^{V439F}	*dnj-11* and *hsp1^{V439F}*	#83	*T7*	Amp^R	This study
#309	pHis^6::SUMO:: hsp-1^{V439F}	*hsp-1^{V439F}*	#125	*T7*	Amp^R	This study
#180	pHis^6::SUMO:: dnj-11$^{\Delta SANT}$	*Δ452-589 dnj-11*	#46	*T7*	Amp^R	This study

RBS = ribosome binding-site

RNAi vectors

Nr.	Plasmid	Inserted gene(s)	Basic vector	Promoter	Marker	Reference
#39	ev	/	*pL4440*	*T7*	Amp^R	AG Deuerling
#49	pL4440-dnj-11	*dnj-11*	*pL4440*	*T7*	Amp^R	This study
#77	pL4440-hsp-1	*hsp-1*	*pL4440*	*T7*	Amp^R	This study

Expression in *C. elegans*

Nr.	Plasmid	Inserted gene(s)	Basic vector	Promoter	Marker	Reference
#6	pMA122	*peel-1*	/	*hsp16.41*	Amp^R	Addgene #34873
#7	pCFJ601	*mos1 transposase*	pDEST R4-R3	*eft3*	Amp^R	Frokjaer-Jensen *et al.*, 2012
#19	pPD152.79	*gfp*	/	*dpy-30*	Amp^R	Addgene #1704
#22	pCFJ421	*gfp::H2B*	pDEST R4-R3	*myo2*	Amp^R	Addgene #34876
#54	pDD162	*Cas9* and *empty sgRNA*	/	*eft-3* and *U6*	Amp^R	Dickinson *et al.*, 2013; Addgene #47549
#98	pPD61_125::Avi:: 3xFlag::TEV::GFP	*Avi::3xFlag:: TEV::GFP*	pPD61_ 125	/	Amp^R	AG Deuerling
#262	pCFJ601::dnj-11	*WT-dnj-11* and *m-Cherry*	#7	*dnj-11* and *icd-2*	Amp^R	This study
#263	pCFJ601::dnj-11$^{\Delta SANT}$	*Δ452-589-dnj-11* and *m-Cherry*	#7	*dnj-11* and *icd-2*	Amp^R	This study
#267	pCFJ601::dnj-11 ^{H129Q}	*H129Q-dnj-11* and *m-Cherry*	#7	*dnj-11* and *icd-2*	Amp^R	This study

8.16 Primers

Sequencing

Nr.	Sequence 5'-3'	Description/Gene	Orientation
T3	ATTAACCCTCACTAAAGGGA	pSUMO	Sense
T7	TAATACGACTCACTATAGGG	pSUMO	Antisense
#1698	GTTTTCCCAGTCACGACGTT	pL4440	Sense
#1699	TGGATAACCGTATTACCGCC	pL4440	Antisense
#2741	CTCTTTCGTTGCTGAAAATC	*dnj-11*	Sense
#2742	AGGATGTCGAGAATTTCTAC	*dnj-11*	Sense
#2743	ACCTGGAACCGTGGAGAG	*dnj-11*	Sense
#3707	CACTCGTGCTCGTTTCGAGG	*hsp-1*	Sense

Quantitative PCR (qPCR)

Nr.	Sequence 5'-3'	Description/Gene	Orientation
#1954	ACTCATGTGTCGGTATTTATC	*C12C8.1*	Sense
#1955	ACGGGCTTTCCTTGTTTT	*C12C8.1*	Antisense
#1958	AATGAACCAACTGCTGCTGCTCTT	*F44E5.4*	Sense
#1959	TGTCCTTTCCGGTCTTCCTTTTG	*F44E5.4*	Antisense
#1964	CCTGCATTCGTCGTTTCAAG	*dnj-11*	Sense
#1965	TGAAGGGATGAGGAAGATTTAGAG	*dnj-11*	Antisense
#3088	ATCGAGGAGGTCGACTA	*hsp-1*	Sense
#3089	GGGGCAGAAGATCGATTA	*hsp-1*	Antisense

Cloning/Mutagenesis

Nr.	Sequence 5'-3'	Description/Gene	Orientation
#274	GAACgtcgacATGACTACGGGCAATTTACA	Amplification of spliced *dnj-11* [*SalI*]	Sense
#2749	GAACgtcgacTCATTTCTTATTTTTAACCA	Amplification of spliced *dnj-11* [*SalI*]	Antisense
#3124	TAGCtctagaATGACTACGGGCAATTTACA	Amplification of spliced *dnj-11* [*XbaI*]	Sense
#679	GCGCggatccATGTTTTCTTTACTACCCTAACC	Amplification of *Zuo1* [*BamHI*]	Sense
#3643	CCAAgatatcTCACACGAAGTAGACAACAAGC	Amplification of *Zuo1* [*EcoRV*]	Antisense
#3634	TGATCTTCTAGTCCAAGTAATATC	SANT domain deletion	Sense
#3635	GGCTTGCTTTTCATTTTCTTTG	SANT domain deletion	Antisense
#3641	TGAGAGCTCCGTCGACAA	SANT domain deletion (spliced)	Sense
#3637	TTTGAAGCATCAGCCGGACAAGA	DNJ-11^{H129Q} mutation	Sense
#3638	ACCTTTTGACGATCTGAAATAATTCTC	DNJ-11^{H129Q} mutation	Antisense
#3639	ACACTGGGCCACTGTACG	N-terminus deletion of *dnj-11* (2-35 aa)	Sense
#3640	CATACCACCAATCTGTTCTCTGTG	N-terminus deletion of *dnj-11* (2-35 aa)	Antisense

Nr.	Sequence 5'-3'	Description/Gene	Orientation
#3699	CCAACCAGGATTCTTGATCCAGG	HSP-1^{V439F} mutation	Sense
#3700	TTATCAGAATAGGTTGTGAAG	HSP-1^{V439F} mutation	Antisense
#3100	ATAAGAATGCGGCCGCTGTCGAC CTGCAGAAGAGGAGAAATTAACC ATGAGTAAGCATAACGCTG	pSUMO insertion of spliced *hsp-1* with RBS [*NotI*]	Sense
GPI_1	TGGCGGCCGCTCTAGAATAATAC GACTCACTATAGGGAGACCATGG	Amplification GPI (85 aa)	Sense
GPI_2	AACCATCATCATCATCATGGCCTC CACGCCCCTGGACT	Amplification GPI (85 aa)	Antisense

Restriction enzyme sites are marked in lower case letters

8.17 RNAi (Mammalian cell culture)

RNAi	Target Sequence	Origin
HSPA14, J-021084-09 (#1)	GGGCUGGUGUGGUUGCAAA	Dharmacon™
HSPA14, J-021084-09 (#2)	CCUGUGUGGCCGUCUAUAA	Dharmacon™
HSPA14, J-021084-09 (#3)	AUGAAGAGAUUGUUGGAUU	Dharmacon™
HSPA14, J-021084-12 (#4)	GUUGUUGCUUACUCAGAAA	Dharmacon™
Ctrl. siRNA	annealed, double-stranded siRNA	Qiagen, Hilden, Deutschland

8.18 Enzymes

Enzyme		Origin
XbaI	(20,000 U/mL)	New England Biolabs GmbH, USA
SalI-HF	(20,000 U/mL)	New England Biolabs GmbH, USA
BamHI-HF	(20,000 U/mL)	New England Biolabs GmbH, USA
EcoRV	(20,000 U/mL)	New England Biolabs GmbH, USA
NotI-HF	(20,000 U/mL)	New England Biolabs GmbH, USA
BsaI	(10,000 U/mL)	New England Biolabs GmbH, USA
Phusion Polymerase		AG Deuerling
T4 DNA Ligase	(400,000 U/mL)	New England Biolabs GmbH, USA
His-Ulp1		AG Deuerling
DNaseI		Sigma-Aldrich
RNase A (10 mg/mL)		Thermo Fisher Scientific GmbH
Antarctic Phosphatase (5,000 U/mL)		New England Biolabs GmbH, USA
Pyruvate Kinase		Roche Diagnostics GmbH, Mannheim

All digestion reactions with listed restriction enzymes were performed in 1x CutSmart buffer

8.19 Antibodies

Primary antibody	Immunogen	Dilution for WB	Origin
anti-Actin (mouse; monoclonal)	gizzard lysate	1:3,000	DSHB (JLA20)
anti-PAS-7 (mouse; monoclonal)	full length PAS-7	1:5,000	DSHB (CePAS7)
anti-DNJ-11 (rabbit serum; polyclonal)	DNJ-11 Exon 3	1:5,000	AG Deuerling
anti-HSP-1 (rabbit; peptide antibody)	edeklkdkispedkkkiedk	1:1,000	Davids Biotechnologie GmbH
anti-HSP-1 (rabbit; polyclonal)	HSP-1	1:7,500	Prof. Dr. Janine Kirstein, University Bremen
anti-NAC-complex (rabbit serum; polyclonal)	full length NAC	1:5,000	AG Deuerling
anti-uL16 (rabbit; polyclonal)	human uL16 9-35 aa	1:1,000	Biomol (#AP17603a)
anti-uL24 (rabbit serum; polyclonal)	full length uL24	1:1,000	AG Deuerling
anti-Tubulin (hybridoma supernatant)	full length Tubulin	1:100	AG T.U. Mayer, University of Konstanz
anti- Zuo1 (rabbit serum; polyclonal)	full length Zuo1	1:10,000	AG Deurling
anti-GFP (mouse; monoclonal)	full length WT GFP	1:5,000	Convance (MMS-118P)
anti-HSPA14 (rabbit; monoclonal)	human HSPA14 aa 50-150	1:1,000	Abcam (ab108612)
anti-HistoneH3 (rabbit; polyclonal)	human H3 N-terminal peptide	1:4,000	Novus Biologicals (NB500-171)
anti-Puromycin (mouse; monoclonal)	Puromycin from *S. alboniger*	1:5,000	Millipore/Merck (MABE343)
anti-p150 (mouse; monoclonal)	rat p150 [Glued] 3-202 aa	1:1,000	BD BD Transduction Laboratories (610473)
anti-GAPDH (mouse; monoclonal)	fragment of human GAPDH	1:10,000	Biomol (#20035)
anti-Hsp70 (mouse; monoclonal)	human Hsp70 1-641 aa	1:1,000	Santa Cruz (sc-69705)
anti-MPP11 (rabbit; monoclonal)	C-terminal synthetic peptide	1:1,000	Cell Singaling Technology (#12844)

Secondary antibody	Dilution for WB	Origin
anti-Rabbit-IgG (HRP coupled) polyclonal	1:10,000	Dianova GmbH , Hamburg
anti-Mouse-IgG (HRP coupled) polyclonal	1:10,000	Dianova GmbH , Hamburg

8.20 Molecular biology kits

Kit	Manufacturer
QIAprep® Spin Miniprep Kit	Qiagen, Hilden, Deutschland
QIAquick® Gel Extraction Kit	Qiagen, Hilden, Deutschland
QuantiTect® Reverse Transcription Kit	Qiagen, Hilden, Deutschland
RNeasy Mini Kit®	Qiagen, Hilden, Deutschland
NEBuilder® HiFi DNA Assembly Cloning Kit	New England Biolabs GmbH, USA
Q5®Site-Directed Mutagenesis Kit	New England Biolabs GmbH, USA
MEGAquick-spin™ Total Fragment DNA Purification Kit	iNtRON Biotechnology, Korea
DNA-spin™ Plasmid DNA Purification Kit	iNtRON Biotechnology, Korea
mMESSAGE mMACHINE™ T7 Transcription Kit	Thermo Fisher Scientific GmbH
RNA Clean & Concentrator Kit	Zymo Research, USA

8.21 Service providers

Service	Facility
DNA sequencing	Eurofins GATC Biotech GmbH
HPLC-purified synthetic oligonucleotides	biomers.net GmbH
Mass spectrometry (protein identification)	Proteomics Centre University of Konstanz

8.22 Software

Software	Company
Prism for macOS (Version 8.0.1)	GraphPad Software, Inc.
Fiji (ImageJ)	Wayne Rasband (NIH)
SnapGene®, Version 3.2.1	GSL Biotech LLC, Chicago
PeakTrak V1.1	Teledyne Isco, Inc.

9. Methods

9.1 *C. elegans* methods

9.1.1 Worm culture

All *C. elegans* strains used in this study were cultured as described before (Brenner, 1974). During experiments worms were kept at 20°C (plates and liquid culture), whereas stocks were stored on plates at 15°C. Small NG plates were applied for worm stocks and RNAi experiments. For assays, which premise high amounts of nematodes, chunks of NG plates were placed on HG plates and cultivated at 20°C.

9.1.2 Generation of transgenic strains

For localization studies, the *gfp::dnj-11* knock-in strain was generated using the CRISPR/Cas9 technique (Dickinson *et al*, 2013; Paix *et al*, 2014). Therefore, the sgRNA was inserted into the Cas-9 encoding plasmid #54 using the Q5® Site-Directed Mutagenesis Kit (Qiagen) and primer pair #3626 and sgRNA rev. The homologous repair template (HRT) was amplified via PCR using the plasmid #98 as template and the primers #3627 and #3628. By this amplification a glycin-rich linker was inserted between GFP and DNJ-11 to ensure proper functionality and folding of the two proteins. Microinjection in N2 worms was performed using 50 ng/µl Cas9/sgRNA template, 50 ng/µl HRT and 2.5 ng/µL pCFJ90 (*myo-2::mCherry*) as co-injection marker (Mello *et al*, 1991). Transgenic nematodes were directly screened for GFP fluorescence as described before (Paix *et al*, 2014). Unfortunately, *in vivo* the *Avi::3xFLAG::TEV* moiety was not expressed resulting in GFP-DNJ-11 only.

C. elegans strains expressing DNJ-11 variants were generated by injection of miniMos transposon vectors containing DNJ-11^{WT} (#262) or DNJ-11^{QPD} (#267) and DNJ-11$^{\Delta SANT}$ (#263) under the native promoter and 3'-UTR into N2 worms. Each injection mix included co-injection markers as follows: 10 ng/µL miniMos-based vector, 5 ng/µL CFJ421 (#22), 5 ng/µL pPD152.79 (#19), 50 ng/µL pCFJ601 (#7), 10 ng/µL pMA122 (#6) and 20 ng/µL DNA ladder. Germline expression was controlled by co-integration of a mCherry marker gene under control of the ubiquitous *icd-2* promoter and 3'-UTR. Transgenic strains were finally crossed with the *dnj-11(bc212)* strain and homozygous progenies were screened as described before (Paix *et al*, 2014).

9.1.3 Worm synchronization

Bleaching solution	11.25 mL sterile ddH_2O
	0.75 mL 5 M NaOH
	3.0 mL sodium-hypochlorite solution

Synchronized worm cultures were prepared via bleaching. All worms were lysed except the eggs, which are insusceptible to the bleaching solution.

For this purpose, NG plates containing starved L1 *C. elegans* larvae were placed on HG plates. The plates were incubated for at least 2 days at 20°C to obtain high amounts of young adults harboring a high proportion of eggs. After incubation agar pieces were removed, the plates were covered with 5 mL M9 buffer and incubated 5 min on a shaker to detach all worms. Worms were washed off and transferred into a sterile 15 mL flacon tube. Clumps were removed by several inverting steps and the nematodes were subsequently washed by centrifugation at 1,800*g* for 1 min in a swing-out rotor. Washing steps were repeated until the supernatant was clear. Afterwards worms were incubated with 15 mL bleaching solution for 5 min followed by three washing steps with M9 at 3,000*g* for 1 min. The pellet including nematode debris and intact eggs was resuspended in 15 mL M9 and transferred in a sterile flask. *C. elegans* larvae hatched over night at 20°C under constant agitation. The next day, development was resumed by adding *E. coli* food source. To get rid of worm debris during the bleaching procedure, a sucrose cushion step is optional. Therefore, after all bleaching and washing steps lysed worms were resuspended in 5 mL sterile water and an equal volume of 60% sucrose solution (in ddH_2O) was added. The solution was mixed and immediately centrifuged at 500*g* for 5 min in a swing-out rotor. The eggs swimming on top of the sucrose cushion were transferred in a 50 mL falcon and washed with M9 and re-pelleted by centrifugation at 3,000*g* for 3 min. Eggs were finally transferred into a sterile flask as described before.

9.1.4 Harvest *C. elegans* liquid culture

Liquid cultures of *C. elegans* were prepared in baffled flasks with S-medium and *E. coli* food source at 20°C under constant agitation. Depending on the conducted experiment, worms were either harvested at day 1 adult stage or treated with 150 µM Floxuridine at L4 stage to guarantee a synchronized culture by inhibiting egg lay and egg hatching (Mitchell *et al*, 1979).

To harvest the worms, the flask was put on ice for 30 min in a 45° angle to let worms settled to the bottom and were transferred to a falcon tube after aspiration of the medium. Worms were washed several times with ice-cold 0.1 M NaCl by gravity settling on ice until the supernatant became clear. Nematodes were resuspended in 25 mL ice-cold 0.1 M NaCl, and an equal volume of ice-cold

60% (w/v) sucrose solution was added. The sample was immediately mixed and centrifuged at 1,500*g* for 5 min at 4°C. Adult worms form a brown slurry film on top of the cushion which was aspirated off and transferred in a fresh falcon tube. After one final washing step in M9 buffer at 2,300*g* for 5 min at 4°C the worms were transferred with 0.1 M NaCl into a fresh falcon tube and settled via gravity on ice. The supernatant was aspirated off and *C. elegans* were flash frozen in liquid nitrogen and stored at -80°C.

9.1.5 Worm lysis

Worms were lysed using 1x SDS lysis buffer via sonication (10 pulses; Output control level 2; 50% DutyCycle) followed by incubation at 95°C for 5 min and final spin down at full speed in a table top centrifuge. Supernatant was provided with 5x SDS sample buffer. *C. elegans* harvested from liquid culture were lysed twice in a pre-cooled cryo mill for 30 s and 22 Hz. The resulting worm powder was flash frozen and stored at -80°C until use.

9.1.6 RNAi

Knockdown via RNAi was achieved by feeding the worms with *E. coli* HT115(DE3) transformed with the plasmid L4440 coding for the respective dsRNA or the empty vector (ev) control. The worms were subjected to RNAi at the L1 stage. For *hsp-1* knockdown the worms were exposed to RNAi at the L4 stage to prevent larval arrest. Worms were harvested on day 3 of adulthood.

9.1.7 Life span

For life span analyses worms were grown on *E. coli* HT115(DE3) RNAi as food source. The worms were subjected to *dnj-11* or empty vector control (ev) RNAi at L1 larval stage. Every day worms were scored and distinguished by response upon nose touch. Animals with vulval protrusion were censored. For each approach 120 worms were used and the median life span was calculated via the Kaplan-Meier survival curves.

9.1.8 Brood size

The brood size of N2 and mutant *C. elegans* strains was determined by counting the L4 progeny of 60 worms per experiment and strain. For the generation of a semi-synchronized population, an egg lay was performed for 3 h. As soon as the nematodes reached the adult stage they were transferred to a new plate each day. Egg lay was carried out until day 5 of adulthood. The number of progeny

was counted at L4 larval stage by flow cytometry. Data (n=3) were analyzed and significance was determined by an unpaired Student's t-test.

9.1.9 *C. elegans* microscopy

To analyze tissue und subcellular localization of GFP-tagged DNJ-11, worms of different ages were anesthetized with 25 mM levamisole. Images were taken on the confocal laser-scanning microscope Leica TCS SP8. Developmental stages of transgenic strains on NG plates were recorded by brightfield microscopy at the Leica DM5500B microscope. Images were adjusted using cropping and contrast tools of ImageJ software.

9.1.10 *C.elegans* cryostocks

For *C. elegans* cryo-conservation freshly starved L1 larvae were washed off NG plates with S-buffer. Same volume of S-buffer supplemented with 30% (v/v) glycerol was added and obtained samples were split in several 1.8 mL cryo-tubes. Tubes were gently frozen at -80°C.

9.2 *Saccharomyces cerevisiae* methods

Yeast strains were grown in YPD or in minimal medium (-His) at depicted temperatures.

9.2.1 Yeast transformation

Transformation-mixture	400 mM lithium-acetate
	40% (w/v) PEG-3350
	137 mM β-ME

Transformation-mixture was prepared freshly before each experiment. To start, 3 µL denatured carrier DNA (10 mg/mL fish sperm DNA boiled at 95°C for 10 min), 1 µg plasmid DNA and 100 µL transformation-mixture were mixed. Subsequently, one large yeast colony was resuspended in the prepared solution and thoroughly mixed by vortexing. The cells were incubated for 30 min at 37°C by constant agitation and afterwards pelleted via centrifugation for 2 min at 1,700*g* in a microcentrifuge. After discarding the supernatant, the cell pellet was resuspended in 100 µL ddH_2O and plated out on selective medium.

9.2.2 NaOH lysis

Yeast cells were lysed using the quick NaOH lysis method. Either the pellet of 1 mL of cells (OD_{600}=1) or one large colony was resuspended in 200 µL 0.1 M NaOH. Cells were incubated 10 min at RT and the OD_{600} was measured using 10 µL lysate and 990 µL ddH_2O. After centrifugation of the lysate the supernatant was discarded, and the cells were resuspended in appropriate amount of 1x SDS sample buffer. For Western Blot analysis OD_{600} = 1 were loaded.

9.2.3 Growth analysis (Spot test)

Stationary overnight cultures grown in synthetic complete media without histidine (SD-His) were diluted to 0.4 OD_{600} with 1.5 mL with ddH_2O. Afterwards, 240 µL of the dilutions were pipetted into a microtiter plate to prepare five-fold serial dilutions in sterile ddH_2O. The dilutions were spotted on SD-His plates and incubated at different temperatures (20°C, 30°C and 37°C) for several days. Intermediate results were documented.

9.3 Cell culture methods

HEK293 cells were cultivated under standard conditions (37°C, 5% CO_2, 95% humidity) in DMEM medium (see 8.10).

9.3.1 Transfection of HEK293 cells with siRNA

HEK293 cells were transfected with siRNA either in 24-well plates (validation of knockdown efficiency) or in 10 cm dishes. Three different concentrations (1 nM, 5 nM and 25 nM) of four different siRNAs (see 8.17) were tested. Stock solutions (10 µM) of siRNA were prepared in 1x siRNA buffer (see 8.3). Control siRNA was used in a concentration of 25 nM (pre-test) and 5 nM in 10 cm dishes. Lipofectamin and siRNA were both mixed with OptiMEM® medium in two separate tubes. The siRNA mixture was transferred into the tube containing Lipofectamin and both components were mixed thoroughly. The solution was incubated for 20 min at RT and then provided in 24 wells or 10 cm dishes. The mixture was overlaid with HEK293 cells in DMEM medium. Cells were cultivated for 24, 48 or 72 h and knockdown efficiency was tested using immunoblotting.

Table 1: Transfection mixtures

24-well	Tube 1	Tube 2	Cell number	DMEM medium
Opti-MEM	100 µL	100 µL	9×10^4	1 mL
Lipofectamin	2 µL	/		
siRNA	/	x µL		
10 cm dish				
Opti-MEM	1000 µL	1000 µL	1.4×10^6	10 mL
Lipofectamin	24 µL	/		
siRNA	/	x µL		

9.3.2 Harvest and lysis of HEK293 cells

Transfected HEK293 cells were harvested by dispensing cells in fresh medium (1 mL/24 well or 10 mL/10 cm dish). Cells were transferred into a reaction tube and centrifuged for 3 min at 400*g* and washed once with 1x PBS . Cell numbers were determined using the LUNA™ Automated Cell Counter. Cells were again pelleted at 400*g* for 3 min and finally resuspended in 2x SDS sample buffer to reach a concentration of 5,000 cells/µL. Per sample the lysate of 25,000 cells was analyzed by immunoblotting.

9.4 Molecular cloning

9.4.1 Plasmid purification

Vectors were extracted and purified from *E. coli* with the help of the QIAprep® Spin Miniprep Kit or DNA-spin™ Plasmid DNA Purification Kit according to the manufacturer's protocol. DNA was eluted from the column with 30-50 µL ddH_2O due to requested DNA concentration. Plasmid DNA applied in microinjection approaches was purified with the QIAprep® Spin Miniprep Kit and eluted in 30 µL EB buffer. The microinjection mix for *C. elegans* was also prepared in EB buffer and centrifuged for 15 min at full speed in a table top centrifuge before usage.

9.4.2 Reverse transcription

For amplification purposes *C. elegans* cDNA was prepared by total RNA extraction (RNeasy Mini Kit®) and following reverse transcription. Worm powder was solved in 350 µL RLT buffer and sonicated six times (Output control level 2; 50% DutyCycle). Cell depris were pelleted by full speed centrifugation for 2 min. The supernatnat was applied on a column and RNA was

purified according to the manufacturer's protocol. Finally, the RNA was eluted in 30 µL ddH_2O and 1,000 ng total RNA was reverse transcripted via QuantiTect®Reverse Transcription Kit. Genomic DNA was removed by addition of 1 µL Wipeout buffer in an end volume of 10 µL and subsequent incubation for 2 min at 42°C, followed by a cool down on ice for 5 min. For reverse transcription 2.2 µL 5x RT buffer, 0.55 µL RT primer mix and 0.55 µL reverse transcriptase were added. The reaction was incubated 15 min at 42°C, 3 min at 95°C and cooled down to 4°C.

9.4.3 Polymerase chain reaction (PCR)

The polymerase chain reaction was used to amplify specific DNA fragments from a vector template or total cDNA. Each 50 µL PCR approach included 200-500 ng DNA template, 1x Phusion buffer, 0.2 mM dNTP mix (stock: 10 mM), 1 µM of each primer (stock: 10 µM) and 1 µL Phusion polymerase in an end volume of 50 µL. The amplification was performed in thermal cyclers (Analytic Jena). 6x Loading Dye was added to the samples and the whole sample volume was loaded onto a preparative 1% agarose gel.

Table 2: PCR program

	Temperature	Time	Cycle
Primary denaturing	98°C	5 min	1x
Denaturing	98°C	20 s	
Annealing	55°C	20 s	32x
Elongation	72°C	2,000 bp/min	
Finale elongation	72°C	10 min	1x
Cooling down	8°C	∞	

9.4.4 Restriction digest

During cloning procedure PCR products or vectors were digested in 1x CutSmart buffer (stock: 10 x) with 1 µL restriction enzyme(s). The reaction volume was adjusted to an end volume of 50-60 µL with sterile ddH_2O. Digestion took place at 37°C for 2 h. Digested PCR products or vectors were loaded onto an 1% preparative agarose gel.

9.4.5 Agarose gel electrophoresis

To separate DNA fragments according to their size, agarose gel electrophoresis was applied using an 1% (w/v) agarose gel in 1x TAE and provided with 10% (v/v) Midori Green. Separation took place at a constant current of 120 V. As size standards the 1 kb or 100 bp Gene Ruler Marker® was used. Bands were visualized under UV light.

9.4.6 Gel extraction

Amplified or digested DNA fragments were cut out of the agarose gel using a sharp scalpel. Extraction was conducted with the QIAquick® Gel Extraction Kit or MEGAquick-spin™ Total Fragment DNA Purification Kit, according to the manufacturer's instructions. DNA was eluted from the column with 50 µL (after digestion) or 43 µL (after amplification, before digestion) sterile ddH_2O.

9.4.7 Dephosphorylation of vector DNA and ligation

In order to prevent religation of the linearized vector DNA, 40 µL extracted plasmid was dephosphorylated using 5 units Antarctic Phosphatase (AP) and 1x Antarctic Phosphatase Buffer in an end volume of 50 µL. The sample was incubated at 37°C for 45 min and the reaction was stopped by heat inactivation for 5 min at 70°C.
Following formula was applied to calculate the ligation approach of vector and insert during standard cloning procedures using a molar ratio of 3/1 (Insert/Vector):

$$ng\ Insert = \frac{ng\ Vector\ x\ Insert\ (bp)}{Vector\ (bp)} \times molar\ ratio\ {}^{Insert}/_{Vector}$$

9.4.8 DNA assembly

For recombinant protein purification, pSUMO vectors were generated using the NEBuilder® HiFi DNA Assembly Cloning Kit. Inserts were amplified from cDNA using the suitable primers (see 8.16) whereas the pSUMO vector was linearized via *BsaI* digestion. Ligation of vector and insert was conducted in a final volume of 10 µL including 5 µL NEBuilder® HiFi DNA Assembly Master Mix and a molar Insert/Vector ratio of 2/1 (see 9.4.7). The reaction was incubated at 50°C for 15 min and finally transformed in chemically competent *E. coli* cells.

9.4.9 Q5 Mutagenesis

Primers for mutagenesis reactions were created via NEBaseChanger®. Mutagenesis of vectors was performed with the Q5® Site-Directed Mutagenesis Kit following the manufacturer's instructions. The approach was downscaled using 12.5 ng template DNA, 6.25 µL 2 x Q5® Hot Start High-Fidelity Master Mix, 0.63 µL of forward and reverse primer (stock 10 µM) and 4.5 µL nuclease free water. After KLD (**K**inase **L**igase **D**pnI) reaction the DNA was immediately transformed in chemically competent *E. coli* cells.

9.4.10 Heat shock transformation of chemically competent *E. coli*

During this thesis three different chemically competent *E. coli* strains were transformed with vectors. DH5αZ1 cells were used during standard cloning procedures. RNAi experiments were conducted with HT115 cells, which were transformed with modified pL4440 vectors. For recombinant protein expression BL21(DE) /pRARE cells were used.
DNA was added to ice-cold 50 µL bacterial cells and incubated for 20 min on ice. After heat shock for 90 s at 42°C the cells were shortly cooled down on ice and provided with 1 mL LB medium. For phenotypic expression *E. coli* cells were incubated at 37°C for 60 min under constant agitation. The cells were pelleted by centrifugation and plated on LB-plates provided with the required antibiotic(s). The plates were incubated over night at 37°C.

9.5 Biochemical methods

9.5.1 Bradford assay

Protein concentrations were measured via the Bradford assay using 1 mL 1x Bradford solution and 1 µL of proteins (amount of protein was adjusted, if protein solution was low concentrated). After 10 min incubation at RT absorbance was measured in triplicates at 595 nm and protein concentration was calculated via dividing the values by 0.06.

9.5.2 BCA assay

Due to disturbance of SDS in the Bradford assay, protein concentrations of worm lysates were also measured via the BCA assay. As a standard curve 0-20 µg BSA were adjusted in 50 µL (ddH_2O), respectively. Protein samples were diluted 1:50 in ddH_2O and both, standard and protein samples, were mixed with 1 mL BCA working solution (see 8.3). Samples were incubated 15 min at 60°C and

500 r.p.m in a thermoblock. After short cool-down on ice the absorbance was measured at 562 nm. Protein concentrations were calculated using the standard BCA curve.

9.5.3 SDS polyacrylamide gel electrophoresis

SDS gels were prepared for Coomassie staining, whereas Bis-Tris gels were used for Western Blot analysis. Polyacrylamide gels were prepared as follows:

Table 3: 10% SDS gel

	Stacking gel	Separation gel
Acrylamide/Bisacrylamide (37.5:1)	2.0 mL	3.25 mL
Buffer	2.5 mL	2.5 mL
ddH_2O	6.5 mL	4.2 mL
10% APS	0.1 mL	0.05 mL
TEMED	0.02 mL	0.02 mL

Separation via 1x SDS running buffer

Table 4: 10% Bis-Tris gel

	Stacking gel	Separation gel
Acrylamide/Bisacrylamide (37.5:1)	0.7 mL	1.75 mL
Buffer	1.5 mL	1.5 mL
ddH_2O	3.0 mL	2.0 mL
10% APS	0.031 mL	0.037 mL
TEMED	0.015 mL	0.01 mL

Separation via 1x MOPS running buffer

Proteins were concentrated in the stacking gel using a constant current of 100 V. The actual separation took place at 150 V.

9.5.4 Western blot

Transfer of separated protein samples onto a nitrocellulose membrane was performed via standard protocols using 1x Western Blot transfer buffer and 100V for 1 h. The membrane was blocked with 5% milk powder in 1x TBS-T for 1 h changing the milk solution at least three times in between. Primary antibodies were diluted in 3% milk powder TBS-T (polyclonal) or 1x TBS-T (monoclonal), respectively (see 8.19). Incubation was performed at 4°C over night under constant agitation followed by three washing steps with 1x TBS-T the next day. The membrane was finally incubated with secondary HRP-coupled antibodies for 1 h (see 8.19). Chemiluminescence was detected by

covering the membrane with ECL solution and readout via the Chemiluminescence imager Fusion SL.

9.5.5 qPCR

For quantitative PCR total *C. elegans* RNA was extracted via the RNeasy Mini Kit® and reverse transcripted using the QuantiTect® Reverse Transcription Kit according to the manufacturer's instructions. The cDNA was diluted 1:2 with ddH_2O and the PCR reaction was performed with the ABI 7500 Fast Real-Time PCR System (Applied Biosystems) using the GoTaq SYBR®Green mix (Promega). For each reaction 1 µL cDNA, 5 µL SYBRGreen master mix, 3.5 µL ddH_2O and 0.25 µL of forward and reverse primer were used. *Ama-1* served as a reference gene and relative mRNA levels were calculated by the $2^{-(\Delta\Delta Ct)}$ method.

Table 5: qPCR program

	Temperature	Time	Cycles
Initial denaturation	95°C	2 min	1x
Denaturation	95°C	3 s	35x
Annealing	60°C	30 s	
Melting curve	65-95°C	5 s	0.5°C/step

$Ct \longrightarrow cycle\ threshold$ (cycle number when the PCR generated fluorscence is distinguishable from the background noise)

$$\Delta Ct = Ct(gene\ of\ interest) - Ct(housekeeping\ gene)$$

$$\Delta\Delta Ct = \Delta Ct(treated\ sample) - \Delta Ct(untreated\ sample)$$

$$\text{Fold gene expression} = 2^{-(\Delta\Delta Ct)}$$

9.5.6 Polysome profile analysis

Lysis buffer

30 mM HEPES-KOH pH 7.4
50 mM KOAc
5 mM $MgCl_2$
5% (w/v) mannitol
100 µg/mL cycloheximide
2 mM β-ME
1 x Complete protease inhibitor cocktail

Worms were cultivated in liquid culture in S-medium in presence of *E. coli* OP50 as food source at 20°C under constant agitation. On day 2 of adulthood *C. elegans* were harvested on ice in 0.1 M NaCl and separated from bacteria via sucrose flotation. After an additional washing step, the nematodes were flash frozen in liquid nitrogen. Worm pellets were ground to powder using a pre-cooled cryo mill for 30 s at 22 Hz. An aliquot was resuspended in lysis buffer and centrifuged at 18,000*g* for 15 min at 4°C. The supernatant was adjusted to 20 A_{260} and 500 µL were loaded on a sucrose gradient (15% - 45% in lysis buffer). Ribosomal species were separated via ultracentrifugation (TH-641; Sorvall) at 39,000 r.p.m for 2.5 h (4°C). Fractionation of the gradients was achieved with a density gradient fractionator monitoring the A_{254}. Received data were processed with PeakTrak V1.1. Aliquots of the collected fractions were subjected to immunoblot analysis.

9.5.7 Ribosome sedimentation assay

Lysis buffer

20 mM HEPES-KOH pH 7.4
50 mM KOAc
2 mM $Mg(OAc)_2$
2 mM DTT
1 mM PMSF
100 µg/mL cycloheximide
1 x Complete protease inhibitor cocktail

Frozen *C. elegans* pellets (day 2 of adulthood) were ground twice in a pre-cooled cryo mill for 30 s at 22 Hz. Frozen powder was resuspended in lysis buffer and centrifuged at 20,000*g* for 10 min at 4°C in order to get rid of cell deposits and protein aggregates. The supernatant was filtrated and adjusted to 4.5 A_{260} in 600 µL lysis buffer containing different KOAc concentrations. For ribosome sedimentation 1.5 A_{260} (200 µL) lysate was loaded on 600 µL sucrose cushion (lysis buffer without cycloheximide + 25% (w/v) sucrose) and centrifuged at 200,000*g* for 90 min at 4°C. The ribosomal pellet was dissolved in lysis buffer with the appropriate salt concentration. The supernatant as well as the total lysate were precipitated with a final concentration of 20% TCA for 90 min on ice. After centrifugation for 30 min at 20,000*g* the precipitate was washed twice with ice-cold acetone for 10 min at 20,000*g*. Total, supernatant and pellet fractions were analyzed via immunoblotting.

9.5.8 Co-immunoprecipitation

Lysis buffer	50 mM Tris-HCl pH 7.5
	150 mM NaCl
	2 mM EDTA
	1 mM EGTA
	0.5% NP-40
	1 x Complete protease inhibitor cocktail

C. elegans were ground to powder using a cryo mill (30 s, 22 Hz). The powder was subsequently resuspended in lysis buffer and samples were incubated on ice for 10 min. To get rid of cell debris the lysate was centrifuged at 13,000*g*. The supernatant was filtrated through a 0.45 µm cellulose filter (Sartorius), and protein concentration was adjusted to 10 µg/µL in 300 µL and afterwards incubated with an anti-DNJ11 antibody. After incubation under constant rotation for one hour at 4°C, 30 µL Protein A Magnetic Beads were added and again the samples were incubated for one hour at 4°C. The beads were finally washed four times with lysis buffer and elution was achieved by adding 25 µL 2 x SDS sample buffer and heating up to 99°C for 5 min at 900 r.p.m in a thermomixer.

9.5.9 Protein purification

Lysis buffer	50 mM Na-PO_4 pH 8.0
	300 mM NaCl
	6 mM $MgCl_2$
	10% glycerol
	10 mM imidazole
	2 mM β-ME
	2 mM PMSF
	1x protease inhibitors (Aprotinin, Leupeptin, Pepstatin)
Dialysis buffer	20 mM Na-PO_4 pH 7.4
	25 mM NaCl
	6 mM $MgCl_2$
	2 mM β-ME
	5% glycerol

Protein buffer	40 mM HEPES-KOH pH 7.4
	100 mM KOAc
	5 mM $MgCl_2$
	1 mM β -ME
	10% glycerol

For recombinant protein expression *E. coli* BL21(DE3) /pRARE cells were transformed with either His^6-SUMO-DNJ-11, His^6-SUMO-HSP-1, His^6-SUMO-DNJ-13 or for co-expression His^6-SUMO-DNJ-11/HSP-1 (ceRAC or N-ceRAC: 2-42aa of DNJ-11). Cells were cultivated at 20°C and protein expression was induced at OD_{600} 0.6-0.8 by 1 mM IPTG overnight. Bacteria were harvested and subsequently lysed via French Press (2x 1,100 psi) in lysis buffer and one spatula of *DNase I* (for purification of HSP-1 and ceRAC 5 mM ATP were added to lysis buffer). Lysates were centrifuged twice for 20 min at 30,000*g* (4°C) and the supernatant was incubated with Protino® Ni-NTA matrix for 60 min at 4°C. After several washing steps with wash buffer (lysis buffer with 20 mM imidazole without PMSF and protease inhibitors; for HSP-1 and ceRAC with 5 mM ATP) the proteins were eluted in elution buffer (wash buffer with 250 mM imidazole). The His6-SUMO-tag was cleaved by Ulp1 (8 µg/mg protein) overnight in dialysis buffer. As an additional purification step proteins were loaded on ion-exchange chromatography columns (HSP-1 and ceRAC: anion exchanger MonoQ® 5/50 GL, 1 mL; DNJ-11 and DNJ-13: cation exchanger MonoS®5/50 GL, 1 mL; both GE Healthcare) and eluted in 500 µL fractions via linear salt gradient of 25 CV (dialysis buffer 25-750 mM NaCl; for purification of HSP-1 and ceRAC 5 mM ATP were added). Samples containing DNJ-11 or DNJ-13 were dialyzed in protein buffer, flash frozen in liquid nitrogen and stored at -80°C. In case of HSP-1 and ceRAC the proteins were further purified by a gelfiltration step on a Superdex®200 Increase 10/300 (GE Healthcare) column in protein buffer.

9.5.10 Purification of firefly luciferase

Lysis buffer	30 mM $NaPO_4$ pH 8
	500 mM NaCl
	5 mM $MgCl_2$
	10% glycerol
	1 mM PMSF
	1 mM β-ME
	1x protease inhibitors (Aprotinin, Leupeptin, Pepstatin)

Low/High salt wash	30 mM $NaPO_4$ pH 8
	50 mM/1 M NaCl
	5 mM $MgCl_2$
	10% glycerol
	1 mM β-ME
Elution buffer	30 mM $NaPO_4$, pH 8
	50 mM NaCl
	5 mM $MgCl_2$
	10% glycerol
	1 mM β-ME
	250 mM imidazole
Low salt/High salt buffer	30 mM $NaPO_4$, pH 8
	50 mM/750 mM NaCl
	5 mM $MgCl_2$
	10% glycerol
	1 mM β -ME

To purify firefly luciferase, BL21(DE) /pRARE *E. coli* cells were transformed with the plasmids #1422 and #747. Precultures (in presence of Ampicillin, Chloramphenicol and Spectinomycin) were grown at 30°C to a final OD_{600} of 0.6-0.8. The culture was switched to 20°C and overnight expression was induced by the addition of 1 mM IPTG. Cells were harvested and lysed in lysis buffer (+ one spatula of *DNase I*) via French Press (2x 1,100 psi). The lysate was centrifuged twice for 20 min at 30,000*g* (4°C) and the supernatant was subsequently incubated with 2 g Protino® Ni-IDA for one hour at 4°C under constant agitation. The slurry was transferred into a column and the matrix was washed with 40 mL high salt wash buffer followed by 40 mL low salt wash buffer. His^6-Luciferase was eluted from the column with five times 5 mL in elution buffer. Fractions containing firefly luciferase were pooled and dialyzed overnight in dialysis buffer. For additional purification the sample was loaded on an anion exchange column (MonoQ®5/50 GL, 1 mL, GE Healthcare) and eluted via a linear salt gradient of 25 CV (50-750 mM NaCl). Pure luciferase was found in the flow through fraction whereas all impurities were bound to the column. The flow through was dialyzed overnight in protein buffer (see 9.5.9).

9.5.11 Purification of *C. elegans* 80S ribosomes

Lysis buffer	50 mM HEPES-KOH pH 7.4
	0.5% NP-40
	6 mM $MgCl_2$
	300 mM NaCl
	20 µM Phenanthrolin
	1 mM PMSF
	2 mM DTT
	1 x Complete protease inhibitor cocktail
60% Sucrose cushion	60% (w/v) sucrose
	50 mM HEPES-KOH pH 7.4
	50 mM KCl
	10 mM $MgCl_2$
	5 mM EDTA
	1 x Complete protease inhibitor cocktail
Resuspension buffer	50 mM HEPES-KOH pH 7.4
	150 mM KCl
	1 mM DTT
10-40% Sucrose gradients	10% and 40% (w/v) sucrose
	50 mM HEPES-KOH pH 7.4
	120 mM KCl
	4 mM $MgCl_2$
	1 mM DTT
	1 x Complete protease inhibitor cocktail
Storage buffer	20 mM HEPES-KOH pH 7.4
	100 mM KCl
	5 mM $MgCl_2$

For *C. elegans* 80S ribosome preparation asynchronous N2 worm pellets were ground to powder using a pre-cooled cryo mill for 1 min at 30 Hz. The resulting powder was resolved in lysis buffer

under constant agitation and centrifuged at 12,000*g* for 10 min at 4°C. The lysate was divided and loaded on 60% sucrose cushions. To pellet all ribosomes the lysate was centrifuged at 244,000*g* for 20 h at 4 °C. Resulting pellets were solved in resuspension buffer and incubated with 1 mM puromycin for 30 min on ice to release nascent polypeptides. Ribosomes were centrifuged at 20,000*g* for 10 min at 4°C. To separate the different ribosomal species the supernatant was loaded on multiple 10-40% sucrose gradients and centrifuged at 99,500*g* for 17 h. Ribosomes were fractionated with a density gradient fractionator and hereafter the 80S fractions were concentrated (100,000 MWKO) accompanied by buffer exchange into storage buffer.

9.5.12 *In vitro* ribosome binding

Ribo buffer	30 mM HEPES-KOH pH 7.4
	120 mM/300 mM KOAc
	5 mM $MgCl_2$
	1 mM β-ME
	1x Complete protease inhibitor cocktail

To test for *in vitro* ribosome binding, proteins (0.5 µM, 1 µM or 4 µM) and 80S ribosomes (0.5 µM or 1 µM) were mixed in Ribo buffer and incubated for 30 min at 18°C. Samples were loaded on a 25% sucrose cushion prepared in Ribo buffer and centrifuged at 220,000*g* for 90 min at 4°C. To prepare soluble proteins the supernatant was precipitated via 20% TCA and the resulting pellet was resuspended in Protein sample buffer. The ribosomal pellet was resuspended in Ribo buffer by constant agitation and finally mixed with sample buffer. Same volumes of supernatant and pellet fractions were analyzed by immunoblotting.

9.5.13 Single turn-over ATPase assay

ATP mix	20 mM ATP
	12 µCi [α^{32}P]-ATP
Reaction buffer A	25 mM HEPES-KOH pH 7.6
	50 mM KCl
	10 mM $MgCl_2$

The ATPase activities of HSP-1 and ceRAC were determined under single turn-over conditions. The HSP-1-ATP and ceRAC-ATP complexes (final volume 50 µL) were formed by mixing HSP-1

or ceRAC (final concentration 30 µM) and 2 µL of ATP-mix in reaction buffer A and leaving the mixture for two min on ice. The complex was isolated at 4°C by size exclusion chromatography on Sephadex G-50 (GE Healthcare) columns, pre-saturated with 1 mL of a BSA solution (1 mg/mL) and pre-equilibrated with three column volumes of buffer A. Twenty fractions (2 drops/fraction) were collected. The first four fractions containing radioactivity as detected by a Geiger counter were pooled, divided into 6.5 µL aliquots, snap frozen in liquid nitrogen and kept at -80°C. For the ATPase activity determination HSP-1-ATP or ceRAC complexes were thawed in a water bath at 20°C and, after withdrawal of 0.5 µL for the 0 time point, mixed with 44 µL reaction buffer containing either no cofactors or 1 µM DNJ-11, DNJ-13, or ceRAC. At different time points a 2 µL aliquot was spotted onto a PEI Cellulose TLC plate. Developing the plates in the TLC solution (400 mM LiCl, 10% acetic acid) separated ADP from ATP. Dried plates were exposed to FI-screens overnight and relative amounts of ATP and ADP were quantified by Fuji FLA 2000 Phosphoimager.

9.5.14 Luciferase refolding assay

Denaturing buffer	25 mM HEPES-KOH pH 7.4
	50 mM KCl
	15 mM $MgCl_2$
	1 mM ATP
	10 mM DTT
	0.05 mg/mL BSA
	5 M GdmCl

Luminescence buffer	75 mM HEPES-KOH pH 7.4
	50 mM KCl
	15 mM $MgCl_2$
	1 mM ATP
	2 mM DTT
	0.05 mg/mL BSA
	240 µM coenzyme A
	0.1 mM luciferin
	10 mM PEP
	50 µg/mL pyruvate kinase

Luciferase refolding activity was measured as previously described (Sun *et al*, 2012). Recombinant luciferase (2.5 µM) was chemically denatured for 45 min at RT in denaturing buffer. To test for refolding activity, denatured luciferase was diluted 1:125 (0.02 µM) and incubated with 3.2 µM HSP-1/ceRAC/N-ceRAC and 0.8 µM DNJ-13/ceRAC in luminescence buffer. Luminescence was measured in 96-well LIA-plates (Greiner Bio-One, Solingen, Germany) over 2 h at RT in a multimode reader.

To test for holding chaperone function of NAC, 0.02 µM luciferase was preincubated in the presence or absence of 0.02 µM NAC variants for 15 min at RT before addition of the Hsp70/JDP system.

9.5.15 Peptide-binding analysis

Peptide-binding of HSP-1 and ceRAC was tested by size exclusion chromatography using a dansyl-labelled small peptide, D-NR peptide (NRLLLTGC labelled with dansyl chloride; 7 kDa). 5 µM HSP-1 or ceRAC were incubated with 80 µM D-NR peptide in presence or absence of 1.25 µM DNJ-13 or ceRAC in protein buffer supplemented with 5 mM ATP (see 9.5.9) for 30 min at 20°C. Samples were loaded on a Superdex®200 Increase 10/300 column (GE Healthcare) and fractions were subsequently measured in a multimode reader in order to detect fluorescence of the D-NR peptide (λ_{ex} = 335 nm, λ_{em}= 525 nm).

9.5.16 Preparation of insoluble protein samples

Lysis buffer	30 mM HEPES-KOH pH 7.4
	50 mM KOAc
	5 mM $MgCl_2$
	5% (w/v) mannitol
	2 mM β-ME
	1 x Complete protease inhibitor cocktail

SDS protein lysis buffer	62.5 mM Tris-HCl pH 6.8
	1 mM EGTA pH 8
	2% SDS
	10% sucrose
	1 x Complete protease inhibitor cocktail

For total soluble lysate, *C. elegans* were ground in a cryo mill and solved in lysis buffer. The worms were sonicated four times with six pulses (Duty Cycle 50%; output control 2) and centrifuged for 20 min at 19,000*g*. The supernatant represents the soluble protein fraction.
After determination of the A_{260}, the pellet was washed once in 1 mL lysis buffer (+ 0.08% digitonin) by incubation for 5 min on ice and centrifugation for 20 min at 19,000*g* at 4°C. The resulting pellet was extracted by dissolving in appropriate volume of SDS protein buffer compared to soluble A_{260}. The pellet was sonicated two times for ten pulses (Duty Cycle 50%; output control 2) and heated for 5 min at 95°C. The sample was centrifuged for 3 min at 19,000*g* at RT. The final supernatant contains the insoluble protein fraction. Soluble and insoluble protein fractions were analyzed by immunoblotting.

9.5.17 Generation and *in vitro* translation of non-stop mRNAs

Non-stop transcript templates were generated by PCR as previously described (Sharma *et al*, 2010). In brief, the T7 promoter (TAATACGACTCACTATAGGGAGA) needed for *in vitro* transcription was included in the 5' end of the forward primer. The reverse primer encoded five C-terminal methionines for radioactive [S^{35}]-labeling and a terminal valine residue to stabilize the tRNA-nascent chain complex. PCR was performed on a plasmid containing the human gene GPI (glucose-6-phosphate isomerase) and the PCR product were purified by gel extraction. DNA templates were *in vitro* transcribed using the mMESSAGE mMACHINE™ T7 Transcription Kit according to manufacturer's protocol. RNA was purified with RNA Clean & Concentrator Kit. Non-stop mRNAs were *in vitro* translated using rabbit reticulocyte lysate (0.5 µg RNA in a 25 µL translation reaction). Translation reactions were performed at 26°C for 20 min in the presence of 1 mCi/mL [S^{35}]-methionine.

9.5.18 Purification of RNCs

RNC wash buffer	50 mM HEPES-KOH pH 7.5
	500 mM KOAc
	5 mM $Mg(OAc)_2$
Crosslinking buffer	50 mM HEPES-KOH pH 7.0
	100 mM NaCl
	5 mM $MgCl_2$
	0.1% NP-40
	1x Complete protease inhibitor cocktail

Translation reactions were layered on a 25% (w/v) sucrose cushion in RNC wash buffer and centrifuged at 200,000*g* for 90 min at 4°C. The ribosomal pellets were resuspended in DSS crosslinking buffer by constant agitation for 1 h on ice.

9.5.19 DSS crosslinking

RAC variants were added to the resuspended RNCs at a concentration of 2 µM, and incubated at 20°C for 15 min. DSS was added at a final concentration of 125 µM and crosslinking was performed for 10 min at 20°C. The reaction was quenched with 60 mM Tris-HCl pH 7.5 for 5 min at 20 °C. [S^{35}]-Methionine labelled tRNA-NCs and crosslinked complexes were separated by SDS–PAGE and visualized by autoradiography.

9.6 Computational analysis

9.6.1 Sequence alignment

Protein sequences of Ssz1 and Zuotin homologs were blasted and extracted from UniProt database. Multiple sequence alignments were performed with CLUSTALW and processed with CLC Sequence Viewer 7.7.1.

9.6.2 Molecular dynamics simulations

All molecular dynamics simulations were obtained by GROMACS version 2016.4 and 2019.1 (Pronk *et al*, 2013; Abraham *et al*, 2015) using the CHARMM36m (Huang *et al*, 2016; Bjelkmar *et al*, 2010) force field together with the tip3p11 (Jorgensen *et al*, 1983) water model. The simulation box was set to dodecahedron shape and defined in such a way that the minimum distance of the structure and the box was at least 2.0 nm (to accommodate possible unfolding of the DNJ-11N peptide and allow for mobility of the interdomain linker). Subsequently the protein was solvated with water and neutralized by sodium chloride. Three independent simulations were started with different initial conditions.

The following simulation settings have been used. The Leap frog integrator was utilized together with H-bonds being constrained by the LINCS algorithm (Hess *et al*, 1997) in order to enable a time-step of 2 fs. Long range Coulomb interactions were calculated by particle mesh Ewald (PME) (Essmann *et al*, 1995) method with a cutoff of 1.2 nm. A modified cutoff scheme for short-ranged electrostatic and Lenard Jones interactions of 1.2 nm, where a switching function is applied to

smoothly approach the cutoff between 1.0 and 1.2 nm, was used. The neighbor list was updated every 20 steps. Initially, all systems were energy minimized with steepest-descent algorithm for 5000 steps. In the next step an equilibration simulation followed (100 ps) in a canonical (NVT) ensemble was carried out where heavy atoms have been position restrained. The actual production simulations (a total of approximately 600 ns) were carried out in an isobaric-isothermal (NPT) ensemble without position restraints. The temperature was maintained at 298 K by using the Velocity-rescaling algorithm (Bussi *et al*, 2007) with a coupling time of 0.1 ps. Constant pressure was maintained at 1 atm using isotropic Parrinello-Rahman pressure coupling (Parrinello & Rahman, 1981)with a pressure relaxation time of 5 ps.

10. Abbreviations

°C	degree Celsius
A. thaliana	*Arabidopsis thaliana*
a.u.	arbitrary units
A_{260}	absorbance at 260 nm
aa	amino acid
ADP	adenosine diphosphate
Amp^R	Ampicillin resistance
APS	ammonium persulfate
atm	atmosphere
ATP	adenosine triphosphate
B. malayi	*Brugia malayi*
BCA	bicinchoninic acid
bis-tris	bis-(2-hydroxy-ethyl)-amino-tris(hydroxymethyl)-methane
bp	base pairs
BSA	bovine serum albumin
Btt	BTf Three
C. briggsae	*Caenorhabditis briggsae*
C. elegans	*Caenorhabditis elegans*
C. thermophilum	*Chaetomium thermophilum*
Cam^R	Chloramphenicol resistance
ceRAC	C. elegans RAC
CV	column volumes
D. magna	*Daphnia magna*
D. melanogaster	*Drosophila melanogaster*
ddH_2O	double-distilled water
DMEM	Dulbecco's Modified Eagle Medium
DMSO	dimethyl sulfoxide
dsRNA	double-stranded RNA
DSS	disuccinimidyl suberate
DTT	dithiothreitol
E. coli	*Escherichia coli*
e.g.	for example
EDTA	ethylendiaminetetraacetic acid
Egd	Enhancer of Gal4 DNA binding
et al.	lat.: „et alii" (and others)
ev	empty vector
FCS	fetal calf serum
Fig.	figure
fs	femtosecond(s)
GdmCl	guanidinium chloride
GFP	green fluorescent protein
h	hour(s)
H. sapiens	*Homo sapiens*
HEK	human embryonic kidney
HEPES	4-(2-hydroxyethyl)-1-piperazineethanesulfonic
HG	high growth
HPD	histidine-proline-aspartate
HRP	horse reddish peroxidase
Hsc	constitutively expressed heat shock protein

Hsp	heat shock protein
IP	immunoprecipitation
IPTG	isopropyl β-D-1-thiogalactopyranoside
JPD	J-domain protein
K	Kelvin
kb	kilobases
kDa	kilodalton
KOAc	potassium acetate
L	liter(s)
mA	milliampere
mCi	millicurie
MeOH	methanol
Met	methionine
min	minute(s)
mM	millimolar
MOPS	3-MOrpholinoPropane-1-Sulfonic acid
mRNA	messenger ribonucleic acid
NAC	nascent polypeptide-associated complex
NaOH	sodium hydroxide
NAT	N-acetyltransferase
NBD	nucleotide-binding domain
NEF	nucleotide exchange factor
NG	normal growth
ns	nano seconds
O. volvulus	*Onchocerca volvulus*
OD_{600}	optic density at 600 nm
PBS	phosphate Buffered Saline
PCR	polymerase chain reaction
PEP	phosphoenolpyruvate
pH	Pondus Hydrogenii
PMSF	phenylmethylsulfonylfluoride
PolyQ	polyglutamine
ps	picosecond(s)
r.p.m	rounds per minute
RAC	ribosome-associated complex
RNA	ribonucleic acid
RNAi	RNA interference
RNC	ribosome-nascent-chain complex
RT	room temperature
s	second(s)
S. cerevisiae	*Saccharomyces cerevisiae*
S. pombe	*Schizosaccharomyces pombe*
SANT	Swi3, Ada2, No-cor, TFIIIB
SBD	substrate-binding domain
SD	standard deviation
SDS	sodium dodecyl sulfate
SDS-PAGE	SDS polyacrylamide gel electrophoresis
sgRNA	single guide RNA
siRNA	small interfering RNA
SRP	signal recognition particle
Ssa	stress seventy family A
Ssb	stress seventy family B

Ssz	stress seventy family Z
TAE	tris-acetate
TBS	tris-buffered saline
TBS-T	tris-buffered saline with tween 20
TCA	trichloracetic acid
TEMED	tetramethylethylenediamine
UBA	ubiquitin-associated
Ulp	Ubl-specific protease 1
V	Volt
v/v	volume per volume
w/o	without
w/v	weight per volume
WB	Western Blot
WT	wildtype
YPD	yeast extract peptone dextrose
Zuo1	Zuotin
β-ME	β-mercaptoethanol

11. Acknowledgements (Danksagung)

Auf dieser Seite möchte ich nun allen Menschen danken, die mich während meiner Arbeit unterstützt und begleitet haben.

An erster Stelle möchte ich mich ganz herzlich bei Prof. Dr. Elke Deuerling bedanken. Vielen Dank für die Zuteilung dieses spannenden Projektes. Die Arbeit hat mich in vieler Hinsicht geprägt und mir die Möglichkeit gegeben mich weiterzuentwickeln. Zudem möchte ich mich für jegliche Unterstützung und die stets offene Tür bedanken. Es war eine sehr lehrreiche Zeit, und ich bin dankbar, dass ich meine Ideen bezüglich des Projektes jederzeit umsetzen konnte.

Mein Dank gilt auch Dr. Martin Gamerdinger für seine Unterstützung, den wissenschaftlichen Input und die fachlichen Diskussionen. Danke, dass Du Dir für jede erdenkliche Frage Zeit genommen hast. Durch die Zusammenarbeit konnte ich sehr viel lernen.

Ein besonderer Dank geht an meine Laborkolleginnen Karina Gense, Sabine Schmidt, Annalena Wallisch, Sina Blessing und Sandra Fries. Ich danke Euch für die gegenseitige Hilfe und die tolle Zeit, die wir gemeinsam verbringen durften. Karina, Sabine und Lena, vielen Dank für Euren Rückhalt.

Ein herzliches Dankeschön gilt Renate Schlömer für ihre Geduld und Hilfsbereitschaft in Bezug auf alle Laborfragen. Danke für die tolle Zusammenarbeit.

Dr. Christina Schlatterer, Erika Oberer-Bley, Dr. Stefan Kreft, Ulrike Dahl und Gundula Hunaeus danke ich für die Hilfe und Unterstützung.

Ein großer Dank geht an die Kooperationspartner, die mich während der Bearbeitung des Projektes unterstützt haben: Prof. Dr. Matthias Mayer, Dr. Roman Kityk, Dr. Christoph Globisch und Prof. Dr. Christine Peter. Ein großer Dank auch an das Team der Proteomics Facility der Universität Konstanz.
Prof. Dr. Thomas U. Mayer danke ich für die Bereitstellung des Zellkulturlabors. Hier ein großes Dankeschön an Dr. Beata Rymarczyk und Lars Henschke für die Einweisung und Unterstützung.

Ein großer Dank gilt auch Dr. Julia Reuther, Dr. Ann-Kathrin Ott und Dr. Anne Hanebuth für die Motivation und Hilfsbereitschaft zu Beginn meiner Doktorarbeit.

Ich bedanke mich bei den Gutachtern meiner Arbeit: Prof. Dr. Elke Deuerling und Prof. Dr. Jörg Hartig.

Bei der Universität Konstanz und der Konstanz Research School Chemical Biology (KoRS-CB) bedanke ich mich für das Weiterbildungsangebot.

Ich danke all meinen Freunden für ihre Unterstützung während meiner Zeit in Konstanz. Ein besonderer Dank geht an Sarah, Nicole und Beata. Zudem bedanke ich mich bei Franziska Schmidt-Thieme für Ihre Hilfe bei der Gestaltung in Adobe Illustrator.

An letzter Stelle, aber ein Dank, der besonders von Herzen kommt, geht an meine Eltern. Ich danke Euch für Eure Unterstützung auf allen Ebenen, die Motivation und die offenen Ohren. Auf meinem gesamten Weg habt Ihr mich jederzeit bestärkt, an mich geglaubt und mir immer den Rücken freigehalten. Ohne Euch wäre Vieles nicht möglich gewesen. Herzlichen Dank!

12. Figure licenses

Figure 1

License Number: 4576510436620

Nature Reviews Molecular Cell Biology by NATURE PUBLISHING GROUP. Reproduced with permission of NATURE PUBLISHING GROUP in the format Thesis/Dissertation via Copyright Clearance Center.

Figure 2

License Number: 4576501175728

Annual review of biochemistry by ANNUAL REVIEWS. Reproduced with permission of ANNUAL REVIEWS in the format Thesis/Dissertation via Copyright Clearance Center.

Figure 5

Under Creative Commons Attribution (CC BY 4.0) license

Figure 7

License Number: 4595401371286

Trends in Biochemical Sciences by ELSEVIER. Reproduced with permission of ELSEVIER in the format Thesis/Dissertation via Copyright Clearance Center.

Figure 10

License Number: 4576520119729

Nature structural & molecular biology by NATURE PUBLISHING GROUP. Reproduced with permission of NATURE PUBLISHING GROUP in the format Thesis/Dissertation via Copyright Clearance Center.

13. Literature

Abraham MJ, Murtola T, Schulz R, Páll S, Smith JC, Hess B & Lindah E (2015) Gromacs: High performance molecular simulations through multi-level parallelism from laptops to supercomputers. *SoftwareX* **1–2:** 19–25

del Alamo M, Pechmann S, Hogan DJ, Albanese V, Frydman J & Brown PO (2011) Defining the Specificity of Cotranslationally Acting Chaperones by Systematic Analysis of mRNAs Associated with Ribosome-Nascent Chain Complexes. *PLoS Biol.* **9:** e1001100

Albanèse V, Reissmann S & Frydman J (2010) A ribosome-anchored chaperone network that facilitates eukaryotic ribosome biogenesis. *J. Cell Biol.* **189:** 69–81

Aloia L, Gutierrez A, Caballero JM & Croce L Di (2015) Direct interaction between Id1 and Zrf1 controls neural differentiation of embryonic stem cells. *EMBO Rep.* **16:** 63–70

Anfinsen CB (1973) Principles that Govern the Folding of Protein Chains. *Science (80-.).* **181:** 223–230

Anger AM, Armache JP, Berninghausen O, Habeck M, Subklewe M, Wilson DN & Beckmann R (2013) Structures of the human and Drosophila 80S ribosome. *Nature* **497:** 80–85

Arnold A, Rahman MM, Lee MC, Muehlhaeusser S, Katic I, Gaidatzis D, Hess D, Scheckel C, Wright JE, Stetak A, Boag PR & Ciosk R (2014) Functional characterization of C. elegans Y-box-binding proteins reveals tissue-specific functions and a critical role in the formation of polysomes. *Nucleic Acids Res.* **42:** 13353–13369

Bakshi S, Siryaporn A, Goulian M & Weisshaar JC (2012) Superresolution imaging of ribosomes and RNA polymerase in live Escherichia coli cells. *Mol. Microbiol.* **85:** 21–38

Balchin D, Hayer-Hartl M & Hartl FU (2016) In vivo aspects of protein folding and quality control. *Science (80-.).* **353:** aac4354

Ban N, Beckmann R, Cate JH, Dinman JD, Dragon F, Ellis SR, Lafontaine DL, Lindahl L, Liljas A, Lipton JM, Warren AJ, Williamson JR, Wilson D, Yonath A & Yusupov M (2014) A new system for naming ribosomal proteins. *Curr Opin Struct Biol* **24:** 165–169

Ban N, Nissen P, Hansen J, Moore PB & Steitz TA (2000) The Complete Atomic Structure of the Large Ribosomal Subunit at 2.4 Å Resolution. *Science (80-.).* **289:** 905–920

Bashan A & Yonath A (2008) Correlating ribosome function with high-resolution structures. *Trends Microbiol.* **16:** 326–335

Beckmann R, Spahn CMT, Eswar N, Helmers J, Penczek PA, Sali A, Frank J & Blobel G (2001) Architecture of the Protein-Conducting Channel Associated with the Translating 80S Ribosome. *Cell* **107:** 361–372

Ben-Shem A, Garreau de Loubresse N, Melnikov S, Jenner L, Yusupova G & Yusupov M (2011) The Structure of the Eukaryotic Ribosome at 3.0 A Resolution. *Science (80-.).* **334:** 1524–1529

Ben-Shem A, Jenner L, Yusupova G & Yusupov M (2010) Crystal Structure of the Eukaryotic Ribosome. *Science (80-.).* **330:** 1203–1209

Berisio R, Schluenzen F, Harms J, Bashan A, Auerbach T, Baram D & Yonath A (2003) Structural insight into the role of the ribosomal tunnel in cellular regulation. *Nat. Struct. Biol.* **10:** 366–370

Bjelkmar P, Larsson P, Cuendet MA, Hess B & Lindahl E (2010) Implementation of the CHARMM Force Field in GROMACS: Analysis of Protein Stability Effects from Correction Maps, Virtual Interaction Sites, and Water Models. *J. Chem. Theory Comput.* **6:** 459–466

Bloss TA, Witze ES & Rothman JH (2003) Suppression of CED-3-independent apoptosis by mitochondrial βNAC in Caenorhabditis elegans. *Nature* **424:** 1066–1071

Boorstein WR, Ziegelhoffer T & Craig EA (1994) Molecular Evolution of the HSP70 Multigene Family. *J Mol Evol* **38:** 1–17

Boyer L a, Latek RR & Peterson CL (2004) The SANT domain: a unique histone-tail-binding module? *Nat. Rev. Mol. Cell Biol.* **5:** 158–163

Boyer LA, Langer MR, Crowley KA, Tan S, Denu JM & Peterson CL (2002) Essential Role for the SANT Domain in the Functioning of Multiple Chromatin Remodeling Enzymes. *Mol. Cell* **10:** 935–942

Bracher A & Verghese J (2015) The nucleotide exchange factors of Hsp70 molecular chaperones. *Front. Mol. Biosci.* **2:** 1–9

Brehme M, Voisine C, Rolland T, Wachi S, Soper JH, Zhu Y, Orton K, Villella A, Garza D, Vidal M, Ge H & Morimoto RI (2014) A Chaperome Subnetwork Safeguards Proteostasis in Aging and Neurodegenerative Disease. *Cell Rep.* **9:** 1135–50

Brenner S (1974) The genetics of Caenorhabditis elegans. *Genetics* **77:** 71–94

Bukau B, Weissman J & Horwich A (2006) Molecular Chaperones and Protein Quality Control. *Cell* **125:** 443–451

Bussi G, Donadio D & Parrinello M (2007) Canonical sampling through velocity rescaling. *J. Chem. Phys.* **126:**

Cassada RC & Russell RL (1975) The Dauerlarva, a Post-Embryonic Nematode Developmental elegans Variant of the Caenorhabditis. *Dev. Biol.* **46:** 326–342

Cheetham ME & Caplan AJ (1998) Strcuture, function and evolution of DnaJ: conservation and adaptation of chaperone function. *Cell Stress Chaperones* **3:** 28–36

Chen D-H, Huang Y, Liu C, Ruan Y & Shen W-H (2014) Functional conservation and divergence of J-domain-containing ZUO1/ZRF orthologs throughout evolution. *Planta* **239:** 1159–73

Chitale S & Richly H (2017) DICER and ZRF1 contribute to chromatin decondensation during nucleotide excision repair. *Nucleic Acids Res.* **45:** 5901–5912

Chojnacki S, Cowley A, Lee J, Foix A & Lopez R (2017) Programmatic access to bioinformatics tools from EMBL-EBI update: 2017. *Nucleic Acids Res.* **45:** W550–W553

Coburn C & Gems D (2013) The mysterious case of the C. elegans gut granule: death fluorescence, anthranilic acid and the kynurenine pathway. *Front. Genet.* **4:** 151

Conz C, Otto H, Peisker K, Gautschi M, Wölfle T, Mayer MP & Rospert S (2007) Functional characterization of the atypical Hsp70 subunit of yeast ribosome-associated complex. *J. Biol. Chem.* **282:** 33977–33984

Craig EA & Jacobsen K (1985) Mutations in Cognate Genes of Saccharomyces cerevisiae hsp7O Result in Reduced Growth Rates at Low Temperatures. *Mol. Cell. Biol.* **5:** 3517–3524

Craig EA & Marszalek J (2017) How Do J-Proteins Get Hsp70 to Do So Many Different Things? *Trends Biochem. Sci.* **42:** 355–368

Cuéllar J, Martín-Benito J, Scheres SHW, Sousa R, Moro F, López-Vïas E, Gómez-Puertas P, Muga A, Carrascosa JL & Valpuesta JM (2008) The structure of CCT-Hsc70NBD suggests a mechanism for Hsp70 delivery of substrates to the chaperonin. *Nat. Struct. Mol. Biol.* **15:** 858–864

David DC, Ollikainen N, Trinidad JC, Cary MP, Burlingame AL & Kenyon C (2010) Widespread protein aggregation as an inherent part of aging in C. elegans. *PLoS Biol.* **8:** e1000450

Deng JM & Behringer RR (1995) An insertional mutation in the BTF3 transcription factor gene leads to an early postimplantation lethality in mice. *Transgenic Res.* **4:** 264–269

Deuerling E, Gamerdinger M & Kreft SG (2019) Chaperone Interactions at the Ribosome. *Cold Spring Harb. Perspect. Biol.***:** a033977

Deuerling E, Schulze-Specking A, Tomoyasu T, Mogk A & Bukau B (1999) Trigger factor and DnaK cooperate in folding of newly synthesized proteins. *Nature* **400:** 693–696

Diamant S & Goloubinoff P (1998) Temperature-Controlled Activity of DnaK - DnaJ - GrpE Chaperones : Protein-Folding Arrest and Recovery during and after Heat Shock Depends on the Substrate Protein and the GrpE Concentration. *Biochemistry* **37:** 9688–9694

Dickinson DJ, Ward JD, Reiner DJ & Goldstein B (2013) Engineering the Caenorhabditis elegans genome using Cas9-triggered homologous recombination. *Nat. Methods* **10:** 1028–34

Dragovic Z, Shomura Y, Tzvetkov N, Hartl FU & Bracher A (2006) Fes1p acts as a nucleotide exchange factor for the ribosome-associated molecular chaperone Ssb1p. *Biol. Chem.* **387:** 1593–1600

Essmann U, Perera L, Berkowitz ML, Darden T, Lee H & Pedersen LG (1995) A smooth particle mesh ewald potential. *J. Chem. Phys.* **103:** 8577–8592

Ferbitz L, Maier T, Patzelt H, Bukau B, Deuerling E & Ban N (2004) Trigger factor in complex with the ribosome forms a molecular cradle for nascent proteins. *Nature* **431:** 590–596

Fiaux J, Horst J, Scior A, Preissler S, Koplin A, Bukau B & Deuerling E (2010) Structural analysis of the ribosome-associated complex (RAC) reveals an unusual Hsp70/Hsp40 interaction. *J. Biol. Chem.* **285:** 3227–34

Flynn GC, Pohl J, Floccot MT & Rothman JE (1991) Peptide-binding specificity of the molecular chaperone BiP. *Nature* **353:** 726–730

Fujii K, Susanto TT, Saurabh S & Barna M (2018) Decoding the Function of Expansion Segments in Ribosomes. *Mol. Cell* **72:** 1013-1020.e6

Gaiser AM, Kaiser CJO, Haslbeck V & Richter K (2011) Downregulation of the Hsp90 system causes defects in muscle cells of Caenorhabditis elegans. *PLoS One* **6:** e25485

Gamerdinger M (2016) Protein quality control at the ribosome : focus on RAC , NAC and RQC. *Essays Biochem* **40:** 203–212

Gamerdinger M, Hanebuth MA, Frickey T & Deuerling E (2015) The principle of antagonism ensures protein targeting specificity at the endoplasmic reticulum. *Science* **348:** 201–7

Gautschi M, Lilie H, Fünfschilling U, Mun A, Ross S, Lithgow T, Rücknagel P & Rospert S (2001) RAC, a stable ribosome-associated complex in yeast formed by the DnaK-DnaJ homologs Ssz1p and zuotin. *Proc. Natl. Acad. Sci. U. S. A.* **98:** 3762–3767

Gautschi M, Mun A, Ross S & Rospert S (2002) A functional chaperone triad on the yeast ribosome. *Proc. Natl. Acad. Sci. U. S. A.* **99:** 4209–14

Ghosh JC, Dohi T, Kang BH & Altieri DC (2008) Hsp60 Regulation of Tumor Cell Apoptosis. *J. Biol. Chem.* **283:** 5188–5194

Goloubinoff P & Rios PDL (2007) The mechanism of Hsp70 chaperones: (entropic) pulling the models together. *Trends Biochem. Sci.* **32:** 372–380

Gracheva E, Chitale S, Wilhelm T, Rapp A, Byrne J, Stadler J, Medina R, Cardoso MC & Richly H (2016) ZRF1 mediates remodeling of E3 ligases at DNA lesion sites during nucleotide excision repair. *J. Cell Biol.* **213:** 185–200

Greene MK, Maskos K & Landry SJ (1998) Role of the J-domain in the cooperation of Hsp40 with Hsp70. *Proc. Natl. Acad. Sci. U. S. A.* **95:** 6108–6113

Greiner J, Ringhoffer M, Taniguchi M, Hauser T, Schmitt A, Dohner H & Schmitt M (2003) Characterization of several leukemia-associated antigens inducing humoral immune responses in acute and chronic myeloid leukemia. *Int J Cancer* **106:** 224–231

Guhathakurta D, Palomar L, Stormo GD, Tedesco P, Johnson TE, Walker DW, Lithgow G, Kim S & Link CD (2002) Identification of a novel cis-regulatory element involved in the heat shock response in Caenorhabditis elegans using microarray gene expression and computational methods. *Genome Res.* **12:** 701–712

Gumiero A, Conz C, Gesé GV, Zhang Y, Weyer FA, Lapouge K, Kappes J, Von Plehwe U, Schermann G, Fitzke E, Wölfle T, Fischer T, Rospert S & Sinning I (2016) Interaction of the cotranslational Hsp70 Ssb with ribosomal proteins and rRNA depends on its lid domain. *Nat. Commun.* **7:** 13563

von der Haar T (2008) A quantitative estimation of the global translational activity in logarithmically growing yeast cells. *BMC Syst. Biol.* **2:** 1–14

Hageman J & Kampinga HH (2009) Computational analysis of the human HSPH/HSPA/DNAJ family and cloning of a human HSPH/HSPA/DNAJ expression library. *Cell Stress Chaperones* **14:** 1–21

Hanebuth MA, Kityk R, Fries SJ, Jain A, Kriel A, Albanese V, Frickey T, Peter C, Mayer MP, Frydman J & Deuerling E (2016) Multivalent contacts of the Hsp70 Ssb contribute to its architecture on ribosomes and nascent chain interaction. *Nat. Commun.* **7:** 13695

Harrison CJ, Hayer-hartl M, Liberto M Di, Hartl F & Kuriyan J (1997) Crystal Structure of the Nucleotide Exchange Factor GrpE Bound to the ATPase Domain of the Molecular Chaperone DnaK. *Science (80-.).* **276:** 431–436

Hartl FU (1996) Molecular chaperones in cellular protein folding. *Nature* **381:** 571–580

Hartl FU, Bracher A & Hayer-Hartl M (2011) Molecular chaperones in protein folding and proteostasis. *Nature* **475:** 324–32

Haslbeck M & Vierling E (2015) A First Line of Stress Defense : Small Heat Shock Proteins and Their Function in Protein Homeostasis. *J. Mol. Biol.* **427:** 1537–1548

Hatzold J & Conradt B (2008) Control of apoptosis by asymmetric cell division. *PLoS Biol.* **6:** 771–784

Heschl MFP & Baillie DL (1990) The HSP70 multigene family of Caenorhabditis elegans. *Comp. Biochem. Physiol. - B* **96:** 633–637

Hess B, Bekker H, Berendsen HJC & Fraaije JGEM (1997) LINCS: A Linear Constraint Solver for molecular simulations. *J. Comput. Chem.* **18:** 1463–1472

Hipp MS, Kasturi P & Hartl FU (2019) The proteostasis network and its decline in ageing. *Nat. Rev. Mol. Cell Biol.*

Huang J, Rauscher S, Nawrocki G, Ran T, Feig M, De Groot BL, Grubmüller H & MacKerell AD (2016) CHARMM36m: An improved force field for folded and intrinsically disordered proteins. *Nat. Methods* **14:** 71–73

Huang K, Ghose R, Flanagan JM & Prestegard JH (1999) Backbone Dynamics of the N-Terminal Domain in E. Coli DnaJ Determined by 15N- and 13CO-Relaxation Measurements. *Biochemistry* **38:** 10567–10577

Huang P, Gautschi M, Walter W, Rospert S & Craig EA (2005) The Hsp70 Ssz1 modulates the function of the ribosome-associated J-protein Zuo1. *Nat. Struct. Mol. Biol.* **12:** 497–504

Hundley H, Eisenman H, Walter W, Evans T, Hotokezaka Y, Wiedmann M & Craig E (2002) The in vivo function of the ribosome-associated Hsp70, Ssz1, does not require its putative peptide-binding domain. *Proc. Natl. Acad. Sci.* **99:** 4203–4208

Hundley HA, Walter W, Bairstow S & Craig EA (2005) Human Mpp11 J protein: ribosome-tethered molecular chaperones are ubiquitous. *Science* **308:** 1032–4

Imamura T, Komatsu S, Ichikawa D, Miyamae M, Okajima W, Ohashi T, Kiuchi J, Nishibeppu K, Kosuga T, Konishi H, Shiozaki A, Fujiwara H, Okamoto K, Tsuda H & Otsuji E (2018) Overexpression of ZRF1 is related to tumor malignant potential and a poor outcome of gastric carcinoma. *Carcinogenesis* **39:** 263–271

Jaiswal H, Conz C, Otto H, Wölfle T, Fitzke E, Mayer MP & Rospert S (2011) The chaperone network connected to human ribosome-associated complex. *Mol. Cell. Biol.* **31:** 1160–1173

Jha S & Komar AA (2011) Birth , life and death of nascent polypeptide chains. *Biotechnol. J.* **6:** 623–640

Jorgensen WL, Chandrasekhar J, Madura JD, Impey RW & Klein ML (1983) Comparison of simple potential functions for simulating liquid water. *J. Chem. Phys.* **79:** 926–935

Kaiser CM & Liu K (2018) Folding up and Moving on—Nascent Protein Folding on the Ribosome. *J. Mol. Biol.* **430:** 4580–4591

Kamath RS, Fraser AG, Dong Y, Poulin G, Durbin R, Gotta M, Kanapin A, Le Bot N, Moreno S, Sohrmann M, Welchman DP, Zipperlen P & Ahringer J (2003) Systematic functional analysis of the Caenorhabditis elegans genome using RNAi. *Nature* **421:** 231–7

Kampinga HH, Andreasson C, Barducci A, Cheetham ME, Cyr D, Emanuelsson C, Genevaux P, Gestwicki JE, Goloubinoff P, Huerta-Cepas J, Kirstein J, Liberek K, Mayer MP, Nagata K, Nillegoda NB, Pulido P, Ramos C, De los Rios P, Rospert S, Rosenzweig R, et al (2018) Function, evolution, and structure of J-domain proteins. *Cell Stress Chaperones* **24:** 7–15

Karbstein K (2011) Inside the 40S ribosome assembly machinery. *Curr. Opin. Chem. Biol.* **15:** 657–663

Kaschner LA, Sharma R, Shrestha OK, Meyer AE & Craig EA (2015) A conserved domain important for association of eukaryotic J-protein co-chaperones Jjj1 and Zuo1 with the ribosome. *Biochim. Biophys. Acta* **1853:** 1035–45

Kaymak A, Sayols S, Papadopoulu T & Richly H (2018) Role for the transcriptional activator ZRF1 in early metastatic events in breast cancer progression and endocrine resistance. *Oncotarget* **9:** 28666–28690

Khatter H, Myasnikov AG, Natchiar SK & Klaholz BP (2015) Structure of the human 80S ribosome. *Nature* **520:** 640–645

Khusainov I, Vicens Q, Bochler A, Myasnikov A, Chicher J, Marzi S, Romby P, Yusupova G, Yusupov M & Hashem Y (2016) Structure of the 70S ribosome from human pathogen Staphylococcus aureus. *Nucleic Acids Res.* **44:** 10491–10504

Kim YE, Hipp MS, Bracher A, Hayer-Hartl M & Ulrich Hartl F (2013) Molecular Chaperone Functions in Protein Folding and Proteostasis. *Annu. Rev. Biochem.* **82:** 323–255

Kirstein-Miles J, Scior A, Deuerling E & Morimoto RI (2013) The nascent polypeptide-associated complex is a key regulator of proteostasis. *EMBO J.* **32:** 1451–68

Kirstein J, Arnsburg K, Scior A, Szlachcic A, Guilbride DL, Morimoto RI, Bukau B & Nillegoda NB (2017) In vivo properties of the disaggregase function of J-proteins and Hsc70 in Caenorhabditis elegans stress and aging. *Aging Cell* **16:** 1414–1424

Kityk R, Kopp J & Mayer MP (2018) Molecular Mechanism of J-Domain-Triggered ATP Hydrolysis by Hsp70 Chaperones. *Mol. Cell* **69:** 227-237.e4

Kityk R, Kopp J, Sinning I & Mayer MP (2012) Structure and Dynamics of the ATP-Bound Open Conformation of Hsp70 Chaperones. *Mol. Cell* **48:** 863–874

Kityk R, Vogel M, Schlecht R, Bukau B & Mayer MP (2015) Pathways of allosteric regulation in Hsp70 chaperones. *Nat. Commun.* **6:** 8308

Klaips CL, Jayaraj GG & Hartl FU (2018) Pathways of cellular proteostasis in aging and disease. *J. Cell Biol.* **217:** 51

Knorr AG, Schmidt C, Tesina P, Berninghausen O, Becker T, Beatrix B & Beckmann R (2019) Ribosome–NatA architecture reveals that rRNA expansion segments coordinate N-terminal acetylation. *Nat. Struct. Mol. Biol.* **26:** 35–39

Koplin A, Preissler S, Llina Y, Koch M, Scior A, Erhardt M & Deuerling E (2010) A dual function for chaperones SSB-RAC and the NAC nascent polypeptide-associated complex on ribosomes. *J. Cell Biol.* **189:** 57–68

Kosolapov A & Deutsch C (2009) Tertiary interactions within the ribosomal exit tunnel. *Nat. Struct. Mol. Biol.* **16:** 405–411

Kramer G, Rauch T, Rist W, Vorderwülbecke S, Patzelt H, Schulze-Specking A, Ban N, Deuerling E & Bukau B (2002) L23 protein functions as a chaperone docking site on the ribosome. *Nature* **419:** 171–174

Labbadia J & Morimoto RI (2015) The Biology of Proteostasis in Aging and Disease. *Annu. Rev. Biochem.* **84:** 435–64

Lai C, Chou C, Ch L, Liu C & Lin W (2000) Identification of Novel Human Genes Evolutionarily Conserved in Caenorhabditis elegans by Comparative Proteomics. *Genome Res.* **10:** 703–713

Laufen T, Mayer MP, Beisel C, Klostermeier D, Mogk A, Reinstein J & Bukau B (1999) Mechanism of regulation of Hsp70 chaperones by DnaJ cochaperones. *Proc. Natl. Acad. Sci. U. S. A.* **96:** 5452–5457

Lee K, Sharma R, Shrestha OK, Bingman CA & Craig EA (2016) Dual interaction of the Hsp70 J-protein cochaperone Zuotin with the 40S and 60S ribosomal subunits. *Nat. Struct. Mol. Biol.* **23:** 1003–1010

Leidig C, Bange G, Kopp J, Amlacher S, Aravind A, Wickles S, Witte G, Hurt E, Beckmann R & Sinning I (2013) Structural characterization of a eukaryotic chaperone--the ribosome-associated complex. *Nat. Struct. Mol. Biol.* **20:** 23–8

Liberek K, Marszalek J, Ang D, Georgopoulos C & Zylicz M (1991) Escherichia coli DnaJ and GrpE heat shock proteins jointly stimulate ATPase activity of DnaK. *Proc. Natl. Acad. Sci.* **88:** 2874–2878

Lindquist S (1980) Translational efficiency of heat-induced messages in Drosophila melanogaster cells. *J. Mol. Biol.* **137:** 151–158

Liu Y, Hu Y, Li X, Niu L & Teng M (2010) The crystal structure of the human nascent polypeptide-associated complex domain reveals a nucleic acid-binding region on the NACA subunit. *Biochemistry* **49:** 2890–2896

Lopez T, Dalton K & Frydman J (2015) The Mechanism and Function of Group II Chaperonins. *J. Mol. Biol.* **427:** 2919–2930

Lu J & Deutsch C (2005) Folding zones inside the ribosomal exit tunnel. *Nat. Struct. Mol. Biol.* **12:** 1123–1129

Malinverni D, Lopez AJ, De Los Rios P, Hummer G & Barducci A (2017) Modeling Hsp70/Hsp40 interaction by multi-scale molecular simulations and coevolutionary sequence analysis. *Elife* **6:** e23471

Markesich DC, Gajewski KM, Nazimiec ME & Beckingham K (2000) bicaudal encodes the Drosophila beta NAC homolog , a component of the ribosomal translational machinery. *Development* **127:** 559–572

Mayer MP (2010) Gymnastics of molecular chaperones. *Mol. Cell* **39:** 321–331

Mayer MP & Bukau B (2005) Hsp70 chaperones: Cellular functions and molecular mechanism. *Cell. Mol. Life Sci.* **62:** 670–684

Mayer MP & Gierasch LM (2018) Recent advances in the structural and mechanistic aspects of Hsp70 molecular chaperones. *J. Biol. Chem.* **294:** 2085–2097

Mayer MP & Kityk R (2015) Insights into the molecular mechanism of allostery in Hsp70s. *Front. Mol. Biosci.* **2:** 58

Mayer MP, Schröder H, Rüdiger S, Paal K, Laufen T & Bukau B (2000) Multistep mechanism of substrate binding determines chaperone activity of Hsp70. *Nat. Struct. Biol.* **7:** 586–593

McCarty JS, Buchberger A, Reinstein J & Bukau B (1995) The Role of ATP in the Functional Cycle of the DnaK Chaperone System. *J. Mol. Biol.* **249:** 126–137

Mello CC, Kramer JM, Stinchcomb D & Ambros V (1991) Efficient gene transfer in C.elegans: extrachromosomal maintenance and integration of transforming sequences. *EMBO J.* **10:** 3959–70

Meyer AE, Hung N-J, Yang P, Johnson AW & Craig EA (2007) The specialized cytosolic J-protein, Jjj1, functions in 60S ribosomal subunit biogenesis. *Proc. Natl. Acad. Sci. U. S. A.* **104:** 1558–1563

Misselwitz B, Staeck O & Rapoport TA (1998) J Proteins Catalytically Activate Hsp70 Molecules to Trap a Wide Range of Peptide Sequences. *Mol. Cell* **2:** 593–603

Mitchell DH, Stiles JW, Santelli J & Sanadi DR (1979) Synchronous Growth and Aging of Caenorhabditis elegans in the Presence of Fluorodeoxyuridine. *Worm Breeder's Gaz.* **34:** 28–36

Nelson RJ, Heschl MFP & Craig EA (1992) Isolation and characterization of extragenic suppressors of mutations in the SSA hsp70 genes of Saccharomyces cerevisiae. *Genetics* **131:** 277–285

Nillegoda NB, Kirstein J, Szlachcic A, Berynskyy M, Stank A, Stengel F, Arnsburg K, Gao X, Scior A, Aebersold R, Guilbride DL, Wade RC, Morimoto RI, Mayer MP & Bukau B (2015) Crucial HSP70 co-chaperone complex unlocks metazoan protein disaggregation. *Nature* **524:** 247–251

Nillegoda NB, Stank A, Malinverni D, Alberts N, Szlachcic A, Barducci A, De Los Rios P, Wade RC & Bukau B (2017) Evolution of an intricate J-protein network driving protein disaggregation in eukaryotes. *Elife* **6:** e24560

Nillegoda NB, Wentink AS & Bukau B (2018) Protein Disaggregation in Multicellular Organisms. *Trends Biochem. Sci.* **43:** 285–300

Nilsson OB, Hedman R, Marino J, Wickles S, Bischoff L, Johansson M, Müller-Lucks A, Trovato F, Puglisi JD, O'Brien EP, Beckmann R & von Heijne G (2015) Cotranslational Protein Folding inside the Ribosome Exit Tunnel. *Cell Rep.* **12:** 1533–1540

Nissen P, Hansen J, Ban N, Moore PB & Steitz TA (2000) The structural basis of ribosome activity in peptide bond synthesis. *Science (80-.).* **289:** 920–930

Nyathi Y & Pool MR (2015) Analysis of the interplay of protein biogenesis factors at the ribosome exit site reveals new role for NAC. *J. Cell Biol.* **210:** 287–301

O'Brien EP, Vendruscolo M & Dobson CM (2012) Prediction of variable translation rate effects on cotranslational protein folding. *Nat. Commun.* **3:** 868

Ott A-K, Locher L, Koch M & Deuerling E (2015) Functional Dissection of the Nascent Polypeptide-Associated Complex in Saccharomyces cerevisiae. *PLoS One* **10:** e0143457

Otto H, Conz C, Maier P, Wolfle T, Suzuki CK, Jeno P, Rucknagel P, Stahl J & Rospert S (2005) The chaperones MPP11 and Hsp70L1 form the mammalian ribosome-associated complex. *Proc Natl Acad Sci U S A* **102:** 10064–10069

Paix A, Wang Y, Smith HE, Lee C-YS, Calidas D, Lu T, Smith J, Schmidt H, Krause MW & Seydoux G (2014) Scalable and Versatile Genome Editing Using Linear DNAs with Micro-Homology to Cas9 Sites in Caenorhabditis elegans. *Genetics* **198:** 1347–56

Papsdorf K, Sacherl J & Richter K (2014) The balanced regulation of Hsc70 by DNJ-13 and UNC-23 is required for muscle functionality. *J. Biol. Chem.* **289:** 25250–25261

Parrinello M & Rahman A (1981) Polymorphic transitions in single crystals: A new molecular dynamics method. *J. Appl. Phys.* **52:** 7182–7190

Patzelt H, Rüdiger S, Brehmer D, Kramer G, Vorderwülbecke S, Schaffitzel E, Waitz A, Hesterkamp T, Dong L, Schneider-Mergener J, Bukau B & Deuerling E (2002) Binding specificity of Escherichia coli trigger factor. *Proc. Natl. Acad. Sci.* **98:** 14244–14249

Pech M, Spreter T, Beckmann R & Beatrix B (2010) Dual binding mode of the nascent polypeptide-associated complex reveals a novel universal adapter site on the ribosome. *J. Biol. Chem.* **285:** 19679–19687

Pechmann S, Willmund F & Frydman J (2013) The Ribosome as a Hub for Protein Quality Control. *Mol. Cell* **49:** 411–421

Peisker K, Braun D, Wölfle T, Hentschel J, Fünfschilling U, Fischer G, Sickmann A & Rospert S (2008) Ribosome-associated complex binds to ribosomes in close proximity of Rpl31 at the exit of the polypeptide tunnel in yeast. *Mol. Biol. Cell* **19:** 5279–5288

Peisker K, Chiabudini M & Rospert S (2010) The ribosome-bound Hsp70 homolog Ssb of Saccharomyces cerevisiae. *Biochim. Biophys. Acta* **1803:** 662–672

Perales-Calvo J, Muga A & Moro F (2010) Role of DnaJ G/F-rich domain in conformational recognition and binding of protein substrates. *J. Biol. Chem.* **285:** 34231–34239

Pfund C, Huang P, Lopez-Hoyo N & Craig EA (2001) Divergent Functional Properties of the Ribosome-Associated Molecular Chaperone Ssb Compared with Other Hsp70s. *Mol. Biol. Cell* **12:** 3773–3782

Von Plehwe U, Berndt U, Conz C, Chiabudini M, Fitzke E, Sickmann A, Petersen A, Pfeifer D & Rospert S (2009) The Hsp70 homolog Ssb is essential for glucose sensing via the SNF1 kinase network. *Genes Dev.* **23:** 2102–2115

Polier S, Dragovic Z, Hartl FU & Bracher A (2008) Structural Basis for the Cooperation of Hsp70 and Hsp110 Chaperones in Protein Folding. *Cell* **133:** 1068–1079

Pool MR, Stumm J, Fulga TA, Sinning I & Dobberstein B (2002) Distinct modes of signal recognition particle interaction with the ribosome. *Science (80-.).* **297:** 1345–1348

Powers T & Walter P (1996) The nascent polypeptide-associated complex modulates interactions between the signal recognition particle and the ribosome. *Curr. Biol.* **6:** 331–338

Preissler S & Deuerling E (2012) Ribosome-associated chaperones as key players in proteostasis. *Trends Biochem. Sci.* **37:** 274–283

Pronk S, Páll S, Schulz R, Larsson P, Bjelkmar P, Apostolov R, Shirts MR, Smith JC, Kasson PM, Van Der Spoel D, Hess B & Lindahl E (2013) GROMACS 4.5: A high-throughput and highly parallel open source molecular simulation toolkit. *Bioinformatics* **29:** 845–854

Raine A, Ivanova N, Wikberg JES & Ehrenberg M (2004) Simultaneous binding of trigger factor and signal recognition particle to the E . coli ribosome. *Biochimie* **86:** 495–500

Rampelt H, Kirstein-Miles J, Nillegoda NB, Chi K, Scholz SR, Morimoto RI & Bukau B (2012) Metazoan Hsp70 machines use Hsp110 to power protein disaggregation. *EMBO J.* **31:** 4221–4235

Raue U, Oellerer S & Rospert S (2007) Association of protein biogenesis factors at the yeast ribosomal tunnel exit is affected by the translational status and nascent polypeptide sequence. *J. Biol. Chem.* **282:** 7809–7816

Resto VA, Caballero OL, Buta MR, Westra WH, Wu L, Westendorf JM, Jen J, Hieter P & Sidransky D (2000) A putative oncogenic role for MPP11 in head and neck squamous cell cancer. *Cancer Res.* **60:** 5529–5535

Richly H, Rocha-Viegas L, Ribeiro JD, Demajo S, Gundem G, Lopez-Bigas N, Nakagawa T, Rospert S, Ito T & Di Croce L (2010) Transcriptional activation of polycomb-repressed genes by ZRF1. *Nature* **468:** 1124–1128

Rist W, Graf C, Bukau B & Mayer MP (2006) Amide Hydrogen Exchange Reveals Conformational Changes in Hsp70 Chaperones Important for Allosteric Regulation. *J. Biol. Chem.* **281:** 16493–16501

Rodnina M V (2016) The ribosome in action : Tuning of translational efficiency and protein folding. *Protein Sci.* **25:** 1390–1406

Rospert S, Dubaquié Y & Gautschi M (2002) Nascent-polypeptide-associated complex. *Cell. Mol. Life Sci.* **59:** 1632–1639

Rüdiger S, Buchberger A & Bukau B (1997) Interaction of Hsp70 chaperones with substrates. *Nat. Struct. Biol.* **4:** 342–349

Rüdiger S, Mayer MP, Schneider-Mergener J & Bukau B (2000) Modulation of substrate specificity of the DnaK chaperone by alteration of a hydrophobic arch. *J. Mol. Biol.* **304:** 245–251

Saibil H (2013) Chaperone machines for protein folding, unfolding and disaggregation. *Nat. Rev. Mol. Cell Biol.* **14:** 630–642

Saio T, Guan X, Rossi P, Economou A & Kalodimos CG (2014) Structural Basis for Protein Antiaggregation Activity of the Trigger Factor Chaperone. *Science (80-.).* **344:** 1250494

Sankhala RS, Kumar CS, Singh BP, Arangasamy A & Swamy MJ (2012) HSP-1/2, a major protein of equine seminal plasma, exhibits chaperone-like activity. *Biochem. Biophys. Res. Commun.* **427:** 18–23

Schlünzen F, Wilson DN, Tian P, Harms JM, McInnes SJ, Hansen HAS, Albrecht R, Buerger J, Wilbanks SM & Fucini P (2005) The Binding Mode of the Trigger Factor on the Ribosome : Implications for Protein Folding and SRP Interaction. *Structure* **13:** 1685–1694

Schmidt EK, Clavarino G, Ceppi M & Pierre P (2009) SUnSET, a nonradioactive method to monitor protein synthesis. *Nat. Methods* **6:** 275–277

Schröder H, Langer T, Hartl F-U & Bukau B (1993) DnaK, DnaJ and GrpE form a cellular chaperone machinery capable of repairing heat-induced protein damage. *EMBO J.* **12:** 4137–4144

Schuwirth BS, Borovinskaya MA, Hau CW, Zhang W, Vila-Sanjurjo A, Holton JM & Cate JHD (2005) Structures of the bacterial ribosome at 3.5 A resolution. *Science (80-.).* **310:** 827–34

Shaner L, Sousa R & Morano KA (2006) Characterization of Hsp70 binding and nucleotide exchange by the yeast Hsp110 chaperone Sse1. *Biochemistry* **45:** 15075–15084

Sharma A, Mariappan M, Appathurai S & Hegde RS (2010) In vitro dissection of protein translocation into the mammalian endoplasmic reticulum. *Methods Mol. Biol.* **619:** 339–363

Shaye DD & Greenwald I (2011) OrthoList : A Compendium of C . elegans Genes with Human Orthologs. *PLoS One* **6:** e20085

Shi Y, Hong X & Wang C (2005) The C-terminal (331–376) Sequence of Escherichia coli DnaJ Is Essential for Dimerization and Chaperone Activity. *J. Biol. Chem.* **280:** 22761–22768

Shomura Y, Dragovic Z, Chang HC, Tzvetkov N, Young JC, Brodsky JL, Guerriero V, Hartl FU & Bracher A (2005) Regulation of Hsp70 function by HspBP1: Structural analysis reveals an alternate mechanism for Hsp70 nucleotide exchange. *Mol. Cell* **17:** 367–379

Sin O, Michels H & Nollen EAA (2014) Genetic screens in Caenorhabditis elegans models for neurodegenerative diseases. *BBA - Mol. Basis Dis.* **1842:** 1951–1959

Snutch TP, Heschl MFP & Baillie DL (1988) The Caenorhabditis elegans hsp70 gene family: a molecular genetic characterization. *Gene* **64:** 241–255

Sondermann H, Ho AK, Listenberger LL, Siegers K, Moarefi I, Wente SR, Hartl F & Young JC (2002) Prediction of Novel Bag-1 Homologs Based on Structure / Function Analysis Identifies Snl1p as an Hsp70 Co-chaperone in Saccharomyces cerevisiae. *J. Biol. Chem.* **277:** 33220–33227

Sondermann H, Scheufler C, Schneider C, Höhfeld J, Hartl FU & Moarefi I (2001) Structure of a Bag/Hsc70 complex: Convergent functional evolution of Hsp70 nucleotide exchange factors. *Science (80-.).* **291:** 1553–1557

Spahn CM, Beckmann R, Eswar N, Penczek PA, Sali A, Blobel G & Frank J (2001) Structure of the 80S Ribosome from yeast - tRNA-ribosome and subunit-subunit interactions. *Cell* **107:** 373–386

Sun L, Edelmann FT, Kaiser CJO, Papsdorf K, Gaiser AM & Richter K (2012) The lid domain of Caenorhabditis elegans Hsc70 influences ATP turnover, cofactor binding and protein folding activity. *PLoS One* **7:** e33980

Swain JF, Dinler G, Sivendran R, Montgomery DL, Stotz M & Gierasch LM (2007) Hsp70 Chaperone Ligands Control Domain Association via an Allosteric Mechanism Mediated by the Interdomain Linker. *Mol. Cell* **26:** 27–39

Szabo A, Langer T, Schröder H, Flanagan J, Bukau B & Hartl FU (1994) The ATP hydrolysis-dependent reaction cycle of the Escherichia coli Hsp70 system DnaK, DnaJ, and GrpE. *Proc. Natl. Acad. Sci. U. S. A.* **91:** 10345–10349

Teter SA, Houry WA, Ang D, Tradler T, Rockabrand D, Fischer G, Blum P, Georgopoulos C & Hartl FU (1999) Polypeptide flux through bac- terial Hsp70: DnaK cooperates with Trigger Factor in chap- eroning nascent chains. *Cell* **97:** 755–765

The C. elegans Consortium (1998) Genome Sequence of the Nematode C . elegans : A Platform for Investigating Biology. *Science (80-.).* **282:** 2012–2019

Tomic S, Johnson AE, Hartl FU & Etchells SA (2006) Exploring the capacity of trigger factor to function as a shield for ribosome bound polypeptide chains. *FEBS Lett.* **580:** 72–76

Tsai J & Douglas MG (1996) A conserved HPD sequence of the J-domain is necessary for YDJ1 stimulation of Hsp70 ATPase activity at a site distinct from substrate binding. *J. Biol. Chem.* **271:** 9347–9354

Vogel M, Mayer MP & Bukau B (2006) Allosteric regulation of Hsp70 chaperones involves a conserved interdomain linker. *J. Biol. Chem.* **281:** 38705–38711

Voorhees RM & Hegde RS (2015) Structures of the scanning and engaged states of the mammalian SRP-ribosome complex. *Elife* **4:** 1–21

Wall D, Zylicz M & Georgopoulos C (1994) The NH2-terminal 108 amino acids of the Escherichia coli DnaJ protein stimulate the ATPase activity of DnaK and are sufficient for λ replication. *J. Biol. Chem.* **269:** 5446–5451

Walther DM, Kasturi P, Zheng M, Pinkert S, Vecchi G, Ciryam P, Morimoto RI, Dobson CM, Vendruscolo M, Mann M & Hartl FU (2015) Widespread Proteome Remodeling and Aggregation in Aging C. elegans. *Cell* **161:** 919–932

Wang L, Zhang W, Wang L, Zhang XC, Li X & Rao Z (2010) Crystal structures of NAC domains of human nascent polypeptide-associated complex (NAC) and its αNAC subunit. *Protein Cell* **1:** 406–416

Wang M, Weiss M, Simonovic M, Haertinger G, Schrimpf SP, Hengartner MO & von Mering C (2012) PaxDb, a Database of Protein Abundance Averages Across All Three Domains of Life. *Mol. Cell. Proteomics* **11:** 492–500

Wegrzyn RD, Hofmann D, Merz F, Nikolay R, Rauch T, Graf C & Deuerling E (2006) A conserved motif is prerequisite for the interaction of NAC with ribosomal protein L23 and nascent chains. *J. Biol. Chem.* **281:** 2847–2857

Weyer FA, Gumiero A, Gesé GV, Lapouge K & Sinning I (2017) Structural insights into a unique Hsp70-Hsp40 interaction in the eukaryotic ribosome-associated complex. *Nat. Struct. Mol. Biol.* **24:** 144–151

Wiedmann B & Prehn S (1999) The nascent polypeptide-associated complex (NAC) of yeast functions in the targeting process of ribosomes to the ER membrane. *FEBS Lett.* **458:** 51–54

Wiedmann B, Sakai H, Davis TA & Wiedmann M (1994) A protein complex required for signal-sequence-specific sorting and translocation. *Nature* **370:** 434–440

Willmund F, Del Alamo M, Pechmann S, Chen T, Albanèse V, Dammer EB, Peng J & Frydman J (2013) The cotranslational function of ribosome-associated Hsp70 in eukaryotic protein homeostasis. *Cell* **152:** 196–209

Wilson DN & Beckmann R (2011) The ribosomal tunnel as a functional environment for nascent polypeptide folding and translational stalling. *Curr. Opin. Struct. Biol.* **21:** 274–282

Yam AYW, Albanèse V, Lin HTJ & Frydman J (2005) Hsp110 cooperates with different cytosolic Hsp70 systems in a pathway for de novo folding. *J. Biol. Chem.* **280:** 41252–41261

Yan W, Schilke B, Pfund C, Walter W, Kim S & Craig EA (1998) Zuotin, a ribosome-associated DnaJ molecular chaperone. *EMBO J.* **17:** 4809–4817

Yarmolinsky MB & Haba GLDL (1959) Inhibition By Puromycin of Amino Acid Incorporation Into Protein. *Proc. Natl. Acad. Sci.* **45:** 1721–1729

Yonath A, Leonard KR & Wittmann HG (1987) A tunnel in the Large Ribosomal Subunit Revealed by Three-Dimensional Image Reconstruction. *Science (80-.).* **236:** 813–816

Yonath AE, Müssig J, Tesche B, Lorenz S, Erdmann VA & Wittmann HG (1980) Crystallization of the large ribosomal subunits from Bacillus stearothermophilus. *Biochem. Int.* **1:** 428–435

Young R & Bremer H (2015) Polypeptide-chain-elongation rate in Escherichia coli B/r as a function of growth rate. *Biochem. J.* **160:** 185–194

Yusupov MM, Yusupova GZ, Baucom A, Lieberman K, Earnest TN, Cate JHD & Noller HF (2008) Crystal Structure of the Ribosome at 5.5 Å Resolution. *Science (80-.).* **292:** 883–897

Zhang S, Lockshin C, Herbert a, Winter E & Rich a (1992) Zuotin, a putative Z-DNA binding protein in Saccharomyces cerevisiae. *EMBO J.* **11:** 3787–3796

Zhang Y, Berndt U, Gölz H, Tais A, Oellerer S, Wölfle T, Fitzke E & Rospert S (2012) NAC functions as a modulator of SRP during the early steps of protein targeting to the endoplasmic reticulum. *Mol. Biol. Cell* **23:** 3027–3040

Zhang Y, Ma C, Yuan Y, Zhu J, Li N, Chen C, Wu S, Yu L, Lei J & Gao N (2014) Structural basis for interaction of a cotranslational chaperone with the eukaryotic ribosome. *Nat. Struct. Mol. Biol.* **21:** 1042–6

Zhang Y & Zuiderweg ERP (2004) The 70-kDa heat shock protein chaperone nucleotide-binding domain in solution unveiled as a molecular machine that can reorient its functional subdomains. *Proc. Natl. Acad. Sci.* **101:** 10272–10277

Zhuravleva A, Clerico EM & Gierasch LM (2012) An interdomain energetic tug-of-war creates the allosterically active state in Hsp70 molecular chaperones. *Cell* **151:** 1296–1307

14. Appendix

The Hsp70 system in *C. elegans*

RNAi phenotype key

Bmd	body morphology defects	**Pvl**	protruding vulva
Dpy	dumpy phenotype	**Rup**	ruptured phenotype
Emb	embryonic lethal	**Sle**	slow embryonic development
Gro	growth defective	**Spd**	spindle defective early embryo
Lva	larval arrest	**Ste**	sterility
Lvl	larval lethal	**Unc**	uncoordinated locomotion
Mlt	molt defect	**WT**	wildtype

Table A1: Hsp70s

Worm gene	Ensembl ID	Description	RNAi phenotype
Cytoplasm			
hsp-70	C12C8.1	• Member of Hsp70 family	WT
F11F1.1	F11F1.1	• Expressed in hypodermis and intestine	WT
hsp-1	F26D10.3	• Hsp70A • heat shock cognate (Hsc70) • expressed throughout development • closely related to *S. cerevisiae* SSA • only mildly heat inducible	Emb, Ste, Lva
F44E5.4	F44E5.4	• enriched in intestine, nervous system and sensillum	WT
F44E5.5	F44E5.5		WT
Endoplasmic reticulum			
hsp-3	C15H9.6	• ortholog of human GRP78 • not heat shock induced	Dpy, Lva
hsp-4	F43E2.8	• homolog of the mammalian chaperone BiP • strongly induced by heat shock • expressed in several tissues like the epithelial, alimentary, nervous and reproductive system	Emb, Lva
stc-1	F54C9.2	• highest abundance in the L1 larval stage • expressed in intestine	Unc, Mlt, Lvl, WT, Emb, Lva

Table A2: J-domain proteins (JDPs; Hsp40s)

Worm gene	Ensembl ID	Description	RNAi phenotype
Cytoplasm			
dnj-1	B0035.14	• ortholog of human DNAJB12 • involved in celluar protein complex assembly • localizes to ER membrane • expressed vulvla muscle and in head and tail neurons	Unc
dnj-2	B0035.2	• transmembrane domain	WT
dnj-3	C01G10.12	• enriched in nervous, reproductive, muscular and alimentary system • transmembrane domain	WT
dnj-4	C01G8.4	• ortholog of human DNAJC4 • expressed in nervous system • transmembrane domain	WT
dnj-5	C04A2.7	• ortholog of human DNAJC14	N/A
dnj-8	C56C10.13	• ortholog of human DNAJC16 • thioredoxin domain • transmembrane domain	N/A
rme-8	F18C12.2	• ortholog of human DNAJC13 • involved in development and mechanosensory behavior • expressed in coelomocytes, hypodermis, muscle cells and reproductive system • involved in receptor-mediated and fluid-phase endocytosis in coelomocytes	N/A
dnj-11	F38A5.13	• orthologous to the mammalian ZRF1/MIDA1/MPP11/DNAJC2 family of ribosome-associated molecular chaperones • two C-terminal SANT-domains • regulates asymmetric cell division and mitotic spindle orientation in the neurosecretory-motor neuron (NSM) • expressed in alimentary, muscular, reproductive and nervous system	WT, Emb
dnj-12	F39B2.10	• ortholog of human DNAJA1 • heat shock protein binding activity, unfolded protein binding, metal binding • expressed in excretory, alimentary, reproductive and muscular system	Emb,Spd
dnj-13	F54D5.8	• ortholog of human DNAJB1/4/5 family • homolog of *S. cerevisiae* Sis1 • unfolded protein binding activity	WT
dnj-14	K02G10.8	• ortholog of human DNAJC5 family • transmembrane domain • involved in determination of adult lifespan, neurotransmitter secretion and locomotion	WT
dnj-16	R74.4	• enriched in neurosecretory-motor neuron (NSM), germline, intestine and AFD (thermosensory neuron)	WT
dnj-17	T03F6.2	• prokaryotic heat shock protein, Zinc finger, C2H2 type • ortholog of human DNAJC21 • predicted nucleic acid and zinc ion binding activity • expressed in head neurons	N/A

Worm gene	Ensembl ID	Description	RNAi phenotype
dnj-18	T04A8.9	• ortholog of human DNAJA3 family • transmembrane domain	N/A
dnj-19	T05C3.5	• ortholog of human DNAJA2 family • heat shock protein binding activity, unfolded protein binding, metal binding	WT
dnj-20	T15H9.7	• ortholog of human DNAJB11 family • heat shock protein binding activity • expressed in hypodermis and intestine	N/A
dnj-23	T24H10.3	• ortholog of human DNAJC9 family	WT, Unc
dnj-24	W03A5.7	• ortholog of human DNAJB6/7/8 family • localizes to the nucleus	N/A
dnj-25	W07A8.3	• ortholog of human DNAJC6 family and cyclin G associated kinase • involved in receptor-mediated endocytosis • expressed in hypodermis and pharynx	N/A
dnj-26	Y39C12A.8	• ortholog of human DNAJC18/B12/B14 family • three transmembrane domains	N/A
dnj-28	Y54E10BL.4	• ortholog of human DNAJC3 • expressed in hypodermis, head, intestine and tail • Tetratricopeptide-like helical domain (TPR)	N/A
dnj-30	Y71F9B.16	• ortholog of human DNAJC8 family	N/A
F54F2.9	F54F2.9	• ortholog of human DNAJC1 family • transmembrane domain • two C-terminal SANT domains • DNA binding activity • Expressed in coelomocytes, intestine and head neurons	WT
Endoplasmic reticulum			
dnj-27	Y47H9C.5	• ortholog of human DNAJC10 family • Thioredoxin/protein disulfide isomerase • expression induced upon ER stress via IRE-1/ XBP-1 • involved in ER-associated degradation (ERAD) • expressed in muscles, hypodermis, the alimentary and reproductive system	N/A
dnj-29	Y63D3A.6	• resides also in cytoplasm • Sec63 domain • two transmembrane domains	WT
dnj-7	C55B6.2	• ortholog of human DNAJC3 family • misfolded protein binding activity • protein kinase inhibitor activity • involved in ER unfolded protein response (UPS) • expressed in body wall muscles, head, pharynx and reproductive system	WT
Mitochondrion			
dnj-10	F22B7.5	• ortholog of human DNAJA3 family • predicted unfolded protein binding activity • involved in embryo and larval development • expressed in head, intestine, pharynx and tail	N/A
dnj-15	F38A5.13	• ortholog of human HSCB (HscB mitochondrial iron-sulfur cluster co-chaperone)	WT
dnj-21	F39B2.10	• ortholog of human DNAJC15/19 family • transmembrane domain	WT, Lva
dnj-22	F54D5.8	• ortholog of human DNAJC17 family	Unc,Rup,Stp,Gro, Lva,Sle

Table A3: Nucleotide-exchange factors (NEFs)

Worm gene	Ensembl ID	Description	RNAi phenotype
Cytoplasm			
bag-1	F57B10.11	• homolog of human BAG-1	WT
unc-23	H14N18.1	• homolog of human BAG2	Unc,WT,Rol
Hsp110	C30C11.4	• involved in protein disaggregation	Emb,Gro,Lvl,Bmd, Rup,Lva,Unc,Pvl
Endoplasmic reticulum			
T14G8.3	T14G8.3	• ortholog of hypoxia-upregulated vertebrate proteins such as human HYOU1 • involved in ER unfolded protein response	WT
T24H7.2	T24H7.2	• ortholog of hypoxia-upregulated vertebrate proteins such as human HYOU1 • involved in ER unfolded protein response	WT
Mitochondrion			
GrpE	C34C12.8	• Ortholog of human GRPEL1/2	N/A

Manuscript (submitted May 2019)

Recruitment of a classical Hsp70 as subunit of the ribosome-associated complex

Nadine Sachs[1], Annalena Wallisch[1], Roman Kityk[2], Lukas Rohland[2], Christoph Globisch[3], Christine Peter[3], Matthias P. Mayer[2], Martin Gamerdinger[1]* and Elke Deuerling[1]*

[1]Department of Biology, Molecular Microbiology, University of Konstanz, 78457 Konstanz, Germany
[2]Center for Molecular Biology of Heidelberg University (ZMBH), DKFZ-ZMBH Alliance, 69120 Heidelberg, Germany
[3]Department of Chemistry, Computational and Theoretical Chemistry, University of Konstanz, 78457 Konstanz, Germany

*corresponding authors: martin.gamerdinger@uni-konstanz.de; elke.deuerling@uni-konstanz.de

ABSTRACT

The ribosome-associated complex (RAC) assists co-translational protein folding. RAC consists of a ribosome binding J-domain protein (Zuotin) and an atypical Hsp70 (Ssz) that lacks ATPase activity. This unique chaperone complex organization is assumed to be evolutionary conserved in eukaryotes. However, while Zuotin-related proteins are present in all organisms, Ssz homologs appear to be absent in many species including nematodes and several arthropods. In the nematode *C. elegans*, we found that a conventional, catalytically-active cytosolic Hsp70 (HSP-1) forms a stable heterodimeric complex with the Zuotin homolog DNJ-11. Strikingly, complex formation via the N-terminal domain of DNJ-11 induces a remodeling of the canonical Hsp70 function resulting in repressed ATPase and substrate binding activity. Nevertheless, on the ribosome, the complexed Hsp70 directly binds nascent chains via the canonical peptide binding cleft. Thus, in addition to Ssz-like proteins also classical Hsp70s can serve as RAC subunit and bind nascent substrates with low-affinity during co-translational protein folding. Moreover, our findings highlight for the first time the reconfiguration of a canonical Hsp70 by complex formation with a J-domain protein that negatively regulates the Hsp70 cycle.

INTRODUCTION

RAC is a eukaryotic heterodimeric chaperone complex consisting of a J-domain protein (JDP; yeast = Zuotin; human = MPP11/DnaJC2) and an ATPase-deficient Hsp70 homolog (Ssz; Hsp70L1/HSPA14). The JDP subunit of RAC directly interacts with the ribosome and facilitates *de novo* protein folding by acting via its J-domain as an ATPase-stimulating partner of an additional catalytically-active Hsp70[1–3]. In yeast this partner is a specialized ribosome binding Hsp70 called Ssb, whereas in human cells a conventional cytosolic Hsp70 cooperates with RAC[4,5]. The Ssz subunit is essential for RAC to act as a J-domain protein cofactor[4]. However, the function of Ssz-like Hsp70 proteins in RAC is poorly understood. Like canonical Hsp70s, Ssz-like Hsp70s consist of an N-terminal nucleotide binding domain (NBD) and a C-terminal substrate binding domain (SBD). Biochemical data, however, showed that yeast Ssz and human Hsp70L1 bind but do not hydrolyze ATP[2,5]. In support of this, the crystal structure of the ATP binding domain of Ssz revealed a typical Hsp70-like fold, but crucial catalytic residues present in canonical Hsp70s are mutated in the catalytic center of Ssz[6]. A second major difference between Ssz and classical Hsp70s lies in the SBD. In classical Hsp70s, the SBD consists of a β-sandwich (SBDβ) that contains the substrate binding cleft, and an α-helical lid domain (SBDα) that closes over the SBDβ upon ATP hydrolysis in the NBD, resulting in high affinity substrate binding[7,8]. In Ssz-like Hsp70s, however, the SBD is truncated lacking the entire SBDα. Both, the catalytic inactivity of the NBD and the truncation of the SBD strongly suggest that Ssz-like proteins bind substrates, if at all, with lower affinity. A direct substrate interaction is not proven yet and the role of Ssz-like proteins in RAC remains enigmatic.

The RAC system has been investigated in yeast and human cells. In these species, the unusual complex organization of RAC between a ribosome binding JDP and a truncated, ATPase-deficient Hsp70 is conserved. This suggests that catalytic inactivity and loss of high-affinity substrate binding of the Hsp70 subunit are intrinsic and essential parts of the RAC function. To test this hypothesis, we investigated the evolutionary conservation of RAC in eukaryotes and, strikingly, found that Ssz-like proteins are absent in many species. Here, we characterize the RAC system in one of those species, *Caenorhabditis elegans*, and show that classical active Hsp70s can be functionally remodeled to act as a RAC subunit.

RESULTS

Catalytically-inactive Ssz-like Hsp70s are not universally conserved in eukaryotes

To investigate the evolutionary conservation of the RAC system in eukaryotes, we performed NCBI BLAST searches on the server of the European Bioinformatics Institute[9] with the sequence of yeast Ssz and human Hsp70L1 as queries to the UniRef90 database of clusters of 90% mutually identical sequences and retrieved 1000 sequence clusters corresponding to 5200 and 3267 sequences, respectively (Supplementary Fig. 1). The retrieved sequences were aligned using CLUSTAL Ω and analyzed for specific features of Hsp70L1/Ssz and classical Hsp70 proteins. We did not detect any unique features for Hsp70L1/Ssz. All residues that are conserved through all Hsp70L1/Ssz-like proteins are also conserved as the same residues in classical Hsp70s. In contrast, classical Hsp70s share a number of sequence features that are not conserved in Hsp70L1/Ssz, including residues known to be important for ATP hydrolysis and allosteric regulation [10], suggesting that Hsp70L1/Ssz have lost both the ability to hydrolyze ATP and allosteric control through degenerative mutations that were not counter-selected by natural selection, consistent with biochemical data on yeast Ssz[2]. As a consequence, Hsp70L1/Ssz were much less conserved than classical Hsp70s and over larger evolutionary distances Hsp70L1/Ssz proteins were no closer related to each other than to classical Hsp70s. Thus, proteins were considered to be Hsp70L1/Ssz like, if the degree of sequence identity was at least 30%, the length was between 500 and 600 amino acids and if they showed replacements in conserved residues important for ATP hydrolysis and allostery in classical Hsp70s.

From the search of the UniRef90 database with Ssz we almost exclusively retrieved sequences of fungal organisms that either matched the characteristics of Ssz or were classical Hsp70s. From the search with the Hsp70L1 sequence we obtained Hsp70L1 like sequences from many metazoan organisms but none from nematodes or plants. To be more specific we used the human Hsp70L1 and the yeast Ssz sequence to search the UniProtKB taxonomic subsets of Vertebrata, Nematoda, Arthropoda, and Viridiplantae (Fig. 1a-d). Again, no Hsp70L1-like sequences were obtained from nematodes and plants and very few from arthropods, however, from each of the major Arthropoda clades Crustacea, Myriapoda, Chelicerata and Insecta. Using the few Hsp70L1 sequences obtained from Arthropoda to search the Arthropoda subset, we retrieved a total of 65 sequences from 35 different organisms, notably lacking several completely sequenced organisms like Drosophila species (Fig. 1b). To verify whether an Hsp70L1 like protein is missing in *Drosophila melanogaster*, we performed a BLAST search using the human Hsp70L1 on FlyBase (https://flybase.org/) retrieving all Hsp70-like protein sequences. Similarly, we extracted all Hsp70 like protein sequences of *Caenorhabditis elegans* from the WormBase (https://wormbase.org/) and of the *Arabidopsis thaliana* genome database (https://www.arabidopsis.org/). No sequences that matched the above-mentioned characteristics of Hsp70L1/Ssz were obtained for *D. melanogaster* or for *C. elegans*. In contrast, we found an Hsp70L1 homolog in *Arabidopsis* and used it to search the UniProtKB taxonomic subset of Viridiplantae, retrieving some 150 Hsp70L1 like sequences (Fig. 1d). These data suggest that the Hsp70 component of RAC is absent in nematodes and several arthropods, whereas it is present in vertebrates and many other metazoa and in plants and fungi. In contrast, when we used the sequence of the human Zuotin homolog MPP11/DnaJC2 in similar BLAST searches, we obtained a large number of homologous sequences from all taxonomic subsets tested (Fig. 1e-h). These data suggest variations of the RAC system during evolution and challenges the assumption that a catalytically-inactive Hsp70 subunit is critical for RAC function.

Characterization of the Zuotin ortholog of *C. elegans*

To gain insight into the structure and function of non-canonical RAC systems that lack Ssz-like proteins, we investigated the Zuotin ortholog DNJ-11 of the nematode *C. elegans*. DNJ-11 shares a similar domain structure and high sequence identity (34.5% and 23.5%, respectively) with human MPP11/DnaJC2 and yeast Zuotin (Fig. 2a and Supplementary Fig. 2a).

DNJ-11 chromosomally tagged with GFP localizes to the cytosol and shows highest expression in the reproductive system of adult worms as well as in embryos, consistent with its supposed role in *de novo* protein synthesis (Fig. 2b). To test whether DNJ-11 indeed represents the Zuotin ortholog of *C. elegans*, we investigated its ability to reversibly bind to translating ribosomes. Polysome analysis of young adult *C. elegans* worms revealed that a large fraction of DNJ-11 co-migrates with 80S ribosomes and polysomes (Fig. 2c). Moreover, ribosome sedimentation analyses showed that the ribosome interaction was salt-sensitive (Supplementary Fig. 2b), similar to the ribosome binding mode of Zuotin and MPP11/DnaJC2[11,12]. Ribosome binding of DNJ-11 was further analyzed *in vitro* using purified components. Recombinant DNJ-11 efficiently bound to 80S ribosomes in a saturable manner, demonstrating a direct interaction of DNJ-11 with ribosomes (Fig. 2d). To substantiate that DNJ-11 is indeed a functional Zuotin ortholog, we performed growth complementation studies in *zuo1Δ* yeast cells. Expression of DNJ-11 in yeast was driven by the constitutive GPD promoter and immunoblot analysis confirmed stable expression of the *C. elegans* protein in yeast cells (Supplementary Fig. 2c). Though not as strong as Zuotin, expression of DNJ-11 significantly promoted growth of *zuo1Δ* cells (Fig. 2e), suggesting that DNJ-11 partially complements the co-translational protein folding defect in *zuo1Δ* yeast cells. In sum, these data strongly suggest that DNJ-11 is a *bona fide* functional ortholog of yeast Zuotin.

The DNJ-11-HSP-1 complex exhibits RAC-like features

To investigate whether DNJ-11 acts on its own or in a heterodimeric complex similar to the canonical RAC systems in yeast and human cells, we performed co-immunoprecipitation studies. Pulldown of DNJ-11 in *C. elegans* lysates coprecipitated a second protein in equimolar amounts to DNJ-11 with a molecular mass of about 70 kDa (Fig. 3a, left). The specificity of the pulldown reaction was verified using lysates of DNJ-11 knockout worms (*dnj-11(bc212)*) as negative control (Fig. 3a, right). Strikingly, the 70 kDa interacting protein was identified by mass spectrometry as HSP-1, the constitutively expressed canonical Hsp70 isoform of *C. elegans*[13,14]. In contrast to yeast Ssz and human Hsp70L1, HSP-1 exhibits a conventional Hsp70 domain structure including the SBDα and the highly conserved NBD-SBD linker (Fig. 3b), and residues critical for the catalytic function and allosteric regulation are conserved (Supplementary Fig. 3). Immunoblot analysis confirmed efficient co-immunoprecipitation of DNJ-11 and HSP-1 specifically in wildtype N2 worms but not DNJ-11 knockout worms (Fig. 3a, lower panel). Moreover, the interaction between HSP-1 and DNJ-11 was high-salt resistant (Supplementary Fig. 4a) and the complex did not resolve upon ATP treatment, which releases Hsp70 bound substrates (Supplementary Fig. 4b). These data suggest that DNJ-11 and HSP-1 form a stable heterodimeric chaperone complex *in vivo*. To investigate whether complex formation with HSP-1 is critical for DNJ-11 function *in vivo*, we depleted HSP-1 by RNAi. Knockdown of HSP-1 decreased DNJ-11 protein levels despite increased *dnj-11* mRNA levels (Supplementary Fig. 4 c, d), indicating that DNJ-11 stability in *C. elegans* depends on its complex formation with HSP-1, reminiscent of the yeast and human orthologs that require their specific Hsp70 partner to become functionally active[2,5]. These data suggest that the DNJ-11-HSP-1 complex of *C. elegans* has RAC-like properties.

To further investigate this potential non-canonical RAC, we performed ribosome binding studies *in vitro* with purified components. We co-expressed DNJ-11 and HSP-1 in *E. coli* and could successfully purify a complex with a 1:1 stoichiometry (Fig. 3c). Recombinant HSP-1 on its own only weakly bound to purified 80S ribosomes, whereas HSP-1 in complex with DNJ-11 showed strong binding (Fig. 3d, upper panel). Thus, as expected, through complex formation with the ribosome binding JDP, HSP-1 gets tethered to ribosomes. Ribosome binding of the DNJ-11-HSP-1 complex was salt sensitive (Fig. 3d, lower panel), indicating involvement of electrostatic ribosome contacts similar to the RAC systems from yeast and humans[3,12]. In sum, the *in vivo* and *in vitro* data suggest that in nematodes a classical Hsp70 potentially serves as a RAC subunit.

Remodeling of Hsp70 function in the DNJ-11-HSP-1 complex

HSP-1 is an ortholog of human Hsc70 (HSPA8), the major constitutively expressed Hsp70 chaperone[14,15]. Thus, it is assumed that HSP-1, in addition to its function in the RAC-like complex with DNJ-11, also exhibits ATP-driven chaperone function on its own like its human counterpart. In support of this, our co-immunoprecipitation study revealed that HSP-1 is expressed in vast excess to DNJ-11 (compare input/IP ratios of HSP-1 and DNJ-11 in immunoblot in Fig. 3a), indicating an additional DNJ-11 independent function of HSP-1 in *C. elegans*. Moreover, knockdown of DNJ-11 did not decrease HSP-1 levels, showing that also uncomplexed HSP-1 is stable *in vivo*, in contrast to DNJ-11, which depends on its Hsp70 partner (Supplementary Fig. 4d, e). Consistent with the expected classical Hsp70 chaperone function, HSP-1 strongly promoted *in vitro* refolding of the chaperone model substrate firefly luciferase in cooperation with an additional JDP of *C. elegans*, called DNJ-13 (Fig. 4a, red curve). Moreover, single turnover ATPase measurements showed a strongly induced ATP hydrolysis rate in HSP-1 in the presence of the JDPs, DNJ-13 and DNJ-11 (Fig. 4b) consistent with the classical model of the Hsp70-JDP system. These data demonstrate that HSP-1, which serves as a subunit of a RAC-like complex in nematodes, also acts like a conventional, catalytically-active Hsp70 folding chaperone. Strikingly, however, we found that HSP-1 in the RAC-like complex together with DNJ-11 was significantly functionally remodeled. Whereas DNJ-11 could stimulate the ATPase activity of HSP-1 when added *in trans*, in the RAC-like complex the ATPase activity of HSP-1 was significantly lower (Fig. 4b). Of note, the RAC-like complex between HSP-1 and DNJ-11 only formed when the two encoding genes were co-expressed but not when the individual proteins were purified separately and mixed afterwards, suggesting co-translational complex formation (Supplementary Fig. 4f). Consistent with the lower ATPase rate, the chaperone activity of complexed HSP-1 was strongly repressed evident by the reduced luciferase refolding activity (Fig. 4a, yellow curve). These data suggest that complex formation induces a change in the Hsp70 that either prevents binding of the ATPase-stimulating J-domain or results in an inactivation of the ATPase domain.

In yeast RAC, Zuotin specifically interacts with its N-terminal domain with Ssz[16–18]. To investigate whether this interaction mode is conserved and sufficient to repress the ATPase function of HSP-1, we co-expressed genes encoding the N-terminal domain of DNJ-11 (2-42 aa) and HSP-1 in *E. coli*. A stable complex with a 1:1 stoichiometry was generated (Supplementary Fig. 4g), indicating that the assembly of the *C. elegans* RAC-like complex is at least partially similar to yeast RAC. Strikingly, the purified recombinant complex (DNJ-11N-HSP-1) showed strongly reduced luciferase refolding activity (Fig. 4a, green curve), demonstrating that the interaction of the N-terminal domain of DNJ-11 with HSP-1 is sufficient to repress the canonical Hsp70 function.

Is the reduced stimulation of the ATPase activity responsible for the repressed chaperone activity of HSP-1 in the DNJ-11-HSP-1 complex or are there additional defects? To address this question, we directly investigated substrate binding using the well-established fluorescent Hsp70 peptide substrate, D-NR[19]. As expected, size exclusion chromatography revealed that, in the presence of ATP, HSP-1 stimulated by DNJ-13 did efficiently bind D-NR (Fig. 4c, upper right panel). In contrast, HSP-1 in the DNJ-11-HSP-1 complex did not bind the peptide in the presence of DNJ-13 (Fig. 4c, lower right panel). In sum, the catalytic inactivation, the reduced luciferase refolding activity, and the repressed peptide binding ability strongly suggest that the HSP-1 ATPase-substrate interaction cycle is interrupted upon complex formation with DNJ-11. In this respect, the DNJ-11-HSP-1 complex resembles the RAC systems from yeast and human cells.

Molecular dynamics simulations of DNJ-11N-HSP-1 interaction

Our data show that the N-terminal domain of DNJ-11 (DNJ-11N) is sufficient for complex formation with the Hsp70 partner (Supplementary Fig. 4g). This is similar to yeast RAC where the N-terminal domain of Zuotin (Zuo1N) directly interacts with Ssz[16]. In the yeast RAC structure (5mb9[16]) Zuo1N binds to the hydrophobic groove of the Ssz-NBD where in classical Hsp70s the interdomain linker binds in the ATP-bound state. This Ssz-NBD contact is mediated by Zuotin via

a conserved EPVG motif in a loop region which seems to be conserved in DNJ-11 (^{Zuotin}EPVG/EPAG^{DNJ-11}; Supplementary Fig. 2a)[16]. Moreover, also a helical motif of Zuo1N located directly downstream of the EPVG motif, which interacts with a helical element of the Ssz interdomain linker, seems to be conserved in DNJ-11 (Supplementary Fig. 2a). This suggests that the DNJ-11-HSP-1 complex assembly is at least partially similar to yeast RAC involving interactions of DNJ-11N with the linker binding groove of the HSP-1-NBD and also potentially the HSP-1 interdomain linker. Thus, we selected the Zuo1N-Ssz structure (5mb9[16]) as a template to model the DNJ-11N-
HSP-1 interaction. For the homology modeling we decided to omit the truncated SBD of Ssz which shows clear differences to the complete and functional HSP-1-SBD (Fig. 3b). The template structures were superimposed by the match maker module[20] of chimera using a combination of sequence alignment and structural superposition. The alignment was obtained in chimera[21] by utilizing the CLUSTAL Ω[22] engine. During alignment it was ensured that inserts/deletions compared to the template sequence do not occur in secondary structure motifs but are positioned in loop regions (Supplementary Fig. 5a). Different homology models were obtained by MODELLER[23], and the final model (Fig. 5) was selected according to the lowest zDOPE score[24] and the most favorable interaction pattern between DNJ-11 and HSP-1 that is predominantly located in the linker binding groove (see below).
In order to analyze the stability of the homology model, we performed molecular dynamics simulations. We were especially interested in the stability of the DNJ-11N-HSP-1 interaction but also in the helical propensity of the DNJ-11N peptide and its potential interactions with the interdomain linker of HSP-1. In all simulations, DNJ-11N shows a very high helical propensity with occasional partial unfolding and fast refolding of the helical motif (Supplementary Fig. 5b). The interaction of the conserved EPAG motif with the hydrophobic groove of HSP-1 maintains stable throughout all simulations. The participating amino acids are highlighted in the model sequence alignment (Supplementary Fig. 5a) and reported as contact pairs and hydrogen bonds (Supplementary Fig. 5c, d). In addition to the widely conserved EPAG motif (21-24 aa), also the residues C26, Y27 and E28, which are conserved in nematodes, participate in HSP-1 binding. Interacting residues on the HSP-1 side involve the stretch GIFEV (216-220 aa) in the hydrophobic groove and the residues R172, N175, T178 and Q377, which, in classical Hsp70s, are important residues for interaction with JDPs and allosteric regulation[25]. In contrast to the clear helical preference of DNJ-11N and the surprising stability of its interactions with the hydrophobic groove, we observed a high mobility of the HSP-1 interdomain linker. It continuously changes its position and does not maintain a stable interaction with DNJ-11N (Fig. 5; Supplementary Fig. 5b). In sum, these data suggest that DNJ-11-HSP-1 assembly involves an interaction of the conserved EPAG motif with the interdomain linker binding groove of the HSP-1-NBD. Thus, similar to the yeast RAC system, also in the DNJ-11-HSP-1 complex the NBD-SBD linker is dislocated from the linker binding cleft of the NBD. However, in contrast to yeast RAC, the HSP-1 linker, which is shorter than the linker of Ssz and may lack the helical element that is bound by ZuoN (Fig. 3b), seems not to interact with DNJ-11N, at least in the absence of the SBD.

Functional dissection of the DNJ-11-HSP-1 complex

RAC in yeast and human cells is known to stimulate ATP hydrolysis of an additional catalytically-active Hsp70 chaperone[2,5]. An emerging question is whether the DNJ-11-HSP-1 system of nematodes, in which *per se* a catalytically-active Hsp70 is already present as subunit, similarly acts as a J-domain partner of an extra Hsp70. DNJ-11 harbors like the human and yeast orthologs a conserved HPD motif in the J-domain that is critical for JDPs to stimulate ATP hydrolysis in Hsp70 partner proteins (Supplementary Fig. 2a). To address the potential J-domain function of the DNJ-11-HSP-1 complex *in vivo*, we generated *C. elegans* strains expressing either wildtype DNJ-11 or a mutant variant with an inactivating point mutation in the HPD motif[26], DNJ-11^{H129Q}, from a single integrated transgene in the DNJ-11 knockout background (*dnj-11(bc212)*) (Supplementary Fig. 6a). Co-immunoprecipitation analysis confirmed that DNJ-11^{H129Q} did form a complex with

endogenous HSP-1 *in vivo* similar to wildtype DNJ-11 (Supplementary Fig. 6b). However, while WT-DNJ-11 completely rescued the delayed growth and embryonic lethal phenotypes in *dnj-11(bc212)* animals, DNJ-11^{H129Q} showed only minor rescuing activity (Fig. 6a, b). These data suggest that the J-domain activity of DNJ-11 is critical for DNJ-11-HSP-1 complex function in nematodes, and implicates that it acts as an ATPase-stimulating partner of an additional Hsp70 reminiscent of RAC in yeast and human cells. We speculated that this Hsp70 partner in *C. elegans* could be, in turn, HSP-1, the only constitutively expressed cytosolic Hsp70 in worms. To directly test this possibility, we measured the ATP hydrolysis rate and DN-R peptide binding activity of HSP-1 in the presence and absence of the DNJ-11-HSP-1 complex *in vitro*. Addition of the RAC-like complex indeed stimulated ATP hydrolysis and D-NR peptide binding in HSP-1 (Fig. 6c, d). Moreover, the DNJ-11-HSP-1 complex did also recruit HSP-1 to cycloheximide-stalled ribosome nascent chain complexes (RNCs) purified from *C. elegans* (Fig. 6e). Thus, HSP-1 plays a dual role in co-translational folding, it acts on the one hand as a functionally reconfigured Hsp70 RAC-like subunit, and on the other hand as a catalytically-active Hsp70 partner of the DNJ-11-HSP-1 complex that is stimulated by the J-domain of DNJ-11.

In sum, our data strongly suggest that the DNJ-11-HSP-1 complex constitutes the *C. elegans* RAC system (ceRAC). A remaining question concerns the function of HSP-1 within this non-canonical ceRAC system. HSP-1 is important to stabilize DNJ-11 *in vivo* (Supplementary Fig. 4d), but complex formation seems not to be important for DNJ-11 to stimulate ATP hydrolysis in HSP-1 *in vitro* (compare HSP-1+DNJ-11 in Fig. 4b with HSP-1+DNJ-11-HSP-1 in Fig. 6c). The recruitment of an Hsp70 merely to stabilize an JDP is difficult to envision, rather HSP-1 likely has a more specific function within the complex. Our finding that HSP-1 undergoes a catalytic inactivation in the complex with DNJ-11, indicates that HSP-1 could bind co-translational substrates at least with low-affinity to act as a 'holding' chaperone. To investigate this possibility, we generated *in vitro* translated stalled RNCs harboring radiolabeled nascent chains with a defined length of 85 aa and tested nascent chain binding to HSP-1 and ceRAC variants by chemical crosslinking. Interestingly, HSP-1 alone did not crosslink to the nascent chains, whereas HSP-1 in the complex with DNJ-11 formed crosslink adducts with the radiolabeled nascent chains (Fig. 6f). The interaction with the nascent chain occurred via the canonical Hsp70 peptide binding cleft, as replacement of a residue in HSP-1 occluding the substrate binding pocket[27,28] and predicted to significantly reduce affinity for substrates, ceRAC^{V439F}, abolished nascent chain crosslinking (Fig. 6f). Using this assay, we could not detect an interaction of the nascent chain with yeast RAC (Fig. 6f), though it efficiently bound to ribosomes (Supplementary Fig. 6c), suggesting that the DNJ-11-HSP-1 complex of *C. elegans* is partially functionally different from the yeast RAC system. Furthermore, we tested whether ceRAC^{V439F}, despite deficient to bind substrates directly, is able to recruit an additional HSP-1 to nascent chains via the canonical J-domain function. Indeed, HSP-1 added together with ceRAC^{V439F} to RNCs did form nascent chain crosslink adducts, indicating that high-affinity substrate binding in the complexed Hsp70 is not required to promote nascent chain binding of an additional Hsp70. In sum, these data suggest that HSP-1 within ceRAC indeed interacts with substrates on the ribosome as a 'holding' chaperone that likely contributes to RAC's co-translational protein folding activity in addition to its J-domain function. In support of this, expression of the DNJ-11^{H129Q} variant partially rescued the embryonic lethal phenotype of *dnj-11(bc212)* animals (Fig. 6b), indicating that the J-domain dead mutant ceRAC variant still exerts residual chaperone activity *in vivo*.

DISCUSSION

This study identifies a new type of RAC in which Ssz-like proteins are substituted by conventional Hsp70 chaperones. Complex formation with a Zuotin-related JDP induces a remodeling of the Hsp70 ATPase function resulting in lower substrate binding activity. However, tethered to the ribosomal tunnel exit site via the JDP subunit, the functionally reconfigured Hsp70 is enabled to directly bind nascent polypeptide chains, indicating that, in addition to catalytically-active Hsp70s that are recruited by the J-domain, RAC also provides an intrinsic Hsp70 with low-affinity substrate binding properties to facilitate co-translational protein folding in eukaryotes.

Our finding that a classical Hsp70 can serve as RAC subunit is striking considering that it differs considerably from Ssz-like Hsp70s in regions that are directly involved in the complex formation with Zuotin-related JDPs, including the interdomain linker and the SBD. In Ssz homologs the SBD is largely truncated lacking the entire SBDα lid domain of canonical Hsp70s. Moreover, also the SBDβ, which contains the substrate binding cleft, is incomplete in Ssz-like Hsp70s as it lacks one of the eight β-strands that are present in the canonical SBDβ. In yeast RAC the incomplete β-sandwich of Ssz-SBDβ is directly bound and complemented by a β-strand of the Zuotin N-terminal domain (Zuo1N)[16]. Furthermore, Ssz homologs have a longer interdomain linker that consists of an α-helix and a β-strand, whereas in classical Hsp70s the linker is shorter lacking the α-helical element[16]. In Ssz homologs the linker is detached from the NBD and the Ssz-specific α-helical linker element is bound by Zuo1N[16]. In contrast, in canonical Hsp70s the linker is bound in a cleft of the NBD in the ATP-bound state[29,30]. In yeast Ssz this linker binding cleft is permanently occupied by a loop region of Zuo1N comprising a conserved EPVG motif[16]. In sum, these differences suggest a divergent assembly of the non-canonical RAC system in nematodes compared to the yeast system. Nevertheless, similar to yeast RAC, our data show that like Zuotin the N-terminal domain of DNJ-11 (DNJ-11N) is critical for complex formation with the Hsp70 partner. Moreover, the EPVG motif of Zuo1N that interacts with the linker binding groove of Ssz is conserved in DNJ-11 (^{Zuotin}EPVG/EPAG^{DNJ-11}; Supplementary Fig. 2a). Indeed, our homology model and MD simulations suggest an interaction mode that is at least partially similar to the Zuo1N-Ssz-NBD contact. It is likely that DNJ-11N binds to HSP-1 via the linker binding cleft in the NBD, thereby dislocating the interdomain linker from the NBD in the ATP-bound state, reminiscent of the situation in yeast RAC. In classical Hsp70s, binding of the linker to the NBD is critical for the allosteric communication between the NBD and the SBD and stimulates ATP hydrolysis in the NBD[31]. Thus, occupation of the linker binding groove by DNJ-11N would interfere with the NBD-SBD interdomain allostery and would inhibit the interconversion between the open and closed state, explaining the repressed catalytic folding activity observed for HSP-1 upon complex formation with DNJ-11N.

The catalytic inactivation of HSP-1 within ceRAC has important implications for understanding how RAC facilitates co-translational protein folding. The presence of an Hsp70 with an at least partial SBD is an evolutionary conserved RAC feature. Despite extensive research, however, the role of Ssz-like Hsp70s in canonical RAC systems is poorly understood. Studies in yeast showed that the substrate binding domain of Ssz is not essential for RAC to recruit Ssb to nascent chains[32]. This implicates that the J-domain activity of RAC is functionally separated from the SBDβ of Ssz. The SBDβ of Ssz complemented by Zuo1N is structurally highly similar to canonical SBDβs and should therefore be able to bind substrates with low affinity like canonical Hsp70s in the ATP-bound state. Thus, it was hypothesized that Ssz-like Hsp70s may act as weakly binding 'holding' chaperones to support co-translational protein folding[6,16]. The principle that 'holding' chaperones have a crucial function in the maturation of newly synthesized proteins is well established in bacteria, where the ATP-independent chaperone trigger factor maintains nascent chains in a folding-competent state by preventing local premature misfolds of nascent chains, thereby increasing productive *de novo* protein folding[33–35]. However, a direct binding of substrates to Ssz could not be proven yet. Our

finding that the high-affinity substrate binding ability of HSP-1 is repressed in ceRAC supports the previous 'holding' chaperone hypothesis for RAC. Indeed, our RNC crosslinking experiment demonstrates a binding of nascent chains in the SBDβ of HSP-1. These finding suggest that the Hsp70 subunit of RAC directly exerts a specific chaperone function via its low-affinity substrate binding SBDβ. Thus, RAC likely has a dual chaperone role and depending on the folding requirements, it probably exerts both ATP-driven '(un)folding' activity by acting as a J-domain partner of an extra Hsp70, and low-affinity 'holding' activities either combined or sequentially towards a nascent chain to assist co-translational *de novo* protein folding.

In sum, our study gives structural and functional insights into a new type of RAC in which classical Hsp70s are functionally reconfigured to act as a low-affinity nascent chain 'holding' chaperone. This new concept will pave the way for further experiments aimed at understanding the function of co-translational protein folding chaperones in eukaryotes. Moreover, JDPs usually stimulate ATP hydrolysis of Hsp70s in the presence of substrates more than 1000-fold[36]. Conversely, this study provides the first example where a JDP-Hsp70 interaction interrupts the Hsp70 catalytic cycle. A short N-terminal fragment of a JDP (DNJ-11N) is sufficient to override the catalytic function of Hsp70 (HSP-1) likely by binding to the interdomain linker binding groove of the NBD thereby uncoupling the allosteric regulation of classical Hsp70s resulting in repressed ATP hydrolysis and high-affinity substrate binding activity. This adds a new layer of functional regulation for Hsp70 chaperone activities to our current understanding and thus may inspire the design of Hsp70-specific inhibitors to selectively block or tune down Hsp70 ATPase and chaperone activities. Such type of inhibitors which uncouple the allostery in Hsp70s have promising anti-proliferative activity e.g. in breast cancer models[37].

ACKNOWLEDGEMENTS

We thank the members of our research groups for valuable support and discussion. We also thank Renate Schlömer and Urte Tomasiunaite for technical support, Prof. Barbara Conradt (LMU, Munich) for the *dnj-11(bc212)* strain and Prof. Dr. Janine Kirstein (University of Bremen) for the HSP-1 antibody. We thank the Proteomics Centre of the University of Konstanz for support. Molecular graphics and part of the structural analyses were performed with UCSF Chimera, developed by the Resource for Biocomputing, Visualization, and Informatics at the University of California, San Francisco, with support from NIH P41-GM103311. The authors acknowledge support by the High Performance and Cloud Computing Group at the Zentrum für Datenverarbeitung of the University of Tübingen, the state of Baden-Württemberg through bwHPC and the German Research Foundation (DFG) through grant no INST 37/935-1 FUGG. This work was supported by research grants from the German Science Foundation (DFG; SFB969; A01 and A07 to E.D. and M.G., and MA1278/4-3 to M.P.M.) and by fellowships of the Konstanz Research School Chemical Biology to N.S. and A.W.

AUTHOR CONTRIBUTIONS

Conceptualization, N.S., M.G., and E.D.; N.S. performed all *in vivo* and *in vitro* experiments except, A.W. performed *in vitro* translation and crosslinking studies, R.K. and L.R. performed single turn-over ATPase assays, C.G. performed structural modeling and molecular dynamics simulations, M.P.M conducted phylogenetic analyses. Writing – Original Draft, N.S., and M.G.; Writing - Review & Editing, M.P.M., and E.D.; Supervision, M.P.M., C.P., M.G., and E.D.; Funding Acquisition, M.G., E.D, and M.P.M.

COMPETING INTERESTS

The authors declare no competing interests.

FIGURE LEGENDS

Figure 1: Conservation of Hsp70L1 and MPP11/DnaJC2 in evolution. Results of BLAST searches on UniProtKB taxonomic subsets Vertebrates (**a**, **e**), Arthropods (**b**, **f**), Nematodes (**c**, **g**), and green plants (**d**, **h**) using human Hsp70L1 (**a**), *Daphnia magna* Hsp70L1 (**b**, **c**), *Arabidopsis thaliana* Hsp70L1 (**d**), and human MPP11/DnaJC2 (**e**-**h**) as query. The relative degree of identity (left y-axis, black symbols) and the sequence length (right y-axis, gray symbols) are plotted versus the alignment score from the BLAST search result. Dashed lines indicate to which score the sequence exhibited features of Hsp70L1 (**a**-**d**) and DnaJC2 (**e**-**h**) and below which the sequences belonged to classical Hsp70s (cHsp70, **a**-**d**) and other J-domain proteins (JDPs, **e**-**h**), respectively, as determined by Clustal Ω multiple sequence comparison.

Figure 2: **Characterization of the Zuotin homolog DNJ-11 in *C. elegans*.** (**a**) Schematic showing the domain structure of Zuotin homologs of different eukaryotic species. N, N-terminal domain; J, J-domain; ZHR, Zuotin homology region; CR, charged region. (**b**) Microscope images of *C. elegans* animals (adult worm and embryo) expressing DNJ-11 tagged with GFP (GFP::DNJ-11). The gonad of adult worm is shown enlarged (second row). White arrowheads, gonads; red arrowheads, oocytes; red asterisk, gonad syncytium. Scale bar = 500 µm (body overview) and 20 µm (others). BF, bright field. (**c**) Sucrose density gradient (15-45%) polysome analysis in wild type N2 worms (day-2 adults). Absorbance at 254 nm was recorded and fractions throughout the gradient were analyzed by immunoblotting using DNJ-11 specific antibodies. uL16 served as ribosomal marker. a.u., arbitrary units. (**d**) Purified *C. elegans* 80S ribosomes were incubated with recombinant DNJ-11 and ribosomes were sedimented by sucrose cushion ultracentrifugation. Proteins in the supernatant (S) and pellet (P) were analyzed by immunoblotting. uL16 served as ribosomal marker. (**e**) Growth analysis (4 days, 20°C) of wildtype (wt) and *zuo1Δ* yeast cells transformed with the empty vector (ev) or plasmids encoding *zuo1* (pGPD-*zuo1*) or *dnj-11* (pGPD-*dnj-11*).

Figure 3: DNJ-11 forms a stable complex with HSP-1. (**a**) Co-immunoprecipitation analysis of DNJ-11 in wildtype (N2) and DNJ-11 knockout (*dnj-11(bc212)*) worms. Coomassie stained gel (upper panel) shows proteins in total lysate (input) and DNJ-11 immunocomplexes (IP). The two immunoprecipitated proteins running at ~70 kDa were identified by mass spectrometry as DNJ-11 and HSP-1, as indicated. Levels of DNJ-11 and HSP-1 were additionally analyzed by immunoblotting (lower panel). Δ, IgG heavy chain. (**b**) Schematic showing domain structure of Hsp70 subunits of RAC from different eukaryotic species. NBD, nucleotide binding domain; Linker; interdomain linker; SBDα/β, substrate binding subdomain α and β. (**c**) Size exclusion chromatography elution profile of recombinant DNJ-11-HSP-1 complex. Inset shows SDS-PAGE analysis of proteins in peak fraction stained with Coomassie. a.u., arbitrary units. (**d**) *In vitro* sucrose cushion centrifugation of purified 80S ribosomes incubated with recombinant HSP-1 and DNJ-11-HSP-1 complex at physiological salt (120 mM KOAc, upper panel) and high salt (300 mM KOAc, lower panel) conditions. Proteins in supernatant (S) and pellet (P) were analyzed by immunoblotting. uL24 served as ribosomal marker. *, degradation product.

Figure 4: Remodeling of Hsp70 function in the DNJ-11-HSP-1 complex. (**a**) Chemically denatured luciferase was incubated for 120 min at 20°C with indicated chaperones in the presence of luciferin and an ATP regenerating system. Luciferase refolding was measured by recording luminescence every min. a.u., arbitrary units (**b**) Diagram shows ATP hydrolysis rate (single turnover of ATP [α-^{32}P]) in HSP-1 alone and HSP-1 in complex with DNJ-11 in the presence and

absence of JDPs (DNJ-13, DNJ-11). Data are presented as mean ± SD (n=3). An unpaired Student's t-test was used to assess significance (**p<0.01) (**c**) D-NR peptide binding analyses of HSP-1 (upper panels) and DNJ-11-HSP-1 complex (lower panel) in presence and absence of DNJ-13, as indicated. HSP-1 and DNJ-11-HSP-1 were preincubated with D-NR peptide in the presence of ATP (5 mM) followed by size exclusion chromatography. Diagrams show the fluorescence of D-NR peptide (blue, emission 520 nm) and absorbance of proteins (black, 280 nm) throughout the elution profile. a.u., arbitrary units.

Figure 5: Molecular dynamics simulations of DNJ-11N-HSP-1 interaction. Comparison of the DNJ-11N-HSP-1 structural model with the crystal structure of Zuo1N-Ssz. The NBD and the interdomain linker of HSP-1/Ssz and the interacting loop-helix motif of DNJ-11N/Zuo1N are colored in blue, gray and orange, respectively. Left: Model of DNJ-11N-HSP-1: side chain of residues forming stable interactions between DNJ-11N and HSP-1 during MD simulations are explicitly indicated, colored according to the residue type (gray hydrophobic, green hydrophilic, red negatively charged and blue positively charged). A ghost like representation of various interdomain linker conformations that occurred during the simulations demonstrates its high mobility and the transient nature of its interactions of the NBD-SDB linker with DNJ-11N. Right: The corresponding template structure of Zuo1N-Ssz with the Ssz-specific helical interdomain linker element that is bound by Zuo1N.

Figure 6: Functional dissection of the DNJ-11-HSP-1 complex. (**a**) Microscope images show larval development of wildtype N2 worms, DNJ-11 knockout (*dnj-11(bc212)*), and *dnj-11(bc212)* worms complemented either with wildtype DNJ-11 (WT) or DNJ-11 with a point mutation in the HPD motif (H129Q). Synchronized (Synchr.) L1 larvae were cultivated at 20°C for 48 and 72 hours. L1-L4, larval stages 1-4; A, adult. Scale bar = 1 mm. (**b**) Mean brood size of *C. elegans* worms as in (a). Data are presented as mean ± SD (n=3 with 20 worms per analysis and strain). An unpaired Student's t-test was used to assess significance (*p<0.05; **p<0.01). (**c**) ATP single turnover measurement as in Fig. 4b. Diagram shows ATP hydrolysis rates of HSP-1, DNJ-11-HSP-1, and HSP-1 combined with DNJ-11-HSP-1. Data are presented as mean ± SD (n=3). (**d**) D-NR peptide binding analyses as in Fig. 4c with HSP-1 alone (left) and HSP-1+DNJ-11-HSP-1 (right). (**e**) *In vitro* sucrose cushion centrifugation of purified 80S ribosome nascent chain complexes incubated with recombinant HSP-1, DNJ-11-HSP-1, and HSP-1+DNJ-11-HSP-1 (1:1 ratio). Proteins in ribosomal pellet fraction were analyzed by immunoblotting. uL24 served as ribosomal marker. *, degradation product. (**f**) Chemical crosslinking (DSS) of indicated proteins to *in vitro* translated stalled ribosome nascent chain complexes carrying radiolabeled 85 aa nascent chain (NC) of a model substrate (GPI). Crosslinks between NC-tRNA and proteins (red arrowheads) were visualized by autoradiography. HSP-1^{V439F}, substrate binding mutant. Ctrl, only buffer control.

Supplementary Figure 1: Conservation of Ssz and Hsp70L1 in evolution. Results of BLAST searches on UniRef90 Database of clusters of mutually 90% identical sequences using yeast Ssz and human Hsp70L1 as query. The relative degree of identity (left y-axis, black symbols) and the sequence length (right y-axis, gray symbols) are plotted versus the alignment score from the BLAST search result. Dashed lines indicate to which score the sequence exhibited features of Ssz (**a**) and Hsp70L1 (**b**), respectively, and below which the sequences belonged to classical Hsp70s (cHsp70) as determined by Clustal Ω multiple sequence comparison.

Supplementary Figure 2: Sequence alignments of ribosome-binding JDPs. (**a**) Multiple sequence alignment of Zuotin homologs from different eukaryotic species. Amino acids are colored on the basis of their properties: positively charged (blue), negatively charged (red), hydrophobic (black) and neutral (green). Highlighted features: yellow, motif interacting with Ssz-like Hsp70s[16]; grey, conserved motif critical for J-domain junction[38]; blue, residues involved in 60S binding[17,39]; orange, residues involved in 40S binding[39]; rose, residues highly conserved in all homologs; purple residues

highly conserved in all metazoan DnaJC2 homologs (**b**) *In vivo* ribosome sedimentation assay in wildtype N2 worms (day-2 adults). Indicated proteins in total lysate (T), supernatant (S), and ribosomal pellet (P) were analyzed by immunoblotting. Actin and uL16 served as cytosolic and ribosomal markers, respectively. (**c**) Immunoblot analysis showing expression levels of Zuo1 and DNJ-11 in yeast strains analyzed in Fig. 2e.

Supplementary Figure 3: HSP-1 shares features of catalytically-active Hsp70s. Multiple sequence alignment of Ssz-like Hsp70s (top three) and canonical Hsc70s (lower three). Amino acids are colored on the basis of their properties: positively charged (blue), negatively charged (red), hydrophobic (black) and neutral (green). Highlighted in yellow are conserved residues critical for catalytic ATPase function and allosteric interdomain communication of Hsp70s, which are degenerated in inactive Ssz-like Hsp70s. Residues known to interact with J-domain proteins are highlighted in purple. The interdomain linkers are shown in grey.

Supplementary Figure 4: HSP-1 and DNJ-11 form a stable heterodimeric complex. (**a**) Co-immunoprecipitation of DNJ-11 at indicated salt concentrations. Coomassie stained gel shows proteins in total lysate (input) and DNJ-11 immunocomplexes (IP). Δ, IgG heavy chain. (**b**) Co-immunoprecipitation study as in (a) in the presence and absence of 5 mM ATP, as indicated. Δ, IgG heavy chain. (**c**) QPCR analysis of *hsp-1* and *dnj-11* mRNA levels in wildtype N2 worms upon knockdown of HSP-1 by RNAi. Diagram shows the log2-transformed ratio of transcript levels in HSP-1 RNAi worms compared to empty vector control (ev) animals. *Ama-1* was used as reference gene. Data are presented as mean ± SD (n=2). (**d, e**) Immunoblot analysis of HSP-1 and DNJ-11 protein levels upon knockdown of HSP-1 and DNJ-11 in wildtype N2 worms. Pas-7 served as loading control. Ev, empty vector control RNAi condition. (**f**) Separately purified recombinant HSP-1 and DNJ-11 were incubated at 20°C for 15 min in the presence or absence of 5 mM ATP and DNJ-11 was immunoprecipitated. Coomassie stained gel shows proteins in total (input), supernatant (SN), and immunoprecipitated (IP) fractions. (**g**) HSP-1 and DNJ-11 N-terminal domain fused to 6xHis-SUMO (His^6-SUMO-DNJ-11N) were co-expressed in *E. coli*. Coomassie stained gel shows proteins captured by His binding matrix in the presence of 5 mM ATP.

Supplementary Figure 5: Molecular dynamics (MD) simulations of DNJ-11N-HSP-1 interactions. (**a**) Alignment of Ssz/HSP-1 and Zuotin/DNJ-11 as used in the homology modeling. The blue highlighted regions are corresponding to stable/conserved interactions between HSP-1 and DNJ-11 during MD simulations shown in Fig. 5. (**b**) Snapshots illustrating the high helical propensity of DNJ-11N peptide (orange), including a short unfolding event which is followed by fast refolding into a fully formed helix, and the high mobility of the NDB-SBD linker (grey). Qualitatively similar behavior (albeit without entire unfolding of the DNJ-11N peptide helix) was observed in all three independent simulations. Blue, HSP-1-NBD. (**c, d**) Stable intermolecular contacts (**c**) and hydrogen-bonding residues (**d**) observed during the MD simulations of the DNJ-11N-HSP-1 model.

Supplementary Figure 6: Additional control experiments related to Figure 6. (**a**) Immunoblot expression analysis of indicated proteins in *C. elegans* strains analyzed in Fig. 6a, b. Pas-7 served as loading control. (**b**) Co-immunoprecipitation of DNJ-11 in *dnj-11(bc212)* worms complemented with either wildtype DNJ-11 ($DNJ\text{-}11^{WT}$) or DNJ-11 with a point mutation in the J-domain HPD motif ($DNJ\text{-}11^{H129Q}$). Coomassie stained gel shows proteins in total lysate (input) and DNJ-11 immunocomplexes (IP). Δ, IgG heavy chain. (**c**) Sucrose cushion centrifugation of ribosomes in rabbit reticulocyte lysate incubated with recombinant DNJ-11-HSP-1 complex (left) and yeast RAC (right). Indicated proteins in supernatant (S) and pellet (P) were analyzed by immunoblotting. uL16 served as ribosomal marker.

ONLINE METHODS

***C. elegans* strains.** *Caenorhabditis elegans* strains were cultured as described before[40]. Wildtype strain N2 was obtained from the Caenorhabditis Genetics Center (CGC). The *dnj-11* knockout strain (*dnj-11(bc212)*) was received from B. Conradt (LMU Munich)[41]. The *gfp::dnj-11* knock-in strain was generated using the CRISPR/Cas9 technique[42,43]. Therefore, the sgRNA (TAATAATTATAGATGACTA) targeting the N-terminus of DNJ-11 was inserted into the Cas-9 encoding plasmid (Addgene #47549) using the Q5® Site-Directed Mutagenesis Kit (New England Biolabs). The homologous repair template (HRT) was amplified via PCR using a GFP encoding plasmid (Addgene #1704) as template thereby inserting microhomology arms and a glycine-rich linker between GFP and DNJ-11. Microinjection in N2 worms was performed using 50 ng/µl Cas9/sgRNA plasmid, 50 ng/µl HRT and 2.5 ng/µl pCFJ90 (*myo-2::mCherry*) as co-injection marker[44]. Transgenic nematodes were directly screened for GFP fluorescence as described before[43]. *C. elegans* strains expressing DNJ-11 variants were generated by injection of miniMos transposon vectors[45] containing DNJ-11^{WT} or DNJ-11^{H129Q} under the native promoter and 3'-UTR into N2 worms. Each injection mix included: 10 ng/µl miniMos-based vector, 5 ng/µl CFJ421, 5 ng/µl pPD152.79, 50 ng/µl pCFJ601, 10 ng/µl pMA122, 20 ng/µl DNA ladder. Expression in the germline was controlled by co integration of a mCherry marker gene under control of the ubiquitous *icd-2* promoter and 3'-UTR. Transgenic strains were finally crossed with the *dnj-11(bc212)* strain and homozygous transgenic progenies were isolated.

RNAi. Gene knockdown via RNAi was achieved by feeding *C. elegans* with *E. coli* HT115(DE3) transformed with the plasmid L4440 coding for the respective dsRNA or the empty vector control. The worms were subjected to RNAi at the L1 larval stage. For *hsp-1* knockdown the worms were exposed to RNAi at the L4 larval stage to prevent larval arrest. Worms were harvested on day 3 of adulthood.

Quantitative PCR (qPCR). Total *C. elegans* RNA was extracted via the RNeasy Mini Kit (Qiagen) and reverse transcribed via the QuantiTect Reverse Transcription Kit (Qiagen). PCR reactions were performed with the ABI 7500 Fast Real-Time PCR System (Applied Biosystems) using the GoTaq SybrGreen mix (Promega). *Ama-1* served as a reference gene and relative mRNA levels were calculated by the $2^{-(\Delta\Delta Ct)}$ method.

Polysome analysis. Worms were cultivated in liquid culture in presence of *E. coli* OP50 as food source at 20°C as previously described[46]. On day 2 of adulthood *C. elegans* were harvested on ice in 0.1 M NaCl and separated from bacteria via sucrose flotation. After an additional washing step, nematodes were flash frozen in liquid nitrogen. Worm pellets were ground to powder using a pre-cooled cryo mill (Retsch MM400) for 30 s at 22 Hz. An aliquot was resuspended in lysis buffer (30 mM HEPES-KOH pH 7.4, 50 mM KOAc, 5 mM $MgCl_2$, 5% (w/v) mannitol, 100 µg/ml cycloheximide, 2 mM β-mercaptoethanol, 1 x Complete protease inhibitor cocktail (Roche)) and centrifuged at 18,000*g* for 15 min at 4°C. The supernatant was adjusted to 20 A_{260} and 500 µl were loaded on a sucrose gradient (15% - 45% in lysis buffer). Ribosomal species were separated via ultracentrifugation (TH-641; Sorvall) at 39,000 rpm for 2.5 h (4°C). Fractionation of the gradients was achieved with a density gradient fractionator (Teledyne Isco, Inc.) monitoring the A_{254}, and received data were processed with PeakTrak V1.1 (Teledyne Isco, Inc.). Aliquots of the collected fractions were subjected to immunoblot analysis.

Immunoblotting and antibodies. Separation of protein samples via SDS-PAGE and transfer onto nitrocellulose membranes were performed via standard protocols. For immunodetection of DNJ-11, uL24, Zuotin and Ssz, polyclonal antibodies were raised in rabbits using recombinant proteins as immunogens. HSP-1 was probed by a peptide antibody against a C-terminal amino acid sequence (EDEKLKDKISPEDKKKIEDK) generated by Davids Biotechnologie GmbH or via a

polyclonal HSP-1 antibody (kind gift from Prof. Janine Kirstein, University of Bremen). In addition, following commercial antibodies were used: Actin (DSHB, JLA20), uL16 (Biomol, #AP17603a), Pas-7 (DSHB, CePAS7).

Fluorescence microscopy. To analyze tissue und subcellular localization of GFP-tagged DNJ-11, worms were anesthetized with 25 mM levamisole. Images were taken on the confocal laser-scanning microscope Leica TCS SP8. Images were adjusted using cropping and contrast tools of Image J software.

***In vivo* ribosome sedimentation assay.** Frozen *C. elegans* worms (day 2 of adulthood) were cryogenic grinded in a pre-cooled cryo-mill (Retsch MM400; 30 s at 22 Hz) and powder was resuspended in lysis buffer (20 mM HEPES-KOH pH 7.4, 50 mM KOAc, 2 mM $Mg(OAc)_2$, 2 mM DTT, 1 mM PMSF, 100 µg/ml cycloheximide, 1 x Complete protease inhibitor cocktail (Roche)) and lysates cleared by centrifugation at 20,000*g* for 10 min. The supernatant was filtrated and adjusted to 4.5 A_{260} in lysis buffer containing different KOAc concentrations. For ribosome sedimentation 200 µl of lysate was loaded on 600 µl sucrose cushion (lysis buffer without cycloheximide + 25% (w/v) sucrose) and centrifuged at 200,000*g* for 90 min at 4°C. The ribosomal pellet was resuspended in lysis buffer with the appropriate salt concentration. The supernatant as well as the total lysate were precipitated with a final concentration of 20% TCA. Total, supernatant and pellet fractions were analyzed via immunoblotting.

Co-immunoprecipitation. *C. elegans* worms were cryogenic grinded using a cryo-mill (Retsch MM400, 30 s at 22 Hz). The powder was subsequently resuspended in lysis buffer (50 mM Tris-HCl pH 7.5, 150 mM NaCl, 2 mM EDTA, 1 mM EGTA, 0.5% NP-40 and 1 x Complete protease inhibitor cocktail (Roche)) and incubated on ice for 10 min. To get rid of cell debris the lysate was centrifuged at 13,000*g* for 15 min. The supernatant was filtrated through a 0.45 µm cellulose filter (Sartorius) and protein concentration was adjusted to 10 µg/µl in 300 µl and afterwards incubated with an anti-DNJ11 antibody. After incubation under constant rotation for one hour at 4°C, 30 µl Protein A Magnetic Beads (NEB, S1425S) were added and again the samples were incubated for one hour at 4°C. The beads were finally washed four times with lysis buffer and captured proteins eluted by adding 25 µl 2 x SDS sample buffer (102 mM Tris-HCl pH 6.8, 5 mM EDTA pH 8.0, 286 mM β-mercaptoethanol, 2% (w/v) SDS, 17% (v/v) glycerol, 0.14% (w/v) bromphenolblue) and heating up to 99°C for 5 min at 900 rpm in a thermomixer.

Protein expression and purification. For recombinant protein expression *E. coli* BL21(DE3)/pRARE cells were transformed with either His^6-SUMO-DNJ-11, His^6-SUMO-HSP-1, His^6-SUMO-DNJ-13 or His^6-SUMO-DNJ-11/HSP-1 (ceRAC or N-ceRAC: 2-42aa of DNJ-11). Cells were cultivated at 20°C and protein expression was induced at OD_{600} 0.6-0.8 by 1 mM IPTG overnight. Bacteria were harvested and subsequently lysed via French Press in lysis buffer (50 mM $NaPO_4$ pH 8.0, 300 mM NaCl, 6 mM $MgCl_2$, 10% glycerol, 10 mM imidazole, 2 mM β-mercaptoethanol, 2 mM PMSF, protease inhibitors and DNase I; for purification of HSP-1 and ceRAC 5 mM ATP was added). Lysates were centrifuged twice at 30,000*g* and 4°C and the supernatant was incubated with Ni-NTA matrix (Machery-Nagel) for 60 min at 4°C. After several washing steps with wash buffer (lysis buffer with 20 mM imidazole without PMSF and protease inhibitors; HSP-1 and ceRAC with 5 mM ATP) the proteins were eluted in elution buffer (wash buffer with 250 mM imidazole). The His^6-SUMO-tag was cleaved off by Ulp1 (8 µg/mg protein) overnight in dialysis buffer (20 mM $NaPO_4$ pH 7.4, 25 mM NaCl, 6 mM $MgCl_2$, 2 mM β-mercaptoethanol and 5 % glycerol). As an additional purification step, proteins were loaded onto ion-exchange chromatography columns (anion-exchanger: HSP-1 and ceRAC; cation-exchanger: DNJ-11 and DNJ-13; both GE Healthcare) and eluted via linear salt gradients (dialysis buffer 25-750 mM NaCl; for purification of HSP-1 and ceRAC 5 mM ATP were added). Fractions containing DNJ-11 or DNJ-13 were dialyzed against protein buffer (40 mM HEPES-KOH pH 7.4,

100 mM KOAc, 5 mM $MgCl_2$, 1 mM β-mercaptoethanol, 10% glycerol). HSP-1 and ceRAC were further purified by a size-exclusion chromatography step in protein buffer (Superdex200 increased 10/300 column (GE Healthcare)).

Purification of *C. elegans* 80S ribosomes. Frozen *C. elegans* N2 worm pellets were cryogenic grinded using a pre-cooled cryo-mill (Retsch MM400; 1 min at 30 Hz). The worm powder was resuspended in lysis buffer (50 mM HEPES-KOH pH 7.4, 0.5% NP-40, 6 mM $MgCl_2$, 300 mM NaCl, 20 µM phenanthrolin, 1 mM PMSF, 2 mM dithiothreitol, 1 x Complete protease inhibitor cocktail (Roche)) under constant agitation and centrifuged at 12,000*g* for 10 min at 4°C. The lysate was loaded on 60% (w/v) sucrose cushions (50 mM HEPES-KOH pH 7.4, 50 mM KCl, 10 mM $MgCl_2$, 5 mM EDTA, 1 x Complete protease inhibitor cocktail (Roche)) and centrifuged at 244,000*g* and 4°C for 20 h. Ribosome pellets were resuspended in buffer (50 mM HEPES-KOH pH 7.4, 150 mM KCl, 1 mM dithiothreitol) and incubated with 1 mM puromycin for 30 min on ice to release nascent polypeptides (this step was omitted to obtain ribosome nascent chain complexes used in the analysis shown in Fig. 6e). Ribosomes were cleared by centrifugation at 20,000*g* for 10 min at 4°C and loaded on 10-40% (w/v) sucrose gradients (50 mM HEPES-KOH, pH 7.4, 120 mM KCl, 4 mM $MgCl_2$, 1 mM dithiothreitol and 1 x Complete protease inhibitor cocktail (Roche)) followed by centrifugation at 99,500*g* for 17 h. Ribosomes were fractionated with a density gradient fractionator (Teledyne Isco, Inc.) and fractions containing 80S ribosomes were concentrated (100,000 MWKO) accompanied by buffer exchange into storage buffer (20 mM HEPES-KOH pH 7.4, 100 mM KCl, 5 mM $MgCl_2$).

***In vitro* ribosome binding analysis.** Proteins (0.5 µM, 1 µM or 4 µM) and 80S *C. elegans* ribosomes (0.5 µM or 1 µM) were mixed in Ribo buffer (30 mM HEPES-KOH pH 7.4, 120 mM/300 mM KOAc, 5 mM $MgCl_2$, 1 mM β-mercaptoethanol, 1x Complete protease inhibitor cocktail (Roche)) and incubated for 30 min at 18°C. Samples were loaded on a 25% sucrose cushion prepared in Ribo buffer and centrifuged at 220,000*g* for 90 min at 4°C. Proteins in the supernatant fraction were precipitated with 20% TCA. The ribosomal pellet was resuspended in Ribo buffer by constant agitation and finally mixed with sample buffer. Same volumes of supernatant and pellet fractions were analyzed by immunoblotting.

Single turn-over ATPase assay. The ATPase activities of HSP-1 and ceRAC were determined under single turn-over conditions. The HSP-1-ATP and ceRAC-ATP complexes (final volume 50 µl) were formed by mixing HSP-1 or ceRAC (final concentration 30 µM) and 2 µl of ATP-mix (20 mM ATP, 12 µCi [α^{32}P]-ATP) in reaction buffer A (25 mM HEPES-KOH pH 7.6, 50 mM KCl 10 mM $MgCl_2$) and leaving the mixture for two min on ice. The complex was isolated at 4°C by gel filtration on Sephadex G-50 (GE Healthcare) columns, pre-saturated with 1 ml of a BSA solution (1 mg/ml) and pre-equilibrated with three column volumes of buffer A. Twenty fractions (2 drops/fraction) were collected. The first four fractions containing radioactivity as detected by a Geiger counter were pooled, divided into 6.5 µl aliquots, snap frozen in liquid nitrogen and kept at -80°C. For the ATPase activity determination HSP-1-ATP or ceRAC complexes were thawed in a water bath at 20°C and, after withdrawal of 0.5 µl for the 0 time point, mixed with 44 µl reaction buffer containing either no cofactors or 1 µM DNJ-11, DNJ-13, or ceRAC. At different time points a 2 µl aliquot was spotted onto a PEI Cellulose TLC plate. Developing the plates in the TLC solution (400 mM LiCl, 10% acetic acid) separated ADP from ATP. Dried plates were exposed to FI-screens overnight and relative amounts of ATP and ADP were quantified by Fuji FLA 2000 Phosphoimager.

***C. elegans* brood size calculation.** The brood size of N2 and mutant *C. elegans* strains was determined by counting the progeny of 60 worms per experiment and strain. Progeny numbers were screened until day 5 of adulthood using a worm flow cytometer (Copas, Union Biometrica). Mean progeny per animal was calculated (n=3) and significance determined by an unpaired Student's t-test.

Peptide-binding analysis. Peptide-binding of HSP-1 and ceRAC was tested by size exclusion chromatography using the dansyl-labeled small peptide D-NR (NRLLLTGC labeled with dansyl chloride; 7 kDa). 5 µM HSP-1 or ceRAC were incubated with 80 µM D-NR peptide in the presence or absence of 1.25 µM DNJ-13 or ceRAC in protein buffer (40 mM HEPES-KOH pH 7.4, 100 mM KOAc, 5 mM $MgCl_2$, 1 mM β-mercaptoethanol, 10% glycerol, 5 mM ATP) for 30 min at 20°C. Samples were loaded on a Superdex 200 increased 10/300 column (GE Healthcare) recording the absorbance at 280 nm. Fluorescence in elution fractions was subsequently measured in a microplate reader (BertholdTech TriStar2S) to detect for D-NR peptide (λ_{ex} = 335 nm, λ_{em}= 525 nm).

Luciferase refolding assay. Luciferase refolding activity was measured as previously described[47] with following adaptations. Recombinant luciferase (2.5 µM) was chemically denatured for 45 min at room temperature in denaturing buffer (25 mM HEPES-KOH pH 7.4, 50 mM KCl, 15 mM $MgCl_2$, 1 mM ATP, 10 mM dithiothreitol, 0.05 mg/mL BSA, 5 M GdmCl). To monitor refolding, denatured luciferase was diluted (1:125) in luminescence buffer (25 mM HEPES-KOH pH 7.4, 50 mM KCl, 15 mM $MgCl_2$, 1 mM ATP, 2 mM dithiothreitol, 0.05 mg/mL BSA, 240 µM coenzyme A, 0.1 mM luciferin, 10 mM phosphoenolpyruvate, 50 µg/mL pyruvate kinase) in the presence of 3.2 µM HSP-1/ceRAC/N-ceRAC and 0.8 µM DNJ-13. Luminescence was measured in 96-well LIA-plates (Greiner Bio-One, Solingen, Germany) over 2 h at room temperature in a microplate reader (BertholdTech TriStar2S).

Nascent chain interaction analysis.

In vitro translation of non-stop mRNAs.

Non-stop transcript templates were generated by PCR as previously described[48]. In brief, the T7 promoter (TAATACGACTCACTATAGGGAGA) needed for *in vitro* transcription was included in the 5' end of the forward primer. The reverse primer encoded five C-terminal methionines for radioactive [S^{35}]-labelling and a terminal valine residue to stabilize the tRNA-nascent chain complex. PCR was performed on a plasmid containing the human gene GPI (glucose-6-phosphate isomerase) and the PCR product was cleaned-up by gel extraction (Qiagen). DNA templates were *in vitro* transcribed using the mMESSAGE mMACHINE T7 Transcription Kit according to manufacturer's guidelines (Thermo Scientific). RNA was purified with RNA Clean & Concentrator Kit (Zymo Research). Non-stop mRNAs were *in vitro* translated using rabbit reticulocyte lysate (Promega) (0.5 µg RNA in a 25 µl translation reaction). Translation reactions were performed at 26°C for 20 min in the presence of 1 mCi/ml [S^{35}]-methionine (Hartmann Analytics).

Purification of ribosome nascent chain complexes (RNCs).

Translation reactions were layered on a 25% (w/v) sucrose cushion in RNC wash buffer (50 mM HEPES-KOH pH 7.5, 500 mM KOAc, 5 mM $Mg(OAc)_2$) and centrifuged at 200,000*g* for 90 min at 4°C. The ribosomal pellets were resuspended in DSS crosslinking buffer (50 mM HEPES-KOH pH 7.0, 100 mM NaCl, 5 mM $MgCl_2$, 0,1 % NP-40, 1x Complete protease inhibitor cocktail (Roche)) by constant agitation for 1 h on ice.

DSS crosslinking.

RAC variants were added to the resuspended RNCs at a concentration of 2 µM, and incubated at 20°C for 15 min. DSS (Thermo Fisher Scientific) was added at a final concentration of 125 µM and crosslinking was performed for 10 min at 20°C. The reaction was quenched with 60 mM Tris-HCl pH 7.5 for 5 min at 20 °C. [S^{35}]-methionine labelled tRNA-NCs and crosslinked complexes were separated by SDS–PAGE and visualized by autoradiography.

Yeast complementation analysis. For complementation assays in *S. cerevisiae* wildtype BY4741 (MATa; *his3Δ1; leu2Δ0; met15Δ0; ura3Δ0*) and *Δzuo1* (*his3Δ1; leu2Δ0; met15Δ0; ura3Δ1; YGR285C::kanMX*) cells were transformed with either pGPD-*zuo1* or pGPD-*dnj-11*. Yeast cultures

were adjusted to identical optical density and serial dilutions were spotted on synthetic complete media without histidine (SD-His) and incubated at 20°C for 4 days.

Sequence alignments. Protein sequences of Ssz and Zuotin homologs were blasted and extracted from the UniProt database. Multiple sequence alignments were performed with CLUSTALW and processed with CLC Sequence Viewer 7.7.1.

Molecular dynamics simulations. All molecular dynamics simulations were obtained by GROMACS version 2016.4 and 2019.1[49,50] using the CHARMM36m[51,52] force field together with the tip3p11[53] water model. The simulation box was set to dodecahedron shape and defined in such a way that the minimum distance of the structure and the box was at least 2.0 nm (to accommodate possible unfolding of the DNJ-11N peptide and allow for mobility of the interdomain linker). Subsequently the protein was solvated with water and neutralized by sodium chloride. Three independent simulations were started with different initial conditions.

The following simulation settings have been used. The Leap frog integrator was utilized together with H-bonds being constrained by the LINCS algorithm[54] in order to enable a time-step of 2 fs. Long range Coulomb interactions were calculated by particle mesh Ewald (PME)[55] method with a cutoff of 1.2 nm. A modified cutoff scheme for short-ranged electrostatic and Lenard Jones interactions of 1.2 nm, where a switching function is applied to smoothly approach the cutoff between 1.0 and 1.2 nm, was used. The neighbor list was updated every 20 steps. Initially, all systems were energy minimized with steepest-descent algorithm for 5000 steps. In the next step an equilibration simulation followed (100 ps) in a canonical (NVT) ensemble was carried out where heavy atoms have been position restrained. The actual production simulations (a total of approximately 600 ns) were carried out in an isobaric-isothermal (NPT) ensemble without position restraints. The temperature was maintained at 298 K by using the Velocity-rescaling algorithm[56] with a coupling time of 0.1 ps. Constant pressure was maintained at 1 atm using isotropic Parrinello-Rahman pressure coupling[57] with a pressure relaxation time of 5 ps.

***C. elegans* strains**

dnj-11(bc212)	[*tph-1p::gfp; bc212*]
DEU136	gamSi36 [*gfp::dnj-11*]
DEU137	*dnj-11(bc212);* gamSi37 [*dnj-11p::WT-dnj-11; icd-2p::mCherry*]
DEU139	*dnj-11(bc212)*; gamSi38 [*dnj-11p::H129Q-dnj-11; icd-2p::mCherry*]

REFERENCES

1. Conz, C. *et al.* Functional characterization of the atypical Hsp70 subunit of yeast ribosome-associated complex. *J. Biol. Chem.* **282**, 33977–33984 (2007).
2. Huang, P., Gautschi, M., Walter, W., Rospert, S. & Craig, E. A. The Hsp70 Ssz1 modulates the function of the ribosome-associated J-protein Zuo1. *Nat. Struct. Mol. Biol.* **12**, 497–504 (2005).
3. Gautschi, M. *et al.* RAC, a stable ribosome-associated complex in yeast formed by the DnaK-DnaJ homologs Ssz1p and zuotin. *Proc. Natl. Acad. Sci. U. S. A.* **98**, 3762–3767 (2001).
4. Gautschi, M., Mun, A., Ross, S. & Rospert, S. A functional chaperone triad on the yeast ribosome. *Proc. Natl. Acad. Sci. U. S. A.* **99**, 4209–14 (2002).
5. Jaiswal, H. *et al.* The chaperone network connected to human ribosome-associated complex. *Mol. Cell. Biol.* **31**, 1160–1173 (2011).
6. Leidig, C. *et al.* Structural characterization of a eukaryotic chaperone--the ribosome-associated complex. *Nat. Struct. Mol. Biol.* **20**, 23–8 (2013).
7. Bertelsen, E. B., Chang, L., Gestwicki, J. E. & Zuiderweg, E. R. P. Solution conformation of wild-type E. coli Hsp70 (DnaK) chaperone complexed with ADP and substrate. *Proc. Natl. Acad. Sci.* **106**, 8471–8476 (2009).
8. Mayer, M. P. & Kityk, R. Insights into the molecular mechanism of allostery in Hsp70s. *Front. Mol. Biosci.* **2**, 58 (2015).
9. Chojnacki, S., Cowley, A., Lee, J., Foix, A. & Lopez, R. Programmatic access to bioinformatics tools from EMBL-EBI update: 2017. *Nucleic Acids Res.* **45**, W550–W553 (2017).
10. Mayer, M. P. & Gierasch, L. M. Recent advances in the structural and mechanistic aspects of Hsp70 molecular chaperones. *J. Biol. Chem.* **294**, 2085–2097 (2018).
11. Yan, W. *et al.* Zuotin, a ribosome-associated DnaJ molecular chaperone. *EMBO J.* **17**, 4809–4817 (1998).
12. Otto, H. *et al.* The chaperones MPP11 and Hsp70L1 form the mammalian ribosome-associated complex. *Proc Natl Acad Sci U S A* **102**, 10064–10069 (2005).
13. Guhathakurta, D. *et al.* Identification of a novel cis-regulatory element involved in the heat shock response in Caenorhabditis elegans using microarray gene expression and computational methods. *Genome Res.* **12**, 701–712 (2002).
14. Snutch, T. P., Heschl, M. F. P. & Baillie, D. L. The Caenorhabditis elegans hsp70 gene family: a molecular genetic characterization. *Gene* **64**, 241–255 (1988).
15. Mogk, A., Bukau, B. & Kampinga, H. H. Review Cellular Handling of Protein Aggregates by Disaggregation Machines. *Mol. Cell* **69**, 214–226 (2018).
16. Weyer, F. A., Gumiero, A., Gesé, G. V., Lapouge, K. & Sinning, I. Structural insights into a unique Hsp70-Hsp40 interaction in the eukaryotic ribosome-associated complex. *Nat. Struct. Mol. Biol.* **24**, 144–151 (2017).
17. Lee, K., Sharma, R., Shrestha, O. K., Bingman, C. A. & Craig, E. A. Dual interaction of the Hsp70 J-protein cochaperone Zuotin with the 40S and 60S ribosomal subunits. *Nat. Struct. Mol. Biol.* **23**, 1003–1010 (2016).
18. Fiaux, J. *et al.* Structural analysis of the ribosome-associated complex (RAC) reveals an unusual Hsp70/Hsp40 interaction. *J. Biol. Chem.* **285**, 3227–34 (2010).
19. Gragerov, A., Zeng, L., Zhao, X., Burkholder, W. & Gottesman, M. E. Specific of DnaK-peptide binding. *J. Mol. Biol.* **235**, 848–854 (1994).
20. Meng, E. C., Pettersen, E. F., Couch, G. S., Huang, C. C. & Ferrin, T. E. Tools for integrated sequence-structure analysis with UCSF Chimera. *BMC Bioinformatics* **7**, 1–10 (2006).
21. Pettersen, E. F. *et al.* UCSF Chimera--a visualization system for exploratory research and analysis. *J. Comput. Chem.* **25**, 1605–12 (2004).
22. Sievers, F. *et al.* Fast, scalable generation of high-quality protein multiple sequence alignments using Clustal Omega. *Mol. Syst. Biol.* **7**, (2011).

23. John, B. & Sali, A. Comparative protein structure modeling by iterative alignment, model building and model assessment. *Nucleic Acids Res.* **31**, 3982–3992 (2003).
24. Shen, M.-Y. & Sali, A. Statistical potential for assessment and prediction of protein structures MIN-YI. *Protein Sci.* **15**, 2507–2524 (2006).
25. Kityk, R., Kopp, J. & Mayer, M. P. Molecular Mechanism of J-Domain-Triggered ATP Hydrolysis by Hsp70 Chaperones. *Mol. Cell* **69**, 227-237.e4 (2018).
26. Cheetham, M. E. & Caplan, A. J. Strcuture, function and evolution of DnaJ: conservation and adaptation of chaperone function. *Cell Stress Chaperones* **3**, 28–36 (1998).
27. Rüdiger, S., Mayer, M. P., Schneider-Mergener, J. & Bukau, B. Modulation of substrate specificity of the DnaK chaperone by alteration of a hydrophobic arch. *J. Mol. Biol.* **304**, 245–251 (2000).
28. Mayer, M. P. *et al.* Multistep mechanism of substrate binding determines chaperone activity of Hsp70. *Nat. Struct. Biol.* **7**, 586–593 (2000).
29. Jiang, J., Prasad, K., Lafer, E. M. & Sousa, R. Structural Basis of Interdomain Communication in the Hsc70 Chaperone. *Mol. Cell* **20**, 513–524 (2005).
30. Kityk, R., Kopp, J., Sinning, I. & Mayer, M. P. Structure and Dynamics of the ATP-Bound Open Conformation of Hsp70 Chaperones. *Mol. Cell* **48**, 863–874 (2012).
31. Vogel, M., Mayer, M. P. & Bukau, B. Allosteric regulation of Hsp70 chaperones involves a conserved interdomain linker. *J. Biol. Chem.* **281**, 38705–38711 (2006).
32. Hundley, H. *et al.* The in vivo function of the ribosome-associated Hsp70, Ssz1, does not require its putative peptide-binding domain. *Proc. Natl. Acad. Sci.* **99**, 4203–4208 (2002).
33. Tomic, S., Johnson, A. E., Hartl, F. U. & Etchells, S. A. Exploring the capacity of trigger factor to function as a shield for ribosome bound polypeptide chains. *FEBS Lett.* **580**, 72–76 (2006).
34. Ferbitz, L. *et al.* Trigger factor in complex with the ribosome forms a molecular cradle for nascent proteins. *Nature* **431**, 590–596 (2004).
35. Hoffmann, A. *et al.* Concerted Action of the Ribosome and the Associated Chaperone Trigger Factor Confines Nascent Polypeptide Folding. *Mol. Cell* **48**, 63–74 (2012).
36. Kityk, R., Vogel, M., Schlecht, R., Bukau, B. & Mayer, M. P. Pathways of allosteric regulation in Hsp70 chaperones. *Nat. Commun.* **6**, 8308 (2015).
37. Gestwicki, J. E. & Shao, H. Inhibitors and chemical probes for molecular chaperone networks. *J. Biol. Chem.* **294**, 2151–2161 (2019).
38. Tsai, J. & Douglas, M. G. A conserved HPD sequence of the J-domain is necessary for YDJ1 stimulation of Hsp70 ATPase activity at a site distinct from substrate binding. *J. Biol. Chem.* **271**, 9347–9354 (1996).
39. Zhang, Y. *et al.* Structural basis for interaction of a cotranslational chaperone with the eukaryotic ribosome. *Nat. Struct. Mol. Biol.* **21**, 1042–6 (2014).
40. Brenner, S. The genetics of Caenorhabditis elegans. *Genetics* **77**, 71–94 (1974).
41. Hatzold, J. & Conradt, B. Control of apoptosis by asymmetric cell division. *PLoS Biol.* **6**, 771–784 (2008).
42. Dickinson, D. J., Ward, J. D., Reiner, D. J. & Goldstein, B. Engineering the Caenorhabditis elegans genome using Cas9-triggered homologous recombination. *Nat. Methods* **10**, 1028–34 (2013).
43. Paix, A. *et al.* Scalable and Versatile Genome Editing Using Linear DNAs with Micro-Homology to Cas9 Sites in Caenorhabditis elegans. *Genetics* **198**, 1347–56 (2014).
44. Mello, C. C., Kramer, J. M., Stinchcomb, D. & Ambros, V. Efficient gene transfer in C.elegans: extrachromosomal maintenance and integration of transforming sequences. *EMBO J.* **10**, 3959–70 (1991).
45. Frokjaer-Jensen, C. *et al.* Random and targeted transgene insertion in C. elegans using a modified Mosl transposon. *Nat. Methods* **11**, 529–534 (2014).
46. Gamerdinger, M., Hanebuth, M. A., Frickey, T. & Deuerling, E. The principle of antagonism ensures protein targeting specificity at the endoplasmic reticulum. *Science* **348**, 201–7 (2015).

47. Sun, L. *et al.* The lid domain of Caenorhabditis elegans Hsc70 influences ATP turnover, cofactor binding and protein folding activity. *PLoS One* **7**, e33980 (2012).
48. Sharma, A., Mariappan, M., Appathurai, S. & Hegde, R. S. In vitro dissection of protein translocation into the mammalian endoplasmic reticulum. *Methods Mol. Biol.* **619**, 339–363 (2010).
49. Pronk, S. *et al.* GROMACS 4.5: A high-throughput and highly parallel open source molecular simulation toolkit. *Bioinformatics* **29**, 845–854 (2013).
50. Abraham, M. J. *et al.* Gromacs: High performance molecular simulations through multi-level parallelism from laptops to supercomputers. *SoftwareX* **1–2**, 19–25 (2015).
51. Huang, J. *et al.* CHARMM36m: An improved force field for folded and intrinsically disordered proteins. *Nat. Methods* **14**, 71–73 (2016).
52. Bjelkmar, P., Larsson, P., Cuendet, M. A., Hess, B. & Lindahl, E. Implementation of the CHARMM Force Field in GROMACS: Analysis of Protein Stability Effects from Correction Maps, Virtual Interaction Sites, and Water Models. *J. Chem. Theory Comput.* **6**, 459–466 (2010).
53. Jorgensen, W. L., Chandrasekhar, J., Madura, J. D., Impey, R. W. & Klein, M. L. Comparison of simple potential functions for simulating liquid water. *J. Chem. Phys.* **79**, 926–935 (1983).
54. Hess, B., Bekker, H., Berendsen, H. J. C. & Fraaije, J. G. E. M. LINCS: A Linear Constraint Solver for molecular simulations. *J. Comput. Chem.* **18**, 1463–1472 (1997).
55. Essmann, U. *et al.* A smooth particle mesh ewald potential. *J. Chem. Phys.* **103**, 8577–8592 (1995).
56. Bussi, G., Donadio, D. & Parrinello, M. Canonical sampling through velocity rescaling. *J. Chem. Phys.* **126**, (2007).
57. Parrinello, M. & Rahman, A. Polymorphic transitions in single crystals: A new molecular dynamics method. *J. Appl. Phys.* **52**, 7182–7190 (1981).

Figure 1

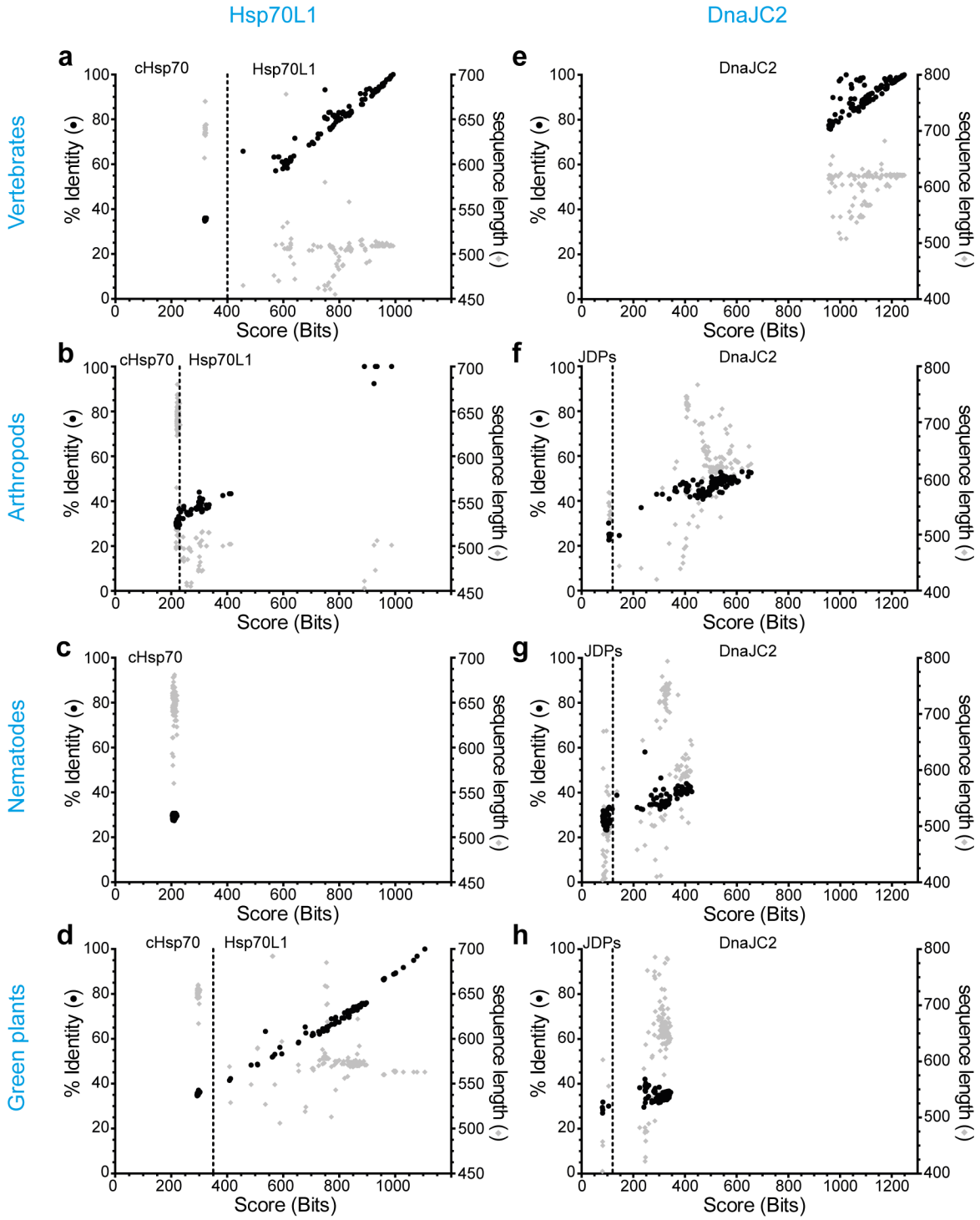
Hsp70L1
DnaJC2
Vertebrates
Arthropods
Nematodes
Green plants
a
b
c
d
e
f
g
h
cHsp70
Hsp70L1
JDPs
DnaJC2
% Identity (•)
sequence length (•)
Score (Bits)

Figure 2

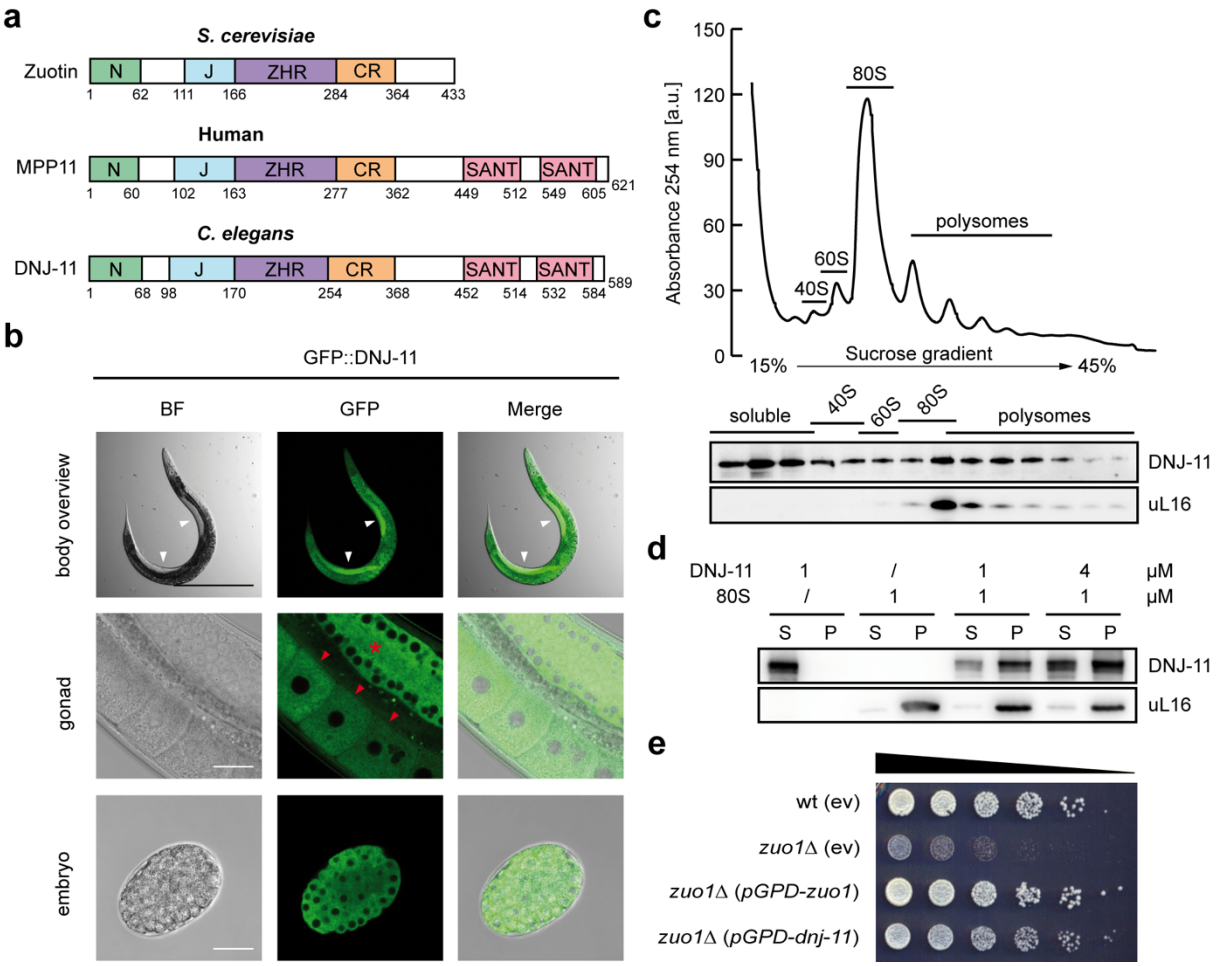
a
S. cerevisiae
Zuotin
N
J
ZHR
CR
1
62
111
166
284
364
433
Human
MPP11
SANT
SANT
60
102
163
277
362
449
512
549
605
621
C. elegans
DNJ-11
68
98
170
254
368
452
514
532
584
589
b
GFP::DNJ-11
BF
GFP
Merge
body overview
gonad
embryo
c
Absorbance 254 nm [a.u.]
150
120
90
60
30
0
80S
60S
40S
polysomes
15%
Sucrose gradient
45%
soluble
40S
60S
80S
polysomes
DNJ-11
uL16
d
DNJ-11
80S
μM
S
P
e
wt (ev)
zuo1Δ (ev)
zuo1Δ (pGPD-zuo1)
zuo1Δ (pGPD-dnj-11)

Figure 3

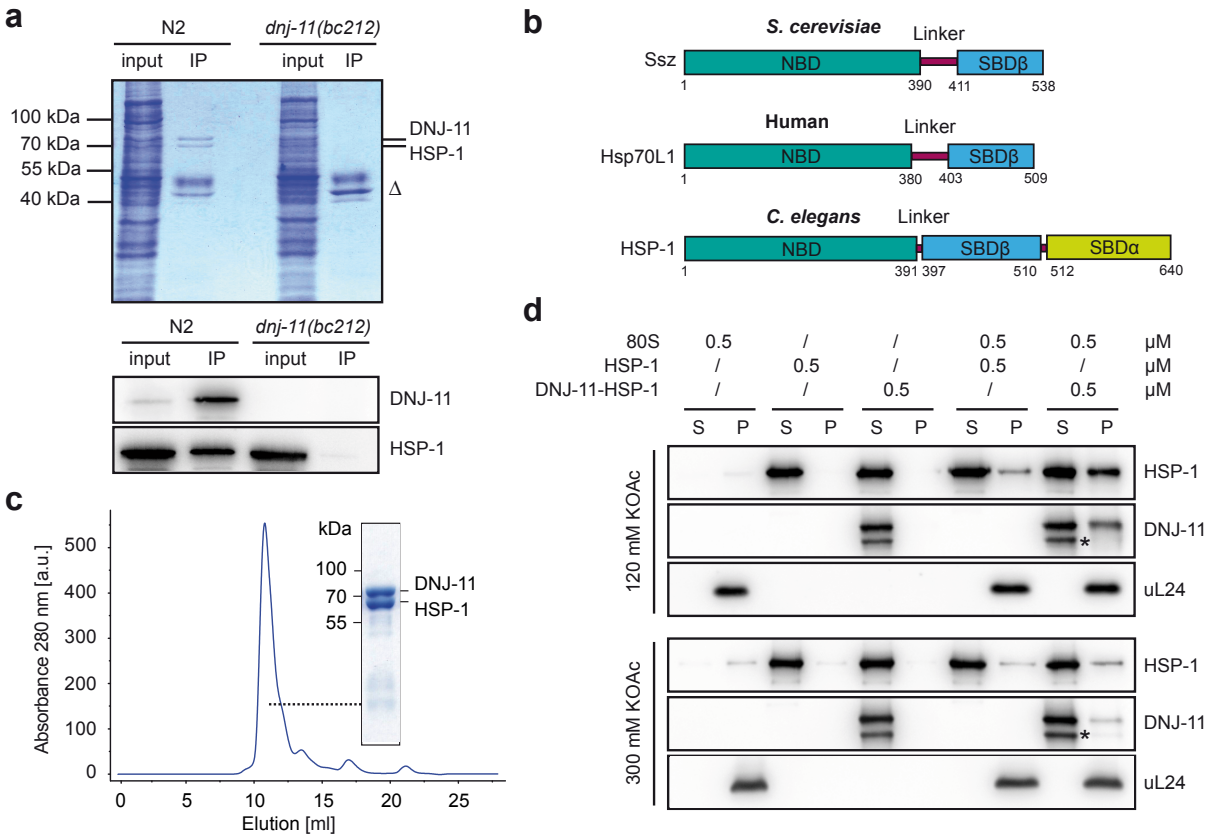
a
N2
dnj-11(bc212)
input
IP
input
IP
100 kDa
70 kDa
55 kDa
40 kDa
DNJ-11
HSP-1
Δ
N2
dnj-11(bc212)
input
IP
input
IP
DNJ-11
HSP-1
b
S. cerevisiae
Linker
Ssz
NBD
SBDβ
1
390
411
538
Human
Linker
Hsp70L1
NBD
SBDβ
1
380
403
509
C. elegans
Linker
HSP-1
NBD
SBDβ
SBDα
1
391
397
510
512
640
c
Absorbance 280 nm [a.u.]
500
400
300
200
100
0
0
5
10
15
20
25
Elution [ml]
kDa
100
70
55
DNJ-11
HSP-1
d
80S
0.5
/
/
0.5
0.5
µM
HSP-1
/
0.5
/
0.5
/
µM
DNJ-11-HSP-1
/
/
0.5
/
0.5
µM
S
P
S
P
S
P
S
P
S
P
120 mM KOAc
HSP-1
DNJ-11
uL24
300 mM KOAc
HSP-1
DNJ-11
uL24

Figure 4

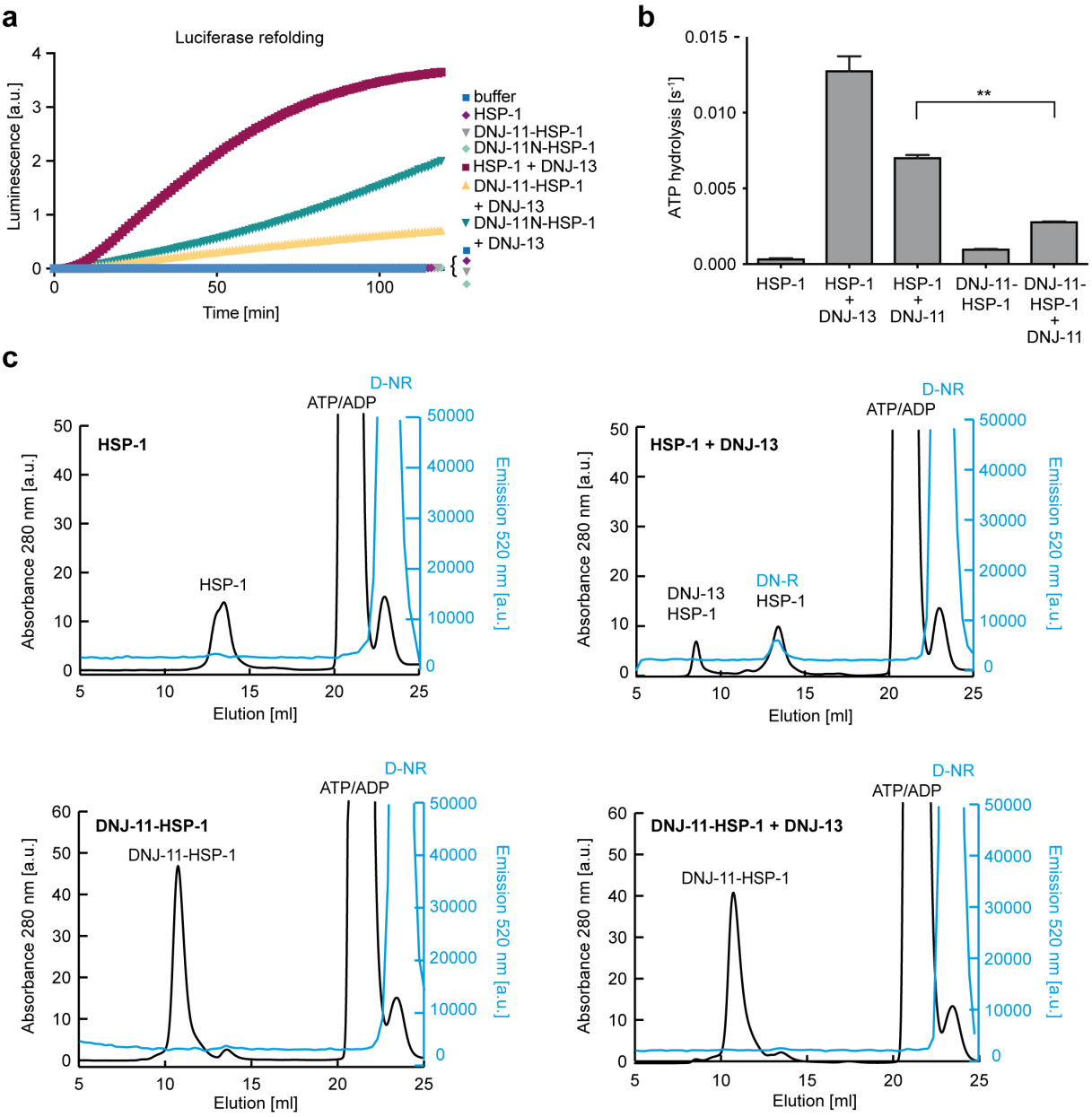
a
Luciferase refolding
Luminescence [a.u.]
Time [min]
buffer
HSP-1
DNJ-11-HSP-1
DNJ-11N-HSP-1
HSP-1 + DNJ-13
DNJ-11-HSP-1 + DNJ-13
DNJ-11N-HSP-1 + DNJ-13
b
ATP hydrolysis [s-1]
**
HSP-1
HSP-1 + DNJ-13
HSP-1 + DNJ-11
DNJ-11-HSP-1
DNJ-11-HSP-1 + DNJ-11
c
HSP-1
HSP-1 + DNJ-13
DNJ-11-HSP-1
DNJ-11-HSP-1 + DNJ-13
Absorbance 280 nm [a.u.]
Emission 520 nm [a.u.]
Elution [ml]
ATP/ADP
D-NR
DN-R
DNJ-13 HSP-1

Figure 5

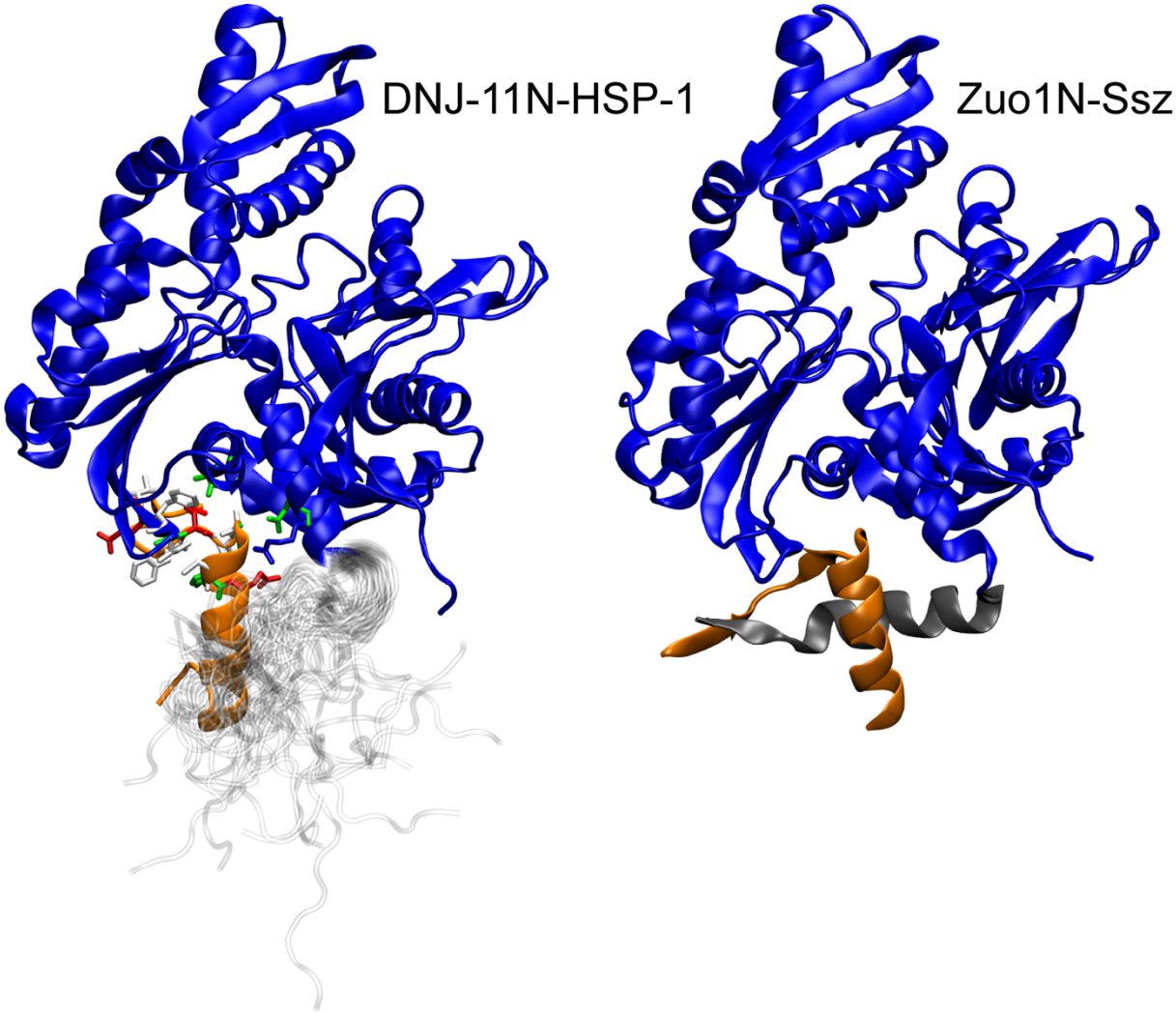

Figure 6

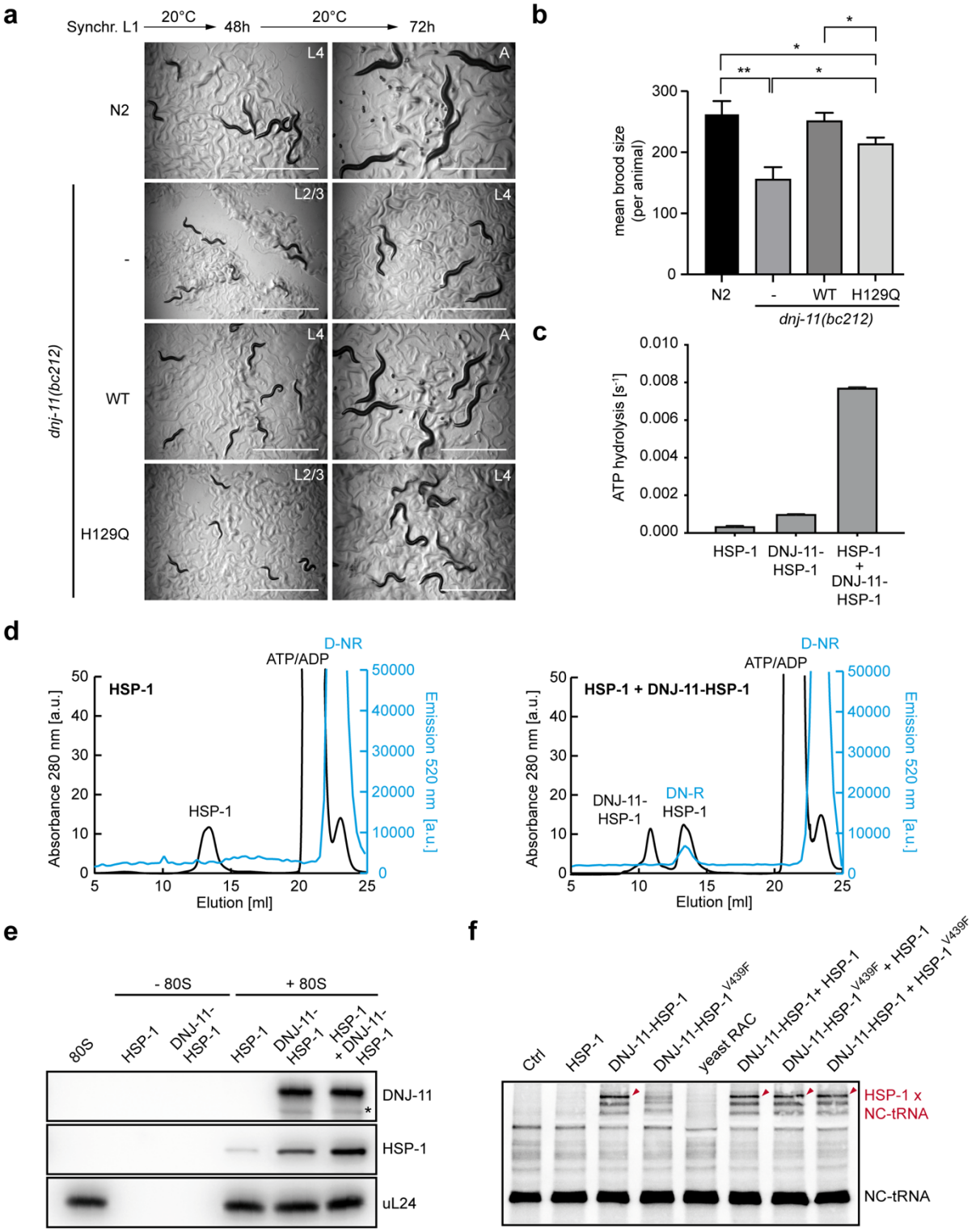
a
Synchr. L1
20°C
48h
20°C
72h
N2
-
WT
H129Q
dnj-11(bc212)
L4
A
L2/3
b
mean brood size (per animal)
N2
-
WT
H129Q
dnj-11(bc212)
c
ATP hydrolysis [s-1]
HSP-1
DNJ-11-HSP-1
HSP-1 + DNJ-11-HSP-1
d
HSP-1
ATP/ADP
D-NR
Absorbance 280 nm [a.u.]
Emission 520 nm [a.u.]
Elution [ml]
HSP-1 + DNJ-11-HSP-1
DNJ-11-HSP-1
DN-R HSP-1
e
- 80S
+ 80S
80S
HSP-1
DNJ-11-HSP-1
HSP-1 + DNJ-11-HSP-1
DNJ-11
HSP-1
uL24
f
Ctrl
HSP-1
DNJ-11-HSP-1
DNJ-11-HSP-1 V439F
yeast RAC
DNJ-11-HSP-1+ HSP-1
DNJ-11-HSP-1 V439F + HSP-1
DNJ-11-HSP-1 + HSP-1 V439F
HSP-1 x NC-tRNA
NC-tRNA

Supplemental Information

Figure S1

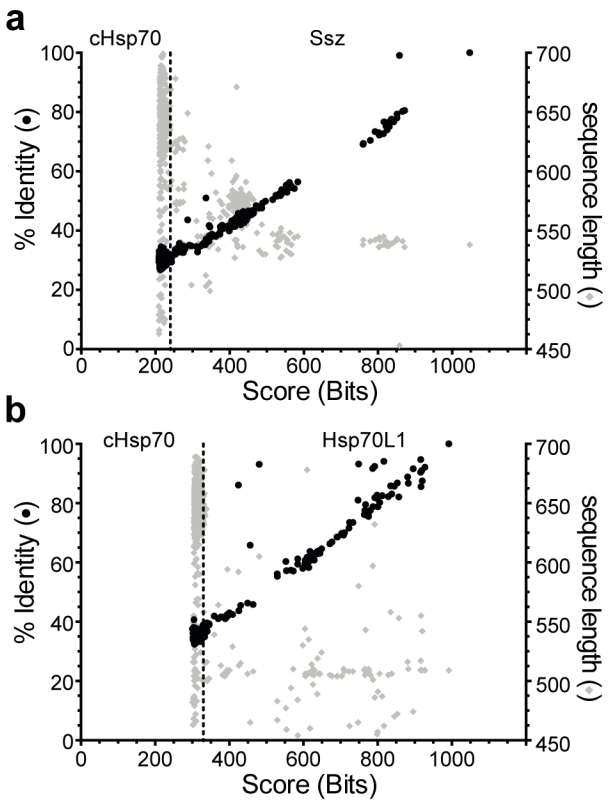

Figure S2

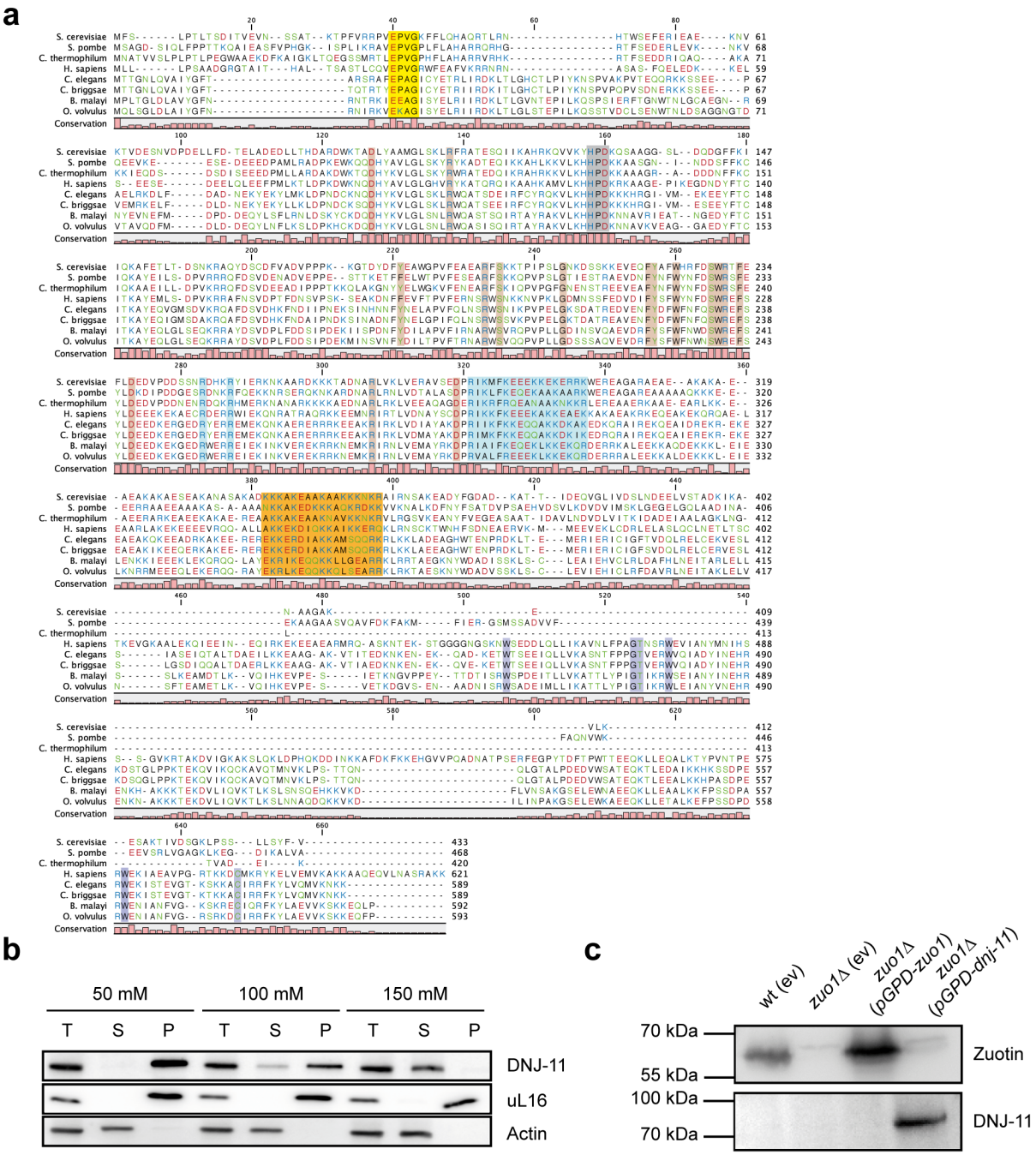
a
S. cerevisiae
S. pombe
C. thermophilum
H. sapiens
C. elegans
C. briggsae
B. malayi
O. volvulus
Conservation
b
50 mM
100 mM
150 mM
T S P T S P T S P
DNJ-11
uL16
Actin
c
wt (ev)
zuo1Δ (ev)
zuo1Δ (pGPD-zuo1)
zuo1Δ (pGPD-dnj-11)
70 kDa
55 kDa
100 kDa
70 kDa
Zuotin
DNJ-11

Figure S3

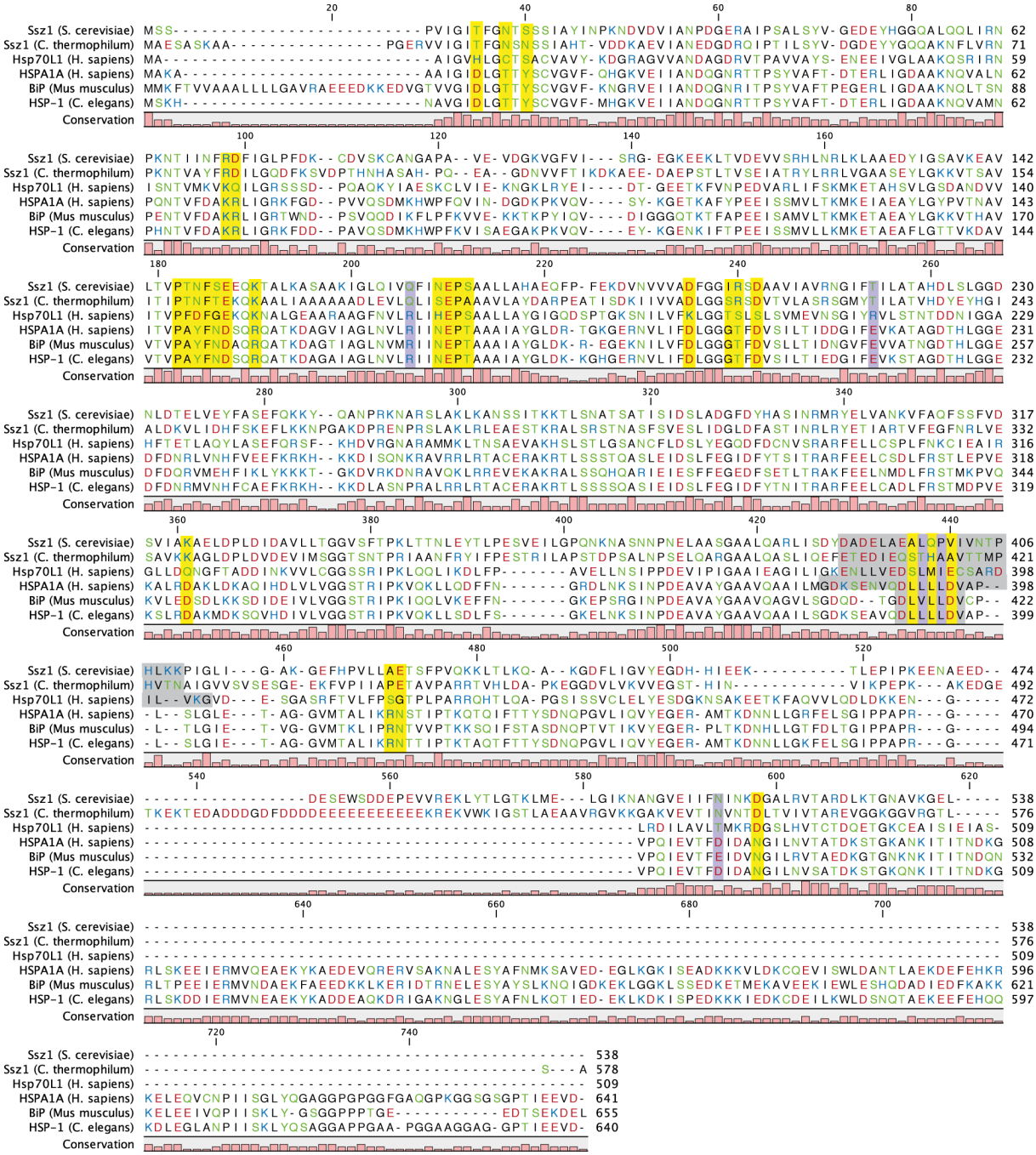
Ssz1 (S. cerevisiae)
Ssz1 (C. thermophilum)
Hsp70L1 (H. sapiens)
HSPA1A (H. sapiens)
BiP (Mus musculus)
HSP-1 (C. elegans)
Conservation

Figure S4

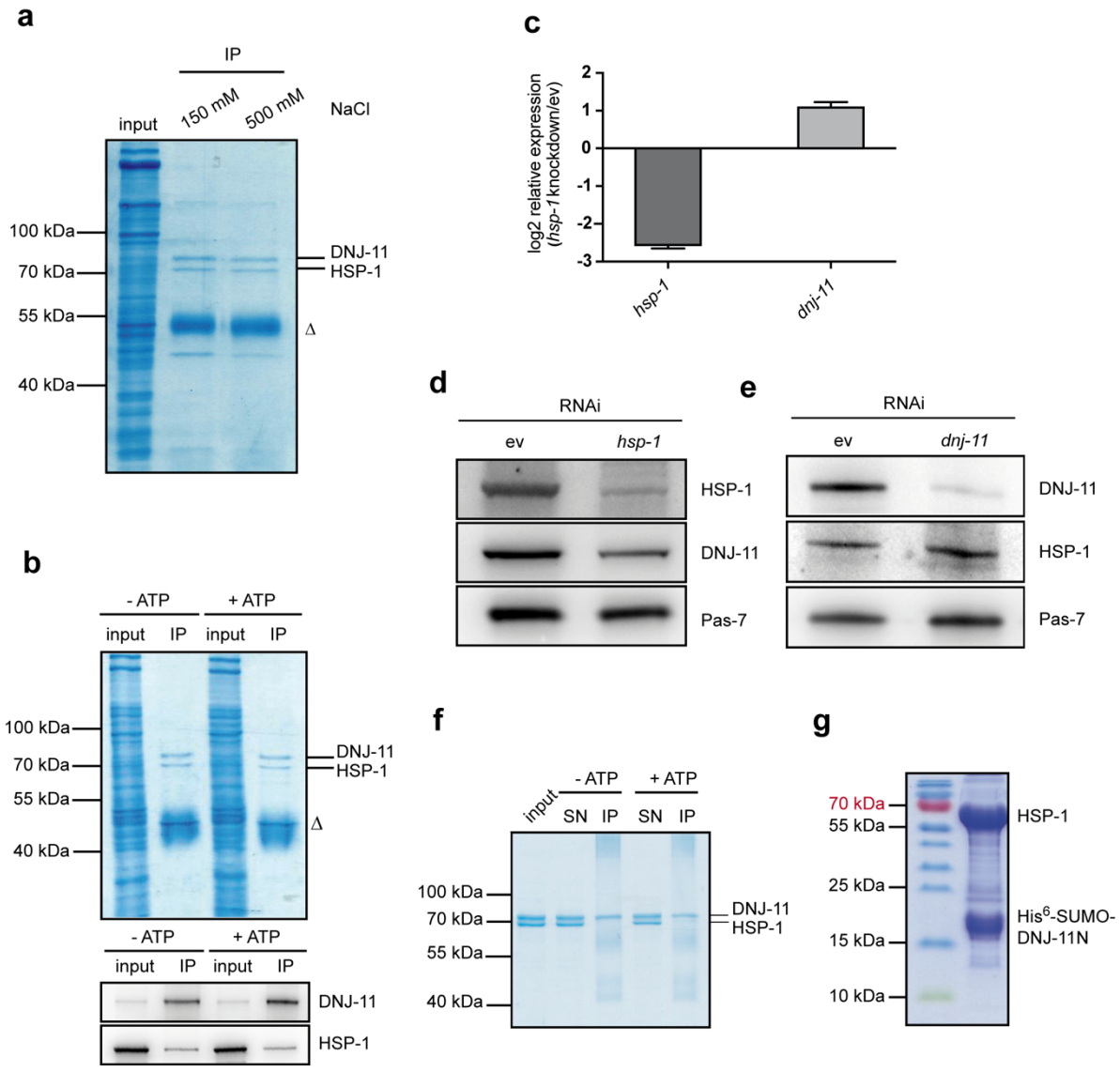
a
IP
input
150 mM
500 mM
NaCl
100 kDa
70 kDa
55 kDa
40 kDa
DNJ-11
HSP-1
Δ
b
- ATP
+ ATP
input
IP
input
IP
100 kDa
70 kDa
55 kDa
40 kDa
DNJ-11
HSP-1
Δ
- ATP
+ ATP
input
IP
input
IP
DNJ-11
HSP-1
c
log2 relative expression
(hsp-1 knockdown/ev)
2
1
0
-1
-2
-3
hsp-1
dnj-11
d
RNAi
ev
hsp-1
HSP-1
DNJ-11
Pas-7
e
RNAi
ev
dnj-11
DNJ-11
HSP-1
Pas-7
f
- ATP
+ ATP
input
SN
IP
SN
IP
100 kDa
70 kDa
55 kDa
40 kDa
DNJ-11
HSP-1
g
70 kDa
55 kDa
25 kDa
15 kDa
10 kDa
HSP-1
His6-SUMO-
DNJ-11N

Figure S5

a

b

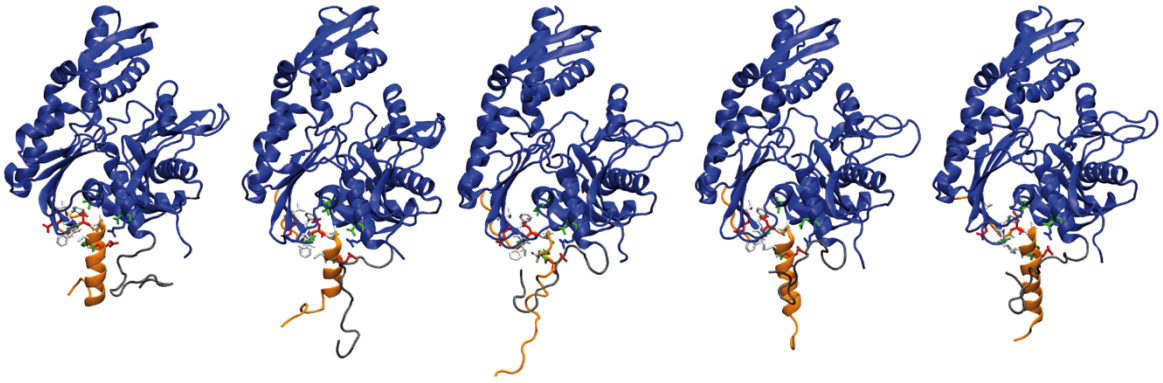

c

Ocuppancy	contact pair			
	HSP1		DNJ-11	
0.669	GLN	377	GLY	24
0.905	GLN	377	ALA	23
0.666	VAL	220	GLU	21
0.812	GLU	219	GLU	21
0.858	GLU	219	PHE	20
0.983	PHE	218	GLU	21
0.948	PHE	218	PHE	20
0.551	ILE	217	TYR	27
0.738	GLY	216	CYS	26
0.772	THR	178	GLU	21
0.681	ASN	175	GLU	21

d

Occupancy	Donor		Acceptor	
0.351	THR	178	GLU	21
0.323	ASN	175	GLU	21
0.227	ASN	175	GLU	21
0.228	ARG	172	PRO	22
0.252	ARG	172	GLU	28
0.267	CYS	26	GLY	216
0.644	GLY	24	GLN	377
0.957	GLU	21	PHE	218

Figure S6

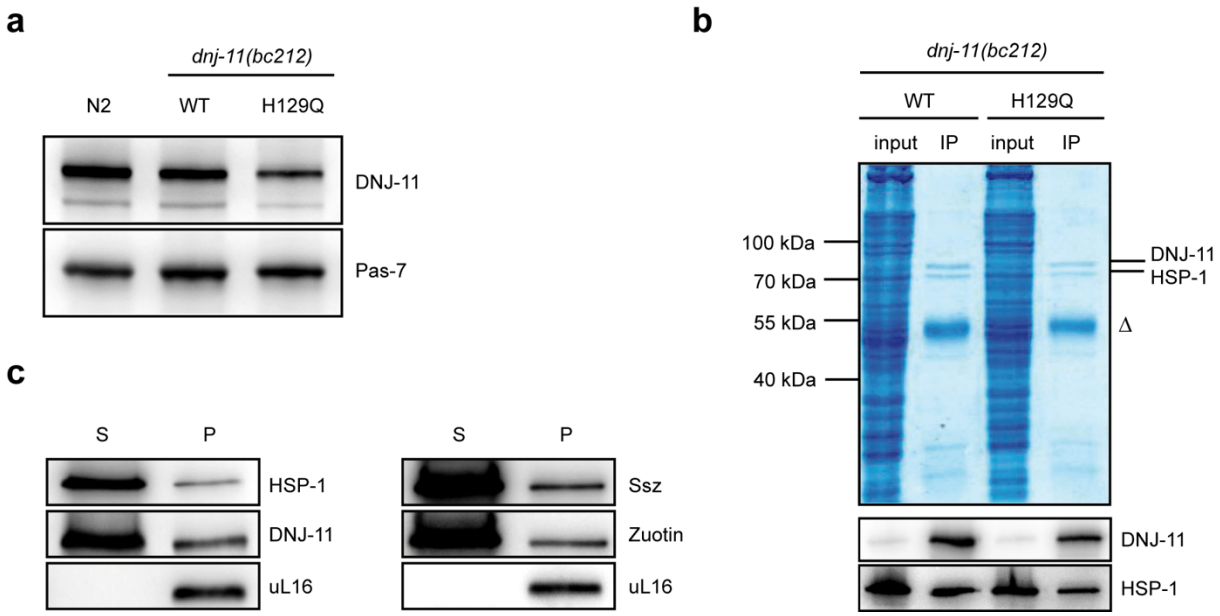
a
dnj-11(bc212)
N2
WT
H129Q
DNJ-11
Pas-7
b
dnj-11(bc212)
WT
H129Q
input
IP
input
IP
100 kDa
70 kDa
55 kDa
40 kDa
DNJ-11
HSP-1
Δ
DNJ-11
HSP-1
c
S
P
HSP-1
DNJ-11
uL16
S
P
Ssz
Zuotin
uL16